Identification of mechanisms that govern regeneration initiation, using the planarian *Schmidtea mediterranea* as a model

INAUGURAL-DISSERTATION

to obtain the academic degree
Doctor rerum naturalium
(Dr. rer. nat.)

submitted to the Department of Biology, Chemistry, Pharmacy
of Freie Universität Berlin
by
Danielle Wenemoser
from Ochsenfurt

January 2011

The work for the thesis presented here was supervised by Assistant-Professor Dr. Peter Reddien, and performed from September 2007 – January 2011, at the Whitehead Institute for Biomedical Research, Cambridge, Massachusetts, USA

1st Reviewer:	Assistant-Professor Dr. Peter Reddien Whitehead Institute for Biomedical Research Massachusetts Institute of Technology
2nd Reviewer:	Prof. Dr. Constanze Scharff Institut für Biologie Freie Universität Berlin

Date of Thesis defense: 14.04.2011

"*Science in the works has two aspects: what could be called day science and night science. Day science employs reasoning that meshes like gears, and achieves results with the force of certainty…Night science on the other hand, wanders blindly. It hesitates, stumbles, falls back, sweats, wakes with a start. Doubting everything, it feels that way, questions itself, constantly pulls itself together…Where thoughts proceed along sinuous paths, tortuous streets, most often blind alleys. At the mercy of chance, the mind frets in a labyrinth, deluged with messages, in quest of a sign, a wink, of an unforeseen connection…Ceaselessly, it goes from hope to disappointment, from exaltation to melancholy. It is impossible to predict whether night science will ever pass to the day condition…When that happens it happens fortuitously, like a freak…What guides the mind, then, is not logic. It's instinct, intuition…Suddenly the landscape shines with blinding light, terrifying, stronger than a thousand suns*."

François Jacob: "The Statue Within", CSHL Press, 1995.

Table of Contents

1 Introduction

1.1 Regeneration and stem cells

The ability to respond to injury and to subsequently restore tissue integrity are fundamental features of multicellular organisms. Amazingly, the human body generates over a billion new cells from various types of stem cells every day (Fuchs and Segre, 2000). Cells that contribute to regeneration can be found in many human tissues, and regeneration in mammals occurs to some degree in the heart (Barbash and Leor, 2006), skeletal muscle (Ehrhardt and Morgan, 2005), bone (Dimitriou et al., 2005), and liver (Fausto et al., 2006; Michalopoulos and DeFrances, 1997) among other tissues. During prenatal development, humans are able to completely recapitulate original tissue architecture in response to injury. However, this ability is lost in adult humans (Colwell et al., 2003). Why can some organisms regenerate so well and others so poorly? What are the key regulatory factors that govern regeneration? The phenomenon of regeneration has puzzled researchers for centuries, yet only recently have these questions begun to be addressed. The fundamental and widespread nature of regenerative processes, and the potential that their study affords for developing novel medical applications, make a cellular and molecular understanding of the events that control regeneration of paramount importance for future research (Pearson, 2001; Slack, 2003; Stocum, 2001).

1.1.1 Regeneration is a common phenomenon throughout the animal kingdom

In contradiction to the common belief that regeneration represents a rare biological phenomenon, regenerative events have been shown to occur in almost all animal phyla (Sánchez Alvarado, 2003). In general, the term regeneration describes events that occur to restore missing tissues or structures, including re-integration with the older, pre-existing tissue. Many organisms can regenerate tissues (or replenish cell numbers) through the action of stem and progenitor cells (Barker et al., 2007; Ito et al., 2005; Jiang et al., 2009; Kragl et al., 2009; Morrison et al., 2006; Oshima et al., 2001; Till and Mc, 1961). The underlying cellular and molecular events are to some degree reminiscent of the events observed during embryogenesis (Sánchez Alvarado, 2004), yet the context in which these two processes occur is different in important ways. During regeneration, as during embryogenesis, self-assembly of new tissues occurs. Regeneration, however, requires the generation of new tissues from older, pre-existing ones, their functional and anatomical integration, and proper re-proportioning of the resulting tissues. Furthermore, regeneration requires that the processes that drive these events be plastic enough to proceed from an infinite number of possible starting conditions, corresponding to the array of possible injuries an organism might sustain (Sánchez Alvarado, 2004).

1.1.2 Different modes of regeneration exist

T. H. Morgan classified two general groups of regeneration: Epimorphosis, which comprises all cases of regeneration that involve proliferation to form new tissue, and morphollaxis (now morphallaxis), where no proliferation occurs but rather pre-existing tissues are directly transformed into new ones (Morgan, 1901). Both of these types of regeneration are used, even together in various species (e.g. planaria). Indeed, there exists a great variety of how regeneration is achieved in the animal kingdom. The polyp hydra is one well-studied example. In these animals, regeneration occurs through direct transformation of the existing parts in the absence of cell proliferation (Park et al., 1970). Urodele amphibians are another well-known model organism studied for their regenerative capacity. These animals are capable of re-growing entire limbs through the transdifferentiation (the direct conversion into another cell type) and dedifferentiation of existing mature cells (Brockes et al., 2001; Kragl et al., 2009). In contrast, regeneration of the human bone relies on the proliferation and differentiation of stem cells that are already present in the tissue (Prockop, 1997). In planarians regeneration occurs through formation of a regeneration blastema from adult stem cells and also involves re-modeling of the pre-existing tissue (Newmark and Sánchez Alvarado, 2002).

While it is clear that regeneration exists in many different contexts, ranging from simple multicellular organisms, such as cnidarians, to complex metazoans, such as humans, it is not known whether these mechanistic variations of the same process share common underlying processes. Likewise, it remains a mystery whether all forms of regeneration are derived from a common ancestor and were simply lost during the evolution of those metazoans that are unable to regenerate, or whether the ability to regenerate was acquired multiple times by different phyla (Sánchez Alvarado, 2003).

1.1.3 Stem cells as the source for new tissue formation

The defining feature of a stem cell is its ability to maintain itself in an undifferentiated state, while generating mature cells of a distinct tissue by differentiation (Reya et al., 2001). Stem cells play an important role in development and regeneration (Weissman, 2000) and can be found in many adult tissues such as heart (Beltrami et al., 2003; Solloway and Harvey, 2003), brain (Capela and Temple, 2002; Uchida et al., 2000), and bone marrow (Spangrude et al., 1988).

Quiescence was long thought to be one of the key features of stem cells. Therefore, label retention using bromodeoxyuridine-labeling (BrdU) was one of the main criteria for the identification of stem cells (Potten and Booth, 2002). However, it has been convincingly shown that stem cells can be fast cycling, for example in the small intestine (Barker et al., 2007). Traditionally, stem cells have been classified by their developmental potential as either totipotent stem cells that can give rise to all embryonic and extra-embryonic tissues, pluripotent stem cells that are

able to produce all tissues within the embryo, multipotent stem cells that produce a subset of cell lineages, or unipotent stem cells that give rise to only one mature cell type (Wagers and Weissman, 2004).

Understanding how stem cell potentiality is maintained and identifying factors that determine “stemness” represent two major areas of current study. For embryonic stem cells, accumulating evidence suggests that a network of transcription factors including Oct3/4, Sox2, c-Myc, Klf-4, and NANOG, prevent differentiation and promote proliferation to maintain and, remarkably, induce the pluripotent state (Boyer et al., 2005; Niwa, 2007; Takahashi and Yamanaka, 2006). For many types of adult stem cells there seems to exist a distinct microenvironment, a physical stem cell niche that ensures proper stem cell proliferation and maintenance (Fuchs et al., 2004). Inside the adult organism most tissues maintain a population of adult slow-cycling stem cells that will proliferate in response to stimulating signals, such as migration factors and growth factors, and either generate new stem cells or differentiate (Blau et al., 2001). In the process of differentiation, stem cells often first enter a transient state of rapid proliferation before they exit the cell cycle and terminally differentiate (Fuchs and Segre, 2000). Their regenerative capacity and plasticity (Forbes et al., 2002) make stem cells not only promising targets for regenerative medicine (Audet, 2004; Gerlach and Zeilinger, 2002; Kume, 2005) and gene therapy (Goessler et al., 2006; Kashofer and Bonnet, 2005; Neff et al., 2006), but also for cancer research as several recent findings indicate that stem cells seem to be involved in the development of certain types of cancer (Guo et al., 2006b; Reya et al., 2001).

Intensive research within the last several years has shed light on many of the signaling mechanisms that govern stem cell proliferation, differentiation, and patterning during development. The mechanisms seem to be very conserved among multicellular organisms. In the development of bilaterian animals, variations of only seven major pathways, namely TGF-ß (transforming growth factor-ß), Wnt (wingless and int, MMTV integration site family), Notch, Hh (hedgehog), nuclear receptor, JAK/STAT (Janus kinase signal transducer and activator of transcription) and receptor tyrosine kinase pathways are believed to perform the bulk of all cell signaling (Pires-daSilva and Sommer, 2003). Together with other factors and pathways that control field and cell-type specification like Hox (homeobox protein), Pax (paired box protein), Distal-less and MASH (achaete-scute homolog) they regulate development in most metazoans (Sánchez Alvarado, 2004). It is therefore possible that subtle variations in the interactions between elements of this toolkit of signaling and patterning mechanisms are sufficient to determine whether an organism is able to regenerate or not.

1.2 Regeneration in the planarian *Schmidtea mediterranea*

All animals suffer risk of injury. Therefore, wound responses are expected to be a common feature of animals throughout the Metazoa. Injuries can elicit a myriad of responses, including cell recruitment, cell proliferation, immunologic responses, and, in some cases, complete regeneration of missing parts. Identification of wound signals and the cellular events that lead to regenerative repair is therefore of fundamental significance. A simple and genetically tractable system in which to study responses to injuries would enable the dissection of the processes that are induced following wounding and that lead to restoration of the injured tissue. Planarians are flatworms that are famous for their ability to regenerate any part of their body (Newmark and Sánchez Alvarado, 2002). The introduction of histological and molecular tools for study of planarian biology—including markers for the stem cells that are involved in regeneration, a complete genome sequence, and strategies for high-throughput RNA interference screening (Reddien et al., 2005a)—make them an attractive system for the investigation of events that happen at wounds and lead to regeneration.

1.2.1 Planarians show remarkable regenerative abilities

The freshwater planarian *Schmidtea mediterranea* is a small free-living flatworm with high regenerative potential (Newmark and Sánchez Alvarado, 2002). Since the first documented description of a tiny piece of a planarian regenerating a complete organism, by Peter Simon Pallas in 1766 (Brøndsted, 1969), researchers have been fascinated by this astonishing regenerative capability.

In the 1880s and early 1900s Thomas Hunt Morgan and Charles Manning Child carried out detailed studies on planarian regeneration, hoping to understand the mechanisms underlying this phenomenon. Inspired by the findings from his experimentation on planarian regeneration, Morgan created the first concept of a morphogenic concentration gradient that establishes and maintains body polarity (Morgan, 1904, 1905). This concept proved to be valid for embryogenesis and metamorphosis. Well-studied examples in *Drosophila melanogaster*, for example, are the BMP (bone morphogenetic protein)-, WNT- and Hedgehog (Hh)-signaling pathways (O'Connor et al., 2006). Despite more than two centuries of research and the fact that many key regulatory events in embryogenesis have been described, the molecular mechanisms of planarian regeneration that puzzled Morgan, still remain poorly understood (Sánchez Alvarado, 2000; Sánchez Alvarado, 2004; Slack, 2003).

Associated with the increasing interest in understanding the mechanisms that control regeneration, planarians have been re-discovered as a model organism for studies on patterning events during regeneration, tissue homeostasis and stem cell regulation (Newmark and Sánchez Alvarado, 2002) (Reddien and Sánchez Alvarado, 2004; Sánchez Alvarado, 2006). Within the last decades a whole set of new methodologies and resources for the study of planarian regeneration

on a cellular and molecular level became available. Their robust regenerative abilities combined with their recently discovered amenability to RNA interference (RNAi) (Sánchez Alvarado and Newmark, 1999), the successful sequencing of more than 99% of the coding regions of the planarian genome in the *Schmidtea mediterranea* genome project (www.genome.wustl.edu), a non-redundant expressed-sequence tag (EST) collection with approximately 10,000 genes(Sánchez Alvarado et al., 2002; Zayas et al., 2005) (Reddien Lab, unpublished data) and the fact that more than 60% of planarian genes are homologous to genes in other organisms (Sánchez Alvarado et al., 2002) make planarians a valuable model organism for addressing long-standing questions in regeneration. Moreover, the development of in situ hybridization techniques on whole animals and cells (Pearson et al., 2009; Reddien et al., 2005b; Umesono et al., 1997), immunohistochemistry (Bueno et al., 1997; Ito et al., 2001), BrdU-labeling (Newmark and Sánchez Alvarado, 2000), flow cytometry (Asami et al., 2002), microarrays (Eisenhoffer et al., 2008) (Peter Reddien, unpublished data), and a recently performed large-scale RNAi screen (Reddien et al., 2005a), provide the tools to gather needed information. Recent case studies on genes required for neoblast function and maintenance (Guo et al., 2006a; Reddien et al., 2005b) have proven the suitability of planarians as a model organism for detailed studies of regeneration and stem cell regulation in vivo. Furthermore, recent findings identified a requirement of the conserved BMP-, WNT-, and Hh-signaling pathways for the establishment of proper axis polarity in planarian regeneration (Gurley et al., 2008; Molina et al., 2007; Petersen and Reddien, 2008, 2009; Reddien et al., 2007; Rink et al., 2009). Therefore findings from studies of regeneration in planarians will not only help to understand basic biological mechanisms in planarians but are likely to improve our understanding of regeneration and stem cell regulation in general.

1.2.2 Planarian biology

In the English literature the term “planarian” generally refers to the taxon Turbellaria, free-living members of the phylum Platyhelminthes. Phylogenetically they are placed in the large taxon Lophotrochozoa, which comprises, together with the Ecdysozoa and the Deuterostomia, all bilaterian animals (Figure 1.1A). Within the Platyhelminthes, *Schmidtea mediterranea* belongs to the Paludicola, freshwater members of the Triclade family (Westheide, 2007). The name is due to the characteristic three main branches of the digestive system, composed of one rostral and two caudolateral blind ending gut branches and a plicate pharynx, which also serves as an anus (Hyman, 1951). They are triploblastic, acoelomate, unsegmented, soft-bodied and dorsoventrally flattened organisms (Hyman, 1951). Their gas exchange relies completely upon diffusion, as they lack any circulatory or respiratory structures (Hyman, 1951). The nervous system consists of bi-lobed cephalic ganglia that are connected to two ventral longitudinal nerve cords, interconnected with lateral commissures (Cebria et al., 2002; Hyman, 1951), and a submuscular

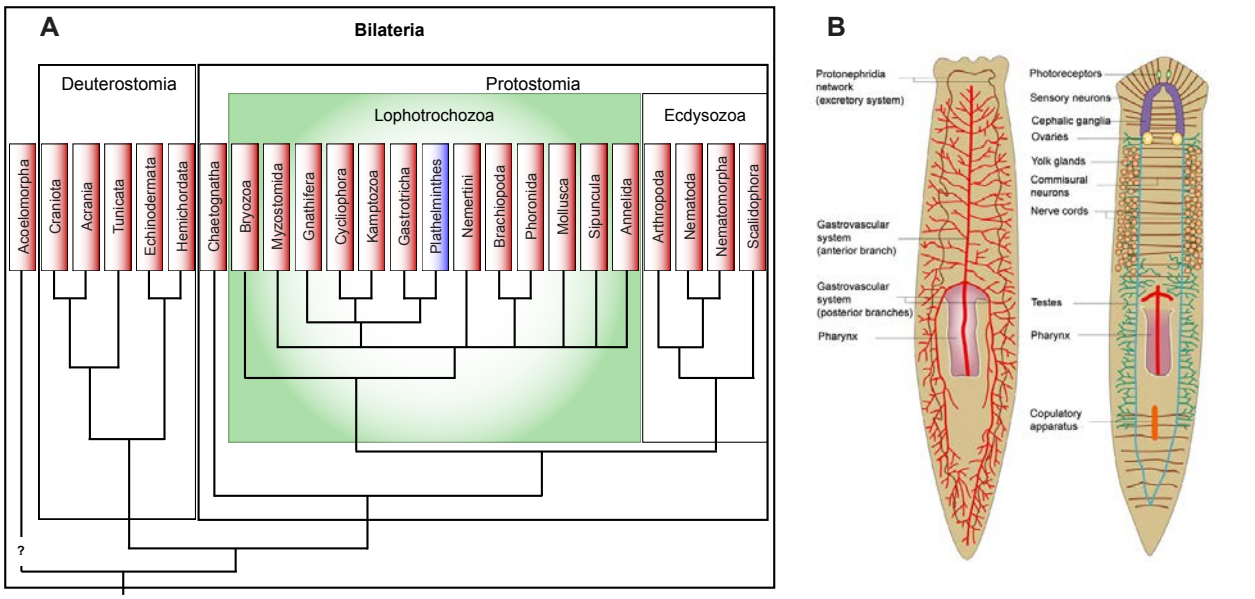

Figure 1.1. Phylogeny and body plan of freshwater planarians. (A) One possible placement of the Platyhelminthes within the phylogenetic tree of the Bilatieria, predominantly based on molecular data (Halanych, 2004). (B) Major anatomical features in two representatives of the triclades. (left) Shown are exclusively the gastrovascular and excretory systems in *Dendrocoelum lacteum*. (right) Reproductive and nervous system in a representative of the genus *Schmidtea*. For better visibility of the testes, the yolk glands are shown only in the anterior region. The oviducts and sperm ducts are not shown. Adapted from the wall charts of Rudolph Leuckart (Newmark and Sánchez Alvarado, 2002).

nervous plexus. Photoreceptors, organized in pigment-cup ocelli, as well as rheoreceptors and chemoreceptors are located in the anterior part of the animal (Figure 1.1B) (Westheide, 2007). The space between the organ systems is filled with a solid mass of tissue called parenchyma. This tissue mainly consists of various types of differentiated cells, such as different types of gland cells, and a distinct type of small, undifferentiated cell referred to as neoblasts (Pedersen, 1959; Westheide, 2007). Depending on environmental influences, planarians can grow and shrink in length and volume. This amazing ability is thought to be accomplished through the daily balance of cell production and cell death (Baguñà and Romero, 1981; Pellettieri and Alvarado, 2007).

Schmidtea mediterranea planarians grow between 1-50 mm in size and are commonly found in springs, freshwater ponds or streams, preying upon insect larvae and other small invertebrates (Hyman, 1951). Reproduction can occur either sexually as cross-fertilizing hermaphrodites, or asexually by transverse fission. A Robertsonian translocation between chromosome 1 and 3 (2n = 8) produced clonal strains that reproduce strictly asexually (Baguñà et al., 1999).

1.2.3 Planarian regeneration relies on a population of adult stem cells

Planarian regeneration requires adult stem cells known as neoblasts (Reddien and Sánchez Alvarado, 2004). The term neoblast originates from Randolph's description of a distinct undifferentiated cell type in *Lumbriculus* (Randolph, 1892) and was later adopted to the undifferentiated

compartment of planarian cells (Buchanan, 1933). Their resemblance to embryonic stem cells and the fact that they can be specifically killed by irradiation prompted the hypothesis that they might be adult stem cells (Wolff and Dubois, 1948). Neoblasts are small cells of 5-10 µm in size with a large nucleus and scant cytoplasm and characteristic chromatoid bodies. Chromatoid bodies are also referred to as nuage in some organisms. They are cytoplasmic ribonucleoprotein complexes that are required for maintenance germ cells of many species and are involved in RNA-processing (Betchaku, 1967; Hayashi et al., 2006; Ikenishi, 1998; Pedersen, 1959). Neoblasts are described as the only known mitotically active somatic cells in the adult planarian (Baguñà, 1989). They are distributed throughout the body, except for two regions that cannot support regeneration of an entire animal when isolated—the region in front of the photoreceptors and the centrally located pharynx (Morgan, 1898; Reddien and Sánchez Alvarado, 2004). Within 2-3 days following amputation of a planarian, an unpigmented structure called a blastema is formed at the wound site and gives rise to some of the new body parts (Reddien and Sánchez Alvarado, 2004). Various studies indicate that neoblasts proliferate following wounding and are the source of new cells for blastema formation (Baguñà, 1976b; Best et al., 1968; Coward et al., 1970; Lindh, 1957; Saló and Baguñà, 1984) (Figure 1.2). However, there has been a history of contradictory results with respect to the spatio-temporal pattern of proliferation. This may in part be due to examination of different species in these studies and the limitations of previously available histological techniques for examination of neoblasts. Two studies, using *Schmidtea mediterranea* (Baguñà, 1976b) and *Dugesia tigrina* (Baguñà, 1976a; Saló and Baguñà, 1984), described an initial maximum in mitotic numbers within 4-12 hours following amputation followed by a second maximum in mitotic numbers occurring more strongly near the wounds by approximately 2-4 days. Because injuries in planarians result in dramatic responses tailored to the identity of missing tissue, the signaling that occurs between the injury site and neoblasts is of great interest for understanding stem cells and their role in regeneration.

Taking advantage of the fact that neoblasts can specifically be killed by irradiation (Wolff, 1962), as they are the only dividing somatic cells in the animal, some groups were able to isolate

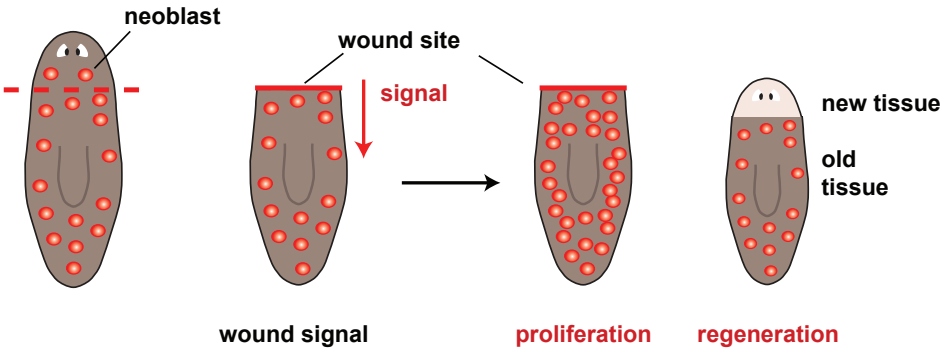

Figure 1.2. Following wounding, neoblasts are signaled to proliferate and give rise to new tissue, which ultimately leads to regeneration.

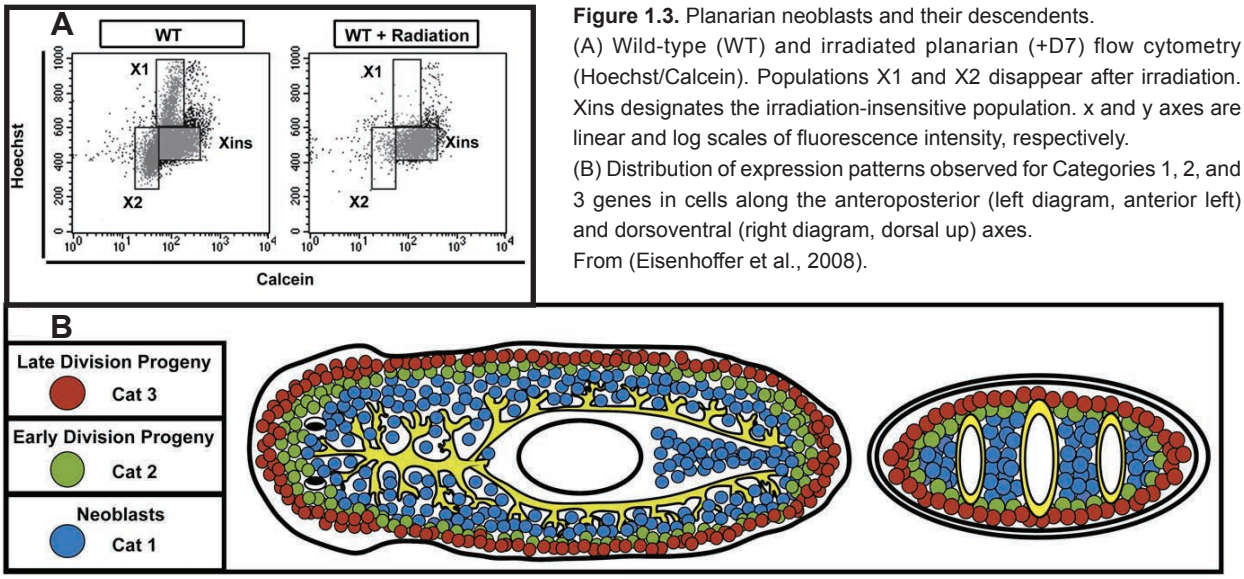

Figure 1.3. Planarian neoblasts and their descendents.
(A) Wild-type (WT) and irradiated planarian (+D7) flow cytometry (Hoechst/Calcein). Populations X1 and X2 disappear after irradiation. Xins designates the irradiation-insensitive population. x and y axes are linear and log scales of fluorescence intensity, respectively.
(B) Distribution of expression patterns observed for Categories 1, 2, and 3 genes in cells along the anteroposterior (left diagram, anterior left) and dorsoventral (right diagram, dorsal up) axes.
From (Eisenhoffer et al., 2008).

different subsets of neoblast-like irradiation-sensitive cells by FACS (Hayashi et al., 2006; Reddien et al., 2005b), using cell labeling with the vital dye Calcein and the DNA stain Hoechst 33342. Mainly two subsets of neoblasts have been identified using FACS analysis, referred to as X1 and X2 (Figure 1.3A). The X1 cells are about 10 µm in size and make up about 2-8% of the total cell number (Reddien et al., 2005b) (Reddien Lab, unpublished data). They appear to be proliferating cells, as shown by quantitative polymerase chain reaction (qPCR) for the genes *pcna* and *mcm2* (Hayashi et al., 2006), in situ hybridization on cells with probe specific for the planarian homolog of cyclin B (Reddien et al., 2005b) and Hoechst labeling (Hayashi et al., 2006; Reddien et al., 2005b). They express the genes for the PIWI-like proteins, *smedwi-1* and *smedwi-2*, the latter of which seems to be required for proper neoblast differentiation (Reddien et al., 2005b). Taken together these findings suggest that planarian neoblasts are a population of adult stem cells, but their potentiality, heterogeneity and cell cycle dynamics remain to be elucidated.

It is unknown whether neoblasts represent a heterogeneous population of cells in different stages of lineage commitment or a homogeneous entity (Sánchez Alvarado and Kang, 2005). The introduction of modern cell biological techniques to address this issue, such as BrdU labeling (Newmark and Sánchez Alvarado, 2000), immunohistochemistry (Guo et al., 2006a; Newmark and Sánchez Alvarado, 2000; Orii et al., 2005), in situ hybridizations (Guo et al., 2006a; Reddien et al., 2005b) and fluorescent-activated cell sorting (FACS) (Asami et al., 2002; Hayashi et al., 2006; Kang and Alvarado, 2009; Reddien et al., 2005b), has begun to shed light on the nature of neoblasts and their immediate progeny, such as their cell cycle dynamics and specifically expressed markers. A recent study identified different categories of neoblast descendents (Eisenhoffer et al., 2008) (Figure 1.3B) that provide useful tools for the future analysis of planarian neoblast differentiation.

1.3 Genes and signaling pathways that are implicated in regeneration and wound-healing

1.3.1 Gene expression changes associated with wound-healing

In *Drosophila* morphogenetic events involving tissue movement, such as embryonic dorsal closure, have been used as models for wound repair. In this system, as well as in wound healing, JUN amino-terminal kinase (JNK) signaling and activation of AP-1 (e.g. JUN and FOS) are crucial for successful closure (Galko and Krasnow, 2004; Martin and Parkhurst, 2004). Similar findings have been reported in mouse models (Koehler et al., 2010; Li et al., 2003). Importantly, a conserved wound repair pathway has been identified that involves function of *grainy head* and activation of extracellular-signal-regulated kinase (ERK) in both *Drosophila* and mice (Mace et al., 2005; Ting et al., 2005), indicating that conserved mechanisms may act to maintain the integrity of various animal barriers. Remarkably, intestinal stem cells of the *Drosophila* midgut proved to be a valuable system for the study wound-induced (e.g. detergent and bacterial ingestion) proliferation (Amcheslavsky et al., 2009; Buchon et al., 2009b; Jiang et al., 2009). Using this system, members of the Hippo signaling pathway, such as Yorkie and Warts (Karpowicz, 2010; Staley, 2010), as well as EGFR signaling (Buchon, 2010) have been identified as factors that mediate intestinal stem cell proliferation following wounding.

In order to distinguish genes that are upregulated directly by wounding from those that are immune response-associated genes, gene expression studies using macrophage-deficient animals were performed (Cooper et al., 2005; Stramer et al., 2008). Data from a study in wounded, macrophage-deficient mouse pups revealed a cluster of about 100 “activation genes” that mainly encode for transcription factors and were upregulated early (i.e., within 30min-3h) and transiently at the wound. Some of these genes are known immediate early genes such as *Egr1 (Krox24)*, *JunB*, *Myc*, *Fosl1*, and *I-Kappa-Bα* (*Nfkbia*). Furthermore, the study identified two further clusters, an “early effector” and a “late effector” cluster. These are upregulated at a later time than the “activation genes” and contain genes that encode extracellular matrix proteins, signaling components, and structural genes required for cell migration. The final cluster of inflammation-independent genes contains genes that may play a role in contact inhibition, such as Ephrin receptors and their ligands, the ephrins, as well as Notch receptors (Cooper et al., 2005). In this study, no analyses on the functional role of identified genes were performed, leaving open the question what role these genes play during the response to wounding.

1.3.2 Regeneration in vertebrate model organisms

Amputation or loss of tissue can be repaired through regeneration in some vertebrates. This is the case in both salamanders (such the newt and the axolotl) and zebrafish (*Danio rerio*), which are capable of replacing or repairing damaged retina, severed spinal cords, injured heart, and

amputated limbs (Antos and Tanaka, 2010). FGF-signaling has been shown to play an important role in zebrafish fin and heart regeneration (Lepilina et al., 2006; Whitehead et al., 2005; Yin et al., 2008). Other mitogenic and patterning factors have been implicated in proliferation of blastemal cells and regeneration, such as Activin-betaA, simplet, and PDGF (Jazwinska et al., 2007; Lee et al., 2009; Lien et al., 2006). Salamander limb regeneration appears to depend on nerve-derived factors (Endo et al., 2004). Notably, nAG, a member of the anterior-gradient family, is released by the Schwann cells of transected nerves and interacts with Prod1 on the surface of blastemal cells, promoting their proliferation (Kumar et al., 2007). However, common transcriptional signatures have been found in comparison of denervated and wild type regenerating limbs, indicating that not all regenerative processes are nerve-dependent (Monaghan et al., 2009).

1.3.3 Transcriptional profiling of liver regeneration

Partial hepatectomy in rats and mice is one of the best-established systems in regeneration research in mammals. During this procedure two-thirds of the liver are surgically removed (Higgins, 1931). The term liver regeneration is a misnomer, because it is in fact a hyperplastic response that involves proliferation of all mature cells in the remnant liver until liver mass is restored, which happens within 1-2 weeks (Higgins, 1931). Major growth factors that are important for this compensatory growth are HGF and TFGa (Burr et al., 1998; Ishii et al., 1995; Mead and Fausto, 1989; Moolten and Bucher, 1967). Studies of differential gene expression identified over 100 immediate early genes that are upregulated in the remnant liver post-hepatectomy (Arai et al., 2003; Haber et al., 1993; Kelley-Loughnane et al., 2002; Mohn et al., 1991; Su et al., 2002). Among these genes are conserved transcription factors that are also upregulated following serum stimulation of tissue culture cells, such as *egr-1*, *c-fos*, *c-jun* (Chavrier et al., 1988; Iyer et al., 1999; Lamph et al., 1988; Muller et al., 1984). It was postulated that these genes are induced by normally latent transcription factors between G0 and G1, before the onset of *de novo* protein synthesis (Taub, 2004). Mitogen-activated kinase signaling, nuclear factor (NF)-kB, signal transducer and activator of transcription 3 (STAT3), and the transcription factor activator protein (AP1) are thought to be involved (Taub, 2004) in activation of these transcription factors. However, it appears that liver regeneration is an extremely complex process and several pathways appear to be activated simultaneously, especially considering the contributing expression changes caused by the immune system (Taub, 2004).

Given the complex nature of the response that is initiated following wounding in vertebrate systems by the contribution of the immune system, and the limitations of studies to a certain organ or tissue type, it is still unclear how valid these findings will be as paradigms for understanding the larger conserved aspects of different types of regeneration in the animal kingdom. Therefore, further studies are required to dissect the molecular mechanisms that underlie

regeneration initiation and to determine whether common programs that govern these events exist.

1.4 Aim of this work

Planarian regeneration requires adult stem cells called neoblasts and amputation is thought to trigger two peaks of neoblast mitoses early in regeneration, a phenomenon that has been historically controversial and therefore requires further investigation. In the first part of this study, I will examine the cellular events that occur during regeneration initiation in planarian neoblasts. I will determine spatial and temporal patterns of neoblast proliferation using the mitotic marker anti-H3P, as well as fluorescence *in situ* hybridizations to label neoblasts and their progeny. Through these studies, I aim to comprehensively describe the nature of the planarian mitotic response to wounding. I will also characterize the key cellular events that happen during regeneration initiation, such as neoblast migration and differentiation. I will use RNAi to identify important features of this wound response. These findings should facilitate future functional studies of regeneration initiation in planarians and contribute to a more complete understanding of regeneration initiation at large.

Responses to sudden and harmful insults, such as wounding, must be quick, robust, and well coordinated. Planarians regenerate efficiently from any mechanical insult. However, the molecular underpinnings that govern this astonishing regenerative ability are to date mainly unknown. In the second part of this study, I will perform differential expression analysis to identify the molecular changes that occur in the pre-existing, differentiated tissue following wounding in planaria. Genes that are upregulated following wounding will be selected as candidate factors that govern regeneration initiation and neoblast proliferation following wounding. I will then use *in situ* hybridizations to probe for expression of these selected candidate genes in order to examine their spatial expression *in vivo*. Additionally, translation inhibition will be used to determine for which of the identified genes are activated independently of protein synthesis. Finally, I will perform RNAi studies on these candidate genes to probe for their potential function in regeneration initiation and neoblast regulation following wounding. Data from the differential expression analysis performed above will also be used to identify genes that are specifically upregulated in planarian neoblasts and their immediate progeny following wounding. I will perform *in situ* hybridizations on identified candidate genes to determine their spatial expression *in vivo*. I will then examine the requirement of protein translation for wound-induced expression of 90 genes (genes that are upregulated in the differentiated tissue and genes that are upregulated in neoblasts) using cycloheximide treatment. Furthermore, effects on wound-induced gene expression by perturbing gene function using RNAi of selected candidate genes will be determined. This functional study will be carried out using the novel NanoString nCounter system, which is able

to accurately measure the expression of large sets of genes across a large set of conditions. This assay will serve to identify genes that are required for specific aspects of the wound-induced transcriptional program. Together, these experiments aim to identify a transcriptional network that underlies the process of regeneration initiation in planarians and identify functional roles for some of the key players.

In the third part of this study, I will focus on two genes encoding planarian homologs of Runt transcription factors identified in part two of this study. I will use *in situ* hybridizations to determine the expression pattern of these genes following wounding. Furthermore, I will use qPCR and fluorescence *in situ* hybridizations to determine the wound-specificity and nature of *runt* expression. To identify the function of wound-induced *runt* expression, I will perform RNAi studies and assay for gross regenerative defects, as well as assess molecular changes that occur following RNAi using microarray analysis. These experiments aim to identify the role of wound-induced *runt* expression in regeneration initiation.

2 Materials and Methods

2.1 Materials

2.1.1 Organisms

Planaria

Schmidtea mediterranea asexual strain CIW4 was maintained as described (Wang et al., 2007) and starved for 1 week before experiments. 4-8mm-long animals were used for immunolabelings and cell-counting experiments; 1-2 mm-long animals were used for in situ hybridizations.

Bacterial strains

Escherichia coli:

Strain	*Genotype*	*Source*
DH10B	F^- *mcr*A Δ(*mrr-hsd*RMS-*mcr*BC) f80*lac*ZΔM15 Δ*lac*X74 *rec*A1 *end*A1 *ara*D139 Δ(*ara, leu*)7697 *gal*U *gal*K I^- *rps*L *nup*G	Invitrogen
HT115	IN(*rrn*D-*rrn*E)1, *rnc14*::ΔTn10	Labstock

2.1.2 Plasmids, Oligonucleotides and Clones

Plasmids

Plasmid	*Source*
pGEM®-T Easy	Promega
pDONRdT7	Labstock
pPR244	Labstock
pBluescript	Labstock

Oligonucleotides

Oligonucleotides were obtained from IDT (Integrated DNA Technologies, Coralville, USA). Gene specific primers were designed using Primer3 (http://frodo.wi.mit.edu/primer3/) and are not listed here for space reasons.

Kits

Name	*Source*
1 Kb Plus DNA Ladder™	Invitrogen

pGEM®-T Vector System I	Promega
QIAprep Spin Miniprep Kit	Qiagen
QIAquick® Gel Extraction Kit	Qiagen
SIGMAFAST™ BCIP/NBT	Sigma-Aldrich
SSC Buffer 20 x Concentrate	Sigma-Aldrich
SuperScript® III First-Strand Synthesis System for RT-PCR	Invitrogen
TSA™ Kit #14 – Tyramide Signal Amplification	Invitrogen
dNTPs	Roche
Vectashield® – Mounting Medium	Vector Labs
Vectashield® – Mounting Medium with DAPI	Vector Labs
MessageAmp™ II aRNA Amplification Kit	Ambion
FirstChoice® RLM-RACE Kit	Ambion
ASAP aRNA Labeling Kit	Perkin Elmer
SYBR® Green PCR master mix	Applied Biosystems

Enzymes

Name	*Source*
Collagenase	Sigma-Aldrich
Proteinase K	Invitrogen
RNase H	Promega
RNase-free DNase	Qiagen
RNasin Ribonuclase Inhibitor	VWR
T7 RNA Polymerase	VWR
Taq DNA Polymerase	Roche Molecular Systems
BP Clonase	Invitrogen

Antibodies

Primary antibodies

Name	*Host*	*Dilution*	*Source*
Anti-arrestin	mouse	1 : 5000	Agata Laboratory, Japan
Anti-Digoxigenin-AP	sheep	1 : 2000	Roche
Anti-Digoxigenin-POD	rabbit	1 : 500	Roche
Anti-Fluorescein-POD	rabbit	1 : 300	Roche
Anti-DNP-POD	rabbit	1 : 100	Perkin-Elmer

Anti-NUCLEOSTEMIN	rabbit	1 : 2000	Reddien Laboratory, USA
Anti-phosphorylated histone H3 (Ser10), clone MC463	rabbit	1 : 50	Millipore Corp.
Anti-SMEDWI-1	rabbit	1 : 2000	Reddien Laboratory, USA

Secondary antibodies			
Name	*host*	*dilution*	*Source*
Anti-mouse Alexa-488	goat	1 : 600	Invitrogen
Anti-rabbit Alexa-568	goat	1 : 600	Invitrogen
Anti-rabbit-HRP	goat	1 : 100	Upstate, Millipore Corp.

2.1.3 Chemicals

Chemicals used in this work are all products of VWR, Sigma-Aldrich, Fisher Scientific, Invitrogen and Roche.

2.1.4 Media

Bacteria Media	
Media	*Ingredients*
2 x YT, pH 7.0	- 16 g / l Bacto Tryptone - 10 g / l Bacto Yeast Extract - 5 g / l NaCl
2 x YT + Tet + Kan	- 2 x YT - 100 µg / ml Kanamycin - 12.5 µg / ml Tetracyclin
Terrific Broth (without K^+ - Salts)	- 12 g / 900 ml Bacto Tryptone - 24 g / 900 ml Bacto Yeast Extract - 4 mL / 900 ml glycerol
10 x K^+ - Salts	- 2.31 g / 100 ml KH_2PO_4 - 12.54 g / 100 ml K_2HPO_4

Planaria Water	
Media	*Ingredients*
1 x Montjuic Salts	- 1.6 mM NaCl - 1.0 mM $CaCl_2$ - 1.0 mM $MgSO_4$ - 0.1 mM $MgCl_2$ - 0.1 mM KCl - 1.2 mM $NaHCO_3$

2.1.5 Buffer and Solutions

All solutions were prepared with deionized MilliQ-water, unless stated otherwise.

General Solutions	
Solution	*Ingredients*
0.5 M EDTA, pH 8.0	- 9.31 g / 50 ml EDTA
1 M $MgCl_2$	- 10.17 g / l $MgCl_2$
1 M Tris, pH 9.5	- 8 g / l Tris-HCl - 116 g / l Tris-Base
1% Agarose gel	- 1 g Agarose - 100 ml TAE buffer/TBE buffer - 5 µl Ethidiumbromide (5 mg / ml)
10 x PBS, pH 7.4	- 80.0 g / l NaCl - 2.0 g / l KCl - 14.4 g / l Na_2HPO_4 - 2.4 g / l KH_2PO_4
10 x TBE buffer	- 108 g / l Tris-Base - 55 g / l Boric Acid - 10 mM EDTA
10% Triton X-100	- 10 ml / 100 ml Triton X-100
10% Tween20	- 10 ml / 100 ml Tween10
5 M NaCl	- 229.2 g / l NaCl
PBT (0.1% Triton X-100)	- 990 ml PBS - 10 ml 10% Triton-X100
PBT (0.3% Triton X-100)	- 970 ml PBS - 30 ml 10% Triton-X100
TAE buffer, pH 8.3	- 40 mM Tris-Acetate - 1 mM EDTA

Fixation	
Solution	*Ingredients*
HCl Solution	- 5.4 ml / 100 ml concentrated HCl
NAC Solution	- 10 g N-acetyl cysteine - 100 ml PBS

5% NAC solution	- 5g N-acetyl cysteine - 100 ml PBS
PBSTx	- 0.1% Triton-X 100 - PBS
Reduction solution	- 50mM DTT - 1% NP-40 - 0.5% SDS - 10x PBS
Proteinase K solution	- 2µg/ml Proteinase-K 0 - 0.1% SDS - 1X PBSTx
Carnoy's	- 60 ml Ethanol - 30 ml Chloroform - 10 ml Glacial Acetic Acid
Bleaching Solution	- 20 ml 30% H_2O_2 - 80 ml Methanol
4% PFA	- 10 ml 16% Paraformaldehyde - 30 ml PBS

Rehydration

Solution	*Ingredients*
75% MeOH / PBT (0.3%)	- 75 ml Methanol - 25 ml PBT (0.3% Triton X-100)
50% MeOH / PBT (0.3%)	- 50 ml Methanol - 50 ml PBT (0.3% Triton X-100)
25% MeOH / PBT (0.3%)	- 50 ml Methanol - 50 ml PBT (0.3% Triton X-100)
75% MeOH / PBT (0.1%)	- 75 ml Methanol - 25 ml PBT (0.1% Triton X-100)
50% MeOH / PBT (0.1%)	- 50 ml Methanol - 50 ml PBT (0.1% Triton X-100)
25% MeOH / PBT (0.1%)	- 50 ml Methanol - 50 ml PBT (0.1% Triton X-100)

in situ Hybridization

Solution	*Ingredients*
Denhardt's	- 10 g / l Ficoll 400 - 10 ml / l polyvinylpyrrolidone - 10 g / l BSA

50% Dextran Sulfate	- 50 g / 100 ml Dextran Sulfate
1 M DTT	154.3 g / l DTT
wHYB	- 500 ml / l Formamide (deionized) - 250 ml / l 20 x SSC - 1 x Denhardt's
PHYB10(-DS)	- 500 ml / l Formamide (deionized) - 250 ml / l 20 x SSC - 1 x Denhardt's - 1 g / l Yeast RNA - 100 mg / l heparin - 0.05% Triton X-100 - 0.05% Tween20 - 5 mM DTT
PHYB10	- 500 ml / l Formamide (deionized) - 250 ml / l 20 x SSC - 1 x Denhardt's - 1 g / l Yeast RNA - 100 mg / l heparin - 0.05% Triton X-100 - 0.05% Tween20 - 5 mM DTT - 5% Dextran Sulfate
HYB	- 50-55% De-ionized Formamide - 5-10% Dextran Sulfate - 5x SSC - 1mg/ml yeast torula RNA - 1% Tween-20
pHYB solution	HYB solution without Dextran Sulfate

Solution	*Ingredients*
MABT, pH 7.5	- 11.67 g / l Maleic Acid - 150 mM NaCl - 0.1% Tween20
AP buffer	- 100 mM Tris pH 9.5 - 50 mM $MgCl_2$ - 100 mM NaCl
Blocking Solution	- 800 ml / l MABT - 100 ml / l heat-inactivated horse serum

2 x SSCT	- 100 ml / l 20 x SSC - 10 ml / l 10% Triton X-100
0.2 x SSCT	- 10 ml / l 20 x SSC - 10 ml / l 10% Triton X-100
75% wHYB / 2 x SSCT	- 75 ml wHYB - 25 ml 2 x SSCT
50% wHYB / 2 x SSCT	- 50ml wHYB - 50 ml 2 x SSCT
25% wHYB / 2 x SSCT	- 50 ml wHYB - 50 ml 2 x SSCT
MeOH / PBT	- 50 ml Methanol - 50 ml PBT (0.1%)
10% PVA	- 100 g / l Polyvinylalcohol
5% PVA / AP	- 100 mM Tris pH 9.5 - 50 mM $MgCl_2$ - 100 mM NaCl - 50 ml / 100 ml 10% PVA
AP buffer variation 2	- 100mM Tris, pH 9.5 - 100mM NaCl - 50mM $MgCl_2$ - 0.1 % Tween-20 - in 10% polyvinylalcohol solution
NBT / BCIP	- 1 NBT / BCIP tablet - 10 ml 10 % PVA
Development buffer	- 4.5µl/ml NBT solution - 3.5µl/ml BCIP solution - AP buffer variation 2
	- 80% Glycerol - 10mM Tris, pH 7.5 - 1mM EDTA

Immunohistochemistry

Solution	*Ingredients*
PBTB	- 30 ml 10% Triton X-100 - 2.5 g BSA - ad 1000 ml PBS

Flow Cytometry and cell isolation	
Solution	*Ingredients*
CMFB, pH 7.3	- 400 mg / l NaH2PO4 - 800 mg / l NaCl - 1200 mg / l KCl - 800 mg / l NaHCO3 - 240 mg / l glucose - 10 g / l BSA - 15mM HEPES
Maceration Solution	- CMFB - 1 mg / ml Collagenase - 0.005% NAC

RNAi feeding	
Solution	*Ingredients*
60% Liver homogenate	- 6 ml blended beef liver - 4 ml Planaria Water

2.1.6 Equipment

Equipment	*Source*
AxioCam HRc/m	Zeiss
FACSCalibur™	Becton Dickinson
Insitu ProVS	Intavis
Mastercycler Epgradient	Eppendorf
Microscope ImagerZ1 with Apotome	Zeiss
Microscope NeoLumar	Zeiss
Nanoject II	Drummond Scientific Company
Stereocope Stemi 2000	Zeiss
Stereoscope Stemi SV6	Zeiss
NanoString Processing Station	NanoString Technologies
NanoString Imaging Station	NanoString Technologies

2.2 Methods

2.2.1 Animals and animal handling

Planarians were raised in Planaria Water at 20˚C in the dark and fed homogenized beef liver every other week. Unless stated otherwise, animals that were starved for at least one week were used for experimentation.

2.2.2 Amputation procedure

For surgery, animals were placed on a voltage regulated cold block (4˚C) and amputated using a trimmed razor blade. Afterwards, animals were placed into Petri dishes with fresh Planaria Water and kept at 20˚C in the dark until further use.

2.2.3 Cycloheximide treatment

Animals were amputated in a dilution of cycloheximide (Sigma) in planaria water (0.1µg/µl; 1:1000 dilution of 100mg/ml in DMSO) and kept in this solution until fixation or RNA extraction. The same procedure was performed with control animals using a 1:1000 dilution of DMSO in planaria water.

2.2.4 Exposure to γ-irradiation

For lethal irradiation (elimination of all neoblasts), planarians were exposed to 6,000 rad (6K, about 72min). For sublethal irradiation planarians were exposed to 1,500 rad (1.5K, about 18min). The same Cesium source was used in both cases (approximately 83rad/min). Animals were used for subsequent experiments 5-7d later, as indicated.

2.2.5 Total RNA isolation

RNA extraction by Trizol (acid guanidinium thiocyanate-phenol-chloroform extraction) is a well-established method for high yield total RNA preparations from whole tissues or cells.
Animals were weighed and 0.75 ml Trizol added to every 0.25 g of sample. After homogenization in a tissue homogenizer at top speed, samples were incubated for 5 minutes at room temperature. 200 µl Chloroform were added to every 750 µl of Trizol and samples were shaken vigorously. After centrifugation at < 12000 g for 15 minutes at 4ºC the aqueous phase was transferred into to a new tube. 500 µl Isopropanol per 750 µl original used Trizol was added and samples were incubated for 10 minutes. After spinning for 10 minutes at < 12000 g, samples were washed with 75% Ethanol and centrifuged at < 7500 g for 5 minutes at 4ºC. Pellets were carefully air dried and resuspended in RNase free water. Samples were stored at -80ºC until use.

2.2.6 Gene cloning

For generation of antisense RNA probes, genes were cloned into pGEM and amplified using T7-promoter-containing primers. For RNAi, genes were cloned into pPR244 using a BP recombination reaction (Invitrogen) to create RNAi entry clones and transformed into DH10B for amplification. Following isolation, the plasmids were then transformed into *E. coli* strain HT115 (Timmons et al., 2001). Clones were confirmed by sequencing.

Gateway cloning of planarian genes from cDNA

First strand cDNA synthesis

For cDNA synthesis, the Superscript III kit (Invitrogen) was used. 10 µL RNA-primer mix was prepared by adding 1µg of planarian RNA, 1 µL of dT primer, 1 µL of 10 mM dNTP and DEPC-treated dH2O to 10µl. The reaction was incubated at 65 ºC for 5 min, then placed on ice for at least 1 min. The 10 µL cDNA synthesis mix for each RT-primer mixture was prepared by adding:

2 µL of 10X RT Buffer
4 µL of 25 mM MgCl2
2 µL of 0.1 mM DTT
1 µL of RNAseOUT
1 µL of Superscript III RT Polymerase

10 µL of cDNA synthesis mix was mixed with each RNA-primer mixture, incubated for 50 min at 50 ºC, and the reaction terminated for 5 min at 85 ºC. Subsequently, reactions were briefly chilled on ice, 1 µL of RNAse H was added to each tube, and samples were incubated for 20 min at 37 ºC.

Amplification of genes from cDNA

For amplification of genes of interest from cDNA, gene specific primers were designed using Primer3 (http://frodo.wi.mit.edu/primer3/). Three different primers were designed as follows per gene for use in two rounds of PCR: **A** primers were designed as 5' gene specific primers for first round amplification, **B** primers were designed as a nested 5' primer for second round amplification, and **C** primers were used in both reactions as the 3' primer. **B** and **C** primers were designed to contain sequences that are complementary to parts of the AA3 and AA4 primers (these append attB sequences that are extended in a later PCR to produce a sequence required for BP recombination):

For **B** primers the following sequence was attached to the 5' end:

5'- AAGCTGGAGCTCCACCGCGG *-GSP-3'*

For **C** primers the following sequence was attached to the 5' end:

5'- GGGCGAATTGGGTACCGGG *- GSP -3'*

Second strand gene-specific PCR reaction:

1 µL of 10 mM dNTP
1 µL of 10 µM **primer A**

1 µL of 10 µM **primer C**
5 µL of 10X Taq Buffer
1 µL of 1st strand template
0.4 µL Taq Polymerase
40.6 µL dH2O

Nested gene-specific PCR:
1 µL of 10 mM dNTP
1 µL of 10 µM **primer B**
1 µL of 10 µM **primer C**
5 µL of 10x Taq Buffer
1 µL of 2nd strand template
0.4 µL Taq Polymerase
40.6 µL of dH2O

Both reactions were run using a "touchdown" strategy (Don et al., 1991), starting with an annealing temperature between 72-79 ºC.

This product was cloned into pGEM and used as a template for RNA probe synthesis by using primers complimentary to the attached attB sites and containing T7 promoter sites, required for *in vitro* transcription.

Adaptor PCR reaction to extend Gateway attB1 and attB2 sites (required for BP recombination):

H20	20.625µL
10xTaq Buffer	2.5µL
10mM dNTP	0.5µL
10µM PWR.AA3	0.3125µL
10µM PWR.AA4	0.3125µL
template	1.0µL
Taq polymerase	0.25µL

For this reaction, Touchdown PCR was again used, this time with a 74 ºC annealing temperature.

These PCR products were PEG (Polyethyleneglycol) purified by mixing the following ingredients:

PCR	25µL
TE (pH8.0)	175µL
PEG (supplied)	100µL

Samples were spun at max speed for 25 min and the supernatant removed. Samples were then resuspended in 20µl H_2O.

For the BP reaction, 1.5µl PEG purified PCR product was mixed with 0.5µl of pPR244 (100ng/µl), and 2µl of TE. 1uL BP clonase was added and mixed by gentle pipetting. Samples were incubated at 25 ºC for 2 hours. Reactions were then briefly spun down and 0.8 µL of Proteinase K solution was added. Samples were then incubated at 37 ºC for 10 min. Reactions were placed on ice to cool down, transformed into competent DH10B cells, screened, and purified plasmid transformed into HT115.

Rapid amplification of cDNA ends (RACE) for complete sequence analysis

For **5' RACE**, a 5' RNA library was created by ligating an adapter to the 5' end of RNA. The reaction was prepared by combining the following components in an RNase-free microfuge tube:

2µl CIP/TAP-treated RNA
1µl 5' RACE Adapter
1µl 10X RNA Ligase Buffer
2µl T4 RNA Ligase (2.5 U/µl)
4µl Nuclease-free Water

Samples were incubated at 37 ºC for one hour.

The ligated RNA was then added to the following in an RNase-free microfuge tube on ice to perform reverse transcription:

2µl Ligated RNA (or minus-TAP control)
4µl dNTP Mix
2µl Random Decamers
2µl 10X RT Buffer
1µl RNase Inhibitor
1µl M-MLV Reverse Transcriptase or Superscript III
8µl Nuclease-free Water

Samples were incubated at 42 ºC for one hour.

For **3' RACE**, reverse transcription was performed by adding the following to an RNase-free microfuge tube on ice:

2µl Ligated RNA (or minus-TAP control)
4µl dNTP Mix
2µl 3' RACE Adapter
2µl 10X RT Buffer
1µl RNase Inhibitor
1µl M-MLV Reverse Transcriptase
8µl Nuclease-free Water

Samples were incubated at 42 ºC for one hour.

Amplification of RACE products for both 5' and 3' RACE was carried out as follows:

1µl RT reaction (from the previous step)
5µl 10X PCR Buffer
4µl dNTP Mix
2µl 5' or 3' RACE gene-specific primer (10 µM)
2µl 5' or 3' RACE Primer
35µl Nuclease-free Water
1µl DNA polymerase

Thermal cycling was performed as follows:

3 mins.: 94°C 35 cycles: 94°C – 30 sec, 60°C – 30 sec, 72°C – 30 sec 7 mins.: 72°C

This amplification step was then repeated using nested RACE primers to produce the final RACE product. RACE products were then cloned to the pGEM vector and sequenced.

2.2.7 RNAi by feeding

RNAi is a powerful method used to investigate the role of a gene of interest through perturbation of gene function. It has been shown that RNAi works effectively in planarians (Newmark et al., 2003; Reddien et al., 2005a}. The double stranded RNA (dsRNA) can either be delivered by direct injection of dsRNA or through feeding of bacteria expressing dsRNA mixed with blended liver.

Food preparation

To prepare bacteria for RNAi feeding, 3 ml of 2 x YT + Kan + Tet were inoculated with HT115 bacteria containing the desired RNAi clone and left shaking overnight at 220 rpm at 37 ºC. The next day, aliquots of these cultures were frozen in 25% glycerol for future use. Subsequently, 3 ml of overnight culture were added to 28 ml pre-warmed 2 x YT + Kan + Tet and incubated at 37 ºC shaking at 200 rpm. The Optical Density (OD) was measured every 30min-1h. At $OD_{0.4}$, cultures were induced with 1 mM IPTG and left shaking at 37 ºC for two more hours. Bacteria were pelleted by spinning at 3700 rpm for 5 minutes and mixed with a 60% liver solution. This mixture was aliquoted and stored at -80ºC until use.

Feeding procedure

At least two hours before feeding, animals were placed into petri dishes with fresh Planarian Water and kept in the dark. 60 µl (for 30 animals) of the thawed liver/bacteria homogenate was mixed with 1.5 µl red food coloring and mixed by pipetting up and down. 20µl aliquots were pipetted into the dish and animals were left eating for > 1 hour, subsequently washed with Planaria Water and kept in the dark at 20ºC. On the two following days, and after that every third day, animals were rinsed twice with fresh water. Prior to the next feeding animals were transferred into a fresh petri dish. Four feedings, at day 0, day 4, day 8 and day 12, were performed. 6 days after the final feeding, animals were amputated.

2.2.8 Histology

For antibody labeling and *in situ* hybridization techniques, animals were fixed either in Carnoy's or in Formaldehyde.

Fixation with Carnoy's

Planarians were placed into glass vials and, after removal of Planarian Water, either killed by addition of HCl-solution for 30 seconds, or 10% NAC/PBS for 5 minutes. This solution was removed and planarians were fixed in Carnoy's on ice for 1.5 hours (NAC) or 2 hours (HCl). Subsequently, specimens were incubated in ice-cold Methanol for 1 hour at -20˚C followed by incubation at room temperature for at least 16 hours in a 6% Hydrogen-peroxide (H_2O_2)/Methanol solution

(to bleach pigment) that had been pre-cooled to the same temperature as samples. After this bleaching step, specimens were rinsed in Methanol twice and either immediately processed or stored at -20˚C until use. Just prior to use, specimen were rehydrated through a MeOH/PBT (0.3%/0.1%) series (MeOH, 75% MeOH/PBT, 50% MeOH/PBT, 25% MeOH/PBT, PBT) for 5 minutes per step.

Fixation with Formaldehyde

Asexual planarians of a length between 2 and 4 mm were starved for one week and transferred either into 1.5ml Eppendorf-tubes (for processing up to 20 worms) or in 15ml Falcon tubes (for processing up to 200 worms). Planarian water was replaced with 5% NAC solution for 5-10 minutes at room temperature (RT). NAC was replaced with 4% Fixative for 15-20 minutes at RT. Fixative was removed and worms were rinsed 1X with PBSTx. PBSTx was replaced with preheated Reduction solution for 5-10 minutes at 37°C. After removal of Reduction solution, worms were rinsed 1X with PBSTx. PBSTx was replaced with 50% Methanol solution for 5-10 minutes at RT. 50% Methanol solution was replaced with 100% Methanol for 5-10 minutes at RT, and then transferred to -20°C for ≥ 1 hour. Specimens were stored at -20°C in MeOH until needed. Methanol was replaced with 6% Bleach solution, under direct light, overnight, at RT and rinsed twice with 100% Methanol the following day. Specimens were then returned to -20°C or used immediately.

Whole-mount antibody labeling

Antibody labeling is a commonly used method to detect the distribution of a protein of interest inside tissue. It is based on the detection of a specific epitope usually by fluorescently labeled antibodies. Signal amount can be enhanced by amplification steps with a secondary antibody or by enzymatic reactions, such as cleavage of fluorescently coupled Tyramide by horse radish peroxidase (HRP). The following procedure was used for all antibody staining with all steps taking place at room temperature. Fixed and rehydrated specimens were transferred into small glass vials or baskets in 24-well plates and blocked in 2-5 ml PBTB (0.3% Triton X-100, 0.25% BSA), for six hours rocking at 130–150 rpm at room temperature. Subsequently, they were incubated in 300 µl primary antibody in PBTB (1:100 rabbit anti-H3P, Millipore; 1:5000 anti-arrestin, Agata Laboratory, Japan; anti-NST 1:2000, Reddien Laboraty, USA; anti-SMEDWI-1 1:2000 Reddien Laboratory, USA) and left rocking at 60–100 rpm overnight. The antibody solution was removed and stored with a final concentration of 5 mM of Sodium Azide at 4ºC for reuse. Specimens were washed once in PBTB for 5 min, followed by an additional wash in PBTB every hour for six hours. 300 µl of the secondary antibody diluted in PBTB (anti-rabbit-HRP 1:150, for Tyramide signal amplification, Invitrogen; anti-mouse Alexa 488/568 1:600) were added to the samples and left rocking over night at 60 – 100 rpm. The following day the antibody solution was removed and after a 5 minute PBTB wash, 6 more 1 hour washes were performed. Samples labeled with a secondary fluorophor-coupled antibody, were mounted in Vectashield®. Specimens that were

labeled with HRP-conjugated antibody were incubated in 200 µl Tyramide (TSA™-Kit #14, 1:200 in Amplification Buffer, Invitrogen) for signal amplification. After removal of the Tyramide solution, samples were washed 5 times for 5 minutes each in PBTB, and subsequently 4 times for 30 minutes each. Specimens were left rocking over night in the fourth wash. The following day, specimens were washed six more times, mounted in Vectashield®, and examined using fluorescence microscopy.

Whole-mount in situ hybridization

in situ hybridizations were performed on formaldehyde fixed animals. All steps were performed at room temperature, with animals rocking or shaking, unless otherwise noted. Animals were first rehydrated in 50% methanol solution for 5 minutes, followed by 5 minutes rinsing in PBSTx. Animals were then treated with Proteinase K for 10 minutes and subsequently fixed in 4% formaldehyde for 10 minutes. After two 5 minutes washes in PBSTx, animals were rinsed in a 1:1 mixture of PBSTx and prehybridization solution (pHYB) for 10 minutes. Animals were then placed in fresh pHYB at 56°C for two hours before being placed in hybridization solution (HYB) containing the desired RNA probe (generally at a 1:800 dilution) at 56°C for greater than 16 hours. The following day, animals were washed twice each in pHYB, pHYB : 2x SSC(1:1), 2x SSC, and 0.2x SSC at 56°C for 30 minutes per wash. Animals were then rinsed in MABT twice for 5 minutes each time. Animals were placed in blocking solution for 1-2 hours and then placed in an anti-DIG solution overnight at 4°C. The following day, animals were rinsed greater than seven times in MABT, for 20 minutes per wash.

For NBT/BCIP detection, animals were incubated in AP-PVA solution for 10 minutes and then developed in NBT/BCIP solution, in the dark, until signal had developed. For time courses and other comparisons, all specimens that were labeled with the same probe were stopped at the same time. Development was stopped by rinsing twice in PBSTx for 10 minutes each wash. Samples were post fixed in 4% formaldehyde, rinsed 2x in PBSTx for 5 minutes each wash, cleared of background signal by rinsing in 100% EtOH for 30 minutes, and rinsed twice more in PBSTx for 5 minutes each wash. Samples were then stored in 80% glycerol for mounting.

For tyramide detection, animals were incubated in PBSTI for 30 minutes and then pre-incubated in tyramide solution without H_2O_2 for 30 minutes. Fresh H_2O_2 was then added to a concentration of 0.002% and animals were left to incubate for 45 minutes. Animals were subsequently rinsed 6x in PBSTx, for 15-20 minutes per wash. Animals were mounted in Vectashield® in the case of single probe tyramide detection. In the case of multiple probe tyramide detection, animals were post-fixed in 4% paraformaldehyde for 45 minutes, rinsed twice in PBSTx for 5 minutes each rinse, rinsed 4x in MABT for 10 minutes each wash and then placed in blocking and antibody solutions as described above containing either anti-Fluorescein or anti-DNP antibodies.

These animals were then washed as described above following antibody treatment and mounted in Vectashield®.

in situ hybridization on sections and cells

Cells and sections were fixed in 4%PFA / PBS for 10 minutes, washed twice in PBS, incubated in a Proteinase K / PBS solution (1µg / ml final concentration) for 10 minutes at room temperature, washed twice in PBS for 5 minutes each, and post-fixed in 4%PFS/PBS for 15 minutes. Two washes in PBS were followed by two more washes in PBT (0.1%). Subsequently, prehybridization was carried out in PHYB10(-DS) at 56ºC in a hybridization oven in a roller drum for two hours. RNA probes were diluted in PHYB10, preheated for 2-5 minutes at 72ºC and kept at 56ºC until use. Samples were hybridized for 36 hours at 56ºC in a roller drum. The next day, animals were washed in a decreasing concentration of wHYB at 56ºC as follows:

10 min 75%wHYB / 25% 2XSSCT
10 min 50%wHYB / 50% 2XSSCT
10 min 25%wHYB / 75% 2XSSCT
2x 30 min 2XSSCT
2x 30 min 0.2XSSCT

Subsequently, animals were transferred to room temperature and washed twice in MABT while rocking. Before antibody labeling, animals were incubated in Blocking Solution for 1 hour, rocking at RT, followed by antibody incubation for 4 hours (anti-DIG-AP, 1:2000 in Blocking Solution, Roche). After two brief rinses and six ten minute washes in MABT, samples were stored overnight. The next day the specimens were equilibrated with two 5 minute washes in AP buffer, followed by 10 minutes in 5%PVA/AP. Development was carried out using NBT/BCIP tablets dissolved in PVA. Animals were kept in the dark, rocking, and development stopped by two 5 min washes with PBS. For storage and image acquisition, animals were fixed in 4%PFA for 30 minutes, washed 2 x 5 minutes with PBS and transferred through a glycerol series, 5 minutes each step (10% glycerol / PBS, 20% glycerol / PBS, 50% glycerol / PBS). Following development and fixation, slides were mounted in Vectashield® with DAPI.

2.2.9 Cell isolation

To obtain single cell suspensions from planarian tissues, animals were placed into petri plate, rinsed once in cold CMFB, and the liquid removed. With the plate on the cold block, heads and tails were cut off, and pieces rinsed in CMFB / NAC (0.05%). Subsequently, the pieces were finely minced using a scalpel and incubated in Maceration Solution for at 30min – 1h at room temperature on a nutator. After two filter steps with 40 µm and 20 µm nylon meshes, suspensions were spun down for 5 minutes at 1250 rpm. Cells were then resuspended in CMFB and applied to slides and fixed in FA solution if cells were used for *in situ* hybridization protocols.

2.2.10 Flow cytometry

Flow cytometry is a useful method for distinguishing between different cell populations in a heterogeneous mixture of cells. This is accomplished through analysis of cells' light scattering properties when exposed to a laser beam. Cells are distinguished based on their relative size (Forward Scatter – FSC), relative granularity/internal complexity (Side Scatter – SSC) or their relative fluorescence intensity if labeled with fluorescent dyes.

500µl of filtered cells, obtained as described above, were incubated in 45µl of Hoechst 33342 (10mg/mL, Molecular Probes) for 30min at RT in the dark. Subsequently, Calcein was added to a final concentration of 100ng/mL and cells were incubated in the dark at RT for another 20min. Cells were spun down, resuspended in fresh CMFB and 5µL/mL PI (stock 1mg/mL) added right before sorting. Small debris was electronically gated out by plotting SSC versus FSC and selecting against small or fragmentized cells, events that appear in the lower left corner and close to the axes. Furthermore, cells were selected for low PI-intensity and high Calcein intensity (i.e., live cells). Hoechst blue versus red plots were used to identify the X1 fraction that is high in DNA content and therefore easily distinguishable from the remainder. All experiments were performed in triplicate. FlowJo software was used for analysis of X1 numbers.

2.2.11 RNA probe synthesis

T7 RNA polymerase is commonly used to synthesize antisense RNA used for transcript detection. In this reaction, a labeled nucleotide (often digoxigenin-labeled dUTP) is incorporated into synthesized RNA and subsequently detected through antibody recognition.

Reactions were performed as follows:

4 µL	PCR product
5 µL	5 x Buffer
2.5 µL	10 x DIG/FL/DNP nucleotides
1.5 µL	RNasin
1 µL	T7 1000 U / µL
11 µL	DEPC dH_2O

This mix was incubated for 1 hour at 37ºC at which point 1 µl of additional T7 was added. Incubation was then allowed to continue for one more hour. DNA was degraded by incubation with RNase-free DNase at 37ºC for 15 minutes. RNA was obtained by precipitation with 0.5 volumes of 7.5M Ammonium Acetate and 2 volumes of ice-cold 100% Ethanol. This was incubated for 30 minutes at -80ºC and centrifuged at maximum speed at 4ºC for 20 minutes. After a wash in 50 µl ice-cold 80% Ethanol, samples were centrifuged at maximum speed at 4ºC for 5 minutes. The pellet was resuspended in 50 µl deionized formamide and the quality of the product was determined by running 4 µl of the product in a 1% Agarose (TBE) gel.

2.2.12 Quantitative Real- Time RT-PCR (qRT-PCR)

For relative quantification studies, two-step qRT-PCR was performed using Applied Biosystems 7300 Real-Time PCR System. 1µl DNase-treated cDNA (obtained as described for the microarray experiments) from samples of interest was mixed with the following:

1 µl	Primer1 (10µM)
1 µl	Primer2 (10µM)
12.5 µl	SYBR Green 2X PCR mix
9.5 µl	dH_2O

Reactions were performed as follows (Volume 25 µl):

Stage	Repetitions	Temperature	Time
1	1	50.0 ∞C	2:00
2	1	95.0 ∞C	10:00
3	40	95.0 ∞C	0:15
		60.0 ∞C	1:00

UDP-Glucose was used as endogenous control primer and samples were calibrated to measurements in the wild type data set. Experiments were performed in triplicate.

2.2.13 Data analyses for imaging

Mitotic density was determined by counting nuclei labeled with the anti-H3P antibody and normalized by the quantified animal area (unless otherwise stated) using the Automatic Measurement program of the AxioVision software (Zeiss, Germany). For quantification of *NB.21.11E*-expressing cells, the complete dorsal domain of cells (about twenty 1µm z-stacks) was photographed from the head and tail regions (335µm from the head or tail tip along the head-to-tail axis were imaged, or ~0.1mm2 of tissue per animal). Numbers were determined using the Automatic Measurement program of the AxioVision software (Zeiss, Germany). For cell *in situ* hybridization quantifications, animals were dissociated and labeled as described above, and the percentage of cells with signal (medium and high expression levels, assigned visually) of the total DAPI+ cell number was calculated.

2.2.14 Microarray experiment

All microarray experiments were performed in biological triplicates. For microarray experiments, RNA was extracted from 10 animals per condition, using TRIZOL, DNase treated by adding 2µl of RNase-free DNase (Qiagen) to up to 20µg of RNA with 5x DNase buffer in 100µl. Samples were incubated 10min at RT and subsequently, RNA was purified using generic Phenol-Chloroform extraction protocols. RNA was amplified using MessageAmp™ II aRNA Amplification Kit (Ambion) and was labeled using ASAP labeling kit (Perkin-Elmer). All experiments were performed in triplicate. For the analysis using RNA from sorted cells, 600,000 cells were collected for each condition

and replicate. Microarray chips were customized arrays (Agilent) 44,000 spots, representing all known *S. mediterranea* ESTs and gene predictions. Hybridization procedures were performed by the "Genome Technology Core" at the Whitehead Institute, Cambridge, MA, USA. Data normalization was carried out by BaRC (Whitehead Institue) using limma (Linear Models for Microarray Data) included in Bioconducter's R package. Data from each chip was first normalized within one chip and subsequently globally. Log2 ratios of mean expression levels (treatment/control) and FDR-adjusted p-values were used for analysis. Further data analysis was carried out using Excel. For analysis of the "differentiated tissue" data set, genes were considered upregulated if a spot was higher than 0.3 log2 ratio in the wild type data set and higher than 0.6 log2 ratio in the irradiated data set at the same time ($p<0.05$). For analysis of the neoblast data set, genes were considered specifically upregulated in the neoblasts if in a tested condition the log2 ratio was >0.3 in the wild type data and at the same time <0.15 in the irradiated data. For analysis of the *Smed-runt-1* RNAi data set, all significantly ($p<0.05$) differentially expressed genes were selected. Cluster 3.0 and Java TreeView were used for clustering and visualization of the microarray data. Homology to genes from other organisms was determined using BLAST.

2.2.15 NanoString experiments

For NanoString nCounter experiments (Geiss et al., 2008), total RNA from drug or RNAi-treated animals (10 per condition, 3 biological replicates) was isolated using TRIZOL and DNase treatment as performed for the microarray experiments. *S. mediterranea* specific code sets were designed by NanoString and hybridization and analysis procedures were performed according to the manufacturer's protocol. Differential expression was assayed from NanoString counts using an overdispersed Poisson model with a Fisher-like exact test, as implemented in Bioconductor's edgeR package (Robinson et al., 2010). A gene was considered differentially regulated if the FDR-adjusted p-value was <0.01.

2.2.16 Phylogenetic analyses

Amino acid sequences were aligned using CLUSTALW (Higgins, 1994; Thompson et al., 1994). The alignments were trimmed using GBlocks (Castresana, 2000). Bayesian analyses were performed using MrBayes (Huelsenbeck and Ronquist, 2001; Ronquist and Huelsenbeck, 2003). Two chains were started and allowed to run for 10 million generations, 1 tree was sampled every 100 generations, and the first 7,500 trees were discarded as burn-in. The phylogenetic tree graphic was generated using FigTree.

3 Results

3.1 Planarian regeneration involves distinct stem cell responses to wounding and tissue absence

3.1.1 Neoblasts respond to wounding in a widespread first mitotic peak and a second localized mitotic peak

Amputation and feeding result in an increase in neoblast proliferation that can last up to seven days (Baguñà, 1976a; Baguñà, 1976b). To investigate neoblast mitoses following wounding, we used an antibody that recognizes Histone H3 phosphorylated at serine 10 (anti-H3P). This mark is present from the onset of mitosis to telophase (Hendzel et al., 1997). Because neoblasts are the only actively dividing somatic cells, and whole-mount antibody labeling can be performed in

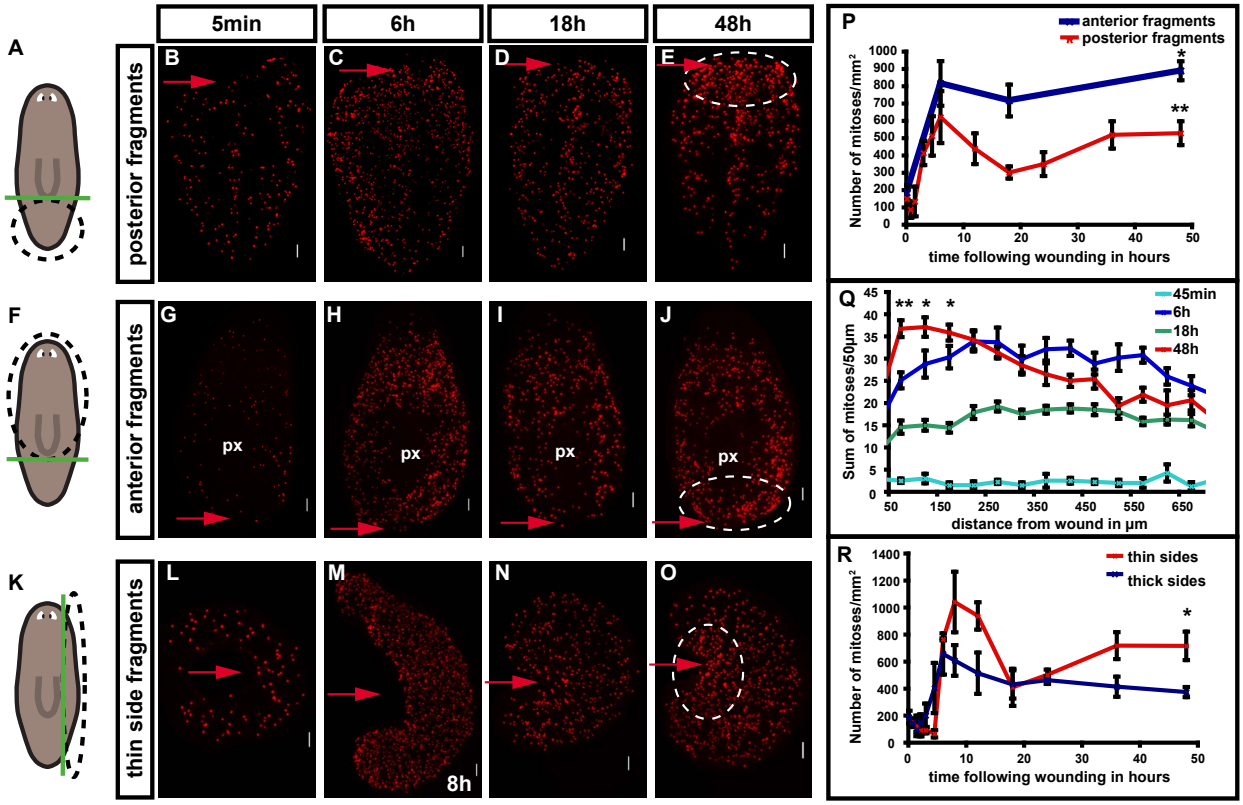

Figure 3.1. Neoblasts respond to amputation with a widespread first mitotic peak and a second, localized mitotic peak.
(A-R) Wounding triggers a widespread first mitotic peak, by 4-10 hours, and a localized, second mitotic peak by 48h. A), F), K) schematics, amputation procedure. Green line, amputation plane. Black dotted circle, region analyzed. Amputated fragments were labeled with an anti-H3P antibody to detect mitoses at indicated timepoints. (P) Change in mitotic density with time following amputation in transversely amputated fragments. Mitotic numbers were significantly higher at 48h versus 18h; **p<0.01, *p<0.05, Student's t-test. (Q) Mitotic numbers at different distances from the wound site in posterior fragments. Numbers were significantly higher at the wound site at 48h versus 6h; **p<0.01, *p<0.05, Student's t-test. (R) Change in mitotic density with time following parasagittal amputation. Mitotic numbers were significantly higher at 48h versus 18h; *p<0.05 by Student's t-test. Red arrows, amputation site. px, pharynx. Circles, wound site at 48h showing increased mitoses. n ≥ 3. Anterior to the top in all images, dorsal view. Scale bars 100µm. All data represent averages ± standard deviation (sd).

planaria, this antibody allows quantification and spatial resolution of neoblast mitoses in entire animal fragments (Newmark and Sánchez Alvarado, 2000).

We established an assay and key time points for examining mitotic patterns in animal posterior (tail) fragments (Figures 3.1A-E, 3.2A-D). A temporally biphasic mitotic pattern occurred following amputation (Figures 3.1A-E, P, 3.2A-F), similar to that observed previously by counting mitotic figures in successive tissue strips (Saló and Baguñà, 1984). After a slight decrease in mitotic density at around 45 minutes (min) – 1 hour (h) (Figures 3.1P, 3.2A), a rapid, 5-fold increase in mitotic numbers occurred, resulting in a first mitotic peak within 6h (Figure 3.1C, P). Significantly, this peak occurred throughout the entire animal fragment, rather than only in cells near the wound. This first peak was followed by a general decrease in mitotic numbers, reaching a minimum by 18h following amputation (Figure 3.1D, P). At this point, mitoses were still 2-fold higher in number than in uninjured animals (Figure 3.1P). Additional wounding applied to tail fragments 6h before the mitotic minimum was not sufficient to increase mitotic numbers; by contrast, a stimulus applied during the mitotic minimum, or later, was sufficient to boost mitotic numbers (Figure 3.3). This observation indicates that the drop in mitotic numbers at 18h is likely not caused by a cessation in wound signaling.

A second change in neoblast division occurred involving an increase in mitotic numbers

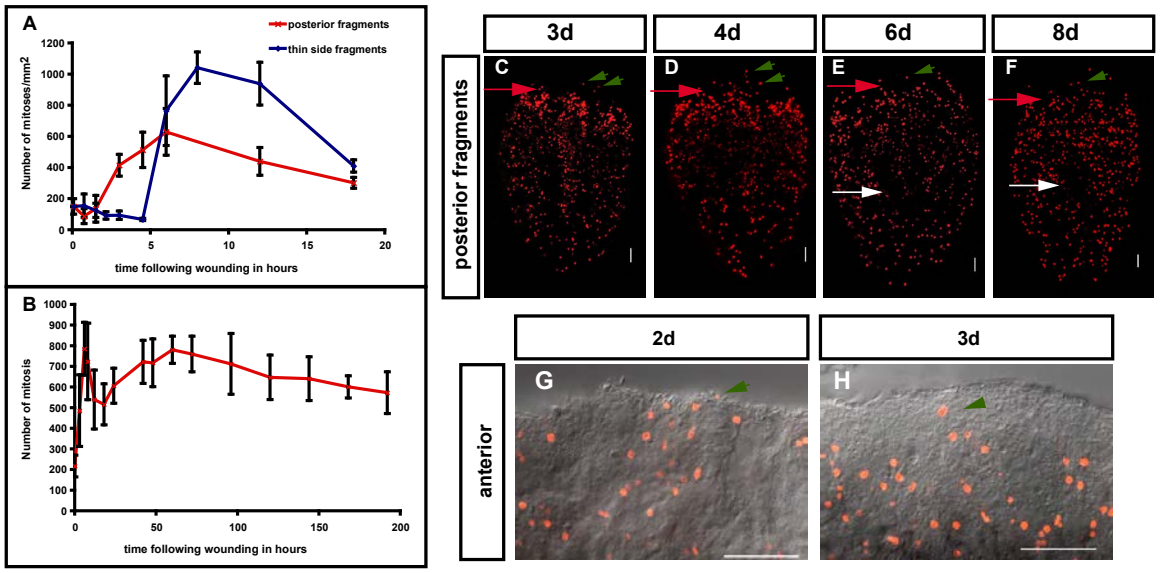

Figure 3.2. Detailed extended time course of neoblast wound response and proliferation in blastema.
(A) Change in mitotic density with time following amputation in amputated posterior tail fragments and thin side fragments during the first 18h following wounding. The thin side fragments display a longer drop in mitotic numbers and a later, but higher, increase during the first mitotic peak. (B) Change in numbers of mitoses with time following amputation in posterior (tail) fragments. Data represent averages. $n \geq 3 \pm$ SD. (C-E) Extended time course on amputated posterior tail fragments, fixed at indicated time points, and labeled with anti-H3P (red). Mitoses stay elevated over the course of eight days following amputation. (G-H) Mitoses (anti-H3P, red) can be found in the blastema proper during regeneration at (G) 2 and (H) 3d 2 and 3d following wounding. Anterior blastemas shown. DIC images were superimposed with fluorescent images. White arrows, pharynx; red arrows, wound site; green arrowheads, mitoses in the blastema. $n \geq 3$. Anterior, top. Scale bars, 100µm.

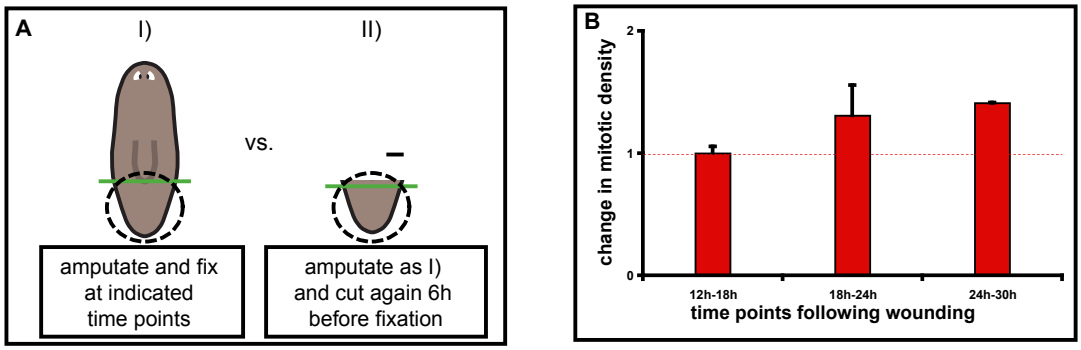

Figure 3.3. The mitotic minimum is not caused by a cessation of wound signaling.
(A-B) Wounding was not sufficient to stop the mitotic decline that leads to the mitotic minimum, indicating cessation of wound signaling does not likely explain the mitotic minimum. A) Schematic depicts amputation procedure. Green lines, wound site. Black circles, area analyzed. B) Change in mitotic density in a 6h time interval at indicated time points in animals amputated twice as in II), normalized by singly amputated animals as in I). Data represent ratio of averages + propagated standard deviation.

near the wound that peaked approximately 48h – 72h following wounding (Figures 3.1E, P, 3.2B-C). This second mitotic peak thus differs from the first peak in that the increase in mitotic numbers is local as opposed to widespread (Figure 3.1E, Q). Mitotic numbers stayed elevated for the following 8 days, but became more evenly distributed throughout the fragment (Figure 3.2B, D-F). Between five and six days following amputation, mitoses were lacking where the newly forming pharynx became visible (Figure 3.2E-F). In contradiction to previous reports (Saló and Baguñà, 1984), we did observe mitoses occasionally in blastemas, particularly in posterior-facing blastemas (Figure 3.2G-H).

To determine whether the biphasic mitotic pattern described above is a general feature of planarian regeneration, a time course of transverse and parasagittal amputations was performed to obtain fragments with posterior (Figure 3.1F-J) and lateral-facing wounds (Figure 3.1K-O). In all cases, a biphasic mitotic pattern was observed, with some differences in the details of the pattern (Figure 3.1P, R). Thin, regenerating side fragments, for instance, had a longer period of decrease in mitotic numbers before the first peak (Figure 3.2A) and a later first peak (8h) than did posterior fragments (Figures 3.1M, R, 3.2A). The overall magnitude of mitotic numbers at the time of the second, localized mitotic peak varied greatly between the different fragment types. However, a local increase at the wound site was always observed (Figure 3.1E, J, O, Q) (hereafter referred to as the second peak). These key aspects of the neoblast wound response – a biphasic pattern mitotic pattern consisting of a first, immediate, and widespread mitotic peak and a second, localized mitotic peak – are explored below.

3.1.2 The magnitude of the first mitotic peak depends on wound size

What aspects of injury result in the rapid and widespread increase in mitoses during the first mitotic peak? To test the influence of wound size, three different surgeries were performed

(Figure 3.4A) and numbers of mitoses were analyzed at 4, 6, and 8h. Strikingly, all wound types tested caused a robust and widespread mitotic increase, even minor injuries that did not elicit or require overt blastema formation. The first wound type (a simple poke in the animal tail using a 10-20µm diameter needle) and the second wound type (a small incision with a blade in the tail tip) caused a more than 4-fold increase in mitotic numbers in the postpharyngeal region (Figure 3.4B). Because a simple piercing of the animal can trigger a mitotic response throughout the planarian body (Figure 3.4C, D), we suggest that the initial response of neoblasts to wounds

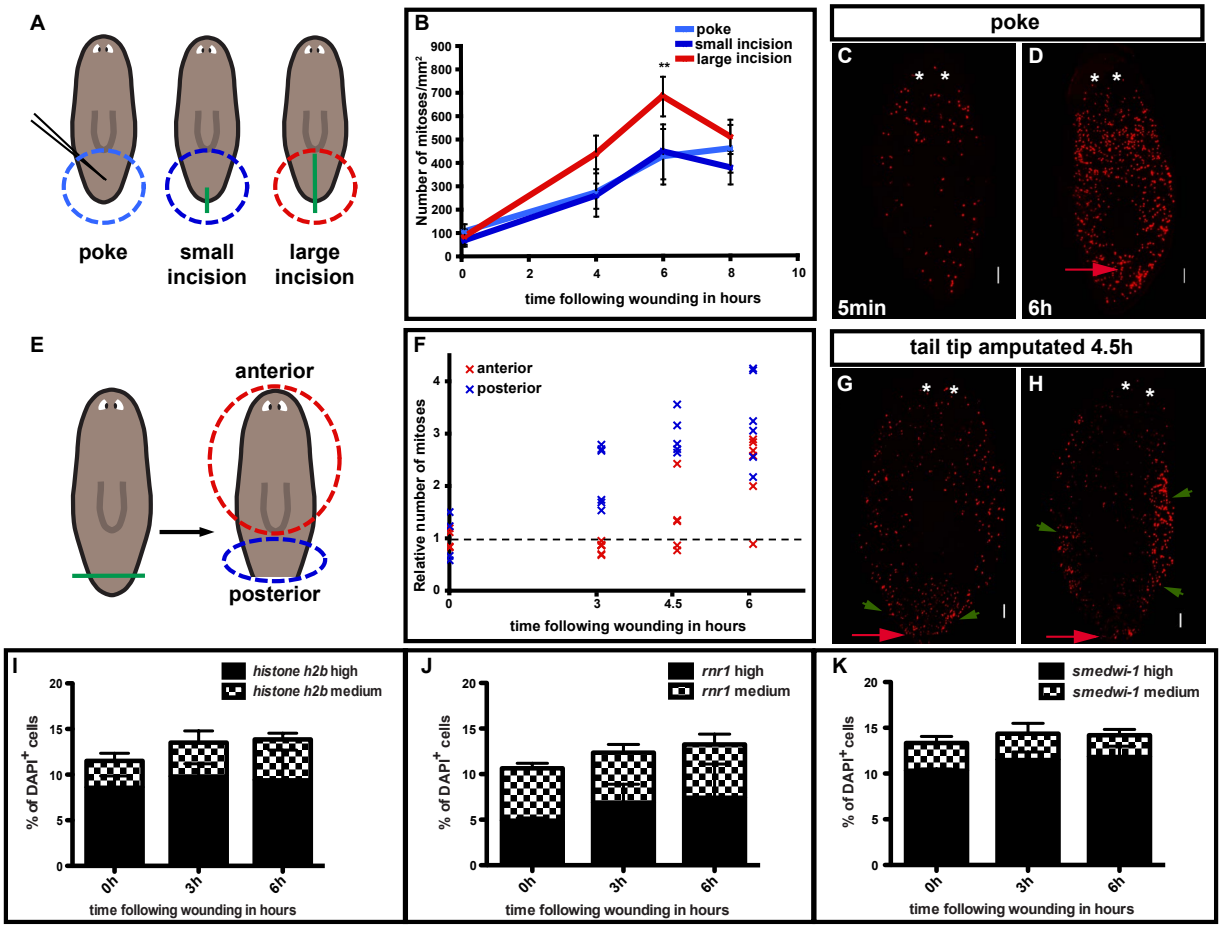

Figure 3.4. The first mitotic peak and the response of neoblasts to wounds.
(A-D) The first mitotic peak magnitude depends on wound size. A) Green lines, wound. Light blue, blue, and red circles, area analyzed. (B) Change in mitotic density with time following wounding. (C-D) A small injury (needle-poke) induces a widespread first mitotic peak by 6h; n ≥ 5. (E-H) The signal that causes the first peak spreads from the wound site. (E) Tail tips were amputated; blue and red circles, area analyzed at right. (F) Change of mitoses in areas far from the wound (anterior) and close to the wound (posterior) following wounding. The number of mitoses for each data point was divided by the average number of mitoses determined for each body region present immediately after amputation (5 min). (G-H) Animals from E) labeled with anti-H3P at 4.5h. Images, stages (G) with mitotic numbers elevated near but not far from the wound (2/8 animals), and (H) with mitotic numbers elevation having spread along the animal periphery (5/8 animals); n ≥ 6. (I-K) The signal that causes the first mitotic peak likely acts on G2/M transition. Graphs, quantification of *in situ* hybridizations on fixed cells from animals macerated at indicated time points, probing for (I) *histone H2B*, (J) *rnr1*, and (K) *smedwi-1* mRNA. The number of S phase-marker-positive cells did not robustly change before the first mitotic peak; n=5, triplicate. Red arrows, wound sites. Anterior to the top, dorsal view. Asterisks, photoreceptors. Scale bars, 100µm in all images. Data represent averages ± sd.

is triggered by disruption of animal integrity. Furthermore, prior data suggested interaction of dorsal and ventral epidermis during wound closure might be inductive for regeneration (Kato et al., 2001; Ogawa et al., 2002). However, because a needle-poke of the dorsal epidermis induced a robust mitotic response, we conclude that dorsal/ventral epidermis interaction is not required for a neoblast wound response.

A large incision, from the tail tip to the pharynx, resulted in a significantly higher increase in mitotic numbers at 6h following wounding than did the two smaller wounds (Figure 3.4B). Therefore, the magnitude of the first mitotic peak scales with wound size. Because planarians can readily seal these injuries along the incision plane, this injury also did not require overt blastema formation for repair. Importantly, none of these surgeries (poke or incision without amputation) resulted in a robust, localized second mitotic peak (this observation is explored further below). Together, these observations indicate that the signal that causes the first mitotic peak is wound size-dependent, with a fast and broad-acting mechanism, and is triggered by any injury – even those not requiring blastema formation for repair – that pierces the epidermis.

3.1.3 The signal that causes the first mitotic peak spreads from the wound site

If there exists a signal that emanates from the wound that is responsible for the first mitotic peak, it should be possible to observe intermediate stages of increase in mitoses as a function of distance from the wound. By 3-4.5h following amputation at the tip of the tail, a wave-like increase in mitoses starting from the wound site was in fact observed (Figure 3.4E-F). At the 3 and 4.5h time points, fragments were found to be in various stages of mitotic elevation (Figure 3.4G-H). By 6h, all but one fragment showed similar mitotic increase in the anterior and the posterior (Figure 3.4F). The mitotic increase was found to spread from near the wound site along the periphery of the animal, before spreading towards the fragment middle (Figure 3.4H). These observations indicate the candidate existence of a diffusion/spreading mechanism that triggers the first mitotic peak.

3.1.4 The signal that causes the first mitotic peak acts mainly on the G2/M transition

The simplest explanation for the rapid increase in mitotic numbers during the first mitotic peak would be action of the inducing signal on G2/M progression, resulting in shortening of G2. Because BrdU can only be applied by injection or feeding (Newmark and Sánchez Alvarado, 2000), which both induce an increase in neoblast proliferation, BrdU-labeling and fraction of labeled mitoses (FLM) experiments cannot easily identify the kinetic changes in cell cycle phases that occur following injury. However, prior FLM experiments indicate that the median length of G2, under conditions of stimulation, is 6h (Newmark and Sánchez Alvarado, 2000). Furthermore, experiments with S-phase inhibitors suggested that roughly half of the mitoses induced by wounding could occur if S phase was blocked (Saló and Baguñà, 1984). Though not conclusive,

these observations are consistent with the idea that acceleration of S-phase does not alone explain the first mitotic peak. In general these observations suggest that approximately half of the mitoses observed at the first peak come from cells that were in S-phase at the time of injury and half come from cells that were in G2. We further reasoned that if the signal that causes the rapid mitotic increase simply accelerates G2, no apparent change in numbers of S-phase cells should be visible. By contrast, if the first peak is explained entirely by a change in the rate of S-phase entry or progression, a robust change in the number of S-phase cells during production of the first mitotic peak should occur. Animals were amputated post-pharyngeally and left to respond to the injury for 0, 3, and 6h. Subsequently, tails were macerated and *in situ* hybridizations were performed on resultant separated and fixed cells. We probed for expression of the planarian homologs of the S-phase-specific transcripts *histone H2B* (Hewitson et al., 2006) and *rnr1* (Bjorklund et al., 1990; Eriksson et al., 1984), as well as *smedwi-1* as a control. The *smedwi-1* gene encodes a planarian homolog of PIWI proteins and is expressed in more than 90% of actively cycling neoblasts (Reddien et al., 2005b). Therefore, it should be expressed in most, if not all cell cycle stages. No significant increase or decrease in the number of cells positive for the S-phase markers or *smedwi-1* was observed (Figure 3.4I-K). Whereas it is possible that changes in multiple phases of the neoblast cell cycle occur, these data support the idea that the wound-specific signal that induces the first mitotic peak causes an acceleration of G2 rather than S-phase.

3.1.5 The localized increase in mitoses at the wound site during the second peak is specific to loss of tissue

Mitoses localize to the wound site by two days following amputation. However, as described above, fragments that were only incised showed no robust second mitotic peak. We also examined animals that were amputated postpharyngeally, and, in addition, had a thin epidermal strip cut off the side of the resulting tail fragments (Figure 3.5A). These fragments possessed a wound

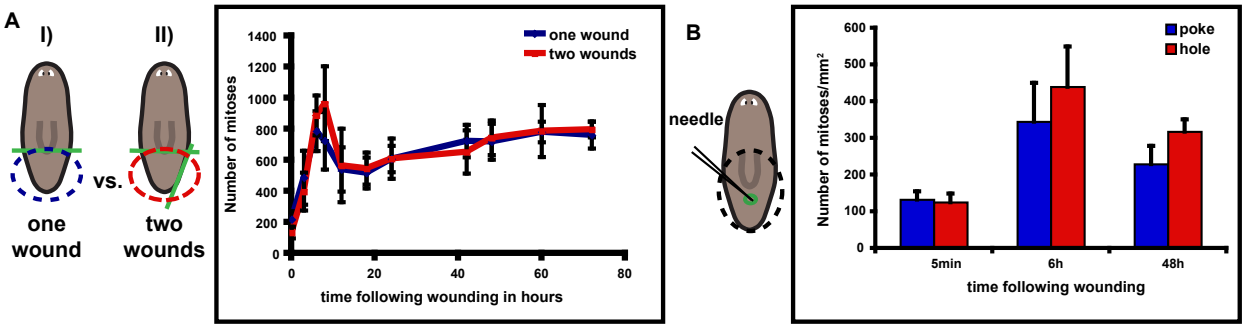

Figure 3.5. Wound size is not the major determinant for the second localized peak.
(A) An increase in wound size does not augment mitotic numbers during the second peak. Schematics depict amputations. Animals were amputated postpharyngeally as in I). A thin, lateral strip of epidermis was cut off as a second wound as in II). Blue and red circles, area analyzed. Animals were fixed at indicated time points and labeled with anti-H3P. Changes in mitotic numbers following wounding is shown. n ≥ 4. (B) Change in mitotic density with time following amputation. n ≥ 5.

surface twice as large as the wounds from simple tail amputation; however, both fragment types were missing approximately the same amount of tissue (the entire midbody and head) and had a similar second mitotic peak (Figure 3.5A). These observations raise the question of what factor(s), if not simply wounding or wound size, trigger the second neoblast-response phase that culminates in the second peak.

We considered the possibility that it is the absence of tissue that is the key determinant in generation of the localized second peak. We compared the wound response of animals injured with a needle poke (diameter 10-20µm) and with a small hole-punch (diameter >50µm); the hole-punch removes tissue, whereas the needle-poke does so only minimally. Significantly, only animals that regenerated from a hole-punch showed a local increase in proliferation at the wound site during the second mitotic peak (Figure 3.6A, B). Areas further away from the wounds had an equal mitotic density for both surgery types (Figure 3.6A, B), and overall mitoses were higher in both surgeries (Figure 3.5B). Because the wounds caused by hole-punch close without

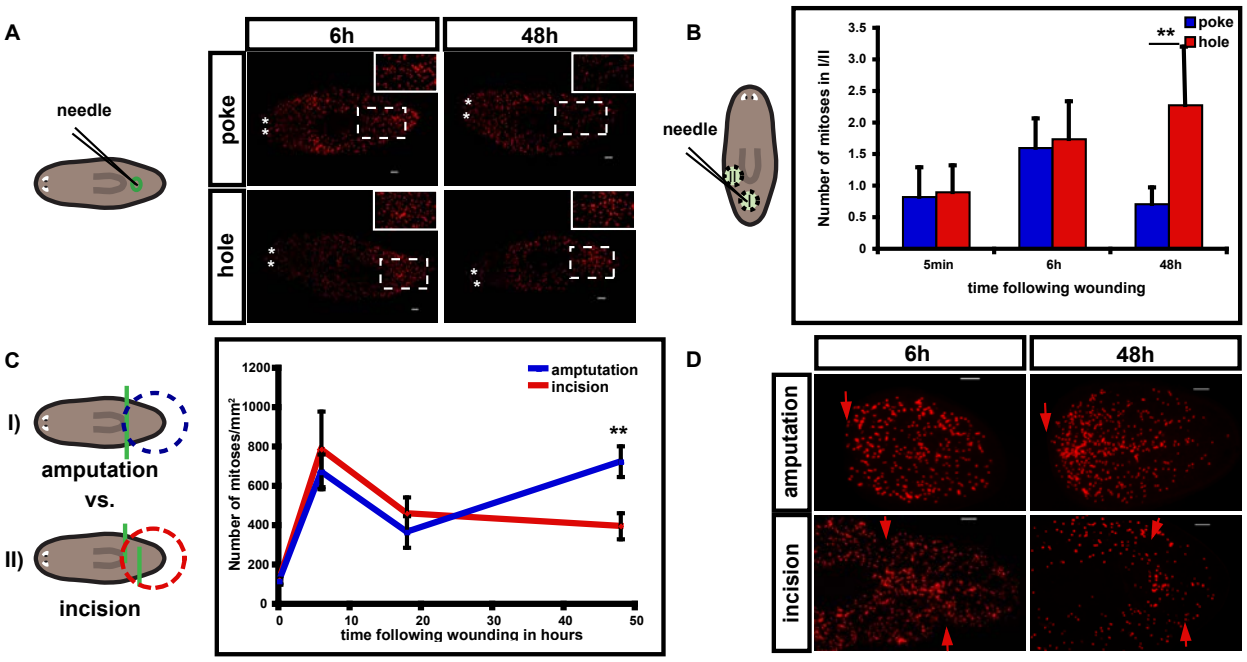

Figure 3.6. The localized, second mitotic peak is specific to loss of tissue.

(A-B) A needle-poke and a hole-punch both induced a strong first peak, but only a hole-punch induced a second, localized peak. Animals were labeled with anti-H3P at indicated timepoints. At left, cartoon schematic depicts the surgical strategy with representative images shown in (A) and quantification shown in (B). Green circles, wound site. A needle was used to inflict piercing of the epidermis (poke, diameter 10-20µm), whereas a broken needle was used to inflict hole-punches (hole, diameter >50µm) that removed a cylindrical region of tissue. Black circles, analyzed areas. (A) Insets, wound-site magnification. (B) At left, cartoon depicts the regions quantified following infliction of poke or hole wounds. Mitotic numbers were determined for two different 267 µm diameter, cylindrical tissue regions (dotted circles): I) centered at the wound site and II) at a region distal from the wound. n ≥ 5. **p<0.01 by Student's t-test.(C-D) Amputations, I), were accomplished by surgical removal of the anterior two-thirds of the body (green line). Incisions, II), were made through the entirety of the body at indicated locations (green lines) and allowed to re-seal. Amputation, I), triggered a localized second mitotic peak, but incisions, II), which caused a larger wound size than in I) but no significant loss of tissue, did not. Blue and red circles, area analyzed. (C) Mitotic density with time following amputation. n ≥ 4. **p<0.01 by Student's t-test. (D) Representative images of animals analyzed in (C). Red arrows, wound site. Bars, 100µm. Data represent averages ± sd.

dorsal-ventral epidermis juxtaposition, the second, localized mitotic peak does not require DV confrontation. These data are consistent with the idea that it is the absence of tissue that triggers the second, localized mitotic peak.

To exclude the possibility that the difference in wound size between the needle-poke and the hole-punch caused the differences in localization of mitoses, we designed a surgery strategy to result in two fragment types; the first I) involved tissue removal and the second II) involved a wound of larger size than I) but with essentially no missing tissue (Figure 3.6C). For both surgeries, mitoses were strongly increased in the analyzed fragments during the first peak. However, only the surgery that resulted in tissue loss (type I, missing the midbody and head) produced a robust second mitotic peak (Figure 3.6C). Importantly, no localization of mitoses was visible at the wound site in fragments that were only incised (type II) (Figure 3.6D). Because mitotic numbers are still elevated at 18h and 48h in these animals as compared to intact animals, possibly due to continued proliferative effects from the first peak, the most prominent difference observed was a local increase in mitoses at the wound site. These observations, together with the data described

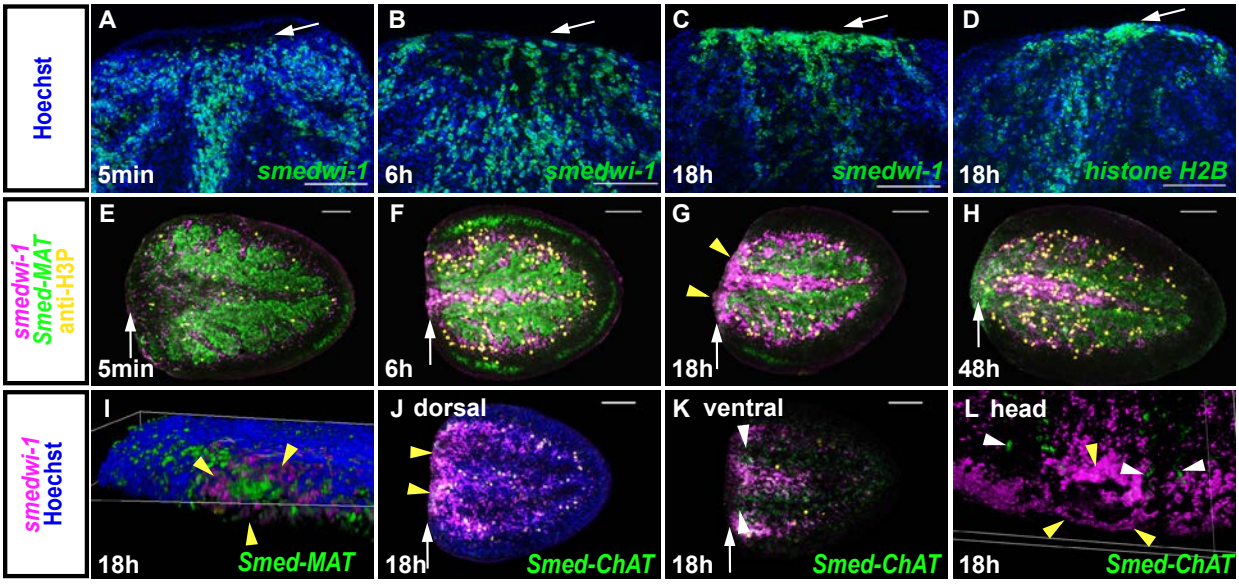

Figure 3.7. Cycling cells are recruited to the wound site and proliferate predominantly near intestinal branches.
(A-D) Cycling cells accumulate at the wound site at 18h following wounding. Wound sites in tail fragments are shown. (A-C) *smedwi-1*$^{+}$ and D) *histone H2B*$^{+}$ cells accumulate at the wound site at 18h (green). Nuclei were labeled with Hoechst (blue). Anterior, to the top. (E-L) Cycling cells accumulate at the tip of gut branches at 18h (yellow arrows), but not at the nerve cords. Tail fragments were labeled with *smedwi-1* (magenta) and anti-H3P (yellow), together with *Smed-MAT* (EG413862, Methionine adenosyltransferase, expressed in the planarian intestine) or *Smed-ChAT* (Choline acetyltransferase, expressed in planarian nerve cords) (green) at indicated timepoints. Anterior, left, except in I) and L). (I) 3D projection showing a gut branch opening (green) surrounded by *smedwi-1*$^{+}$ cells (magenta); anterior-dorsal view. (J) Optical section from dorsal domain of a posterior (tail) fragment. Gut branch outlines can be seen by Hoechst labeling; in this dorsal domain, no *ChAT* expression is found. (K) Optical section from ventral domain of the same tail fragment as J). No accumulation of *smedwi-1*$^{+}$ cells in areas of *ChAT* expression. (L) 3D projection from an anterior (head) fragment showing that the majority of *smedwi-1*$^{+}$ cells accumulates around the single gut branch, but not the nerve cords - *ChAT* $^{+}$ cells (in green, white arrow heads), posterior-ventral view. Images represent superimposed optical sections, except in (J-K). Dorsal view, unless otherwise stated. White arrows, wound site. Yellow arrowheads, *smedwi-1*$^{+}$ cells surrounding gut branches. Bars, 100µm.

above, suggests that it is tissue loss, rather than simple injury itself, that induces the localized, second mitotic peak.

3.1.6 Neoblasts accumulate at the wound site during the mitotic minimum

What changes occur within the neoblast population in the transition from the initial wound response to the second mitotic peak? We determined that, during this phase of decline in mitotic numbers (by 18h), the neoblasts accumulate at injury sites. We performed fluorescent in situ hybridizations with regenerating fragments 5min, 6h, and 18h after amputation using a riboprobe for the neoblast marker, *smedwi-1*. *smedwi-1*$^{+}$ cells accumulated near the wound site by 18h (Figure 3.7A-C). A similar observation was made for cells expressing *histone H2B,* expressed in S-phase (Hewitson et al., 2006) (Figure 3.7D). Of note, at 18h following amputation, the majority of *smedwi-1*$^{+}$ cells accumulated dorsally at the wound site; neoblast proliferation was previously suggested to occur along the planarian nerve cords (Brøndsted, 1969), which are located ventrally. However, most *smedwi-1*$^{+}$ cells at the wound site were found in close vicinity to the remnant intestine branches (Figure 3.7E-H, J), rather than the ventral nerve cords (Figure 3.7I-L). In general, the observed neoblast accumulation at wounds raises the possibility that

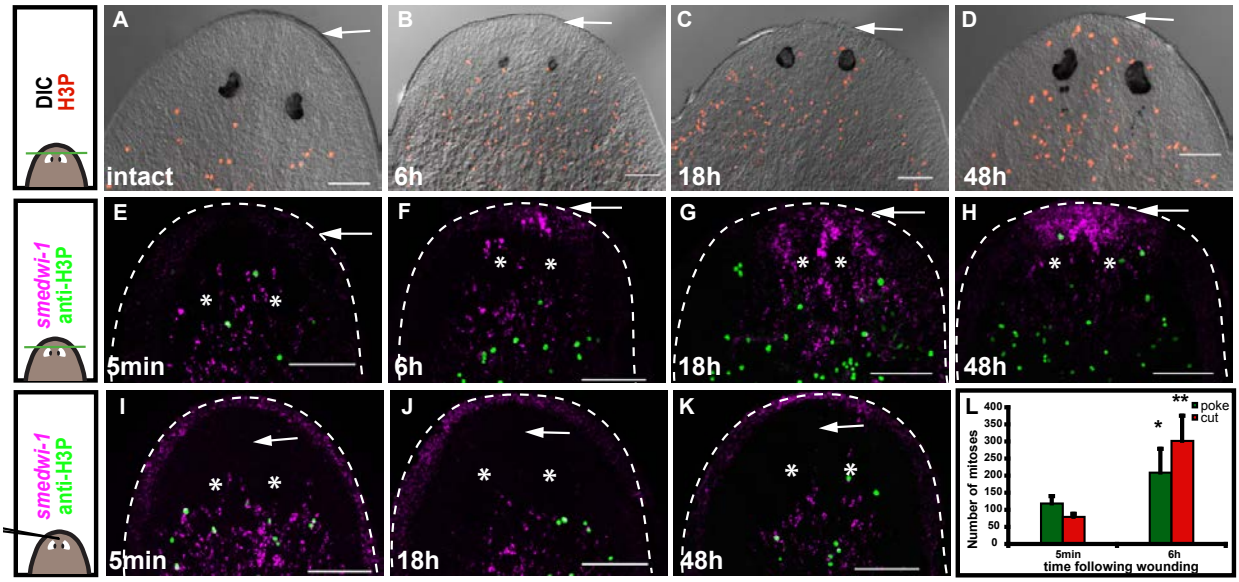

Figure 3.8. Loss of tissue induces neoblast recruitment to wounds.
(A-K) Cartoons at left depict surgery types. Top and middle, amputation of the head tip (green line); bottom, black line indicates site of needle poke. White arrows on images indicate the sites of amputation or needle poke in head tips. White asterisks indicate photoreceptors. Anterior, up. Bars, 100μm. (A-D) Mitotic cells appear in front of the photoreceptors at (C) 18h and (D) 48h after amputation. Differential interference contrast (DIC) image superimposed with image of mitotic cells (anti-H3P, red). (E-K) *smedwi-1*$^{+}$ cells (magenta – fluorescence at animal periphery is non-specific) and mitoses (green) accumulate in head tips (a region normally devoid of neoblasts) at 18h and 48h, respectively, when the head tip was amputated (E-H), but not following a needle-poke (I-K). (L) A head tip needle-poke induces a first mitotic peak. Data represent averages ($n \geq 3$) ± sd. Mitoses were quantified from z-stacks through the entirety of the DV axis from tip of the head to the posterior base of the pharynx. Data were significantly higher at 6h than at 5min; **$p<0.01$ and *$p<0.05$ by Student's t-test.

regeneration initiation may involve signaling from injuries that trigger neoblast migration.

3.1.7 Loss of tissue induces neoblast migration to wound sites

To test the hypothesis that neoblasts are recruited to wounds we amputated animals anterior to the photoreceptors, a region devoid of neoblasts (Newmark and Sánchez Alvarado, 2000). Following amputation, *smedwi-1*$^+$ and H3P$^+$ cells were visible in front of the photoreceptors at 18h and 48h following wounding, respectively (Figure 3.8A-H). Accumulation of *smedwi-1*$^+$ cells was observed at 12h and rare cells seen as early as 6h (Figure 3.8F). We conclude that active recruitment of neoblasts to the site of wounding can occur before or during the minimum in mitoses (by 18h).

This experiment involved amputation in a region where neoblasts do not reside, leaving open the possibility that neoblast recruitment only occurs in cases when no neoblasts are initially present at the wound site. However, as described above, the number of cycling cells increases by 18h at transverse amputation sites (e.g., in tail fragments)—that possess many neoblasts (Figs. Figure 3.7C, D). Mitoses are evenly distributed in the body before 18h following such transverse amputations (Figure 3.1D, I, N); we therefore conclude that the accumulation of neoblasts cannot be explained by local proliferation. In addition, irradiation experiments indicate that neoblasts cannot be produced by differentiated tissues (Wolff and Dubois, 1948), excluding the alternative explanation that de-differentiation occurs at the wound site and explains the greater number of neoblasts observed. Significantly, a poke into the head tip with an injection needle did not cause detectable recruitment of *smedwi-1*$^+$ cells or H3P$^+$ cells (Figure 3.8I-K), despite inducing a first mitotic peak at 6h (Figure 3.8L). Therefore, we conclude that the increase of neoblasts at wounds is the result of neoblast migration and is induced by tissue absence rather than by injury *per se*.

3.1.8 The second mitotic peak is accompanied by neoblast differentiation

In order for tissue replacement to occur, neoblasts must produce differentiated cells. Does this occur in response to injuries during a phase of regeneration initiation, or after initial blastema formation? To distinguish cycling neoblasts from those that have exited the cell cycle and will differentiate, we double-labeled animals with a riboprobe to detect *smedwi-1* mRNA and an antibody to recognize SMEDWI-1 protein (Guo et al., 2006). Cycling cells are *smedwi-1*$^+$/SMEDWI-1$^+$, whereas cells that cease expression of *smedwi-1* and exit the cell cycle will transiently be *smedwi-1*$^-$/SMEDWI-1$^+$ due to protein perdurance (Figure 3.9A). Support for this assertion can be observed by the spatial relationship between these two cell types in intact animals; *smedwi-1*$^-$/SMEDWI-1$^+$ cells are present anterior to the photoreceptors, a region devoid of cycling neoblasts (Guo et al., 2006; Newmark and Sánchez Alvarado, 2000). Furthermore, SMEDWI-1$^+$ cells are eliminated shortly after irradiation (Guo et al., 2006) and can be labeled by a BrdU-pulse chase;

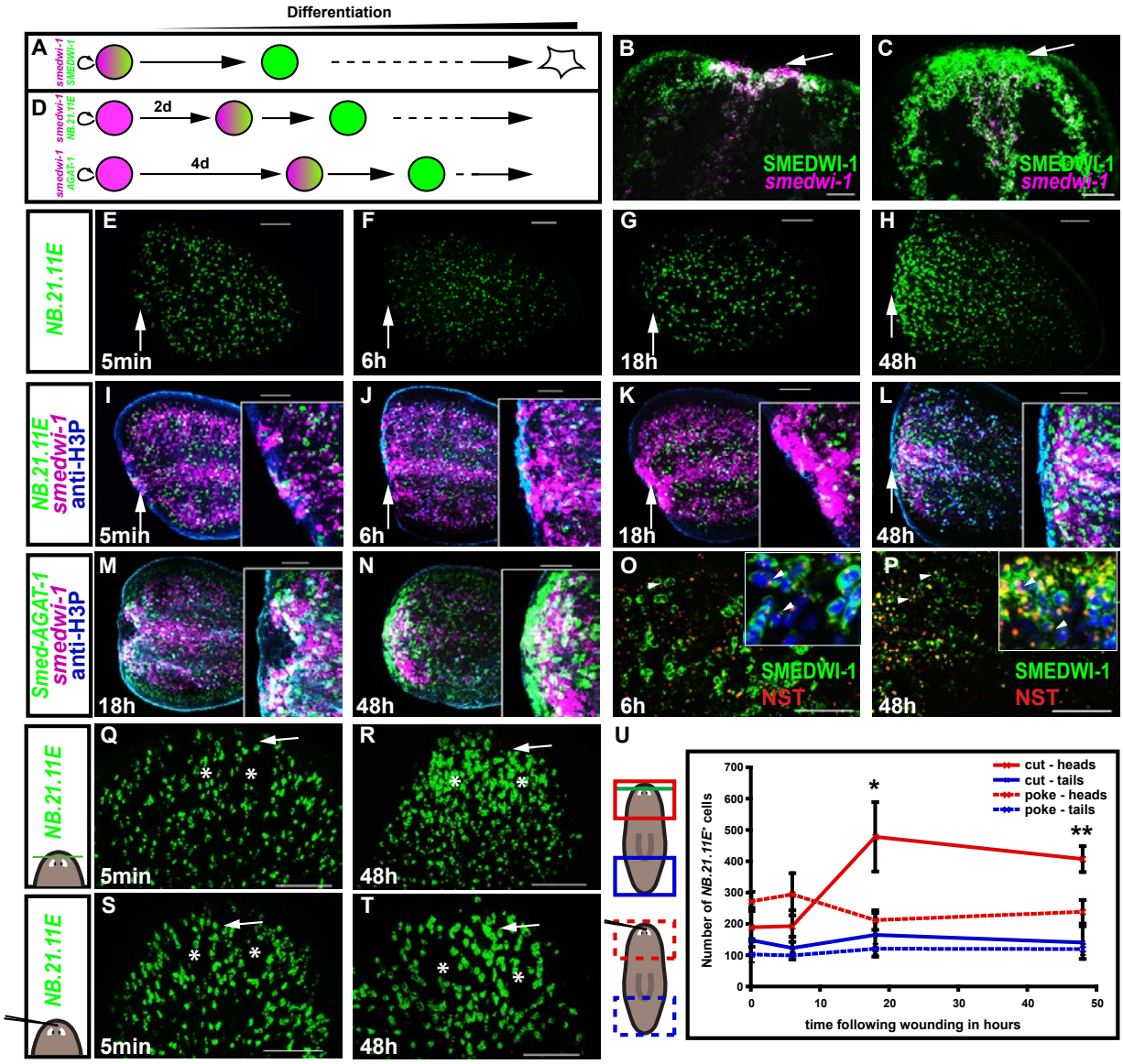

Figure 3.9. The second mitotic peak is accompanied by differentiation and cell growth at the wound site.
(A) Lineage relationship schematic. smedwi-1$^+$(mRNA, magenta)/SMEDWI-1$^+$(protein, green) neoblasts will become SMEDWI-1$^+$ cells as they differentiate. (B-C) Tail fragments probed with anti-SMEDWI-1 antibody (green) and smedwi-1 RNA probe (magenta). White arrow, wound site. Anterior, up. (B) smedwi-1$^+$/SMEDWI-1$^+$ cells accumulate at the wound site of tail fragments at 18h. White arrow, wound site. Anterior, left. (C) A layer of smedwi-1$^-$/SMEDWI-1$^+$ cells formed in front of actively proliferating smedwi-1$^+$/SMEDWI-1$^+$ cells at 48h, indicating increased differentiation. (D) smedwi-1$^+$ neoblasts (magenta) will turn on the NB.21.11E and Smed-AGAT-1 genes (green) as they differentiate. (E-L) Timecourse, following amputation, of tail fragments (E-H) labeled with an NB.21.11E RNA probe (green); (I-L) merge of (E-H) labeling with anti-H3P antibody for mitoses (blue epidermal fluorescence is non-specific), and with a smedwi-1 RNA probe (magenta). Insets, magnified view of wound site. White arrow, wound site. Anterior, left. (M-N) Time course, following amputation, of tail fragments. Smed-AGAT-1$^+$ (EC616230) cells (green) accumulate at the wound site in front of smedwi-1$^+$ cells (magenta) at 48h (mitoses in blue, anti-H3P), indicating increased differentiation. Anterior, left. (O-P) Neoblast descendants at the wound site show an increase in nucleolar size at 48h. Tail fragments labeled with anti-SMEDWI-1 (green) and anti-NST (red) antibodies. NST signal was also found in SMEDWI-1$^+$ cells, white arrowheads. (O) At 6h, NST was localized to a small nuclear region, inset (Hoechst, blue). (P) At 48h, NST signal occupies up to 1/3 of the nucleus.

indicating that the entire SMEDWI-1$^+$ cell population is comprised of neoblasts and their non-dividing descendants. By 18h after amputation, there existed a high density of *smedwi-1*$^+$/SMEDWI-1$^+$ cells at the wound site, many of which expressed *smedwi-1* mRNA strongly (Figure

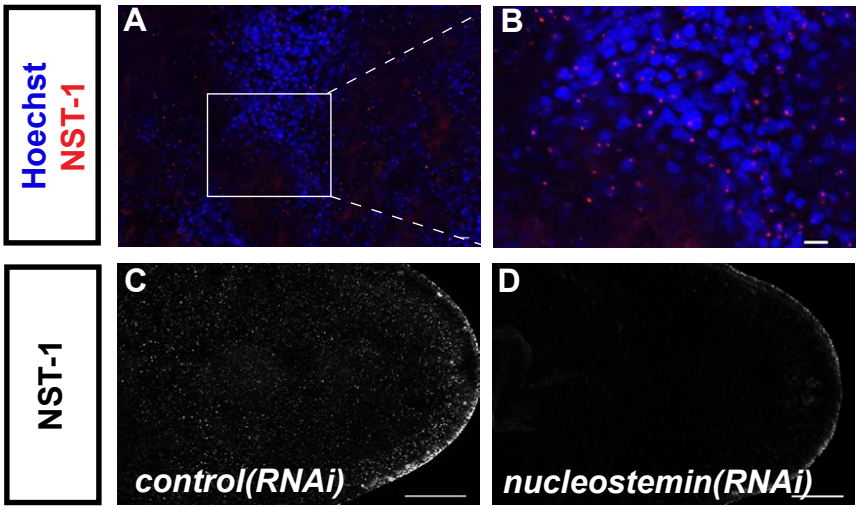

Fig. 3.10. NST-1 protein is localized in the nucleolus and the signal is depleted following 11 days of RNAi. (A-B) NST-1-signal (red) is restricted to a small area in the nucleus, likely the nucleolus. Image in (B) represents magnified view of white rectangular area in (A). Nuclei labeled with Hoechst (blue). (C-D) NST-1 signal was depleted in animals after 11 days of *Smed-nucleostemin(RNAi)*, but not in the control (*unc-22(RNAi)* animals). This demonstrates the specificity of the NST-1 antibody. Images represent superimposed optical sections, in dorsal view. Scale bars, 100µm.

3.9B). By 48h after amputation, however, a layer of mostly *smedwi-1*$^-$/SMEDWI-1$^+$ cells was found in front of the zone of actively cycling cells (*smedwi-1*$^+$/SMEDWI-1$^+$) (Figure 3.9C). These data indicate that before and during the second mitotic peak a proportion of neoblast descendant cells exit the cell cycle and give rise to a layer of non-cycling cells at the wound site. This indicates that signals from wounds trigger increased differentiation at the wound site very early in regeneration—before and during the second mitotic peak.

Three different categories of genes that are expressed in cells that disappear following irradiation were recently identified. These genes are expressed in neoblasts (e.g., *smedwi-1*) and the non-dividing descendant cells of neoblasts (e.g., *NB.21.11E* and *Smed-AGAT-1*) (Eisenhoffer et al., 2008), allowing assessment of neoblast differentiation (Figure 3.9D). It was previously shown that neoblast descendants accumulate at the wound site at 4d following amputation (Eisenhoffer et al., 2008). A thin strip of unpigmented tissue is already visible at the amputation site by 48h, however. To assess differentiation and blastema formation, we assessed the distribution of *NB.21.11E*$^+$ and *Smed-AGAT-1*$^+$ cells in tail fragments (Figure 3.9D, E-N). By 48h after amputation, *NB.21.11E*$^+$ or *Smed-AGAT-1*$^+$ cells were found in front of (proximal to the wound epidermis) the *smedwi-1*$^+$ and H3P$^+$ cells (Figure 3.9L, N). By contrast, *NB.21.11E*$^+$ and *Smed-AGAT-1*$^+$ cells were behind *smedwi-1*$^+$ and H3P$^+$ cells (distal, with respect to the wound epidermis) at 6 and 18h after amputation (Figure 3.9J-K, M). These observations indicate that, first, stem cells are recruited to wounds and second, increased neoblast differentiation occurs at the wound site during the time of the second mitotic peak to initiate blastema formation.

Cells with a high demand for ribosomal biosynthesis, such as highly proliferating or growing cells, typically show an increase in nucleolar size (Frank and Roth, 1998). We raised an antibody against

SMED-NUCLEOSTEMIN (NST), the planarian homolog of mammalian nucleostemin, a nucleolar GTPase that is expressed in proliferating cells/stem cells (Kudron and Reinke, 2008; Tsai and McKay, 2002; Tsai and McKay, 2005). Therefore, NST should serve as a marker of the planarian nucleolus, and was in fact localized to a compartment of the nucleus (Figure 3.10A-B). Within 11 days following *nucleostemin* RNAi, the protein was mostly depleted (Figure 3.10C-D), indicating antibody specificity. Following wounding, SMEDWI-1$^+$ cells at the wound site exhibited a strongly broadened NST signal at 48h compared to 6h-wounded animals (Figure 3.9O-P). This suggests nucleolus broadening and probable increase in ribosome biosynthesis. Most of these SMEDWI-1$^+$ cells have likely exited the cell cycle, as shown by their lack of *smedwi-1* mRNA expression (Figure 3.9C). It is therefore probable that these non-dividing neoblast progeny cells are growing and differentiating (Johnson et al., 1974). The increase in progeny cells and in cells with a broadened NST signal indicates commitment to differentiate at wounds is an early response in regeneration initiation.

We described above that local proliferation at the second peak and neoblast recruitment to wounds are outcomes specific to injuries that remove tissue. To test whether increased formation of non-dividing neoblast descendants is also specific to tissue loss, we utilized different injuries in animal head tips. In fragments where the tip of the head had been amputated, *NB.21.11E*$^+$ cells increased in number at the wound site, but not far away from the wound, at 18h and 48h (Figure 3.9Q-R, U). By contrast, we did not observe accumulation of *NB.21.11E*$^+$ cells at 18h or 48h in animals that were poked in the tip of the head with a needle (Figure 3.9S-U). This observation suggests that it is loss of tissue, rather than simply wounding, that triggers neoblast differentiation at wound sites. Together, our experiments indicate that – in addition to wound detection – tissue absence is detected early in regeneration and that signals from wounds that result in loss of tissue lead to neoblast recruitment, local neoblast division, and neoblast descendant formation at the wound site – coordinately leading to blastema formation. These data are significant in that they indicate a key event in regeneration is the detection of tissue absence and the associated signaling from wounds.

3.1.9 The neoblast wound-response assay as a paradigm to study stem cell-mediated regeneration

Generating responses to wounding is a fundamental biological process. However, study of wound responses in regeneration can be challenging because of a myriad of responses that happen in mammals or because of difficulties in gene function studies in adult organisms. We described here key steps in the response of planarian stem cells to wounds, revealing the cellular underpinnings of planarian regeneration initiation and presenting assays for genetic dissection of wound signaling. RNAi in adult planarians is robust (Newmark et al., 2003), can be performed for many

genes (Reddien et al., 2005a). We established that a decrease in homeostatic neoblast numbers, following RNAi of genes that impact neoblast maintenance, is directly correlated to a decrease in the wound response (Figure 3.11A) and that RNAi of S-phase entry or stress-response related genes caused a stronger effect on the second mitotic peak than the first peak (Figure 3.11B). Importantly, we also found that numbers of mitoses in RNAi animals prior to amputation are not necessarily indicative of the homeostatic neoblast numbers (Figure 3.11C). We suggest, therefore, that assessment of homeostatic neoblast numbers will be an essential control in experiments that examine potential regulators of neoblast proliferation following wounding and that RNAi can be used to dissect features of the wound response (Figure 3.11).

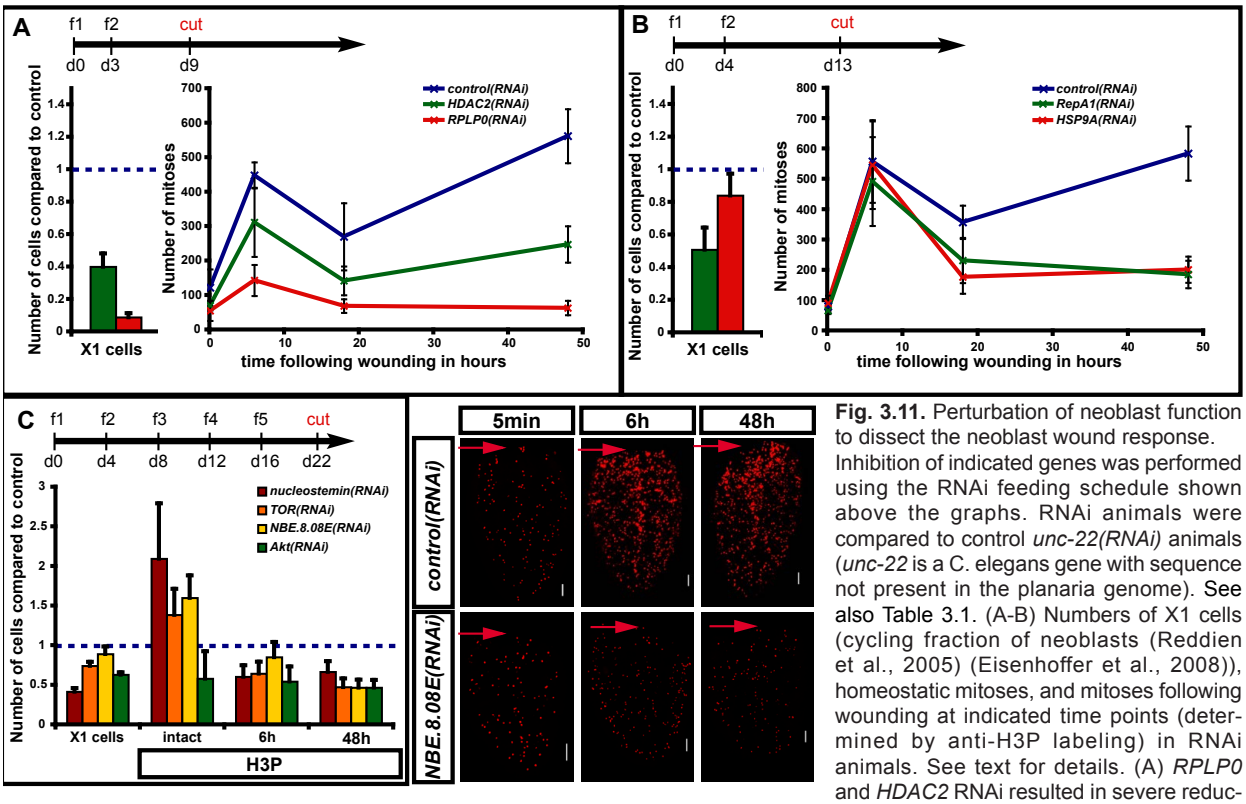

Fig. 3.11. Perturbation of neoblast function to dissect the neoblast wound response. Inhibition of indicated genes was performed using the RNAi feeding schedule shown above the graphs. RNAi animals were compared to control *unc-22(RNAi)* animals (*unc-22* is a C. elegans gene with sequence not present in the planaria genome). See also Table 3.1. (A-B) Numbers of X1 cells (cycling fraction of neoblasts (Reddien et al., 2005) (Eisenhoffer et al., 2008)), homeostatic mitoses, and mitoses following wounding at indicated time points (determined by anti-H3P labeling) in RNAi animals. See text for details. (A) *RPLP0* and *HDAC2* RNAi resulted in severe reduction of all features. (B) *RepA1* and *HSP9A* RNAi resulted in defects in the second, but not first, mitotic peak. (C) *Akt3*, *TOR*, *nucleostemin*, and *NBE.8.08E* RNAi resulted in a slow loss of neoblasts and a decrease of the two mitotic peaks. *TOR*, *nucleostemin*, and *NBE.8.08E* RNAi caused an increase in homeostatic mitoses. *NBE.8.08E* RNAi results in a complete failure of neoblasts to respond to wounding after five weeks of RNAi.

Table 3.1. List of genes inhibitied by RNAi for the wound response assay (Figure 3.11)

Homology	Abbreviation	Functional category	blastema formation*	Gene ID
ribosomal protein LP0	RPLP0	housekeeping	0	NB.6.2f
histone deacetylase2	HDAC2	chromatin remodeling	0-2	H.9.4h
heat shock protein 9A	HSP9A	stress, cell cycle	0-0.5	H.6.5d
replication protein A1	RepA1	DNA replication, stress	0.5-1.5	NB.52.11e
Akt	Akt	cell proliferation, differentiation, apoptosis, metabolism	1-2	DN300225
mTOR	mTOR	nutrient and stress signaling, cell proliferation	0.5-2	de_novo.24889.1
nucleostemin	nucleostemin	ribosomal biogenesis, (stem) cell proliferation	1-2.5	NB.6.8f
unknown	NBE.8.08E	unknown	0.5-2	NB.35.4a

* blastema formation scoring (schedule as in Figure 3.11, n ≥ 6): 0-3, with 0 = no blastema, 3 = control.

3.2 A gene regulatory network that governs regeneration initiation in planarians

3.2.1 A microarray designed to identify a wound response program associated with regeneration initiation in planarians

In order to identify candidate genes that are involved in planarian regeneration initiation, we performed a microarray experiment using RNA extracted from a time course of amputated animals (Figure 3.12). RNA from freshly cut (5min) animals was used as a reference sample and compared to RNA from amputated animals extracted at 30min, 1h, 3h, 6h, and 12h. These time points correspond to important events in the neoblast wound response (Figures 3.1, 3.7). Gene expression changes in differentiated, non-dividing cells are likely to include mitogens and patterning factors that direct neoblast proliferation, migration, and differentiation. We therefore repeated the same microarray experiment with RNA extracted from lethally irradiated, amputated animals. Irradiation eliminates dividing cells and given that neoblasts are the only dividing somatic cells in the animal (Newmark and Sánchez Alvarado, 2000; Reddien and Sánchez Alvarado, 2004), detected expression changes in irradiated animals following wounding can be assigned to the differentiated tissue. To filter out gene expression changes that could simply be caused by irradiation, the overlap of genes that change in both wild type and irradiated animals was chosen as candidate genes to be upregulated in differentiated tissues for further analysis (Figure 3.12).

Because it is likely that important factors governing regeneration initiation will be upregulated following wounding, we focused our analysis on genes that were upregulated, rather than downregulated, in wounded animals as compared to control animals. 463 oligos were associated with significant upregulation following amputation (see Appendix for the full list of oligos, and

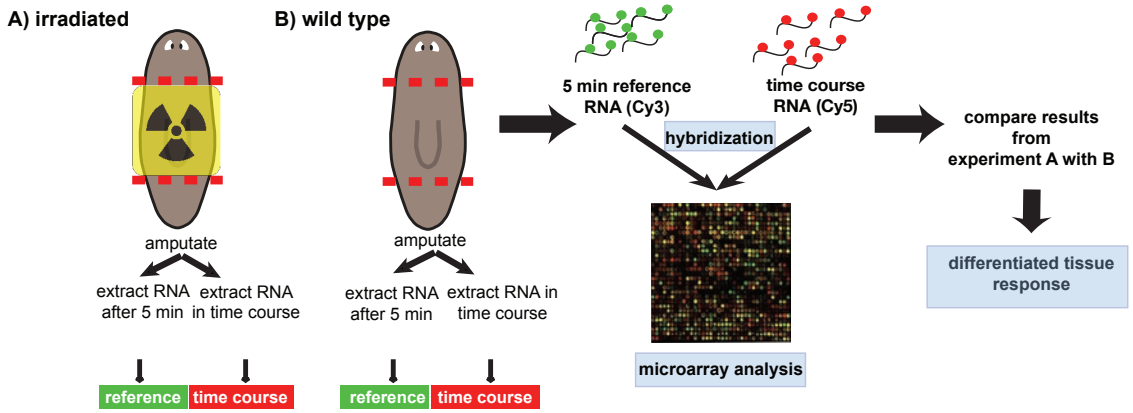

Figure 3.12. A microarray designed to identify wound-induced gene expression.
Cartoon illustrating the microarray design and analysis strategy. To determine wound-induced expression in the differentiated tissue, RNA was isolated from freshly amputated (reference) and amputated fragments at different time points (time course). The same experiment was carried out twice, using (A) lethally irradiated animals (irradiation eliminates neoblasts and their progeny) and (B) wild type animals. The overlap of genes upregulated in data obtained from experiment A and B was used to identify genes that were upregulated in the differentiated tissue, as opposed to neoblasts and their progeny.

the genes they are from).

To validate the differential expression of genes that was determined by microarray analysis and to examine the temporal and spatial properties of wound-induced gene expression, we performed in situ hybridizations on intact and amputated animals. 100 candidate genes were selected based on fold change of differential expression and homology to genes from other organisms ((such as transcription factors, cell signaling and patterning factors, and mitogens) as determined by BLAST. Over 60% of the tested genes showed a clear wound-induced expression pattern in *in situ* hybridization (see Appendix for a complete list). The remainder showed either no expression pattern at all or no clear wound induction. We conclude that the microarray design was well suited to identify genes that are induced in the differentiated tissue following amputation. Two major clusters of genes were apparent: A first set of genes that were strongly expressed within the first 30 minutes to hour following wounding and a second wave of genes that were expressed later, between 3-12h. These findings indicate at least two major temporal signaling events that initiate gene expression following wounding. We will investigate those events in detail below.

3.2.2 Immediate early genes are expressed at wound sites within 30min following injury in a translation-independent manner

The first wave of gene expression occurred within 30min (Figure 3.13A) and was strongly localized to the wound site as determined by *in situ* hybridization. The expression domain expanded toward the middle of the fragment over time and ceased within 6-12h. Expression of these genes was localized subepidermally (Figure 3.13B). In contrast to wound-induced expression, expression of this set of genes in intact animals was weak or absent for many of those genes (Figure 3.13B). Interestingly, many of these genes encode transcription factors (e.g. *egr1, egr1b*, *c-fos*, *jun*, *atf6*) (Chavrier et al., 1988; Iyer et al., 1999; Lamph et al., 1988; Muller et al., 1984; Wang et al., 2000) and signaling proteins (e.g. *PI3K*, *small GTPases*, *protein phosphatase 1*, *traf*, *antigen p97*, and *pim-1/3*) (Beharry et al., 2011; Cen et al., 2010; Cohen, 2002; Inoue et al., 2000; Ives, 1991; Kazlauskas et al., 1992; Woodbury et al., 1980), some of which represent homologs to well established “immediate early” genes from other organisms described in a number of distinct biological contexts. Immediate early genes are genes for which expression is induced rapidly following a defined perturbation or stimulus without requirement of protein translation. Such perturbations/stimuli may include viral infection (Lewis, 1980), learning (Abraham, 1991), response to serum stimulation in tissue culture (Chavrier et al., 1988; Iyer et al., 1999), stress (Schreiber et al., 1991; Wollnik et al., 1993), and wounding (Cooper et al., 2005; Stramer et al., 2008).

Expression of immediate early genes is by definition insensitive to inhibition of protein translation. We therefore amputated planarians in the presence of the translation inhibitor

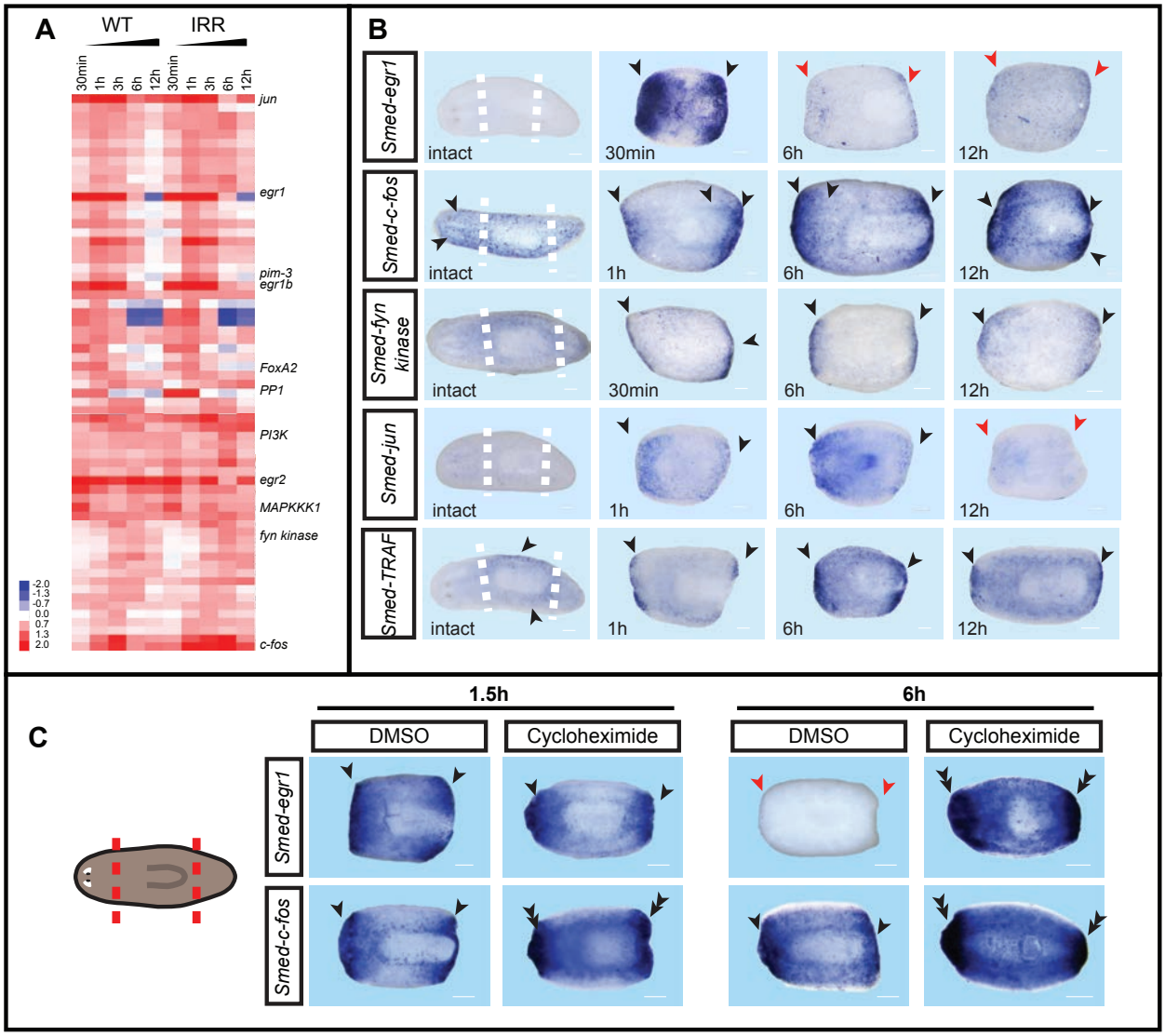

Figure 3.13. Upregulation of early wound-induced gene expression occurs within 30min, is mainly localized to the wound site, and is insensitive to inhibition of protein translation.

(A) Heatmap of genes that are upregulated early ($p<0.05$) in wild type and irradiated animals following wounding. The genes in this cluster mainly encode transcription factors and signaling components and will be referred to as immediate early genes. (B) *In situ* hybridizations on intact and amputated animals probing for genes that were upregulated following wounding. Expression is strongest at the wound site and ceases within 6-12h for some of the genes tested. Probes and time points as indicated. White dotted lines indicate amputation sites. Black arrows, upregulated expression; red arrows, downregulated expression. (C) Induction of immediate early gene expression is insensitive to inhibition of protein translation, whereas their downregulation requires protein translation. Planarians were amputated (as shown in the cartoon to the left) in cycloheximide (0.1µg/µl) or DMSO (1:1000; control) and fixed at indicated time points. *in situ* hybridizations were performed, probing for *egr1* and *c-fos*, representatives of the immediate early gene cluster. Red dotted lines indicate amputation sites. Black arrowheads, upregulated expression; black double arrowheads, overexpression; red arrowheads, downregulated expression. Amputated trunk fragments are shown, anterior to the left. Scale bars, 100µm.

cycloheximide (Schneider-Poetsch et al., 2010), to test whether translation was required for wound-induced expression of genes in the first wave. Amputated animals treated with cycloheximide showed normal expression of putative immediate early genes, such as *egr1* and *c-fos* at 1.5h as compared to control, DMSO-treated animals and therefore their wound-induced

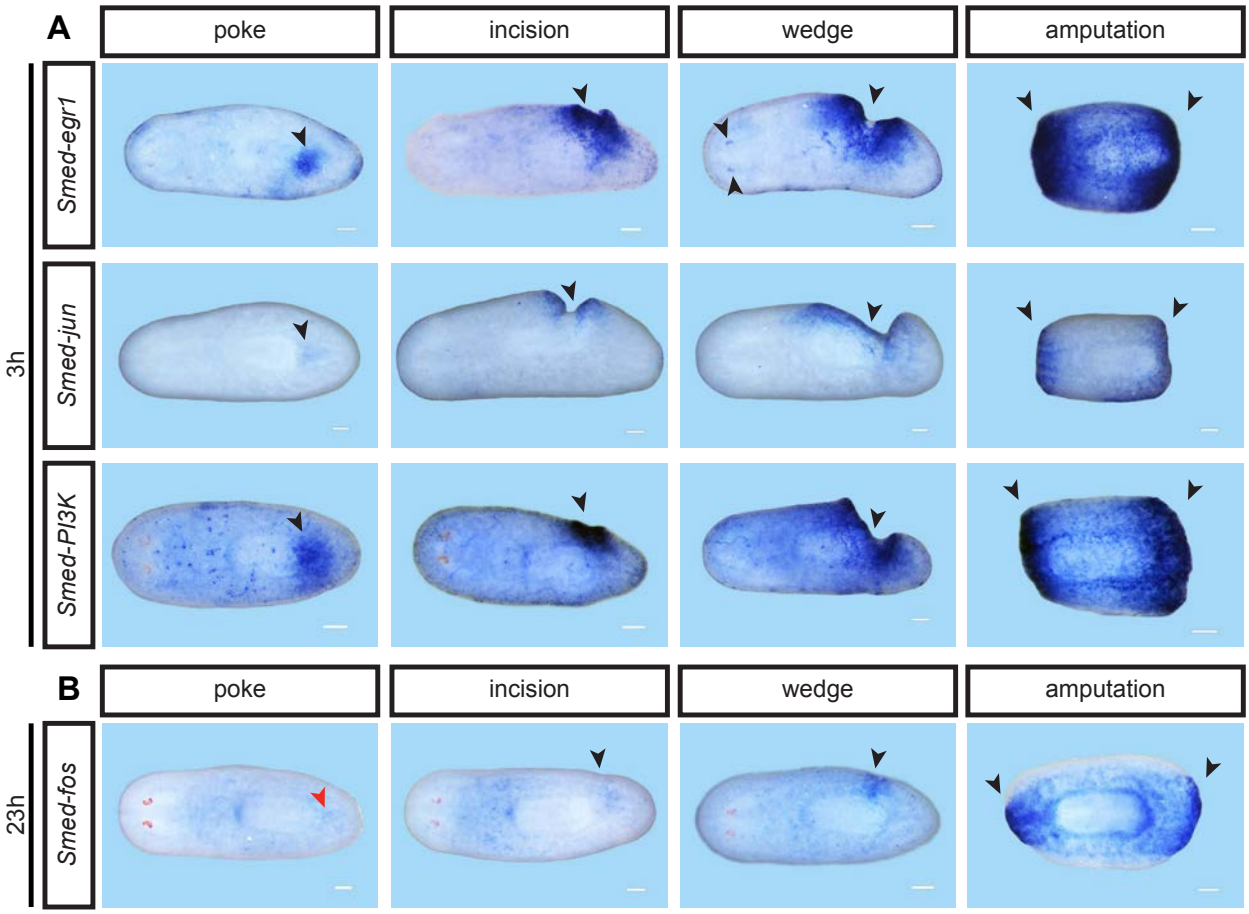

Figure 3.14. Immediate early gene expression following wounding is induced by all kinds of wounds, but maintenance of expression at the wound site at late time points can depend on missing tissue.
(A-B) Animals were either wounded by poking in the tail (using a glass injection needle, poke), incised behind the pharynx (incision), surgically removing a triangle of tissue behind the pharynx (wedge), or amputated pre- and postpharyngeally (amputation) and fixed at indicated time points. *in situ* hybridizations were performed probing for expression of immediate early genes as indicated. (A) Induction of immediate early genes at 3h following wounding occurs at all wounds, albeit to a lesser degree in minor wounds, such as a poke. (B) Expression of *c-fos* is only maintained at major wounds that are associated with missing tissue. Black arrows, wound-induced expression. Red arrowheads, absence of expression. Anterior to the left. Scale bars, 100µm.

expression can be considered insensitive to translation inhibition (Figure 3.13C). However, at 6h following amputation, these genes were strongly upregulated, as compared to control animals in which expression of egr1 was no longer detectable at 6h (Figure 3.13C). This finding suggests that either protein translation is required for degradation of the respective mRNAs or that translation of some gene is required to efficiently downregulate expression of these genes (Lau and Nathans, 1987).

To test whether induction of expression of these genes is specific to the stimulus of removal of tissue, we performed a series of surgeries resulting in different degrees of wounding and tissue loss. The immediate early genes tested were induced at every kind of wound tested at 3h, albeit to a lesser degree in the case of minor wounds. This indicates that expression of immediate early genes is part of the normal wound response and not specific to regeneration per se

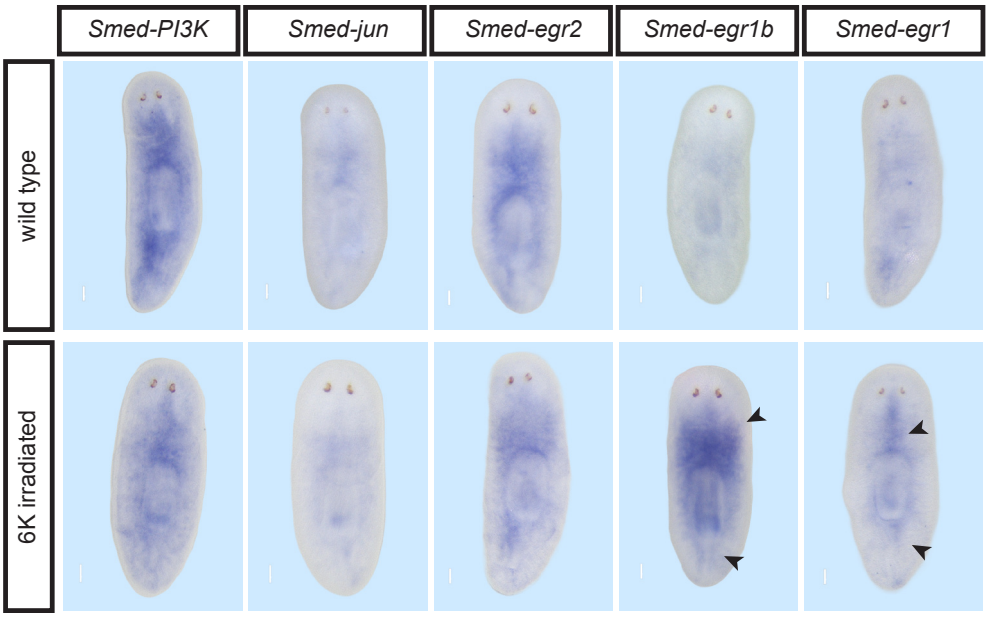

Figure 3.15. Immediate early gene expression can be upregulated in other stress situations, such as following irradiation.
Wild type animals and animals 24h post lethal irradiation (6K) were fixed and *in situ* hybridization probing for expression of immediate early genes was performed, probes as indicated. Two of the 5 genes tested, *egr1b* and *egr1* are visibly upregulated following irradiation (black arrowheads). Anterior to the top. Scale bars, 100µm.

(Figure 3.14A). Despite the finding that immediate early genes are expressed at all wound types at early time points, we found differences at later time points. For example, *c-fos* expression was strongly sustained at the wound site at 23h for surgeries that resulted in missing tissue, but not for surgeries that do not (Figure 3.14B). Continued, long-term *c-fos* expression is therefore connected to formation of new tissue.

In addition to wounding, expression of immediate early genes can be induced by many stress situations, such as exposure to irradiation and during apoptosis (Dragunow et al., 1994; Wan and Ishihara, 2004; Weichselbaum et al., 1994). In planarians, 24h following irradiation, a large number of apoptotic cells can be detected in a pattern that is reminiscent of neoblast localization (Pellettieri et al., 2010). To test for expression of immediate early genes following irradiation, we irradiated animals lethally, fixed 24h later and probed for expression of immediate early genes. A subtle increase in expression was detectable for *egr1* and *egr1b* expression, but not for any other genes tested (Figure 3.15). This indicates that some immediate early genes that are expressed following wounding can also be involved in other stress responses.

To test whether immediate early genes have an essential role in regeneration initiation, we performed RNAi by feeding. No phenotypes were observed for RNAi of *egr1*, *egr1b*, *PI3K* or *jun*; similarly no phenotypes were observed following RNAi of combinations of these genes. However, at this point we do not know whether stronger RNAi would be required to obtain a phenotype and therefore no conclusions can be drawn from these results. *c-fos* RNAi however, resulted in the regeneration defects of cycloptic animals with small blastemas (Figure 3.16A), despite only a partial reduction in *c-fos* mRNA having occurred (Figure 3.16A). Moreover, we observed a diminished neoblast wound response in these RNAi animals, as determined by H3P labeling (Figure 3.16B). We therefore conclude that at least some immediate early genes are required for aspects

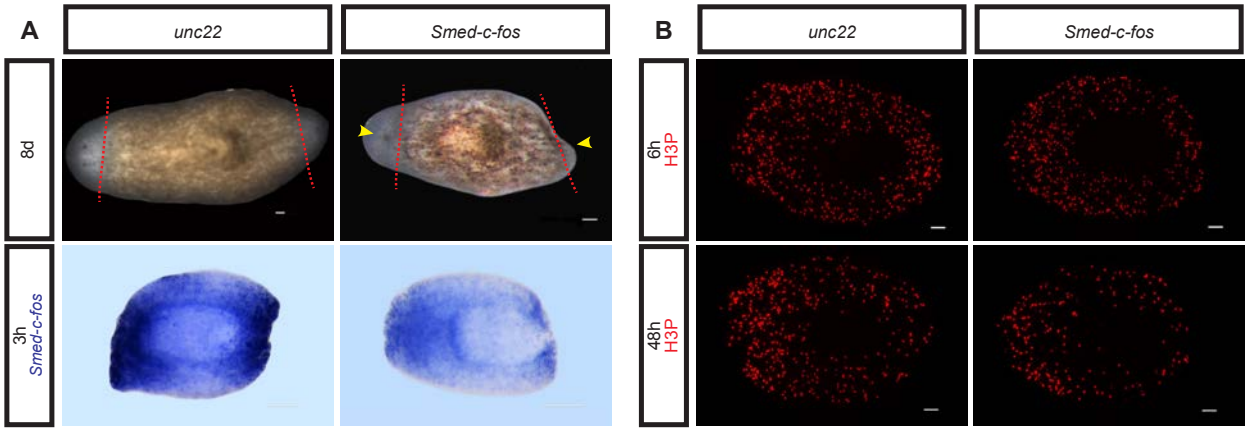

Figure 3.16. Perturbation of function of the immediate early gene *c-fos* leads to regeneration defects and a decrease in the mitotic wound response.
(A-B) Animals were fed control (*unc22*) or *c-fos* RNAi food four times (d0, d4, d8, d12) and amputated 6 days later. Time points as indicated. (A) Upper panel: *c-fos* RNAi causes cycloptic animals with small blastemas and asymmetric posterior blastemas (6/10). Red lines, approximate amputation plane. Lower panel: *in situ* hybridization probing for *c-fos*, showing that *c-fos* RNAi results in a decrease of wound-induced *c-fos* expression. (B) *c-fos* RNAi leads to a decreased mitotic neoblast wound response at 6h and 48h, as assayed by labeling of fragments with anti-H3P antibody. Trunk fragments are shown. Yellow arrows, regeneration defects. Anterior to the left. Scale bars, 100µm.

of regeneration initiation and neoblast proliferation.

3.2.3 A late wave of gene expression is comprised of genes encoding patterning factors and mitogens

Many genes expressed during the late wave of gene expression (3-12h) are predicted to encode patterning factors, mitogens, and matrix remodeling factors (e.g. *wntless* (*Smed-evi*), *wntP-1*, *inhibin*, *noggin-like1* (*nlg1*), *follistatin*, *dally-like*, *delta*, *epiregulin*, *plasminogen*, *tissue factor pathway inhibitor*, *ADAM metalloproteinases*) (Adell et al., 2009; Hooft van Huijsduijnen, 1998; Kocholaty et al., 1952; Lindahl et al., 1994; Molina et al., 2009; Ogawa et al., 2002; Pentek et al., 2009; Petersen and Reddien, 2009; Toyoda et al., 1995; Yan and Lin, 2007) (Figure 3.17A). Genes from the late waves showed a greater variety of expression patterns in amputated animals than did genes from the first wave of expression. Some genes, such as *inhibin*, *nlg1*, *wntless* and *wntP-1*, were expressed at the wound site in a manner similar to immediate early gene expression, but in fewer cells (Figure 3.17B). Unexpectedly, some genes such as a gene encoding a homolog of the Notch ligand Delta (Alton et al., 1989), were densely expressed in seemingly random epidermal cells throughout the fragment between 6-12h, but notably, were excluded from the wound site (Figure 3.17B). Another striking expression pattern was from a gene encoding an unknown protein that became expressed around the entire periphery of the fragment between 6-12h following wounding, including at the wound site, which we named *borderline1* (Figure 3.17B). To test whether this later phase of wound-induced gene expression is sensitive to translation inhibition, we amputated animals in cycloheximide and probed for expression of *nlg1* and *inhibin*,

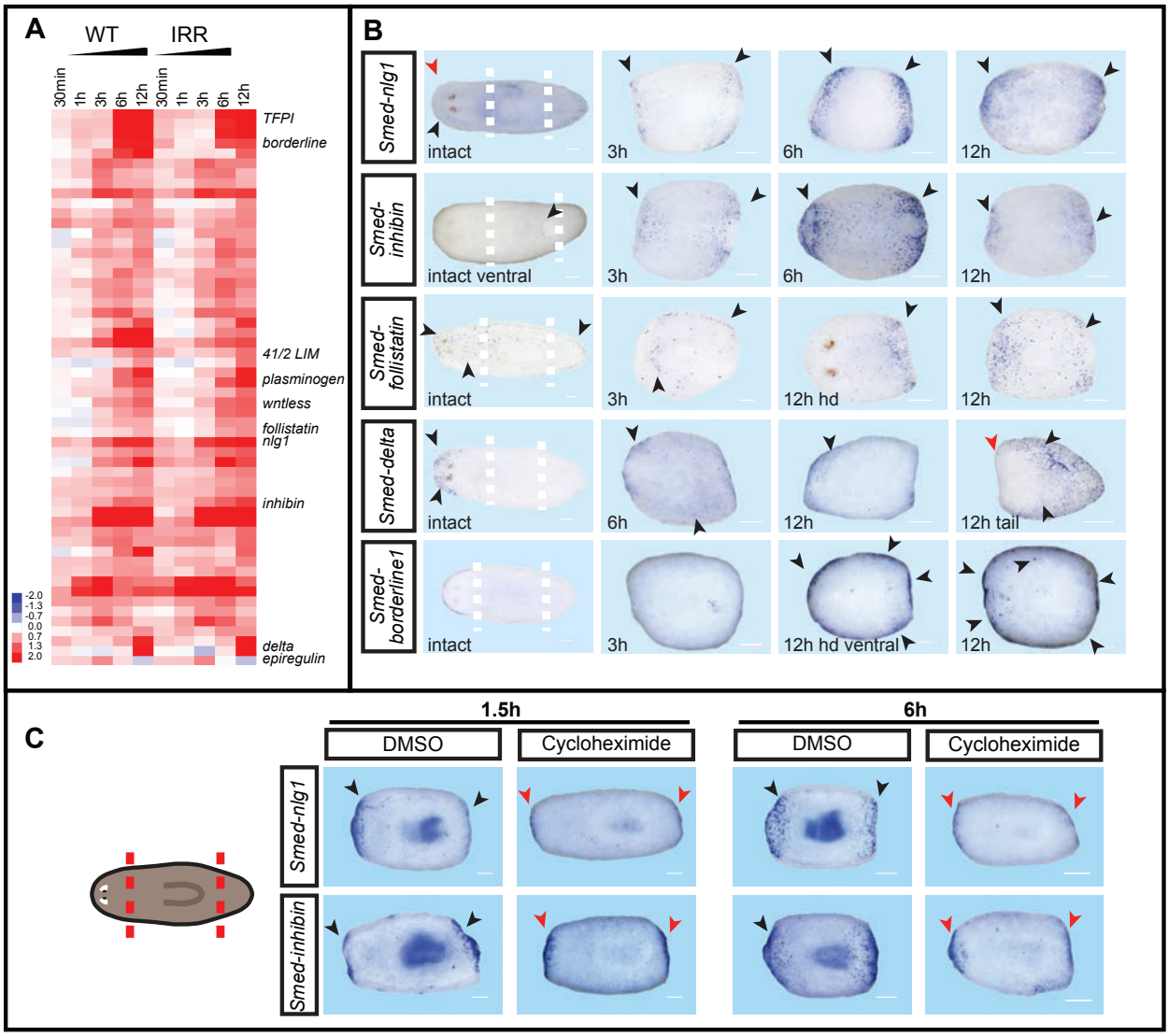

Figure 3.17. Expression of late wave genes is sensitive to translation inhibition, is weaker at the wound site, and may occur in areas away from the wound site

(A) Heatmap of genes that are upregulated ($p<0.05$) late (3-12h) in wild type and irradiated animals following wounding. Many genes in this cluster encode patterning and matrix remodeling factors. (B) *In situ* hybridizations on intact and amputated animals probing for genes that were upregulated following wounding at late time points. Expression is often upregulated at the wound site, but in fewer cells than immediate early gene expression. Some genes are upregulated away from the wound (*delta*) or all around the animal periphery (*borderline1*). Probes and time points as indicated. White lines indicate amputation sites. (C) Wound-induced expression of the late genes shown here, *nlg1* and *inhibin*, depends on protein translation. Planarians were amputated (as shown in the cartoon to the left) in cycloheximide (0.1µg/µl) or DMSO (1:1000; control) and fixed at indicated time points. *In situ* hybridizations were performed, probing for *nlg1* and *inhibin*, representatives of the late gene cluster. It is unclear whether the thin line of expression of *inhibin* at the wound site in cycloheximide-treated animals is background or real expression. Red dotted lines indicate amputation sites. Black arrowheads, upregulated expression; red arrowheads, downregulated expression. Amputated trunk fragments are shown, anterior to the left. Scale bars, 100µm.

as those are two of the earliest genes to be expressed from this late gene cluster. Expression of both genes was undetectable following cycloheximide treatment (Figure 3.17C). This suggests that protein synthesis is required for gene expression of the tested “late wave” genes following wounding.

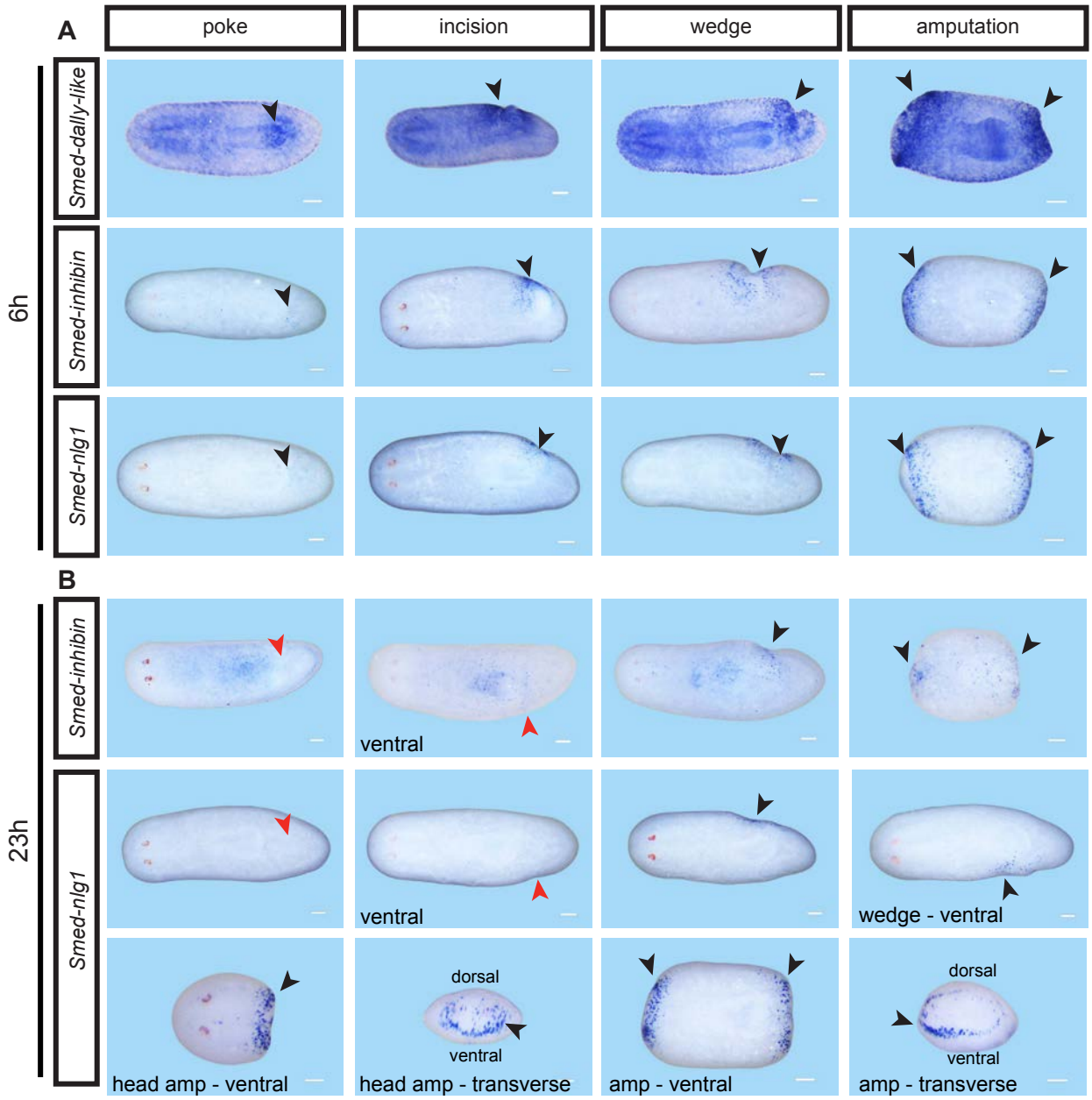

Figure 3.18. Late gene expression is induced by all kinds of wounds and their expression is dynamic.
(A-B) Animals were either wounded by poking animals in the tail (using a glass injection needle, poke), incised behind the pharynx (incision), surgically removing a triangle of tissue behind the pharynx (wedge), or amputated pre- and postpharyngeally (amputation) and fixed at indicated time points. *in situ* hybridizations were performed probing for expression of genes from the late cluster as indicated. (A) Induction of tested late genes at 6h following wounding occurs at all wounds, albeit to a lesser degree in minor wounds, such as a poke. (B) Expression of *inhibin* and *nlg1* at 23h is sustained at wounds that are associated with loss of tissue (wedge, amputation), but not at minor wounds (poke, incision). Expression of *nlg1* is dynamic. At 23h, the expression domain of *nlg1* was restricted to the ventral side of the animal, whereas expression was uniform along the DV axis of the wound at 6h (data not shown). Black arrowheads, wound-induced expression. Red arrowheads, absence of expression. Anterior to the left. Scale bars, 100µm.

To determine whether expression of genes that are expressed in the late wave is specific to loss of tissue or a generic part of the wound response, we performed the same surgeries as described above for the immediate early genes. We found that all of the genes tested were

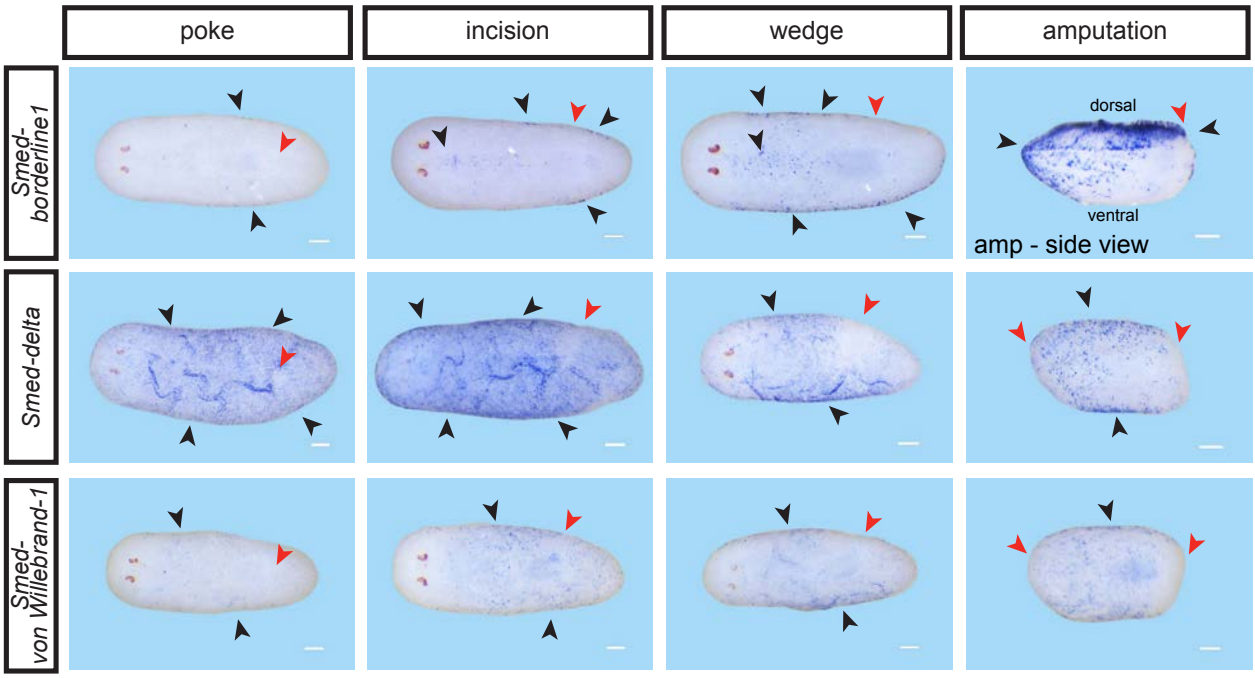

Figure 3.19. Expression of late genes that are expressed away from the wound scales with wound size.
Animals were either wounded by poking animals in the tail (using a glass injection needle, poke), incised behind the pharynx (incision), surgically removing a triangle of tissue behind the pharynx (wedge), or amputated pre- and postpharyngeally (amputation) and fixed at 23h. *In situ* hybridizations were performed probing for expression of genes from the late cluster as indicated. Induction of tested late genes at 23h following wounding is induced by all kinds of wounds, albeit to a lesser degree in minor wounds, such as a poke. Black arrowheads, wound-induced expression. Red arrowheads, absence of expression at the wound site. Anterior to the left. Scale bars, 100µm.

generically induced at all wounds (Figure 3.18), albeit again, to a lesser degree at minor wounds. Remarkably, expression of *nlg1* became polarized towards the ventral side of animals at later time points, after initially being expressed uniformly at earlier time points (Figure 3.18). A similar effect has been observed for the anterior-posterior axis defining patterning factor *wntP-1*, which after generic wound-induced expression, becomes localized to posterior facing wounds at later time points (Petersen and Reddien, 2009).

We described earlier that wound-induced gene expression of some genes occurred predominantly around the periphery of amputated fragments and was excluded from amputation sites, as described earlier for *borderline1* and *delta*, respectively. Remarkably, we found that even minor wounds, such as a poke or an incision induced expression of tested genes in a similar manner, expression around the animal periphery and excluded from wound sites, respectively (Figure 3.19).

Two members of the late wave of wound-induced gene expression, *wntP-1* and *wntless* have been shown to be required for proper patterning in planarian regeneration (Adell et al., 2009; Petersen and Reddien, 2009). We therefore sought to determine whether other candidates from this list also have a role in tissue patterning in planarians. Animals were fed RNAi

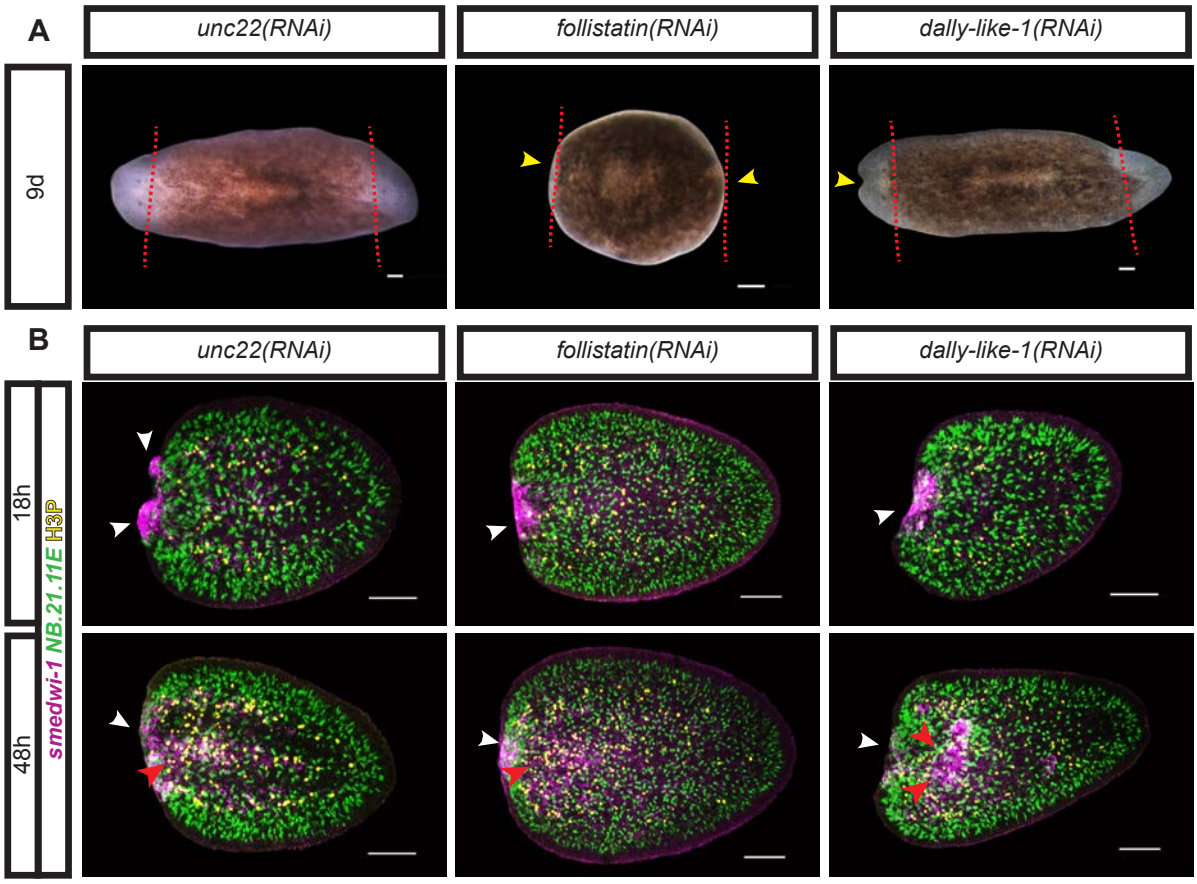

Figure 3.20. Genes from the late cluster are required for blastema formation and patterning.
(A-B) Animals were fed control (*unc22*), *follistatin* or *dally-like-1* RNAi food four times (d0, d4, d8, d12) and amputated 6 days later. Time points as indicated. (A) *follistatin* RNAi causes complete failure of blastema formation (7/7). *dally-like-1* RNAi causes indented blastemas (5/7). Regenerating trunk fragments are shown. Red lines, approximate amputation plane. (B) *dally-like-1(RNAi)* animals show a aberrant localization of neoblasts at 48h following wounding. Accumulation of *smedwi-1*$^{+}$ cells (magenta) at the wound site at 18h, *NB.21.11E* (green) progeny formation at 48h, and mitotic pattern (anti-H3P, yellow) are normal in *follistatin* and *dally-like-1(RNAi)*. At 48h, localization of *smedwi-1*$^{+}$ cells is aberrant (red arrows) in *dally-like-1(RNAi)* animals. Tail fragments are shown. White arrows, wound site, location of neoblast accumulation at 18h and differentiation at 48h. Anterior to the left. Scale bars, 100µm.

food, amputated, and left to regenerate. A number of striking phenotypes were observed. RNAi of a putative *follistatin* homolog, which is expressed at 6-12h at wounds (Figure 3.17B), caused a complete failure in blastema formation (Figure 3.20A). RNAi of a homolog of *dally-like*, another wound-induced gene that is expressed at 3h-12h, produced animals with split blastemas, a phenotype typically observed in animals with defects in BMP-signaling (Figure 3.20A) (Molina et al., 2007; Reddien et al., 2007). Dally-like proteins are glypicans that can be required for BMP signaling in the *Drosophila* wing (Belenkaya et al., 2004). In order to test for effects of gene perturbation on aspects of the neoblast wound response, we fixed another set of RNAi animals immediately, and after 6h, 18h, and 48h. Labeling for neoblasts, neoblast mitoses and progeny showed that the key features of the early neoblast wound response—first and second peak of mitoses, neoblast recruitment and differentiation at the wound site (Chapter 3.1)—were present (Figure 3.20B). Notably, *smedwi-1*$^{+}$-cell localization was aberrant at 48h in *dally-like(RNAi)* animals, likely

a first indicator of the patterning defect, which ultimately results in indented blastemas. Taken these findings together it becomes evident that a number of factors that are expressed during the late wave of wound-induced gene expression are required for proper patterning during regeneration in planarians.

3.2.4 Co-expression of immediate early genes with late wave genes suggests a functional relationship

The spatial similarity of immediate early gene expression with some of the late gene expression led us to ask whether they might be expressed in the same cells. We therefore double-labeled regenerating fragments with RNA probes for genes from each category. Expression of *c-fos* and *egr1*, representatives of the immediate early gene cluster, mostly overlapped (Figure 3.21A). Furthermore, expression of *inhibin* and *nlg1*, representatives of the late gene cluster, co-localized (Figure 3.21B). Interestingly, we also found co-localization of immediate early genes with late genes, as shown here for *c-fos* and *inhibin*, even though *inhibin* was expressed only in a fraction of cells expressing *c-fos* (Figure 3.21C). These findings together with the observation that cycloheximide is required for late, but not immediate early gene induction, suggest a possible role for immediate early genes in the induction of late gene expression.

3.2.5 A microarray study identifies wound-induced genes that are specifically upregulated in neoblasts and their immediate descendants

The microarray experiment described above (Figure 3.12) can also be used to identify genes that are upregulated in the neoblasts following wounding (Figure 3.22A). Genes that are upregulated following wounding in the data set from wild-type animals, but not upregulated in the data from lethally irradiated animals are likely expressed in neoblasts and/or their immediate descendants in response to wounding. Using this strategy, we identified over 900 genes that are candidates to mainly be upregulated in neoblasts and their descendents following wounding. Among these

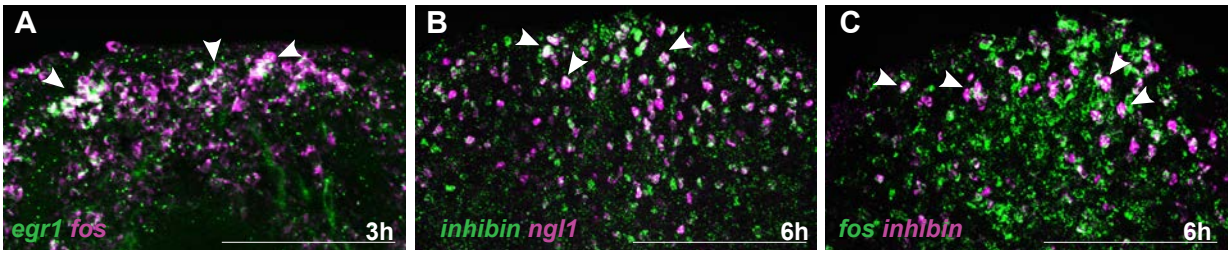

Figure 3.21. Wound-induced gene expression occurs in overlapping cell types.
(A-C) Animals were amputed pre- and postphayngeally and fixed at indicated time points. (A) Wound-induced expression of the immediate early genes *egr1* and *c-fos* co-localizes. (B) Wound-induced expression of the late genes *inhibin* and *nlg1* co-localizes. (C) Wound-induced expression of the immediate early gene *c-fos* and the late gene *inhibin* co-localizes. *inhibin* is expressed in fewer cells. Anterior wound sites of regenerating trunk fragments are shown. White arrowheads, co-labeling. Anterior, top. Scale bars, 100µm.

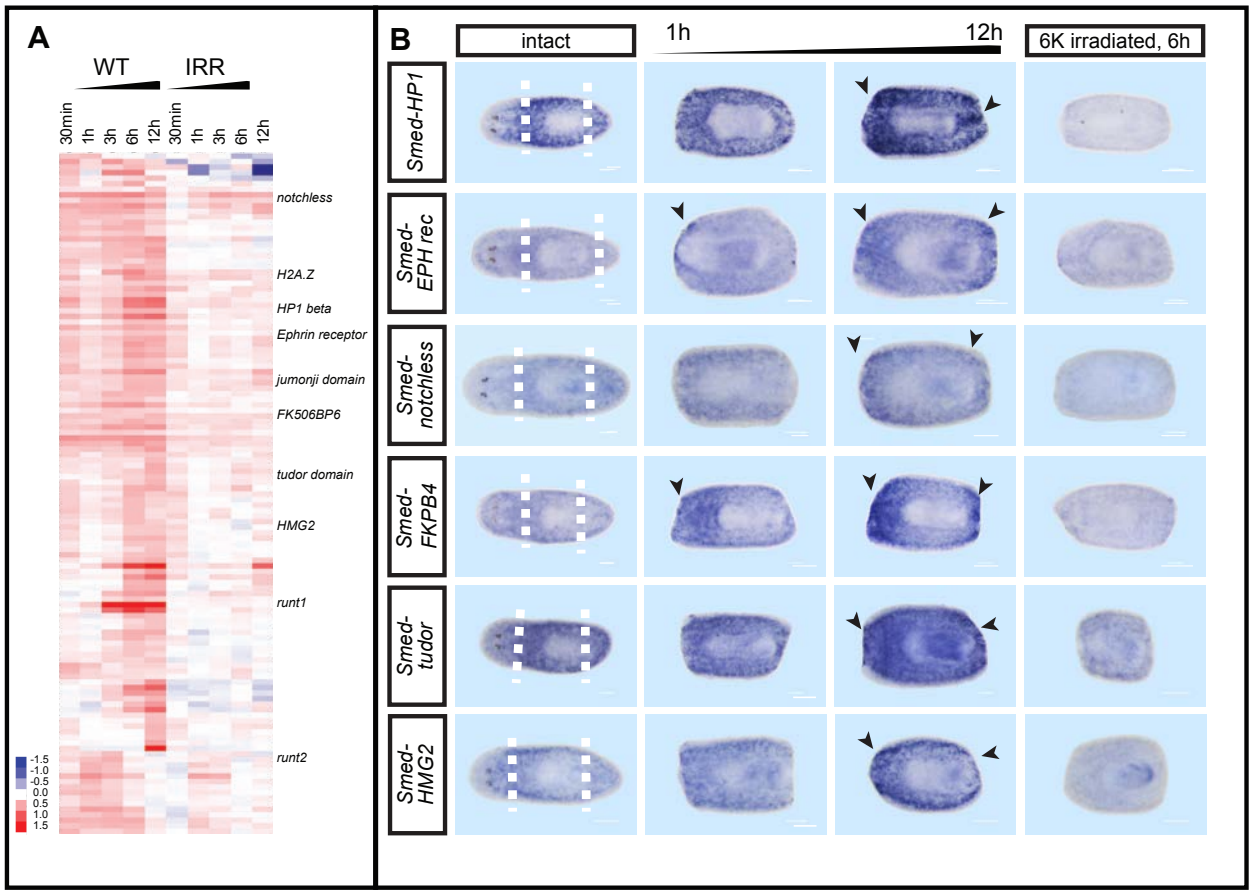

Figure 3.22. Identification of genes that are upregulated in neoblasts and their immediate descendants following wounding. (A) Heatmap of genes that are upregulated ($p<0.05$) wild type, but not irradiated animals following wounding. Genes in this cluster encode transcription factors and chromatin remodeling factors among others. (B) *In situ* hybridizations on intact and amputated animals probing for genes that were upregulated following wounding. Right column shows amputated fragments that were lethally (6K) irradiated 5 days prior to amputation. Expression in the intact animal is mostly in the parenchyma, the area where neoblasts reside. For many genes tested, expression was upregulated in irradiation sensitive cells throughout the fragment and upregulation was in some cases stronger in cells at the wound site. Black arrowheads, upregulated expression. White dotted lines, amputation planes. Amputated trunk fragments are shown, anterior to the left. Scale bars, 100µm.

genes are many encoding transcription factors, chromatin remodeling factors, cell cycle factors, and histone methyltransferases (see Appendix for a selection of genes). We performed an in situ hybridization screen on intact and amputated animals probing for a subset of these genes and found many neoblast-specific expression patterns (Figure 3.22B). Expression was upregulated in parenchymal cells following wounding and often stronger expression at the wound site was observed. Wound-induced expression was found to be irradiation sensitive (Figure 3.22B), suggesting that identified genes are expressed in neoblasts and their immediate descendants. These experiments identified genes that are specifically upregulated in neoblasts and their immediate descendants following wounding, providing useful information about neoblast biology during regeneration initiation, providing some of the first insights into the genetic behavior of neoblasts during regeneration initiation.

3.2.6 Multiplex expression analyses identify five different groups of wound-induced genes

In order to clearly distinguish immediate early (i.e., expression is not sensitive to inhibition of protein translation) and late genes (i.e., expression is sensitive to inhibition of protein translation), we performed multiplex expression analysis using the nCounter platform from NanoString (Geiss et al., 2008). We selected a total of 72 wound-induced genes from the differentiated tissue that had been confirmed by *in situ* hybridization experiments above and some additional genes with functionally interesting homology (Figure 3.23A). Furthermore, we included 18 neoblast/neoblast progeny-specific, wound-induced genes that were identified in the irradiation-sensitive microarray approach described above (Figure 3.22). Among these genes were those encoding cell cycle components, such as *cyclins*, *aurora kinase*, and *ribonucleotide reductase*, as well as chromatin components and two *runt* transcription factors among others (Figure 3.23B) (Chabes et al., 2004; Coffman, 2003; Evans et al., 1983; Heald et al., 1993; Kelly et al., 2010; Lens et al., 2010; Paro and Hogness, 1991). We also included 7 constitutively expressed "housekeeping" genes as a control and for normalization purposes in our probe set. RNA from control and cycloheximide-treated, amputated animals (10 animals per condition, in three biological replicates) was extracted 1.5h and 8h following wounding and probed for differential expression of the selected genes. At 1.5h following wounding, three genes were significantly upregulated in cycloheximide-treated animals (Figure 3.24A), all of which represent genes from the first wave of gene expression. We

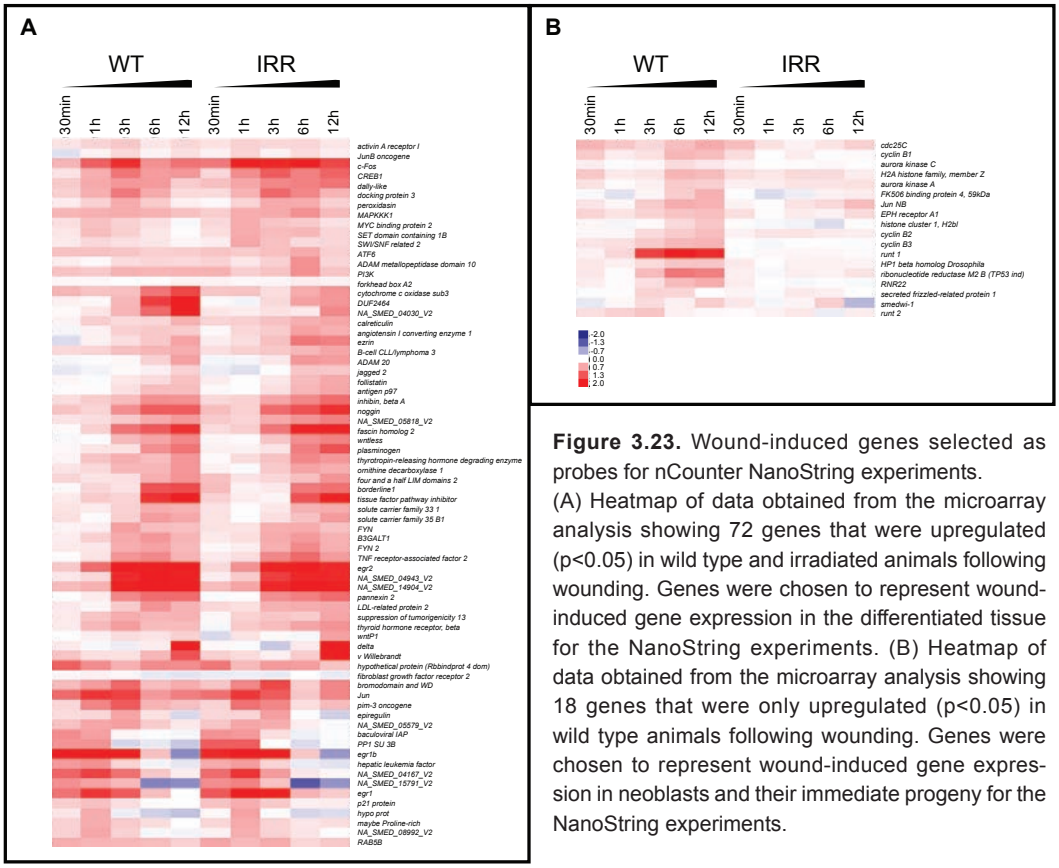

Figure 3.23. Wound-induced genes selected as probes for nCounter NanoString experiments.
(A) Heatmap of data obtained from the microarray analysis showing 72 genes that were upregulated ($p<0.05$) in wild type and irradiated animals following wounding. Genes were chosen to represent wound-induced gene expression in the differentiated tissue for the NanoString experiments. (B) Heatmap of data obtained from the microarray analysis showing 18 genes that were only upregulated ($p<0.05$) in wild type animals following wounding. Genes were chosen to represent wound-induced gene expression in neoblasts and their immediate progeny for the NanoString experiments.

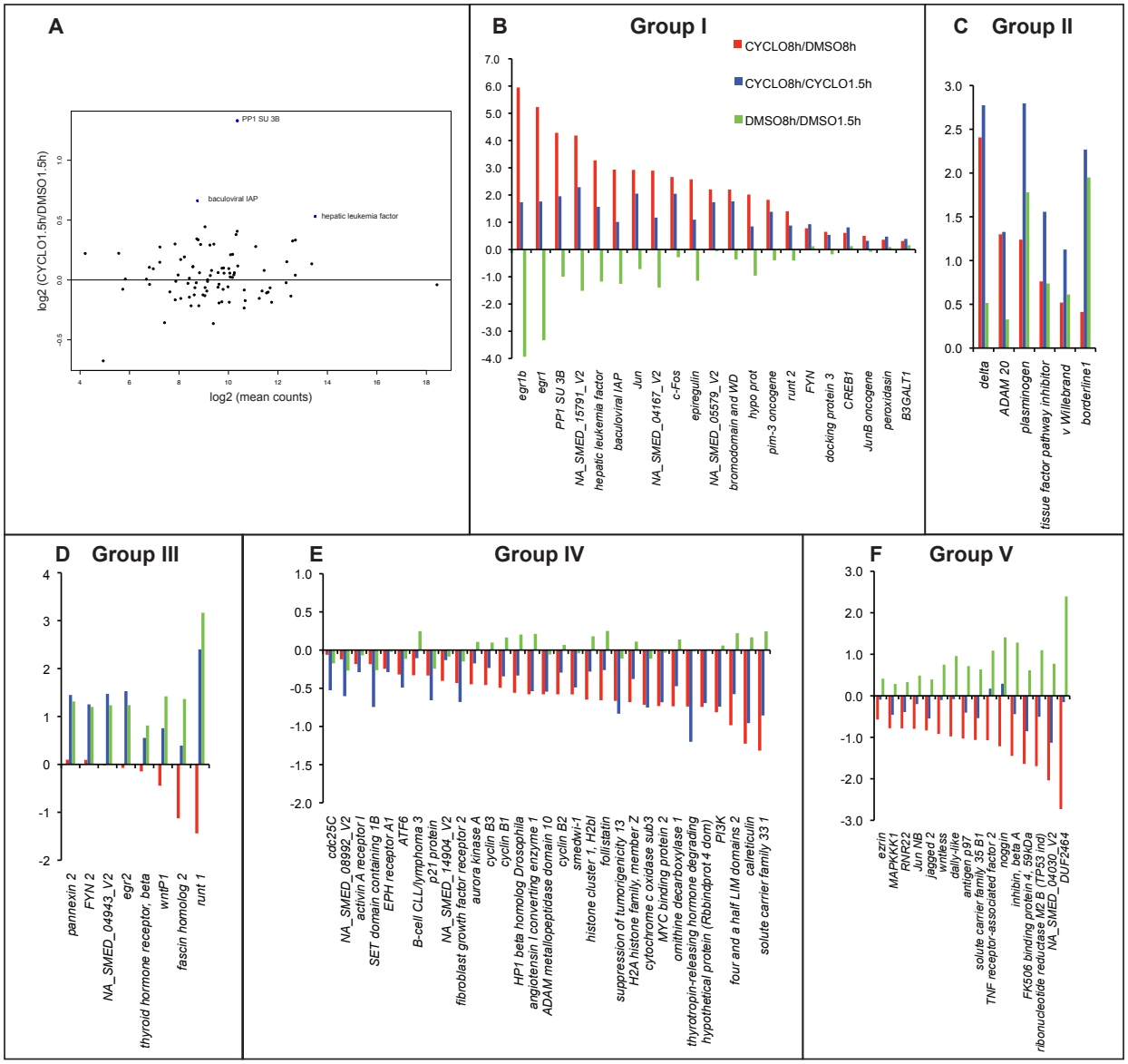

Figure 3.24. Wound-induced genes can be assigned to five different groups by their dependence on protein translation.
(A-E) Animals were amputated in cycloheximide (0.1µg/µl) or DMSO (1:1000; control) and RNA extracted at indicated time points following wounding. RNA hybridizations and counts were performed using the NanoString platform. Expression changes are expressed as log2 ratios. Significant = $p < 0.01$. (A) MA-plot showing log2 ratios and log2 mean count values at 1.5h following wounding of animals amputated in cycloheximide as compared to control (DMSO) animals. Three genes are significantly upregulated following cycloheximide treatment (in blue and labeled). (B-F) Log2 ratios of tested genes are shown. Legend shown in (B) applies to all the following graphs. (B) Expression of group I genes is significantly upregulated 8h following amputation in cycloheximide as compared to non-treated animals and as compared to cycloheximide-treated expression at 1.5h (red, CYCLO8h/DMSO8h and blue bars, CYCLO8h/CYCLO1.5h). Many of these genes are usually downregulated by 8h following wounding (green bars, DMSO8h/DMSO1.5h). (C) Expression of group II genes is also upregulated at 8h following amputation in cycloheximide as compared to non-treated controls and as compared to cycloheximide-treated expression at 1.5h (see red, CYCLO8h/DMSO8h and blue bars, CYCLO8h/CYCLO1.5h). These genes are usually upregulated at 8h following wounding but to a lesser extent (green bars, DMSO8h/DMSO1.5h). (D) Expression of group III genes either does not change or is partially sensitive to translation inhibition, but in all cases, induction still occurs (down in CYCLO8h/DMSO8h, red bars, but up in CYCLO8h/CYCLO1.5h, blue bars). All of these genes are usually upregulated at 8h (green bars, DMSO8h/DMSO1.5h). (E) Expression of group IV genes is downregulated 8h following amputation in cycloheximide (red, CYCLO8h/DMSO8h), but their expression usually does not increase significantly between 1.5h and 8h (green bars, DMSO8h/DMSO1.5h). (F) Expression of group V genes is downregulated 8h following amputation in cycloheximide (red, CYCLO8h/DMSO8h) though expression usually increases between 1.5h and 8h (green bars, DMSO8h/DMSO1.5h).

identified five different groups of genes, classified by their expression profile in amputated wild type and cycloheximide-treated animals (Figure 3.24B-E). Wound-induced expression of group I genes was higher in cycloheximide-treated animals as compared to control animals and therefore not sensitive to translation inhibition. All genes in this group belong to the first wave of gene expression and are usually either downregulated or unchanged between 1.5h and 8h (Figures 3.13A, 3.24B). Genes in group I include *egr1*, *egr1b*, *c-fos*, *jun*, *FYN kinase*, *protein phosphatase 1 (inhibitory subunit 3B)* (*PP1 SU 3B*), *epiregulin*, and the neoblast-specific gene *runt2.* This finding is consistent with the observed expression of *egr1* and *c-fos* described above (Figure 3.13C). Wound-induced expression of group II genes was also higher in cycloheximide-treated animals as compared to control animals and therefore not sensitive to translation inhibition. This group is distinguished from group I by later wound-induced expression (3-12h, members of the late wave) and greater perdurance of expression in wild-type animals (Figure 3.24C). Wound-induced expression of members of this group occurs in areas other than the wound site (Figures 3.17B, 3.19). These genes encode proteins involved in extracellular matrix remodeling and signaling, such as *delta* (Figure 3.24C). These genes represent a second wave of immediate early genes that had not been previously identified. Wound-induced expression of group III genes was either unchanged or marginally lower in cycloheximide-treated animals as compared to control animals (Figure 3.24D). Notably, in all cases, expression of group III genes was induced by wounding in the presence of cycloheximide, albeit often to a lesser degree than in control animals (Figure 3.24D, blue bars). Genes from group III are therefore partially sensitive to translation inhibition. Genes in this group are expressed in the late wave (3-12h) following wounding, including *egr2*, the patterning factor *wntP-1*, and the neoblast-specific gene *runt1*. Expression of group IV genes was lower in cycloheximide-treated animals as compared to control animals at 8h (Figure 3.24E, blue and red bars). Genes in this group encode signaling factors, such as *activin A receptor* (Attisano et al., 1992) and many of the neoblast-specific genes, such as *cdc25C* (Heald et al., 1993), *ephrin receptor* (Xu et al., 1999), *smedwi-1* (Reddien et al., 2005b), and *cyclin B1-3* (Evans et al., 1983). Expression of group IV genes does not usually increase between 1.5h and 8h (Figure 3.24E, green bars). This distinguishes genes from group IV from genes from group V, which usually increase in expression between 1.5h and 8h (Figure 3.24F, green bars). Wound-induced expression of group V genes therefore depends on *de novo* protein synthesis. These genes encode patterning factors such as *inhibin*, *nlg1, noggin*, *wntless*, *dally-like*, and some neoblast-specific genes, such as *rnr2-2* (Chabes et al., 2004) (Figure 3.24F). We therefore conclude that there exist an early and a late wave of immediate early genes (groups I and II, respectively), both of which are overexpressed following inhibition of protein translation and therefore potentially require translation of themselves or other wound-induced genes to be downregulated normally. There additionally exists wound-induced expression of some genes that only partially depends on protein translation

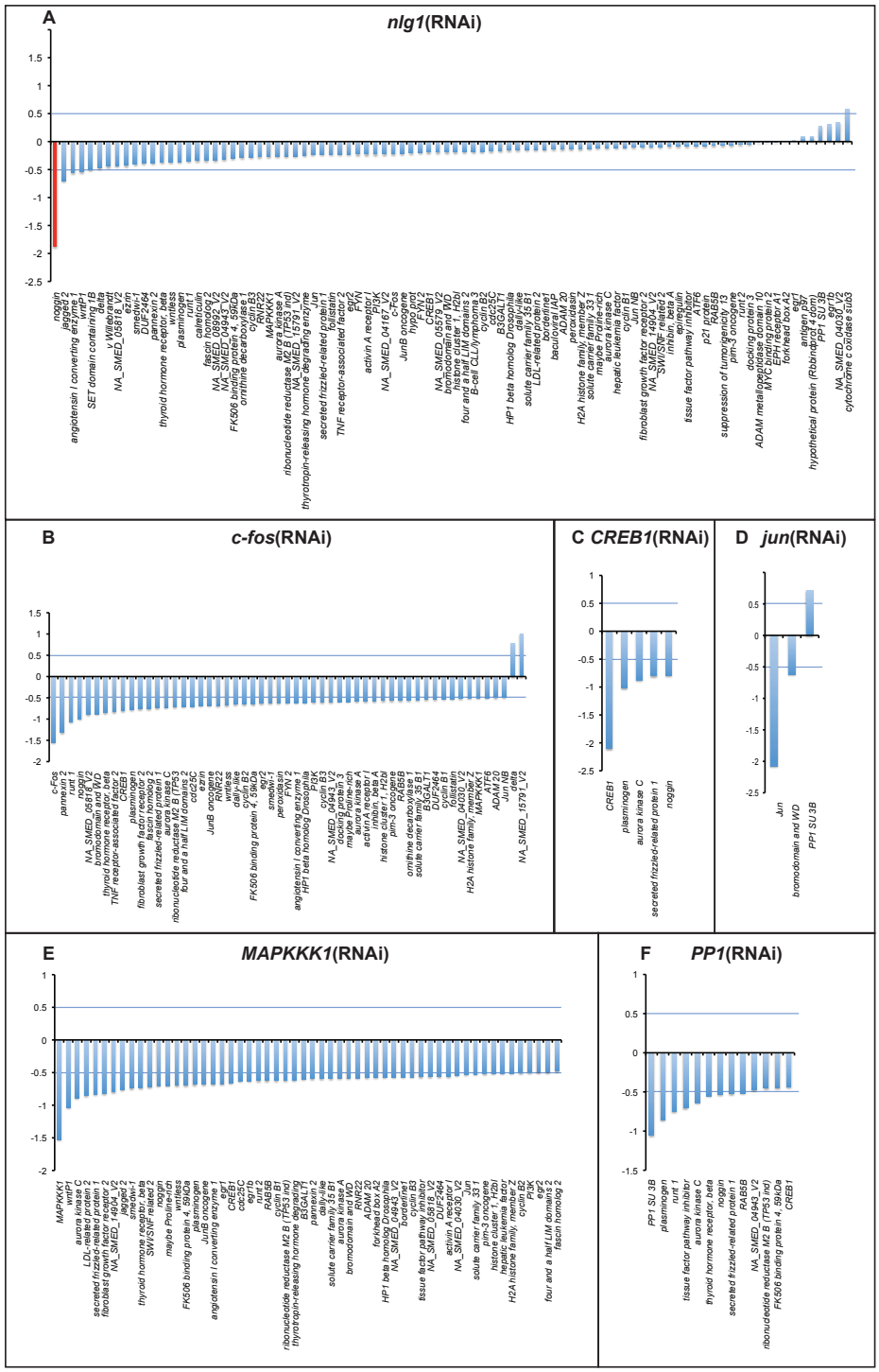

Figure 3.25. RNAi of immediate early gene expression following wounding causes decreased wound-induced expression.
(A-F) Animals were fed RNAi food four times (d0, d4, d8, d12) and amputated 6 days later. RNA was extracted at 3h following wounding, unless otherwise stated. All samples were compared to RNA from control *unc22*(RNAi) animals. RNA hybridizations and counts were performed using the NanoString platform. Expression changes are expressed as log2 ratios. All changes shown are significant ($p<0.01$), except in (A). Note, that in all RNAi conditions the gene whose function is perturbed is downregulated by 50-75%. (A) Effect of *nlg1* (a member of group IV) RNAi on wound-induced gene expression at 7.5h. No genes assayed show significant reduction in gene expression except for *nlg1* itself (red bar, down by 75%). (B) Effect of *c-fos* RNAi on wound-induced gene expression. (C) Effect of *CREB1* RNAi on wound-induced gene expression. (D) Effect of *jun* RNAi on wound-induced gene expression. (E) Effect of *MAPKKK1* RNAi on wound-induced gene expression. (F) Effect of *PP1* RNAi on wound-induced gene expression. Blue lines mark 0.5 log2 ratio (i.e., 1.4-fold change) and were added to facilitate comparison between the different conditions shown. See text for details.

(group III). Finally, there exist two groups of genes that are dependent upon protein translation for wound-induced expression. These two groups are separated by the temporal properties of their wound-induced expression: expression of group IV does not increase between 1.5h and 8h under normal conditions, but expression of group V genes does.

3.2.7 Immediate early genes are required for wound-induced gene expression

We showed that immediate early genes are rapidly upregulated following wounding, in a translation-insensitive manner. Many genes that are expressed in the late wave, however, depend on protein translation for their expression. Therefore we asked whether expression of immediate early genes (mainly group I) is required for expression of genes from the late waves. We performed multiplex expression analysis using the same target genes as described above (Figure 3.23) probing with RNA extracted from animals that had been subjected to four RNAi feedings (10 animals per RNAi, in three biological replicates) for the respective gene. RNA was extracted 3h following amputation from RNAi-treated animals to test the effect of five immediate early genes: *c-fos*, *CREB1*, *jun*, *MAPKKK1*, and *PP1*. Moreover, we included a gene from group IV, *nlg1,* to assay for possible defects that are caused by perturbation of wound-induced expression in general and to assay for function of wound-induced expression of a gene from the late wave of wound-induced gene expression. RNA was extracted at 7.5h following wounding in this condition and the associated control, because of the late wound-induced expression for this gene, and therefore the potentially late effects of wound-induced *nlg1* expression. *nlg1* RNAi did not cause any significant changes in wound-induced gene expression, besides reduction of *nlg1* expression itself (65%) (Figure 3.25A). Because *nlg1* RNAi did not cause changes in wound-induced gene expression, we conclude that significant changes in wound-induced expression are likely specific to the respective treatment and that our selection criteria are stringent enough to exclude the possibility of changes in expression produced simply by noise. Notably, wound-induced expression of genes that were perturbed using RNAi was strongly reduced (50%-75%) in each respective RNAi condition (Figure 3.25A-F). Of the tested immediate early genes, *c-fos* and *MAPKKK1* RNAi showed the strongest effects on wound-induced gene expression (Figure 3.25B, E). 53 and 56 genes were significantly downregulated in *c-fos* and *MAPKKK1*, respectively. 41 of these genes were downregulated in both conditions, potentially indicating common downstream targets. 29 of the downregulated, shared genes represent members of the translation sensitive groups III-V, indicating that *c-fos* and *MAPKKK1* are involved, directly or indirectly, in wound-induced expression of groups III-V. Seven of the shared genes are members of the translation insensitive groups I-II, suggesting a possible requirement of *c-fos* and *MAPKKK1* for immediate early gene expression (note that RNAi treatment began 18 days prior to amputation). The five remaining genes were not significantly affected by cycloheximide treatment and had therefore not been assigned

to any group. Remarkably, two genes were significantly upregulated following *c-fos* RNAi—*delta* and a gene encoding an unknown protein—indicating a possible direct or indirect involvement of *c-fos* in repression of these genes. *CREB1* RNAi and *PP1* RNAi also caused downregulation of genes from groups III-V, suggesting that these genes are involved in the induction of wound-induced late gene expression (Figure 3.25C, F) in planaria. *jun* RNAi did not cause any defects in late gene expression. Instead, two members of group I were aberrantly induced, suggesting a possible role for *jun* in regulation of expression of some immediate early genes (Figure 3.25D). Although *jun* expression was strongly decreased in the RNAi treatment (by 75%) the possibility that the remaining gene products might be sufficient to induce wound response gene expression cannot be excluded. Moreover, the target genes in the NanoString code set represent only one fourth of wound-induced genes and because of this, potential defects might not be visible. Finally, Jun proteins (together with other bZIP transcription factors from the Jun and Fos family) have been described to form the homo- and heterodimeric AP-1 transcription factor (Eferl and Wagner, 2003). It is therefore possible that lack of *jun* function in planaria is compensated by other, functionally similar transcription factors.

Taking these findings together, we conclude that immediate early genes are at least partially required for wound-induced expression of late, translation-sensitive genes. Moreover, products of some immediate early genes that are present prior to wounding might also act as inducers of immediate early gene expression (i.e., *c-fos*, *jun*, *MAPKKK1*).

3.2.8 Identification of factors that regulate wound-induced gene expression

As shown above, wound-induced expression of immediate early genes does not require new protein translation. Instead, it is thought that latent transcription factors are modified directly or indirectly by external stimuli, such as wounding, and act to induce expression of these genes (Taub, 2004). To identify candidate inducers of immediate early gene expression, we selected a small list of candidate genes that had previously been described to be involved in induction of immediate early genes in other systems or that are known to cause regeneration defects when perturbed by RNAi. Importantly, none of the selected genes were upregulated in the wound-induced microarray data set, consistent with roles as “wound-sensing” genes. To test for the effects of these selected genes on wound-induced gene expression, we inhibited expression of each gene prior to amputation through four consecutive RNAi feedings. First, we assessed morphological phenotypes generated through adult tissue turnover (homeostasis) and during regeneration (Figure 3.26A, B). SOS (Son of Sevenless) is a signaling factor that is required for receptor tyrosine kinase signaling, a pathway that is used by most mitogens (Lemmon and Schlessinger, 2010). Perturbation by RNAi of a planarian gene encoding a homolog of *SOS (Smed-SOS)* caused smaller blastemas and asymmetric tail formation during regeneration (Figure

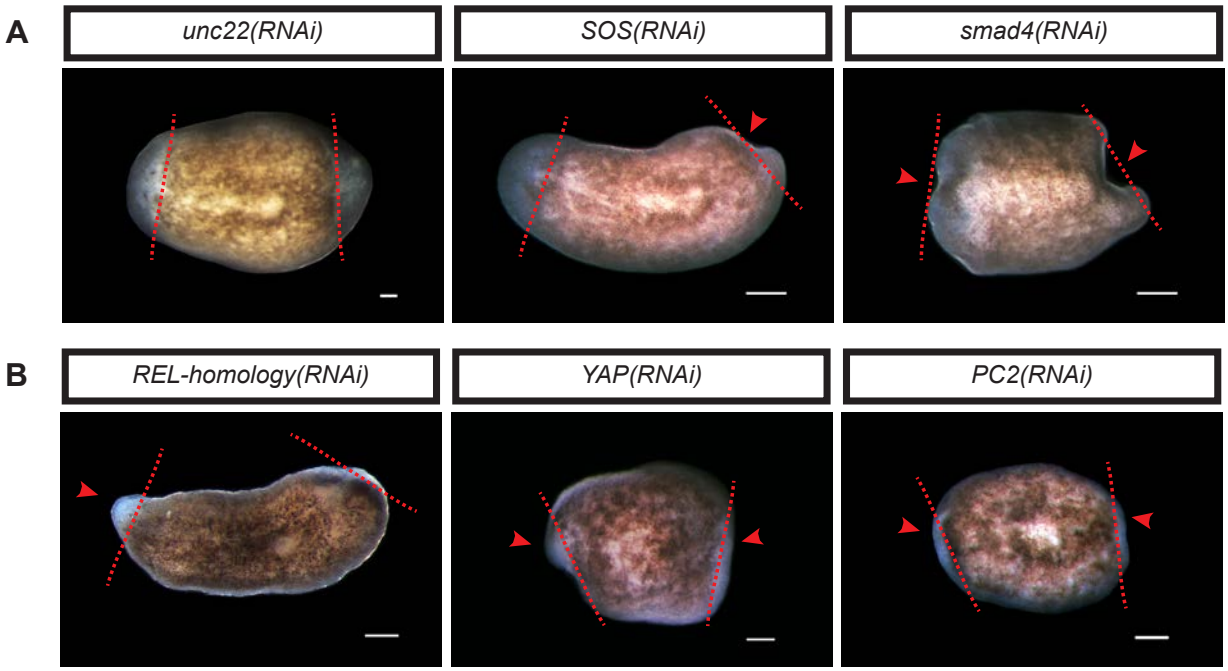

Figure 3.26. Candidate wound-sensor genes are required for normal regeneration
(A-B) Live images of animals that were fed RNAi food for indicated genes four times (d0, d4, d8, d12) and amputated 6 days later. (A) Genes for which RNAi did not cause gross defects during homeostasis prior to amputation, but did cause defects during regeneration. Images were taken at day 11 following amputation. (B) Genes for which RNAi caused defects during homeostasis, as well as during regeneration. Because of decreased survival of regenerating fragments in these conditions, images were taken at the following days following amputation: *REL-homology* d7, *YAP* d10, *PC2* d4. See text for details. Red arrowheads, regeneration defects. Red dotted line, approximate amputation plane. Anterior to the left. Scale bars, 100µm.

3.26A). A gene encoding a homolog of *smad4*, a co-Smad (common-partner Smad) that acts downstream of both BMP and TGFβ-signaling pathways, is required for blastema formation in planaria (Reddien et al., 2005a) (Figure 3.26A). However, RNAi animals appear to have a normal neoblast wound response (Wenemoser and Reddien, 2007), providing an interesting opportunity to identify factors that might be required for blastema formation in a context where the neoblast wound response is functional. SRF is involved in regulation of immediate early gene expression in the brain (Knoll and Nordheim, 2009) and liver regeneration (Latasa et al., 2007). RNAi of a planarian gene encoding a homolog of *SRF* lead to formation of smaller blastemas (Reddien et al., 2005a). Nuclear factor (NF)-κB is rapidly activated in hepatocytes following partial hepatectomy and might therefore play a role in wound-induced gene expression (Taub et al., 1999). RNAi of a putative planarian homolog of (NF)-κB, *REL-homology*, led to severe homeostatic defects. Starting at approximately day 12 following the first RNAi feeding, animals began lysing and blastema formation was subsequently impaired following amputation (Figure 3.26B). YAP (yes-associated protein), or Yorkie, is a negative regulator of Hippo signaling that regulates stem cell proliferation in the *Drosophila* intestine following wounding (Staley, 2010). RNAi of a gene encoding a planarian homolog of YAP, *Smed-YAP* (*YAP*), led to bloating of animals during homeostasis, a sign of malfunction of the excretory system in planaria (Glazer et al., 2010). *YAP(RNAi)* animals

also failed to regenerate (Figure 3.26B), an effect that is not observed for other genes involved in excretory function (Glazer et al., 2010), suggesting that *YAP* may play multiple, independent roles in excretory system maintenance and regeneration initiation. To test for possible involvement of peptide hormones and neuropeptides in wound-induced gene expression, we examined the effects of *proprotein convertase 2* (*PC2)* RNAi, a gene which is required for maturation of peptide hormones and neuropeptides (Muller and Lindberg, 1999), on wound-induced gene expression. *PC2(RNAi)* animals were uncoordinated (Reddien et al., 2005a) and regeneration was impaired (Figure 3.26B). The various regeneration defects produced by RNAi of these genes is consistent with candidate roles in induction of immediate early wound-induced gene expression.

To test the requirement of selected candidate genes for wound-induced expression, we performed multiplex expression analysis using the nCounter platform from NanoString. RNA was extracted from RNAi animals 3h following amputation and effects on wound-induced gene expression were assayed using the same target genes as above (Figure 3.23). RNAi of all tested genes caused changes in wound-induced gene expression (Figure 3.27A-F). *SOS(RNAi)* animals showed downregulation of three genes, *runt1*, *egr2* (both of which are group III genes) and a gene of unknown homology *NA_SMED_14904_V2* (group IV), and upregulation of two unknown genes (Figure 3.27A). This indicates a possible role of receptor tyrosine kinase signaling in regulation of wound-induced gene expression. Remarkably, perturbation of *SRF* function led to a strong decrease of many neoblast-specific genes, such as *cyclin B1-3*, *cdc25C*, and *runt1*, most of which are group IV genes (*runt1*, group III) (Figure 3.27B). This indicates a possible role for *SRF* in the induction of wound-induced gene expression in neoblasts. RNAi of *smad4* caused downregulation of a number of late wave genes that are involved in patterning, including *wntP-1*, *delta*, and *nlg1* (*noggin*) (Figure 3.27C). These findings indicate a requirement of *smad4* for wound-induced expression of some genes that are expressed late and possibly involved in pattern formation during regeneration. *REL-homology(RNAi)* animals displayed downregulation of some genes (such as *nlg1* and *runt1*), but the majority of genes were upregulated in this condition, including genes from all groups (I-V), ranging from immediate early genes (*PP1*, *hepatic leukemia factor*, *bromodomain* and *WD*) to patterning genes that are expressed in the late wave (*follistatin, inhibin, jagged 2*) (Figure 3.27D). This finding indicates that *REL-homology* may play a role in negative regulation of wound-induced gene expression. *YAP(RNAi)* animals, surprisingly, did not show many changes in wound-induced gene expression (Figure 3.27E). Finally, *PC2(RNAi)* animals did not show downregulation of any genes. Instead, four genes were strongly upregulated, including three genes from group II: *plasminogen*, *tissue factor pathway inhibitor*, and *borderline1* (Figure 3.27F).

To validate the results obtained by multiplex expression analysis, we performed *in situ* hybridizations on regenerating *SOS* (Figure 3.28A) and *SRF(RNAi)* (Figure 3.28B) animals, probing

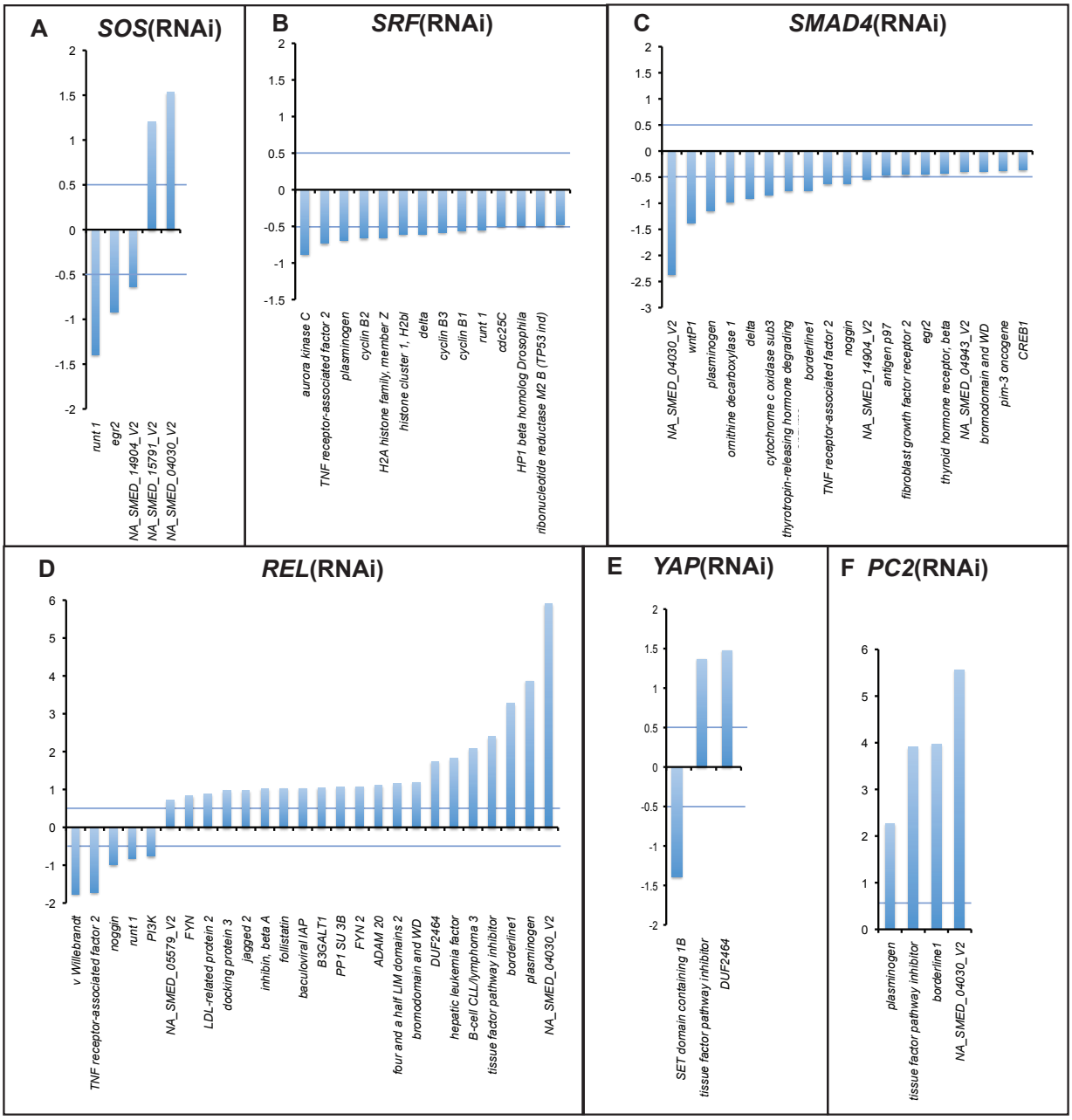

Figure 3.27. Multiplex expression analysis reveals defects in wound-induced gene expression following RNAi of candidate sensor genes.

(A-F) Animals were fed RNAi food four times (d0, d4, d8, d12) and amputated 6 days later. RNA was extracted at 3h following wounding. All samples were compared to RNA from control *unc22(RNAi)* animals. RNA hybridizations and counts were performed using the NanoString platform. Expression changes are expressed as log2 ratios. All changes shown are significant ($p<0.01$). (A) Effect of *SOS* RNAi on wound-induced gene expression. (B) Effect of *SRF* RNAi on wound-induced gene expression. (C) Effect of *smad4* RNAi on wound-induced gene expression. (D) Effect of *REL-homology* RNAi on wound-induced gene expression. (E) Effect of *YAP* RNAi on wound-induced gene expression. (F) Effect of *PC2* RNAi on wound-induced gene expression. Blue lines mark 0.5 log2 ratio (i.e., 1.4-fold change) and were added to facilitate comparison between the different conditions shown. See text for details.

for expression of *runt1* and *cdc25C* (for *SRF(RNAi)*). We found that wound-induced expression of *runt1* at 3h was strongly downregulated in fragments from *SOS* and *SRF(RNAi)* animals. At 6h following wounding, *runt1* expression was increased in fragments from *SRF(RNAi)* animals,

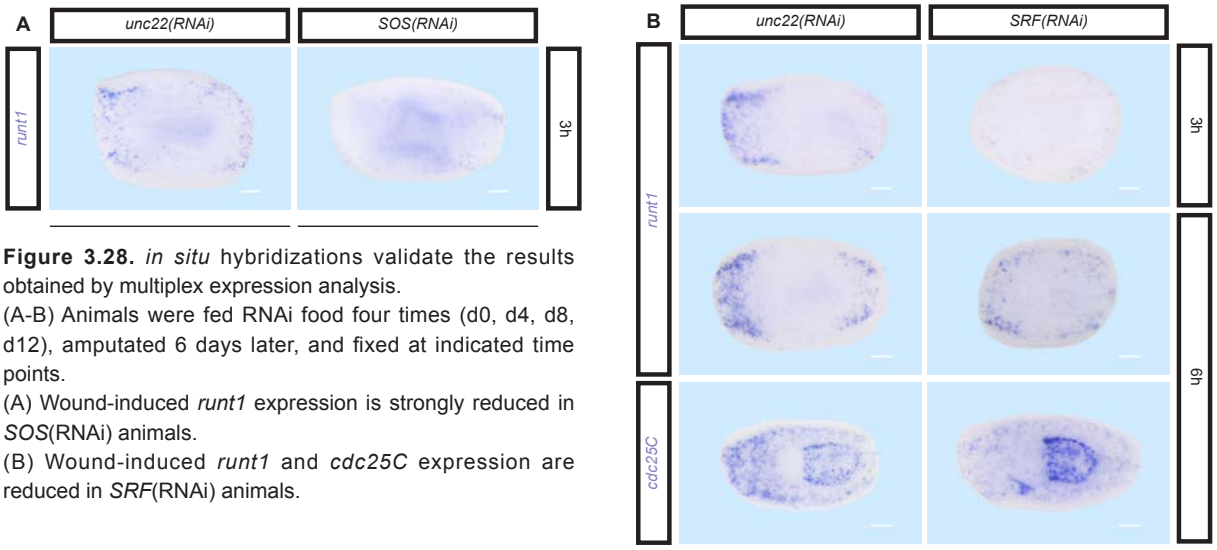

Figure 3.28. *in situ* hybridizations validate the results obtained by multiplex expression analysis.
(A-B) Animals were fed RNAi food four times (d0, d4, d8, d12), amputated 6 days later, and fixed at indicated time points.
(A) Wound-induced *runt1* expression is strongly reduced in *SOS*(RNAi) animals.
(B) Wound-induced *runt1* and *cdc25C* expression are reduced in *SRF*(RNAi) animals.

although detected in less cells than in control animals (Figure 3.28B). We also found that *cdc25C* expression was decreased in fragments from *SRF(RNAi)* animals (Figure 3.28B).

We conclude from these experiments that no gene in this category of genes appears to play a broad role in wound-induced immediate early gene expression.. However, our findings indicate that *SRF* is required for wound-induced gene expression in neoblasts and that *REL-homology* may be required for negative regulation of wound-induced gene expression.

3.3 *Smed-runt1* expression in planarian neoblasts following wounding is required for regeneration of neuronal structures

3.3.1 *Smed-runt1* expression is specific to wounding and is required for photoreceptor formation

Planarian stem cells proliferate rapidly following wounding, are recruited to wound sites, and differentiate to give rise to new tissue. Little knowledge exists about factors that govern these events in planarians. Runt transcription factors are conserved throughout the metazoan kingdom (Sullivan et al., 2008) and have been implicated in the developmental balance between cell proliferation and differentiation in many systems (Coffman, 2003; Nimmo and Woollard, 2008; Zagami et al., 2009). We found two planarian homologs of runt transcription factors, *Smed-runt1* and *Smed-runt2* that become strongly and specifically expressed in a subset of planarian neoblasts following wounding. Both *S. mediterranea* runt homologs cluster with runt homologs from other species rather than other p53/RUNT-type transcription factors, such as p53 and p73 (Figure 3.29A). By *in situ* hybridization, both genes were expressed in irradiation sensitive cells in a spatial and temporal pattern reminiscent of the neoblast wound response (Figure 3.29B, C). In intact animals, both genes are expressed in a pattern that is reminiscent of neuronal cell types,

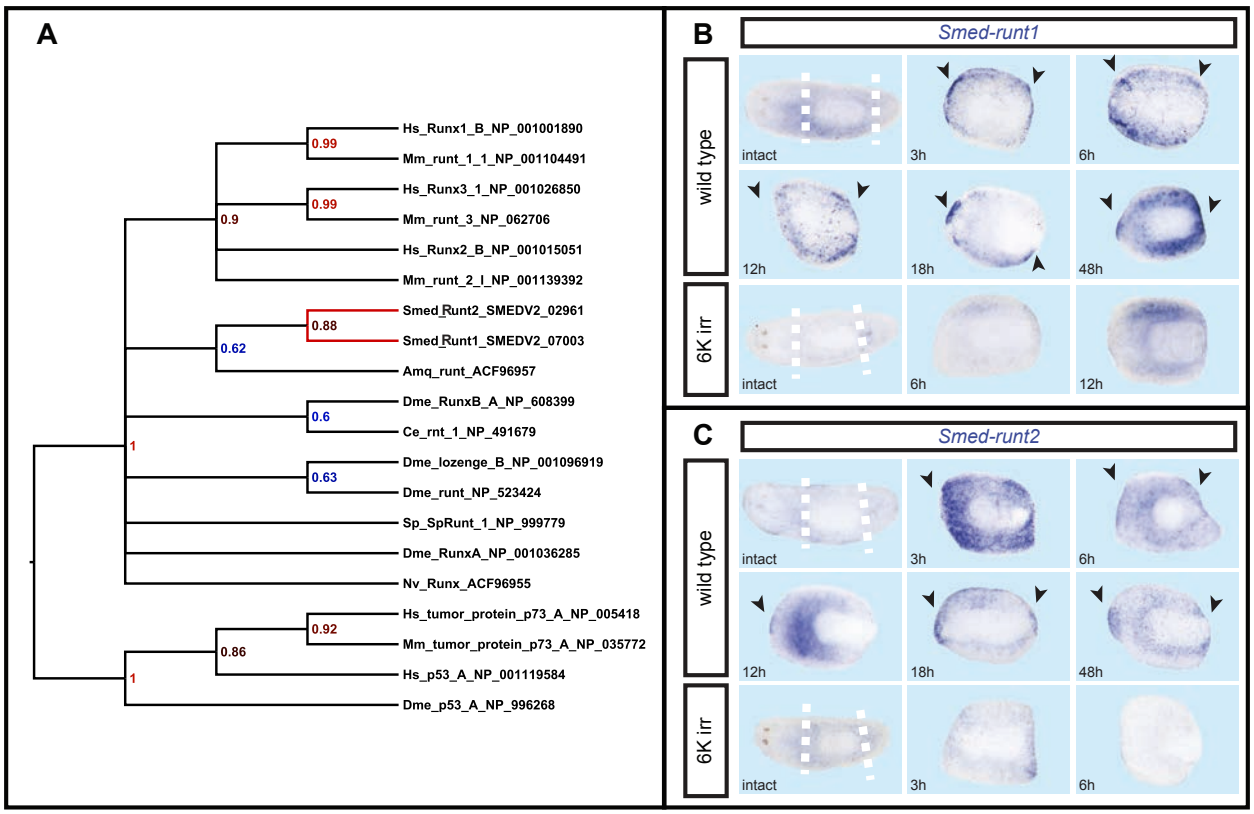

Figure 3.29. Two planarian homologs of *runt* transcription factors are strongly upregulated in irradiation sensitive cells following wounding.
(A) By Bayesian phylogenetic analysis, the two identified planarian homologs of *runt* transcription factors cluster with *runt* transcription factors from other species, rather than other p53/RUNT-type transcription factors. Numbers shown are bootstrap values. (B-C). Wild type and lethally (6K) irradiated animals were amputated pre- and postpharyngeally, fixed at indicated time points and probed for *runt1* (B) and *runt2* (C) expression. Black arrowheads, wound-induced expression. White dotted lines, amputation planes. Amputated trunk fragments are shown, anterior to the left.

but also at very low levels in the parenchyma, where the planarian neoblasts reside (Reddien et al., 2005b). *runt1* was induced strongly in a discrete subset of irradiation sensitive cells between 3-6h following wounding and expression was found in more cells towards the wound site than in the middle of the fragment (Figure 3.29B). *runt2* was expressed predominantly at 3h, in a higher percentage of irradiation-sensitive cells than *runt1* and was distributed more evenly throughout the amputated fragment (Figure 3.29C). Both genes were first expressed broadly and then expression coalesced more strongly towards the wound site at time points that coincide with accumulation of neoblasts at the wound site (12-48h) (Figure 3.29B, C).

runt1(RNAi) animals did not regenerate photoreceptors (Figure 3.30A). Labeling with the photoreceptor neuron marker anti-arrestin antibody (Sakai et al., 2000) revealed that photoreceptor neurons were either absent or aberrantly formed and the optic nerves were severely distorted in these animals (Figure 3.30B). RNAi of *runt2* showed no visible gross regeneration defects by feeding or injection, potentially due to insufficient knockdown.
Increased neoblast proliferation and expansion occurs in many contexts. Feeding (Kang and

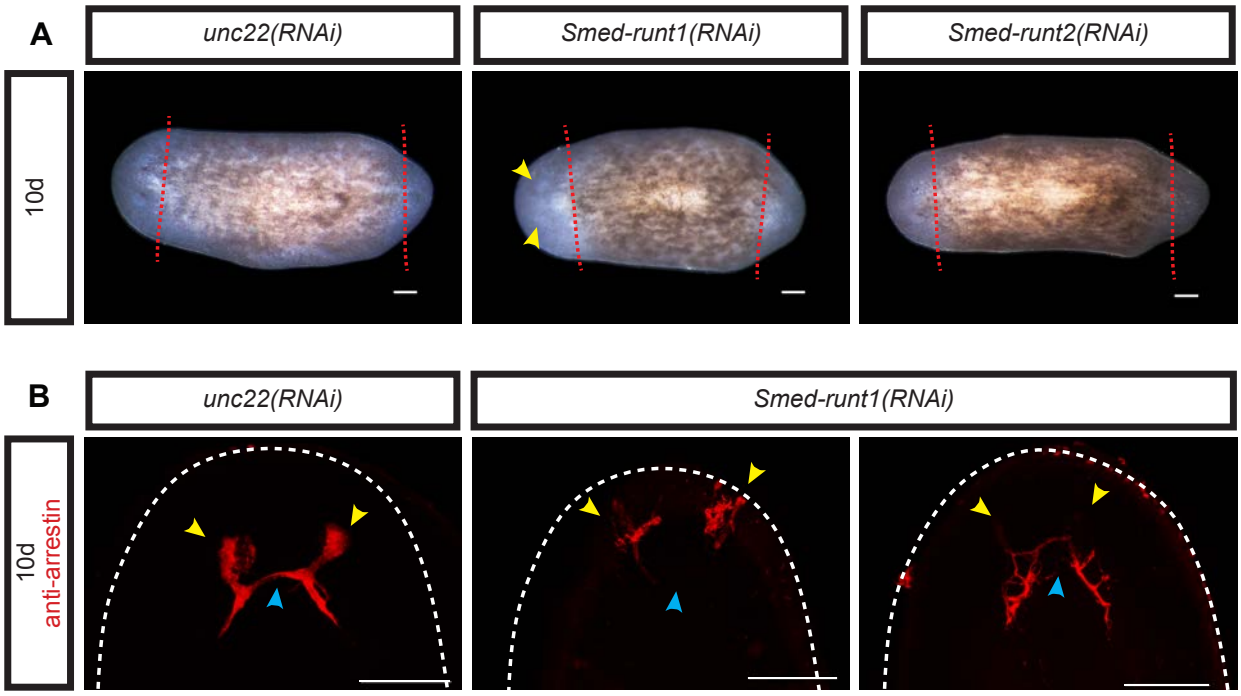

Figure 3.30. *runt1* is required for photoreceptor formation during regeneration.
(A-B) Animals were fed RNAi food for indicated genes four times (d0, d4, d8, d12) and amputated 6 days later. (A) Live images of RNAi animals at day 10 of regeneration. *runt1(RNAi)* animals showed no visible photoreceptor formation (10/10 animals, yellow arrowheads). *runt2(RNAi)* animals showed no gross regeneration defects. Red dotted line, approximate amputation plane. Anterior to the left. (B) Photoreceptor neurons (anti-arrestin antibody, red) are aberrantly placed, deformed, and partially missing in regenerating *runt1(RNAi)* animals (d10). White dotted line, outline of the animal. Yellow (photoreceptors) and blue (optic chiasm) arrowheads, regeneration defects. Anterior to the top. Scale bars, 100µm.

Alvarado, 2009), simple wounding and amputation (Chapter 3.1), as well as partial irradiation (Daniel E. Wagner, unpublished data), induce a wave of neoblast proliferation and expansion, respectively. To test whether induction of *runt1* expression is specific to wounding or occurs in any context of neoblast proliferation or expansion, we performed real time PCR on fed, partially irradiated, wounded and amputated animals at 6h (Figure 3.31A). *runt1* expression was strongly reduced in lethally irradiated animals as compared to intact wild type animals, indicating that *runt1* might be expressed in irradiation-sensitive cells at low levels in the intact animal (Figure 3.31A). Remarkably, *runt1* expression was strongly upregulated in amputated and incised animals (this effect was not observed for the neoblast marker *smedwi-1*, used as a control), but *runt1* expression was not upregulated in fed animals at 6h following the respective treatment (Figure 3.31A). Moreover, the increase in *runt1* expression was twice as high in amputated animals as compared to incised animals (Figure 3.31A). Neither *smedwi-1* expression, nor *runt1* expression were detectable in sublethally irradiated animals (1.K) (Figure 3.31A) and therefore no conclusions can be drawn from this data. To further assess the wound-specificity of *runt1* expression, we performed *in situ* hybridizations at 23h following wounding on animals that had been wounded in different ways (Figure 3.31B). At 23h following wounding, *runt1* expression was

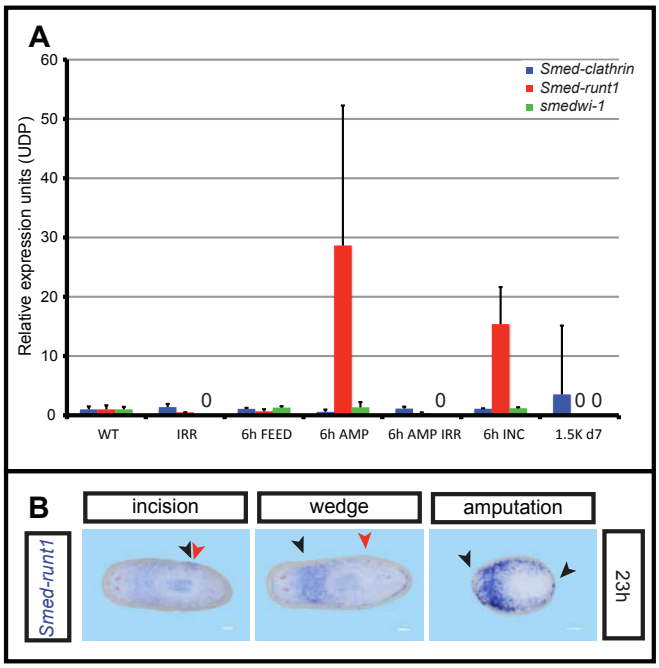

Figure 3.31. Wound-induced *runt1* expression scales with wound size.
(A) Expression of *runt1*, *smedwi-1* (a neoblast gene), and *clathrin* (a constitutively expressed gene) were assessed using qRT-PCR. RNA was extracted from different animals: wild type (WT), lethally (6K) irradiated at 7d following irradiation (IRR), 6h following feeding with egg white (6h FEED), 6h following amputation from wild type (6h AMP) and lethally irradiated (6h AMP IRR), animals with an incision wound (6h INC), and 7d following sublethal irradiation (1.5K d7). Data was calibrated to values obtained from the WT cDNA and *UDP-Glucose* was used as an endogenous control (Relative expression units). *runt1* was almost 30-fold upregulated following amputation in wild type, but not in irradiated animals. This was not observed for expression of *smedwi*-1. A 15-fold upregulation of *runt1* expression was observed in animals that had been incised 6h prior to RNA extraction. 0 = not detectable. (B) Animals were either wounded by poking animals in the tail (poke), incised behind the pharynx (incision), surgically removing a triangle of tissue behind the pharynx (wedge), or amputated pre- and postpharyngeally (amputation) and fixed at 23h. *in situ* hybridizations were performed probing for *runt1* expression. *runt1* expression is easily detectable at wounds that are associated with missing tissue (amputation). Black arrowheads, upregulated expression. Red arrowheads, wound site. White dotted lines, amputation planes. Amputated trunk fragments are shown, anterior to the left.

easily detectable in amputated animals, but less so in poked or incised animals (Figure 3.31B). Taking these findings together, we conclude that wound-induced *runt1* expression scales with wound size and is likely specific to wounding. It is also possible however, that the degree of expression in other contexts of neoblast expansion (such as following feeding) is too low to be detected with our methods.

We wanted to determine whether wound-induced *runt1* expression occurs preferentially in actively cycling cells or other irradiation-sensitive neoblast descendants that were described previously (Eisenhoffer et al., 2008) (Figure 3.32A-H). *runt1* expression at 6h following wounding is detectable by fluorescent *in situ* hybridization (Figure 3.32B, C). Importantly, all *runt1*$^{+}$ cells also labeled positively for the cell cycle marker *histone h2b* (Figure 3.32D), indicating that all cells expressing *runt1* following wounding are cycling (Hewitson et al., 2006). The double-labeling technique is suitable to detect double-positive cells as shown by double labeling of *runt1* with itself (Figure 3.32E). We also found that *runt1* can be expressed in mitotic cells as shown by co-labeling with the mitotic marker anti-H3P (Figure 3.32E). Furthermore, all *runt1*$^{+}$ cells were positive for the X1 marker *smedwi-1* (Figure 3.32F). Despite the fact that the progeny cells labeled with *NB.21.11E* and *Smed-AGAT-1* overlap with other Category 1 markers, such as *smedwi-1* (Eisenhoffer et al., 2008), and show co-labeling with the mitotic marker anti-H3P, we were unable to detect co-localization of these markers with *runt1* (Figure 3.32G, H). This suggests that wound-induced *runt1* expression occurs preferrentially in *smedwi-1*-positive neoblasts, but none of their tested progeny.

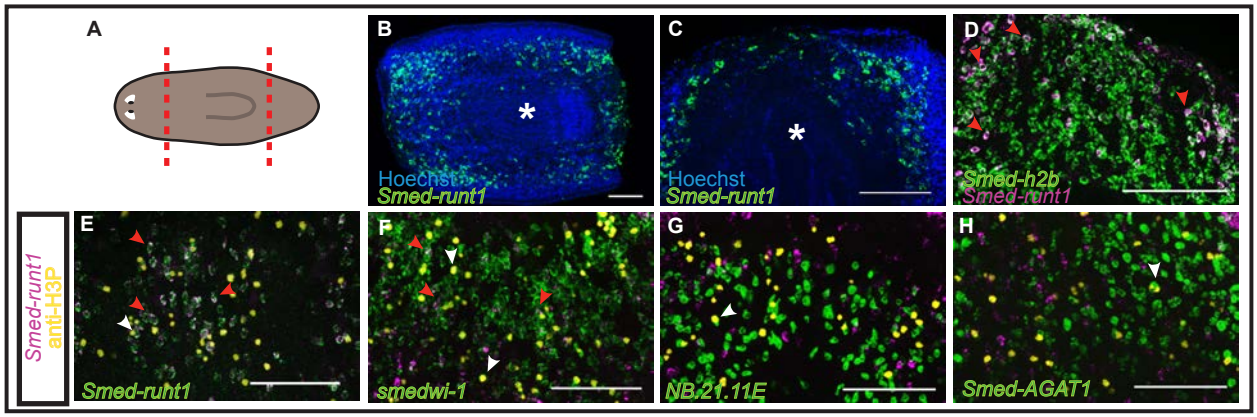

Figure 3.32. *runt1* expression overlaps with expression of neoblast markers, but not with expression of tested neoblast descendant markers.
(A) Cartoon illustrating amputation procedure. (B-H) Animals were amputated pre- and postpharyngeally, fixed at 6h following wounding, and FISH was performed probing for indicated makers. (B-C) *runt1* expression (green) is visible in parenchymally located cells and more expressing cells are visible towards the wound site. Nuclei are labeled with Hoechst (blue). Asterisk, pharynx. (A-B) Anterior, left. (D-H) *runt1* (magenta). (D) *runt1* expression always co-localizes with *histone h2b*. (E) *runt1* (magenta) always co-localizes with *runt1*. (F) *runt1* co-localizes with *smedwi-1*. *runt1* expression does not overlap with (G) *NB.21.11E*- or (H) *AGAT-1* expression. Anterior wound sites of regenerating trunk fragments are shown. Red arrowheads, co-localization of *runt1* expression with expression of second tested marker. White arrowheads, co-localization of marker expression (green) with mitoses (anti-H3P, yellow). Anterior, top, unless otherwise stated. Scale bars, 100µm.

3.3.2 Gene expression analysis reveals a role for *Smed-runt1* in neuronal lineage commitment

runt1 is strongly expressed in a subset of neoblasts following wounding and *runt1(RNAi)* animals do not regenerate photoreceptors following wounding (Figure 3.30). To identify gene expression affected by the role of wound-induced *runt1* expression, we performed a microarray experiment using RNA extracted from *runt1* RNAi animals. RNA was extracted from intact and wounded control (*unc-22*) and *runt1(RNAi)* animals at 9h and 24h following wounding. These time points were chosen to test for a potential effects that occurs downstream of the wound-induced expression at 3-6h and wound site accumulation at 12-18h (Figure 3.29). We showed earlier that wound-induced *runt1* expression occurs only in a subset of *smedwi-1*-positive cells, which make up 2-8% of the total cells in the animal (Reddien et al., 2005b). It is therefore possible that potential expression changes following inhibition of *runt1* function would happen only in a very small number of cells and would be too weak to be detected, when comparing RNA extracted from entire fragments. We therefore decided to also isolate RNA at 9h from the cycling X1 fraction (Eisenhoffer et al., 2008; Reddien et al., 2005b). Most of the X1 cells express *smedwi-1;* and because all *runt1* cells were found to be positive for *smedwi-1*, the X1 fraction will contain the cells that express *runt1* following wounding. Analysis of the microarray data revealed that knockdown of wound-induced *runt1* expression was efficient, at all time points following wounding (Figure 3.33A). However, the data obtained from isolated X1 fractions was found to be the more sensitive than the data obtained from entire fragments and will therefore be discussed here.

Among the genes that were significantly downregulated following wounding in neoblasts

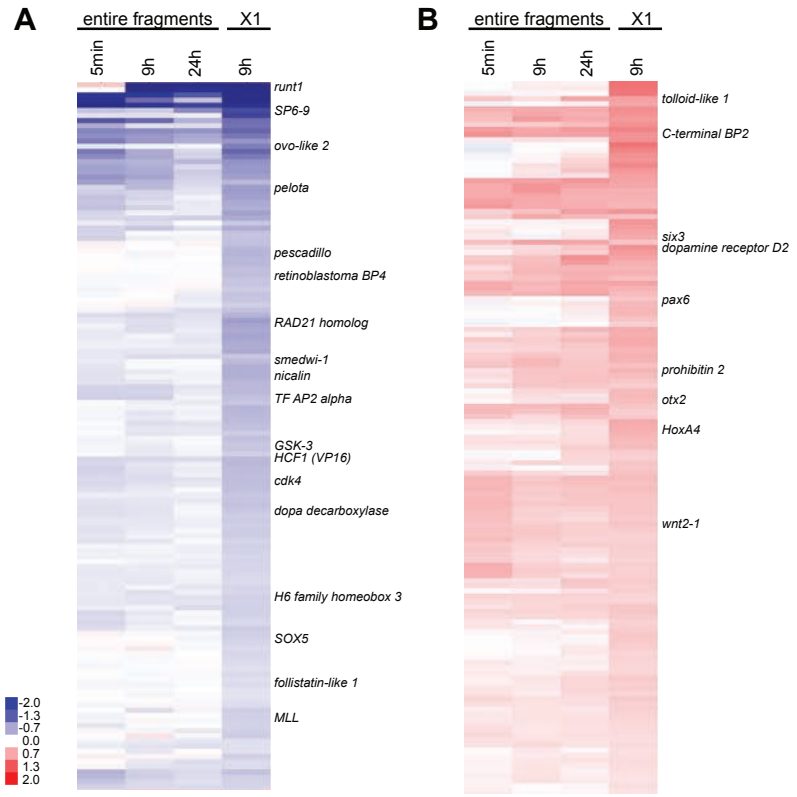

Figure 3.33. *runt1* RNAi causes aberrant expression of transcriptional regulators involved in neuronal development. RNAi animals were fed *runt1* and *unc22* RNAi food four times (d0, d4, d8, d12) and amputated 6 days later. RNA was extracted from entire fragments and from sorted neoblasts (X1) at indicated time points. Significant = $p < 0.05$. Heatmap of genes that are (A) downregulated or (B) upregulated at 9h following wounding in X1 cells isolated from *runt1(RNAi)* animals as compared to control *(unc22)* wounded animals.

isolated from *runt1(RNAi)* animals (Figure 3.33), many encode homologs of transcription factors that have been implicated with neuronal development and specification, such as *Ovo-like2* (Mackay et al., 2006), *SP6-9* (S. Lapan, *submitted*), *H6 family homeobox 3 (HMX2/3)* (Wang et al., 2004), *SRY (sex determining region Y)-box 5 (SOX5)* (Kwan et al., 2008; Lai et al., 2008; Morales et al., 2007) were downregulated. Moreover, other important developmental regulators, such as transcription factor *AP-2 alpha (activating enhancer binding protein 2 alpha) (TFAP2A)* (Milunsky et al., 2008), and *myeloid/lymphoid or mixed-lineage leukemia (trithorax homolog, Drosophila) (MLL)* were downregulated (Klebes et al., 2005). Many of the described genes are involved in proper eye (S. Lapan, *submitted*) or nervous system formation. Moreover, important key players in cell cycle, especially G1/S transition, such as *cdk4* (Tam et al., 1994), *Rb binding protein 4* (Nicolas et al., 2000), *Rad21* (Beauchene et al., 2010), *host cell factor C1 (VP16-accessory protein) (HCF1 (VP16))* (Mangone et al., 2010), *pelota* (Adham et al., 2003), *smedwi-1* (Reddien et al., 2005b), and *pescadillo* (Kinoshita et al., 2001) were downregulated in this data set. *GSK3* and *nicalin*, inhibitors of Wnt- (Rubinfeld et al., 1996) and Nodal/Activin-signaling (Haffner et al., 2004) signaling, respectively, were also downregulated in this data set (Figure 3.33A). Among the genes that were significantly upregulated in neoblasts isolated from *runt1(RNAi)* animals (Figure 3.33B), are genes encoding homologs of nervous system specific and developmentally important transcription factors, such as *six3* (Oliver et al., 1995; Serikaku and Otousa, 1994), *pax6* (Denes et al., 2007; Ericson et al., 1997), *hoxA/D4* (Hunt et al., 1991), *otx2* (Ang et al., 1996; Royet and

Finkelstein, 1995), and other genes involved in brain development, such as *dopamine receptor D2* (Schambra et al., 1994) and *Rac1* (Kumanogoh et al., 2001). Moreover, transcriptional regulators, such *as C-terminal binding protein 2* (Nibu et al., 1998), *prohibitin 2*, the BMP-signaling promoting metalloproteinase *tolloid*, and *wnt2-1*, were upregulated (Figure 3.33B). Together, these data suggest that *runt1* expression following wounding is directly or indirectly required for proper expression of cell cycle components and induction of expression as well as repression of transcriptional regulators that are implicated in eye- and brain-development, and to possibly favor anti-wnt, anti-TGFβ environment.

Taken these findings together, we conclude that *runt1* is upregulated in planarian neoblasts following wounding and that wound-induced expression scales with wound size. Moreover, *runt1* is required for photoreceptor formation during regeneration, which may be due to a requirement for *runt1* in specification of neuronal progenitors following wounding.

4 Discussion

4.1 Wounding and amputation involve distinct responses in planarian neoblasts

Planarian regeneration provides a powerful system for studying the regenerative response of adult stem cells following different types of injuries. Utilizing histological and molecular tools that have only recently become available, we characterized changes in planarian neoblasts that occur following wounding. Two distinct mitotic peaks were apparent early in the process of planarian regeneration, consistent with studies performed previously in *Schmidtea mediterranea* and *Dugesia tigrina* (Baguñà, 1976b; Saló and Baguñà, 1984). We provide evidence that the two described mitotic peaks have distinct properties indicative of two phases of regeneration initiation, with independent underlying signaling events. Together, our data suggest a model for planarian regeneration initiation (Figure 4.1) that involves two phases of wound responses. First, wounds trigger entry into mitosis at long distances (body wide); induction of cell cycle changes distant from the site of injury is a novel property of wound-induced signaling. Second, tissue absence is detected, which triggers recruitment of neoblasts to wounds. Neoblasts are then signaled to divide near the wound and they commit to production of cells at the wound that will exit the cell cycle and differentiate (Figure 4.1).

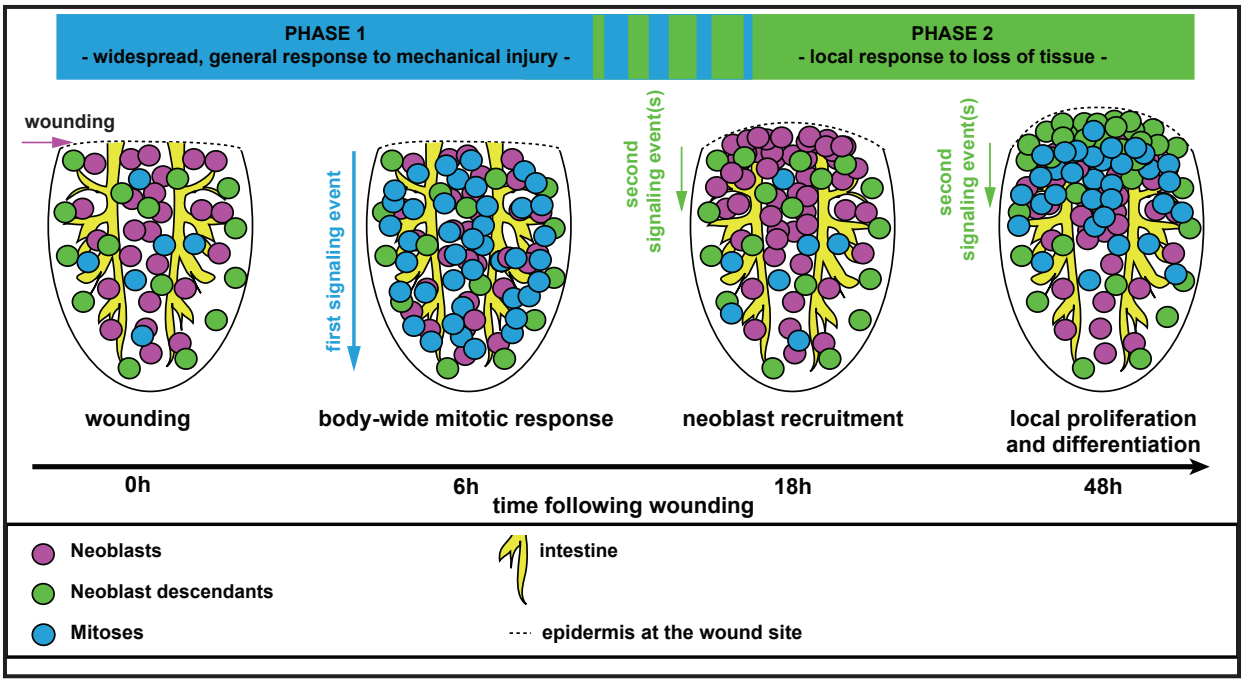

Figure 4.1. Model of the planarian neoblast wound response.
Cartoon summarizing cellular changes during regeneration initiation. Two distinct phases of neoblast responses occur during regeneration initiation. The first phase represents a generic response to injury that spreads quickly from the wound site, is wound-size dependent, and induces increased mitotic entry of neoblasts body-wide. The second phase occurs only when a significant amount of tissue is missing and involves local signals that induce recruitment of neoblasts followed by local proliferation and differentiation at the wound site. Depicted are posterior (tail) fragments.

4.1.1 The response to wounds and the first mitotic peak

We found an immediate and broad increase in mitoses that peaks between 4-10 hours following wounding. An immediate increase in mitotic numbers had been observed before in *S. mediterranea* (Baguñà, 1976b) and *Dugesia tigrina* (Saló and Baguñà, 1984). Surprisingly, a simple poke with a needle sufficed to trigger this body-wide, mitotic response. Our data provide evidence for a broad and fast-acting signal, that scales with wound-size, and that spreads quickly from wounds.

We did not detect robust changes in the numbers of S-phase cells in the first 6h after injury, suggesting that the wound signal acts primarily on G2/M progression of the cell cycle to shorten G2. However, because the number of mitotic cells is very small in comparison to the number of cells in S phase, it is still possible that a minor, undetected change in the S phase cell numbers would be sufficient to cause a 4-10 fold increase in mitotic numbers. Considering data from previous studies (Newmark and Sánchez Alvarado, 2000; Saló and Baguñà, 1984), it seems likely that cells that were both in G2 and S-phase at the time of injury contribute to the first mitotic peak with the increase in mitotic numbers caused by acceleration of G2.

In hydra, it has been shown that 4 hours following head, but not foot amputation, an immediate apoptosis-induced increase of proliferation occurs (Chera et al., 2009). In planarians it has been shown that a simple incision is sufficient to induce a localized increase in apoptosis at the wound site by 4 hours (Pellettieri et al., 2010). Whether this localized cell death is involved in the induction of the broad, first mitotic peak remains to be determined; however, the spatial distributions of mitoses and apoptotic cells following injury differ. Rapid, organ-wide, wound-induced gene expression changes have been described recently in zebrafish heart regeneration (Lepilina et al., 2006). The possibility thus exists that early broad-acting wound signals will be found in many regenerating organisms. The identity of regeneration signals that are induced by wounds and exert influence at long distances is unknown.

4.1.2 The response to missing tissue and the second mitotic peak

Our experiments show that loss of tissue is the key event for recruitment of neoblasts to wounds and their subsequent local proliferation and differentiation during the second mitotic peak. To our knowledge, no prior paradigm has indicated any mechanism by which tissue absence – rather than simply injury – is detected and causes a response in stem cells. Therefore, the molecular mechanisms by which regenerating organisms detect tissue absence will be of great interest for understanding regeneration.

We found that neoblasts are recruited to wound sites involving missing tissue. This indicates the existence of a candidate stem cell migratory signal that is induced following the detection of tissue absence. There exist previous conflicting reports on neoblast migration in

regeneration. In one study, animals with one half of their body irradiated displayed degeneration in the irradiated region unless they were amputated—supporting the idea that amputation induced neoblast recruitment (Wolff and Dubois, 1948). Subsequent studies using tissue grafts and chromosomal and nuclear markers to track neoblasts led to the proposal that neoblast movement is explained through passive spreading by cell division (Salo and Baguñà, 1985; Saló, 1989). Our data use molecular markers of neoblasts and demonstrate the capacity of neoblasts to migrate to wounds in animal head tips—a region normally devoid of neoblasts.

The cells that accumulate at wounds are cycling, but not initially mitotic. Therefore, whereas the initial wound response (the first peak) involves a mitotic response, the missing-tissue response involves migration of cells that proceed through S phase and result in a later, local mitotic peak (the second peak). The observed increase in NUCLEOSTEMIN signal (nucleolar marker) within neoblast progeny cells at wounds suggests these cells have an increased growth rate. Nucleolar size also increases at the wound site in the regenerating organism *Lumbriculus* (Sayles, 1927). At 48h post amputation, we also found an accumulation of neoblast progeny expressing differentiation markers. Because we did not observe a notable decrease in neoblast descendant numbers in areas far away from wounds, this accumulation is probably not due primarily to migration of descendants, but local differentiation. Therefore, there exists a signal induced by tissue loss that induces a greater incidence of differentiation of neoblast progeny, as opposed to retention of neoblast identity, near the wound.

Local accumulation of S-phase cells at wound sites, followed by an increase in mitoses is a phenomenon observed in multiple regenerating systems. For example, S-phase cells accumulate at wounds within 12-24h following posterior amputation in the flatworm *Macrostomum lignano* (Egger et al., 2009), during rodent liver regeneration (Taub, 1996), during zebrafish fin regeneration (Nechiporuk and Keating, 2002), and in *Drosophila* wing disc regeneration (Bosch et al., 2008). In most of these cases, an increase in mitotic numbers is observed within the day following recruitment, suggesting that the recruited cells undergo mitosis. In the wing disc, genetic ablation of cells is sufficient to induce proliferation (Smith-Bolton et al., 2009). In the *Drosophila* midgut, stem cell proliferation can also be augmented in response to different stimuli (e.g. detergent and bacterial ingestion) (Amcheslavsky et al., 2009; Buchon et al., 2009a; Jiang et al., 2009); like the planarian second peak, mitoses were found to peak between one and two days following stimulus exposure. Mechanisms for detection of tissue absence may prove to be an important general feature of animal wound responses and regeneration.

It will be important in future studies to determine whether any heterogeneity of neoblasts that respond to wound signals exists and to characterize in more detail the process of blastema outgrowth. However, our data illuminate a series of events that lead to a blastema: detection of missing tissue leads to signaling that results in neoblast accumulation; some cells produced by

these neoblasts will continue to divide locally and some will leave the stem-cell state near the wound epidermis to initiate blastema formation.

The identification of cellular changes during regeneration initiation in planarians and the establishment of a neoblast wound-response assay provide powerful tools for the molecular dissection of stem cell-mediated regeneration using planarians as a model system. We conclude that regeneration initiation in planarians involves two distinct stem cell responses: an early systemic response to any injury and a later, local response that is uniquely caused by tissue absence, indicating that separate signaling mechanisms exist in regeneration to distinguish between simple injury and loss of tissue.

4.2 A transcriptional network that is associated with planarian regeneration initiation

The ability to restore tissue integrity following wounding and to subsequently repair damaged or lost structures is fundamental to the survival of all multicellular organisms. This task requires a robust and well-coordinated mechanism for rapid induction of factors that are needed for faithful regeneration of the damaged structures. It can therefore be expected that many factors act together to ensure restoration of the appropriate tissue. Immediate early genes are expressed in response to external stimuli in a variety of biological contexts and mediate long-term changes in gene expression (Lewis, 1980;Abraham, 1991;Chavrier et al., 1988; Iyer et al., 1999;Schreiber et al., 1991; Wollnik et al., 1993;Cooper et al., 2005; Stramer et al., 2008). Remarkably, this is also the case during planarian regeneration initiation. We found that following wounding, immediate early genes are induced by latent (i.e., pre-existing) transcription factors, such as serum response factor (SRF) and induce, at least partially, expression of wound-induced factors that are required for body patterning and proper regeneration (Figure 4.2A, B). Two temporally and functionally distinct waves of immediate early gene expression were detected at all types of wounds and that are expressed in the differentiated tissue. Using multiplex expression analysis, probing for wound-induced gene expression in RNAi animals we found that some of the factors which are induced in the first immediate early wave were required for regulation of late wave gene expression (Figure 4.2A). This finding is further supported by the fact that immediate early genes of the first wave were expressed in the same cells as genes from the late wave following wounding. Remarkably, late wound-induced gene expression was also induced by all types of wounding and included factors that are required for proper patterning and regeneration in planaria (Figure 4.2A). This suggests that mechanisms, to restrict the expression of patterning factors to the appropriate tissue following generic wound-induced expression exist and are a common strategy during planarian regeneration initiation. Maintenance of wound-induced gene expression depended on the type and amount of missing structure. Notably, we identified non-wound-induced factors whose function was required for normal wound-induced gene expression—in cells of the

differentiated tissue as well as planarian neoblasts—suggesting that these factors act to mediate signaling from wounds (Figure 4.2A, B). These data provide the first insight into the gene regulatory networks that underlie regeneration initiation in planarians and provide an exciting opportunity to systematically dissect the molecular mechanisms that act to initiate regenerative events. Given that many of the genes we identified function as immediate early genes in other contexts, the possibility also exists that further studies into planarian wound-response factors could shed light on more broadly conserved wound-response mechanisms.

4.2.1 Two temporally and functionally distinct waves of wound-induced immediate early gene expression are observed at all wounds

Our experiments identified two waves of wound-induced gene expression whose induction was independent of *de novo* protein synthesis. Genes of the first wave were expressed within 30min following wounding in subepidermal cells at the wound site and encoded homologs of established immediate early genes, mainly transcription and signaling factors (*jun*, *c-fos*, *egr1*, *egr1b*,

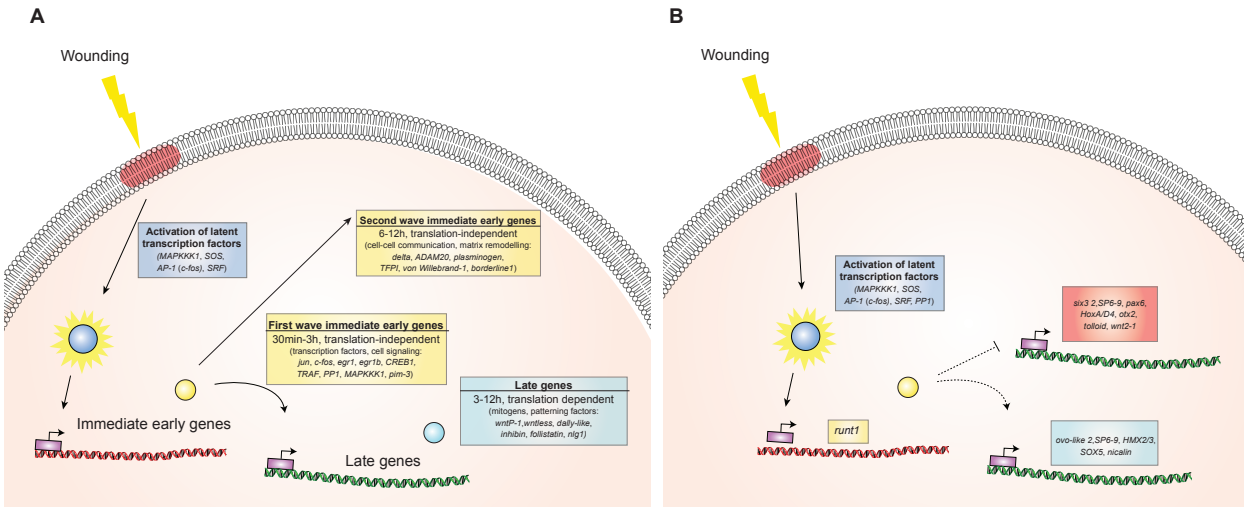

Figure 4.2. Model of the transcriptional network that is associated with regeneration initiation in planarians.
(A-B) Cartoons illustrating the functional relationship of factors that are expressed following wounding. Depicted is a schematized cell, nuclear membrane omitted. Only genes that were identified in this study are represented in the figure. (A) Wound signaling activates functionally and temporally distinct waves of gene expression. First, wound signaling leads to activation of latent transcription factors that consequently activate transcription of immediate early genes. Immediate early genes are expressed in two temporally distinct waves (first wave 30min-3h; second wave 6-12h) and comprise genes that encode homologs of functionally distinct factors (i.e., transcription factors and intracellular signaling versus cell-cell signaling and matrix remodeling). Notably, genes that are upregulated during these two immediate early gene waves are also expressed in very different areas of the wounded animal (i.e., first wave genes were expressed directly at the wound site in subepidermal cells; second wave genes are expressed away from the wound or around the periphery of the fragment in a more superficial layer of cells). Immediate early genes (from the first wave) then act, at least in part, to induce (or in some cases repress, not shown in the figure) expression of wound-induced genes that are expressed in a translation-sensitive manner at later time points following wounding (3-12h). Many genes in this category represent homologs of developmentally important morphogens and factors that are required for patterning of body structures during regeneration and development in planaria and other species. (B) Wound signaling induces expression of cell cycle factors, chromatin components, and transcription factors in planarian neoblasts. Wound signaling in neoblasts is at least in part mediated through a homolog of *serum response factor* (*SRF*). *Smed-runt1* expression is induced in neoblasts upon wounding (*SOS*- and *SRF*-dependent) and acts directly or indirectly (dotted lines), to regulate transcription of factors that are involved in eye and nervous system formation in planaria and other species.

PP1) (Chavrier et al., 1988; Iyer et al., 1999; Lamph et al., 1988; Muller et al., 1984; Wang et al., 2000). Immediate early gene expression was mostly transient and inhibition of protein synthesis led to over-expression of these genes. This phenomenon has been observed in other systems (Campisi et al., 1984; Greenberg et al., 1986; Kelly et al., 1983), and it was shown that absence of protein translation can lead to an increased half-life of the associated mRNAs (Lau and Nathans, 1987). Moreover, it has been postulated that the gene products of immediate early genes are involved in autoinhibition of immediate early gene expression (Skar et al., 1994). Expression of genes of the later immediate early wave was observed between 6-12h following wounding, and this expression displayed high spatial variability with respect to the wound site. Like the first wave of immediate early expression, expression of late immediate early genes was also over-induced following translation inhibition. Genes of this wave encoded mainly homologs of factors that are involved in extracellular matrix remodeling as well as a notch ligand, a member of a developmentally important pathway involved in cell-cell communication (*ADAM20*, *plasminogen*, *tissue factor pathway inhibitor*, *delta*) (Alton et al., 1989; Hooft van Huijsduijnen, 1998; Kocholaty et al., 1952; Lindahl et al., 1994). Despite the temporal and potentially functional distinctions between these two waves, we found that both are generically induced by all types of wounds and that their expression level scales with wound size. Immediate early genes are expressed in many different biological contexts and are considered the “gateway to the genome”, because their expression can be rapidly induced by many factors and they act to regulate required long-term gene expression changes for generation of an appropriate response to a stimulus (Abraham, 1991; Herschman, 1991; Schreiber et al., 1991). In human cells that were stimulated by exposure to growth factors, the temporal difference in induction of immediate early gene waves (referred to as immediate early and delayed primary response genes) was associated with distinct modifications of the chromatin architecture (Thomson et al., 2001; Tullai et al., 2007). It was proposed that this difference is consistent with a functional role of the first immediate early gene wave as mediators, and the second immediate early (delayed primary response) genes as effectors, of growth factor signaling (Tullai et al., 2007). Promoters of immediate early genes in other systems are very complex and hence, allow continuously variable regulation of gene expression (Hazzalin and Mahadevan, 2002).

4.2.3 Late waves of wound-induced gene expression are induced by all types of wounds and include factors that are required for proper patterning during regeneration

Late wound-induced gene expression occurred at 3-12h following wounding and expression was partially or entirely dependent on protein translation. A large proportion of these genes encode homologs of patterning factors (*wntless*, *wntP-1*, *nlg1*, *inhibin*, *dally-like*, *follistatin*), some of which have been shown to be required for proper patterning and regeneration in planaria here

(*dally-like*, *follistatin*) and in previous studies (*wntless*, *wntP-1*) (Adell et al., 2009; Petersen and Reddien, 2009). Wound-induced expression of most genes in this class was observed in subepidermal cells adjacent to the wound site and overlapped with expression of immediate early genes, albeit in fewer cells, consistent with a possible requirement of immediate early gene expression for late gene expression. Remarkably, expression of these genes was also generically induced by all types of wounding. However, long-term expression of these genes was found to require loss of tissue and in some cases expression became axially polarized over time (*nlg1*, *wntP-1*). These later changes in expression suggest a role for some late wave genes in the specification of missing tissue, as they are among the earliest changes in gene expression following wounding that reflect recognition of axial polarity.

4.2.4 Immediate early genes are required for normal wound-induced expression of late wave genes

Studies in other systems demonstrate that immediate early genes transcriptionally regulate downstream effector genes in response to a variety of stimuli in a variety of biological contexts (Herschman, 1991; Winkles, 1998). Our findings indicate that the planarian wound-induced immediate early genes *c-fos* and *MAPKKK1* are required for normal expression of late wave genes following wounding. This defect suggests that these factors may directly regulate later wave gene expression. Alternatively, the possibility also exists that, as RNAi was performed prior to amputation, some of the observed defects in gene expression could be caused by defects in direct mediation of the wound signal. This possibility is particularly relevant given that genes from the immediate early groups I and II are affected in these conditions. Interestingly, many of the wound-induced genes that require function of *c-fos* are also downregulated in *MAPKKK1(RNAi)* animals (a planarian homolog of MAP3K). This is consistent with the observation that in other systems, MAP kinase signaling (JNK, ERK, p38, downstream targets of MAP3K) can activate AP-1 transcription factors, which are homo- and heterodimers of Jun and Fos family proteins, and have been implicated in regulation of various biological processes, including cell proliferation, differentiation, apoptosis, immune responses, and tumorigenesis (Eferl and Wagner, 2003; Hsu et al., 1992). AP-1 transcription factors alter transcription of target genes in response to exposure to a variety of stimuli, ranging from growth factors to stress (Eferl and Wagner, 2003).

4.2.5 A planarian homolog of *SRF* is required for wound-induced gene expression in neoblasts

Our findings indicate that a complex system of factors acts to coordinately regulate wound-induced gene expression, which is required for restoration of damaged tissue in planarians. Importantly, regeneration of missing structures also requires rapid proliferation and differentiation

of planarian neoblasts, the cells that give rise to new tissue. We identified many planarian genes that encode homologs of cell cycle components, chromatin remodeling, and transcription factors (*cyclin B1-3*, *aurora kinase A/C*, *ribonucleotide reductase*, *cdc25C*, *HP1*, *H2A.Z*, *runt1*, *runt2*) (Chabes et al., 2004; Coffman, 2003; Evans et al., 1983; Heald et al., 1993; Kelly et al., 2010; Lens et al., 2010; Paro and Hogness, 1991), which are transcriptionally induced following wounding in the neoblasts. Wound-induced expression of many of these genes (except *runt2*) depends at least partially on protein translation. Here, we demonstrated that a planarian gene encoding a homolog of serum response factor, *SRF*, is required for wound-induced expression of many of these neoblast-specific genes, which is surprising given that many wound-induced neoblast genes were found to be translation sensitive. *runt1* expression was found to be partially sensitive to translation inhibition, making it together with *runt2* a potential direct target of SRF-induced gene expression. SRF is a MADS box transcription factor (Norman et al., 1988) that binds to serum response elements (SRE) to activate transcription of target genes (i.e., immediate early genes) in cooperation with partner proteins, such as members of the TCF (ternary complex factor) family and can act to induce immediate early gene induction (Gille et al., 1992; Poser et al., 2000). Activation of SRF can be mediated by MAPK-signaling (Alberts et al., 1998; Hazzalin and Mahadevan, 2002). Conditional knockout studies in mice have demonstrated that SRF is an essential regulator of neuronal-activity-induced (immediate early) gene expression, neuronal precursor cell migration, and morphological neuron differentiation (Alberti et al., 2005; Etkin et al., 2006; Ramanan et al., 2005). Remarkably, liver-specific conditional *SRF* was also required for induction of cell cycle components during liver regeneration following partial hepatectomy (Latasa et al., 2007). Our findings demonstrate that the planarian homolog of *SRF* is required for induction of wound-induced genes in planarian neoblasts, indicating a potential conservation of the gene regulatory mechanisms that govern regeneration initiation in different species.

4.3 *Smed-runt1* is a Runt transcription factor that acts in planarian neoblasts following wounding and is required for proper regeneration of neuronal structures

We have shown that planarian neoblasts are induced to proliferate following wounding, recruited to the wound site, and induced to differentiate to give rise to missing structures. Consequently, many genes whose expression is induced in neoblasts following wounding encode homologs of factors that are involved in cell proliferation and differentiation. Furthermore, as our data above indicate, some of these genes require *SRF* for normal wound-induced expression (Figure 4.2B).

Two of the genes identified as upregulated in neoblasts following wounding encode homologs of a family of evolutionary conserved Runt transcription factors (Sullivan et al., 2008), which are thought to be important for the decision making process between cell cycle and differentiation (Coffman, 2003) and are involved in many developmentally important processes

in other species. These processes include segmentation, hematopoiesis, and eye development in *Drosophila* (Gergen and Wieschaus, 1985; Li and Gergen, 1999), regulation of lateral hypodermal stem cell (seam cell) divisions in *C. elegans* (Kagoshima et al., 2007), as well as hematopoesis, osteogenesis and neurogenesis in the dorsal root ganglia in mammals, among other roles (Coffman, 2003; Miller et al., 2002; Speck and Gilliland, 2002).

Here, we demonstrated that planarian *runt1* is specifically upregulated following wounding in planarian neoblasts and that *runt1* the number of cells that express *runt1* following wounding, scales with wound size. Moreover, *runt1* expression was required for proper formation of photoreceptor neurons during regeneration. Molecular analysis of *runt1(RNAi)* animals revealed that *runt1* is required in planarian neoblasts for regulation of many transcriptional regulators that are involved in nervous system formation in other species. Remarkably, genes that encode homologs of factors that are involved in eye- and brain development in other species were downregulated in neoblasts from *runt1(RNAi)* animals (*ovo-like2*, *SP6-9*, *HMX2/3*, *SOX5*) (Kwan et al., 2008l; Lai et al., 2008; Mackay et al., 2006; Morales et al., 2007; Wang et al., 2004). Moreover, genes that encode homologs of factors that are involved in morphogen-signaling were also downregulated (*GSK3*, *nicalin*) (Haffner et al., 2004; Rubinfeld et al., 1996). Importantly, GSK3 function has also been associated with neuronal cell development and maintenance in planarians and other species (Adell et al., 2008; Chiang et al., 2009; Hur and Zhou, 2010; Yokota et al., 2010). Neoblasts isolated from *runt1(RNAi)* animals also displayed upregulation of many genes that encode homologs of nervous system specific and developmentally important transcription factors (*six3*, *pax6*, *hoxA/D4*, *otx2*) (Ang et al., 1996; Denes et al., 2007; Ericson et al., 1997; Hunt et al., 1991; Oliver et al., 1995; Royet and Finkelstein, 1995; Serikaku and Otousa, 1994). Homologs of genes that are involved in BMP- and WNT-signaling were also upregulated (*tolloid*, *wnt2-1*) (Petersen and Reddien, 2008; Reddien et al., 2007). These data indicate that wound-induced *runt1* expression in planarian neoblasts is required for proper formation of nervous system structures during regeneration, possibly by acting in neuronal progenitors for specification of specific neuronal lineages (Figure 4.2B). Several studies suggest, that Runt proteins can be required during development in other species for regulation of lineage-commitment in neuronal precursors and in post-mitotic neurons for development of neuronal subtypes (Zagami et al., 2009). This suggests that *runt* transcription factors may play a conserved role during development and regeneration in helping to specify the fate of cells contributing toward new tissue.

5 Abstract / Zusammenfassung

5.1 Abstract

Regeneration requires signaling from a wound site for detection of the wound, and a mechanism that determines the nature of the injury to specify the appropriate regenerative response. *Schmidtea mediterranea* planarians are able to regenerate from essentially any type of injury. They represent an emerging model organism for the study of regeneration and stem cell regulation. The first part of my thesis focuses on identification of cellular changes in planarian stem cells—neoblasts—during regeneration initiation. Neoblasts divide during two spatially and temporally distinct mitotic waves following tissue removal. Prior to the second mitotic wave, neoblasts were recruited to wound sites, and subsequently induced to differentiate, but only at wounds that were associated with loss of tissue. This indicates that separate stem cell responses exist following wounding that distinguish between simple injury and loss of tissue.

The second part of my thesis identifies a transcriptional network that is associated with regeneration initiation in planarians. Wounding induces two temporally and functionally distinct waves of immediate early gene expression that do not require *de novo* protein synthesis. Some of the products from the first immediate early gene wave, such as *c-fos*, then act to induce genes of the late, translation-sensitive wave of wound-induced gene expresseion, some of which are required for patterning during regeneration. A homolog of Serum response factor (*SRF*) is required for wound-induced induction of genes that are specifically expressed in neoblasts, which is consistent with findings in mouse models during liver regeneration, suggesting that conserved mechanisms may exist to induce regenerative events in different species.

Smed-runt1, a planarian homolog of Runt transcription factors, which have a evolutionary conserved role in cell fate specification, is expressed specifically in planarian neoblasts following wounding. Inhibition of *Smed-runt1* function, using RNA interference, leads to aberrant nervous system regeneration. Gene expression analysis on such animals indicates that *Smed-runt1* acts early following wounding in neoblasts to regulate expression of genes that encode developmentally important factors relevant to nervous system formation in other organisms.

5.2 Zusammenfassung

Zur Regeneration benötigt es Signale, die von der Wunde ausgesendet werden und die der Erkennung der Wundstelle dienen. Ausserdem bedarf es eines Mechanismus, der die Art der Verwundung identifiziert, um die angebrachten regenerativen Schritte einzuleiten. Planarien der Gattung *Schmidtea mediterranea*, können sich von nahezu jeglicher Art der Verwundung regenerieren und sind ein zunehmend anerkannter Modelorganismus zur Erforschung von Regeneration und Stammzellregulation. Der erste Teil meiner Doktorarbeit konzentriert sich auf die Charakterisierung der zellbiologischen Veränderungen, die in den Neoblasten, den Stammzellen von Planarien, während der ersten regenerativen Ereignisse vorgehen. Nach der Entfernung von Gewebe, findet die Zellteilung der Neoblasten in zwei zeitlich und räumlich unterschiedlichen Wellen statt. Vor Beginn der zweiten Teilungswelle, werden Neoblasten zur Stelle der Verwundung rekrutiert und anschliessend ihre Differenzierung induziert. Dies geschieht jedoch nur, wenn die Verwundung Entfernung von Gewebe involvierte. Dies weist darauf hin, dass unterschiedliche Wundantworten der Stammzellen existieren, die zwischen einfacher Verwundung und Gewebsverlust unterscheiden.

Der zweite Teil meiner Doktorarbeit, charakterisiert ein transkriptionelles Netzwerk, das mit den ersten regenerativen Ereignissen verknüpft ist. Verwundung induziert die Expression von zwei zeitlich und funktionell unterschiedlichen Wellen von “immediate early” Genen. Ein Vorgang, der unabhängig von *de novo* Proteinsynthese ist. Einige der Produkte der ersten “immediate early” Genexpressionswelle, zum Beispiel *c-fos*, aktivieren die Expression der späten Gene. Expression der späten Gene ist abhänging von *de novo* Proteinsynthese. Einige Vertreter dieser Gruppe spielen eine wichtige Rolle in der Regeneration der korrekten Strukturen. Ein Homolog von Serum response factor (*SRF*) wird für die wund-induzierte Genexpression in Neoblasten benötigt; ein ähnlicher Effekt, der auch während der Leberregeneration von Mäusen beobachtet wurde, was darauf hindeutet, dass konservierte Mechanismen existieren könnten, die Regenerationsvorgänge in verschiedenen Spezies induzieren.

Smed-runt1, ist ein Homolog von Runt Transkriptionsfaktoren in Planarien, die eine evolutionär konservierte Rolle in der Spezifizierung von Zellschicksalen spielen. Nach Verwundung wird *Smed-runt1* ausschliesslich in Neoblasten exprimiert. Inhibierung der Funktion von *Smed-runt1* durch RNA Interferenz, führt zur abnormalen Regeneration von neuronalen Strukturen. Genexpressionsanalyse solcher Tiere deutet darauf hin, dass *Smed-runt1* zu einem frühen Zeitpunkt nach Verwundung in Neoblasten aktiv ist, und die Expression von Genen reguliert, die wichtig für die Entwicklung neuronaler Strukturen in anderen Organismen sind.

6 References

Abraham, W., Dragunow, M., Tate, WP. (1991). The role of immediate early genes in the stabilization of long-term potentiation. Mol Neurobiol *5*, 297-314.

Adell, T., Marsal, M., and Salo, E. (2008). Planarian GSK3s are involved in neural regeneration. Development Genes and Evolution *218*, 89-103.

Adell, T., Salo, E., Boutros, M., and Bartscherer, K. (2009). Smed-Evi/Wntless is required for beta-catenin-dependent and -independent processes during planarian regeneration. Development *136*, 905-910.

Adham, I.M., Sallam, M.A., Steding, G., Korabiowska, M., Brinck, U., Hoyer-Fender, S., Oh, C., and Engel, W. (2003). Disruption of the pelota gene causes early embryonic lethality and defects in cell cycle progression. Molecular and Cellular Biology *23*, 1470-1476.

Alberti, S., Krause, S.M., Kretz, O., Philippar, U., Lemberger, T., Casanova, E., Wiebel, F.F., Schwarz, H., Frotscher, M., Schutz, G.*, et al.* (2005). Neuronal migration in the murine rostral migratory stream requires serum response factor. Proc Natl Acad Sci U S A *102*, 6148-6153.

Alberts, A.S., Geneste, O., and Treisman, R. (1998). Activation of SRF-regulated chromosomal templates by Rho-family GTPases requires a signal that also induces H4 hyperacetylation. Cell *92*, 475-487.

Alton, A.K., Fechtel, K., Kopczynski, C.C., Shepard, S.B., Kooh, P.J., and Muskavitch, M.A. (1989). Molecular genetics of Delta, a locus required for ectodermal differentiation in *Drosophila*. Dev Genet *10*, 261-272.

Amcheslavsky, A., Jiang, J., and Ip, Y.T. (2009). Tissue damage-induced intestinal stem cell division in *Drosophila*. Cell Stem Cell *4*, 49-61.

Ang, S.L., Jin, O., Rhinn, M., Daigle, N., Stevenson, L., and Rossant, J. (1996). A targeted mouse Otx2 mutation leads to severe defects in gastrulation and formation of axial mesoderm and to deletion of rostral brain. Development *122*, 243-252.

Antos, C.L., and Tanaka, E.M. (2010). Vertebrates That Regenerate as Models for Guiding Stem Cells. Cell Biology of Stem Cells *695*, 184-214.

Arai, M., Yokosuka, O., Chiba, T., Imazeki, F., Kato, M., Hashida, J., Ueda, Y., Sugano, S., Hashimoto, K., Saisho, H.*, et al.* (2003). Gene expression profiling reveals the mechanism and pathophysiology of mouse liver regeneration. Journal of Biological Chemistry *278*, 29813-29818.

Asami, M., Nakatsuka, T., Hayashi, T., Kou, K., Kagawa, H., and Agata, K. (2002). Cultivation and characterization of planarian neuronal cells isolated by fluorescence activated cell sorting (FACS). Zoolog Sci *19*, 1257-1265.

Attisano, L., Wrana, J.L., Cheifetz, S., and Massague, J. (1992). Novel activin receptors: distinct genes and alternative mRNA splicing generate a repertoire of serine/threonine kinase receptors. Cell *68*, 97-108.

Audet, J. (2004). Stem cell bioengineering for regenerative medicine. Expert Opin Biol Th *4*, 631-644.

Baguñà, J. (1976a). Mitosis in Intact and Regenerating Planarian *Dugesia-Mediterranea* N-Sp .1. Mitotic Studies during Growth, Feeding and Starvation. Journal of Experimental Zoology *195*, 53-64.

Baguñà, J. (1976b). Mitosis in Intact and Regenerating Planarian *Dugesia-Mediterranea* N-Sp .2. Mitotic Studies during Regeneration, and a Possible Mechanism of Blastema Formation. Journal of Experimental Zoology *195*, 65-79.

Baguñà, J., Carranza, S., Pala, M., Ribera, C., Giribet, G., Arnedo, M.A., Ribas, M., and Riutort, M. (1999). From morphology and karyology to molecules. New methods for taxonomical identification of asexual populations of freshwater planarians. A tribute to Professor Mario Benazzi. Ital J Zool *66*, 207-214.

Baguñà, J., and Romero, R. (1981). Quantitative-Analysis of Cell-Types during Growth, Degrowth and Regeneration in the Planarians *Dugesia-Mediterranea* and *Dugesia-Tigrina*. Hydrobiologia *84*, 181-194.

Baguñà, J., Saló, E., and Auladell, C. (1989). Regeneration and pattern formation in planarians. III. Evidence that neoblasts are totipotent stem cells and the source of blastema cells. Development *107*.

Barbash, I.M., and Leor, J. (2006). Myocardial regeneration by adult stem cells. Isr Med Assoc J *8*, 283-287.

Barker, N., van Es, J.H., Kuipers, J., Kujala, P., van den Born, M., Cozijnsen, M., Haegebarth, A., Korving, J., Begthel, H., Peters, P.J.*, et al.* (2007). Identification of stem cells in small intestine and colon by marker gene Lgr5. Nature *449*, 1003-U1001.

Beauchene, N.A., Diaz-Martinez, L.A., Furniss, K., Hsu, W.S., Tsai, H.J., Chamberlain, C., Esponda, P., Gimenez-Abian, J.F., and Clarke, D.J. (2010). Rad21 is required for centrosome integrity in human cells independently of its role in chromosome cohesion. Cell Cycle *9*, 1774-1780.

Beharry, Z., Mahajan, S., Zemskova, M., Lin, Y.W., Tholanikunnel, B.G., Xia, Z., Smith, C.D., and Kraft, A.S. (2011). The Pim protein kinases regulate energy metabolism and cell growth. Proc Natl Acad Sci U S A *108*, 528-533.

Belenkaya, T.Y., Han, C., Yan, D., Opoka, R.J., Khodoun, M., Liu, H., and Lin, X. (2004). *Drosophila* Dpp morphogen movement is independent of dynamin-mediated endocytosis but regulated by the glypican members of heparan sulfate proteoglycans. Cell *119*, 231-244.

Beltrami, A.P., Barlucchi, L., Torella, D., Baker, M., Limana, F., Chimenti, S., Kasahara, H., Rota, M., Musso, E., Urbanek, K.*, et al.* (2003). Adult cardiac stem cells are multipotent and support myocardial regeneration. Cell *114*, 763-776.

Best, J.B., Hand, S., and Rosenvol.R (1968). Mitosis in Normal and Regenerating Planarians. Journal of Experimental Zoology *168*, 157-&.

Betchaku, T. (1967). Isolation of Planarian Neoblasts and Their Behavior in Vitro with Some Aspects of Mechanism of Formation of Regeneration Blastema. Journal of Experimental Zoology *164*, 407-&.

Bjørklund, S., Skog, S., Tribukait, B., and Thelander, L. (1990). S-phase-specific expression of mammalian ribonucleotide reductase R1 and R2 subunit mRNAs. Biochemistry *29*, 5452-5458.

Blau, H.M., Brazelton, T.R., and Weimann, J.M. (2001). The evolving concept of a stem cell: Entity or function? Cell *105*, 829-841.

Bosch, M., Baguna, J., and Serras, F. (2008). Origin and proliferation of blastema cells during regeneration of *Drosophila* wing imaginal discs. International Journal of Developmental Biology *52*, 1043-1050.

Boyer, L.A., Lee, T.I., Cole, M.F., Johnstone, S.E., Levine, S.S., Zucker, J.R., Guenther, M.G., Kumar, R.M., Murray, H.L., Jenner, R.G.*, et al.* (2005). Core transcriptional regulatory circuitry in human embryonic stem cells. Cell *122*, 947-956.

Brockes, J.P., Kumar, A., and Velloso, C.P. (2001). Regeneration as an evolutionary variable. J Anat *199*, 3-11.

Brøndsted, H.V. (1969). Planarian Regeneration (Pergamon Press, London).

Buchanan (1933). Regeneration in Phagocata gracilis (Leidy). Phys Zool *6*, 185-204.

Buchon, N., Broderick, N.A., Chakrabarti, S., and Lemaitre, B. (2009a). Invasive and indigenous microbiota impact intestinal stem cell activity through multiple pathways in *Drosophila*. Gene Dev *23*, 2333-2344.

Buchon, N., Broderick, N.A., Poidevin, M., Pradervand, S., and Lemaitre, B. (2009b). *Drosophila* Intestinal Response to Bacterial Infection: Activation of Host Defense and Stem Cell Proliferation. Cell Host Microbe *5*, 200-211.

Buchon, N., Broderick, NA., Kuraishi, T., Lemaitre, B. (2010). *Drosophila* EGFR pathway coordinates stem cell proliferation and gut remodeling following infection. BMC Biol *8*, 152.

Bueno, D., Baguñà, J., and Romero, R. (1997). Cell-, tissue-, and position-specific monoclonal antibodies against the planarian *Dugesia (Girardia) tigrina*. Histochem Cell Biol *107*, 139-149.

Burr, A.W., Toole, K., Chapman, C., Hines, J.E., and Burt, A.D. (1998). Anti-hepatocyte growth factor antibody inhibits hepatocyte proliferation during liver regeneration. Journal of Pathology *185*, 298-302.

Campisi, J., Gray, H.E., Pardee, A.B., Dean, M., and Sonenshein, G.E. (1984). Cell-cycle control of c-myc but not c-ras expression is lost following chemical transformation. Cell *36*, 241-247.

Capela, A., and Temple, S. (2002). LeX/ssea-1 is expressed by adult mouse CNS stem cells, identifying them as nonependymal. Neuron *35*, 865-875.

Castresana, J. (2000). Selection of conserved blocks from multiple alignments for their use in phylogenetic analysis. Molecular Biology and Evolution *17*, 540-552.

Cebria, F., Kudome, T., Nakazawa, M., Mineta, K., Ikeo, K., Gojobori, T., and Agata, K. (2002). The expression of neural-specific genes reveals the structural and molecular complexity of the planarian central nervous system. Mech Dev *116*, 199-204.

Cen, B., Mahajan, S., Zemskova, M., Beharry, Z., Lin, Y.W., Cramer, S.D., Lilly, M.B., and Kraft, A.S. (2010). Regulation of Skp2 levels by the Pim-1 protein kinase. J Biol Chem *285*, 29128-29137.

Chabes, A.L., Bjorklund, S., and Thelander, L. (2004). S Phase-specific transcription of the mouse ribonucleotide reductase R2 gene requires both a proximal repressive E2F-binding site and an upstream promoter activating region. J Biol Chem *279*, 10796-10807.

Chavrier, P., Zerial, M., Lemaire, P., Almendral, J., Bravo, R., and Charnay, P. (1988). A gene encoding a protein with zinc fingers is activated during G0/G1 transition in cultured cells. Embo J *7*, 29-35.

Chera, S., Ghila, L., Dobretz, K., Wenger, Y., Bauer, C., Buzgariu, W., Martinou, J.C., and Galliot, B. (2009). Apoptotic Cells Provide an Unexpected Source of Wnt3 Signaling to Drive Hydra Head Regeneration. Developmental Cell *17*, 279-289.

Chiang, A., Priya, R., Ramaswami, M., VijayRaghavan, K., and Rodrigues, V. (2009). Neuronal activity and Wnt signaling act through Gsk3-beta to regulate axonal integrity in mature *Drosophila* olfactory sensory neurons. Development *136*, 1273-1282.

Coffman, J.A. (2003). Runx transcription factors and the developmental balance between cell proliferation and differentiation. Cell Biol Int *27*, 315-324.

Cohen, P.T. (2002). Protein phosphatase 1--targeted in many directions. J Cell Sci *115*, 241-256.

Colwell, A.S., Longaker, M.T., and Lorenz, H.P. (2003). Fetal wound healing. Front Biosci *8*, S1240-S1248.

Cooper, L., Johnson, C., Burslem, F., and Martin, P. (2005). Wound healing and inflammation genes revealed by array analysis of 'macrophageless' PU.1 null mice. Genome Biol *6*, R5.

Coward, S.J., Hirsh, F.M., and Taylor, J.H. (1970). Thymidine Kinase Activity during Regeneration in Planarian *Dugesia-Dorotocephala*. Journal of Experimental Zoology *173*, 269-&.

Denes, A.S., Jekely, G., Steinmetz, P.R.H., Raible, F., Snyman, H., Prud'homme, B., Ferrier, D.E.K., Balavoine, G., and Arendt, D. (2007). Molecular architecture of annelid nerve cord supports common origin of nervous system centralization in bilateria. Cell *129*, 277-288.

Dimitriou, R., Tsiridis, E., and Giannoudis, P.V. (2005). Current concepts of molecular aspects of bone healing. Injury *36*, 1392-1404.

Don, R.H., Cox, P.T., Wainwright, B.J., Baker, K., and Mattick, J.S. (1991). 'Touchdown' PCR to circumvent spurious priming during gene amplification. Nucleic Acids Res *19*, 4008.

Dragunow, M., Beilharz, E., Sirimanne, E., Lawlor, P., Williams, C., Bravo, R., and Gluckman, P. (1994). Immediate-early gene protein expression in neurons undergoing delayed death, but not necrosis, following hypoxic-ischaemic injury to the young rat brain. Brain Res Mol Brain Res *25*, 19-33.

Eferl, R., and Wagner, E.F. (2003). AP-1: a double-edged sword in tumorigenesis. Nat Rev Cancer *3*, 859-868.

Egger, B., Gschwentner, R., Hess, M.W., Nimeth, K.T., Adamski, Z., Willems, M., Rieger, R., and Salvenmoser, W. (2009). The caudal regeneration blastema is an accumulation of rapidly proliferating stem cells in the flatworm *Macrostomum lignano*. Bmc Dev Biol *9*, -.

Ehrhardt, J., and Morgan, J. (2005). Regenerative capacity of skeletal muscle. Curr Opin Neurol *18*, 548-553.

Eisenhoffer, G.T., Kang, H., and Sánchez Alvarado, A. (2008). Molecular analysis of stem cells and their descendants during cell turnover and regeneration in the planarian *Schmidtea mediterranea*. Cell Stem Cell *3*, 327-339.

Endo, T., Bryant, S.V., and Gardiner, D.M. (2004). A stepwise model system for limb regeneration. Dev Biol *270*, 135-145.

Ericson, J., Rashbass, P., Schedl, A., BrennerMorton, S., Kawakami, A., vanHeyningen, V., Jessell, T.M., and Briscoe, J. (1997). Pax6 controls progenitor cell identity and neuronal fate in response to graded shh signaling. Cell *90*, 169-180.

Eriksson, S., Graslund, A., Skog, S., Thelander, L., and Tribukait, B. (1984). Cell cycle-dependent regulation of mammalian ribonucleotide reductase. The S phase-correlated increase in subunit M2 is regulated by de novo protein synthesis. J Biol Chem *259*, 11695-11700.

Etkin, A., Alarcon, J.M., Weisberg, S.P., Touzani, K., Huang, Y.Y., Nordheim, A., and Kandel, E.R. (2006). A role in learning for SRF: deletion in the adult forebrain disrupts LTD and the formation of an immediate memory of a novel context. Neuron *50*, 127-143.

Evans, T., Rosenthal, E.T., Youngblom, J., Distel, D., and Hunt, T. (1983). Cyclin: a protein specified by maternal mRNA in sea urchin eggs that is destroyed at each cleavage division. Cell *33*, 389-396.

Fausto, N., Campbell, J.S., and Riehle, K.J. (2006). Liver regeneration. Hepatology *43*, S45-53.

Forbes, S.J., Vig, P., Poulsom, R., Wright, N.A., and Alison, M.R. (2002). Adult stem cell plasticity: new pathways of tissue regeneration become visible. Clin Sci *103*, 355-369.

Frank, D.J., and Roth, M.B. (1998). ncl-1 is required for the regulation of cell size and ribosomal RNA synthesis in Caenorhabditis elegans. Journal of Cell Biology *140*, 1321-1329.

Fuchs, E., and Segre, J.A. (2000). Stem cells: a new lease on life. Cell *100*, 143-155.

Fuchs, E., Tumbar, T., and Guasch, G. (2004). Socializing with the neighbors: stem cells and their niche. Cell *116*, 769-778.

Galko, M.J., and Krasnow, M.A. (2004). Cellular and genetic analysis of wound healing in *Drosophila* larvae. Plos Biology *2*, 1114-1126.

Geiss, G.K., Bumgarner, R.E., Birditt, B., Dahl, T., Dowidar, N., Dunaway, D.L., Fell, H.P., Ferree, S., George, R.D., Grogan, T.*, et al.* (2008). Direct multiplexed measurement of gene expression with color-coded probe pairs. Nat Biotechnol *26*, 317-325.

Gergen, J.P., and Wieschaus, E.F. (1985). The localized requirements for a gene affecting segmentation in *Drosophila*: analysis of larvae mosaic for runt. Dev Biol *109*, 321-335.

Gerlach, J.C., and Zeilinger, K. (2002). Adult stem cell technology - prospects for cell based therapy in regenerative medicine. Int J Artif Organs *25*, 83-90.

Gille, H., Sharrocks, A.D., and Shaw, P.E. (1992). Phosphorylation of transcription factor p62TCF by MAP kinase stimulates ternary complex formation at c-fos promoter. Nature *358*, 414-417.

Glazer, A.M., Wilkinson, A.W., Backer, C.B., Lapan, S.W., Gutzman, J.H., Cheeseman, I.M., and Reddien, P.W. (2010). The Zn Finger protein Iguana impacts Hedgehog signaling by promoting ciliogenesis. Developmental Biology *337*, 148-156.

Goessler, U.R., Riedel, K., Hormann, K., and Riedel, F. (2006). Perspectives of gene therapy in stem cell tissue engineering. Cells Tissues Organs *183*, 169-179.

Greenberg, M.E., Hermanowski, A.L., and Ziff, E.B. (1986). Effect of Protein-Synthesis Inhibitors on Growth-Factor Activation of C-Fos, C-Myc, and Actin Gene-Transcription. Molecular and Cellular Biology *6*, 1050-1057.

Guo, T., Peters, A.H., and Newmark, P.A. (2006a). A bruno-like Gene Is Required for Stem Cell Maintenance in Planarians. Dev Cell *11*, 159-169.

Guo, W., Lasky, J.L., and Wu, H. (2006b). Cancer stem cells. Pediatr Res *59*, 59R-64R.

Gurley, K.A., Rink, J.C., and Alvarado, A.S. (2008). beta-catenin defines head versus tail identity during planarian regeneration and Homeostasis. Science *319*, 323-327.

Haber, B.A., Mohn, K.L., Diamond, R.H., and Taub, R. (1993). Induction-Patterns of 70 Genes during 9 Days after Hepatectomy Define the Temporal Course of Liver-Regeneration. J Clin Invest *91*, 1319-1326.

Haffner, C., Frauli, M., Topp, S., Irmler, M., Hofmann, K., Regula, J.T., Bally-Cuif, L., and Haass, C. (2004). Nicalin and its binding partner Nomo are novel Nodal signaling antagonists. Embo Journal *23*, 3041-3050.

Halanych, K.M. (2004). The new view of animal phylogeny. Annual Review of Ecology, Evolution, and Systematics 35, 229-256.

Hayashi, T., Asami, M., Higuchi, S., Shibata, N., and Agata, K. (2006). Isolation of planarian X-ray-sensitive stem cells by fluorescence-activated cell sorting. Dev Growth Differ *48*, 371-380.

Hazzalin, C.A., and Mahadevan, L.C. (2002). MAPK-regulated transcription: a continuously variable gene switch? Nat Rev Mol Cell Biol *3*, 30-40.

Heald, R., McLoughlin, M., and McKeon, F. (1993). Human wee1 maintains mitotic timing by protecting the nucleus from cytoplasmically activated Cdc2 kinase. Cell *74*, 463-474.

Hendzel, M.J., Wei, Y., Mancini, M.A., Van Hooser, A., Ranalli, T., Brinkley, B.R., Bazett-Jones, D.P., and Allis, C.D. (1997). Mitosis-specific phosphorylation of histone H3 initiates primarily within pericentromeric heterochromatin during G2 and spreads in an ordered fashion coincident with mitotic chromosome condensation. Chromosoma *106*, 348-360.

Herschman, H.R. (1991). PRIMARY RESPONSE GENES INDUCED BY GROWTH-FACTORS AND TUMOR PROMOTERS. Annu Rev Biochem *60*, 281-319.

Hewitson, T.D., Kelynack, K.J., and Darby, I.A. (2006). Histochemical localization of cell proliferation using in situ hybridization for histone mRNA. Methods Mol Biol *326*, 219-226.

Higgins, D.G. (1994). CLUSTAL V: multiple alignment of DNA and protein sequences. Methods Mol Biol *25*, 307-318.

Higgins, G.M.a.A., R. M. (1931). Experimental pathology of the liver. I. Restoration of the liver of the white rat following partial surgical removal. Arch Pathol *12*, 186-202.

Hooft van Huijsduijnen, R. (1998). ADAM 20 and 21; two novel human testis-specific membrane metalloproteases with similarity to fertilin-alpha. Gene *206*, 273-282.

Hsu, J.C., Bravo, R., and Taub, R. (1992). Interactions among LRF-1, JunB, c-Jun, and c-Fos define a regulatory program in the G1 phase of liver regeneration. Mol Cell Biol *12*, 4654-4665.

Huelsenbeck, J.P., and Ronquist, F. (2001). MRBAYES: Bayesian inference of phylogenetic trees. Bioinformatics *17*, 754-755.

Hunt, P., Gulisano, M., Cook, M., Sham, M.H., Faiella, A., Wilkinson, D., Boncinelli, E., and Krumlauf, R. (1991). A Distinct Hox Code for the Branchial Region of the Vertebrate Head. Nature *353*, 861-864.

Hur, E.M., and Zhou, F.Q. (2010). GSK3 signalling in neural development. Nat Rev Neurosci *11*, 539-551.

Hyman, L.H. (1951). The Invertebrates: Platyhelminthes and Rhynchocoela The acoelomate bilateia (New York, McGraw-Hill Book Company Inc.).

Ikenishi, K. (1998). Germ plasm in *Caenorhabditis elegans*, *Drosophila* and *Xenopus*. Development Growth & Differentiation *40*, 1-10.

Inoue, J., Ishida, T., Tsukamoto, N., Kobayashi, N., Naito, A., Azuma, S., and Yamamoto, T. (2000). Tumor necrosis factor receptor-associated factor (TRAF) family: adapter proteins that mediate cytokine signaling. Exp Cell Res *254*, 14-24.

Ishii, T., Sato, M., Sudo, K., Suzuki, M., Nakai, H., Hishida, T., Niwa, T., Umezu, K., and Yuasa, S. (1995). Hepatocyte Growth-Factor Stimulates Liver-Regeneration and Elevates Blood Protein Level in Normal and Partially Hepatectomized Rats. J Biochem-Tokyo *117*, 1105-1112.

Ito, H., Saito, Y., Watanabe, K., and Orii, H. (2001). Epimorphic regeneration of the distal part of the planarian pharynx. Dev Genes Evol *211*, 2-9.

Ito, M., Liu, Y.P., Yang, Z.X., Nguyen, J., Liang, F., Morris, R.J., and Cotsarelis, G. (2005). Stem cells in the hair follicle bulge contribute to wound repair but not to homeostasis of the epidermis. Nature Medicine *11*, 1351-1354.

Ives, H.E. (1991). GTP binding proteins and growth factor signal transduction. Cell Signal *3*, 491-499.

Iyer, V.R., Eisen, M.B., Ross, D.T., Schuler, G., Moore, T., Lee, J.C.F., Trent, J.M., Staudt, L.M., Hudson, J., Boguski, M.S.*, et al.* (1999). The transcriptional program in the response of human fibroblasts to serum. Science *283*, 83-87.

Jazwinska, A., Badakov, R., and Keating, M.T. (2007). Activin-betaA signaling is required for zebrafish fin regeneration. Curr Biol *17*, 1390-1395.

Jiang, H.Q., Patel, P.H., Kohlmaier, A., Grenley, M.O., McEwen, D.G., and Edgar, B.A. (2009). Cytokine/Jak/Stat Signaling Mediates Regeneration and Homeostasis in the *Drosophila* Midgut. Cell *137*, 1343-1355.

Johnson, L.F., Abelson, H.T., Green, H., and Penman, S. (1974). Changes in Rna in Relation to Growth of Fibroblast .1. Amounts of Messenger-Rna, Ribosomal-Rna, and Tertiary Rna in Resting and Growing Cells. Cell *1*, 95-100.

Kagoshima, H., Nimmo, R., Saad, N., Tanaka, J., Miwa, Y., Mitani, S., Kohara, Y., and Woollard, A. (2007). The *C. elegans* CBFbeta homologue BRO-1 interacts with the Runx factor, RNT-1, to promote stem cell proliferation and self-renewal. Development *134*, 3905-3915.

Kang, H., and Alvarado, A.S. (2009). Flow Cytometry Methods for the Study of Cell-Cycle Parameters of Planarian Stem Cells. Dev Dynam *238*, 1111-1117.

Karpowicz, P., Perez, J., Perrimon, N. (2010). The Hippo tumor suppressor pathway regulates intestinal stem cell regeneration. Development *137*, 21064-21069.

Kashofer, K., and Bonnet, D. (2005). Gene therapy progress and prospects: Stem cell plasticity. Gene Ther *12*, 1229-1234.

Kato, K., Orii, H., Watanabe, K., and Agata, K. (2001). Dorsal and ventral positional cues required for the onset of planarian regeneration may reside in differentiated cells. Dev Biol *233*, 109-121.

Kazlauskas, A., Kashishian, A., Cooper, J.A., and Valius, M. (1992). GTPase-activating protein and phosphatidylinositol 3-kinase bind to distinct regions of the platelet-derived growth factor receptor beta subunit. Mol Cell Biol *12*, 2534-2544.

Kelley-Loughnane, N., Sabla, G.E., Ley-Ebert, C., Aronow, B.J., and Bezerra, J.A. (2002). Independent and overlapping transcriptional activation during liver development and regeneration in mice. Hepatology *35*, 525-534.

Kelly, K., Cochran, B.H., Stiles, C.D., and Leder, P. (1983). Cell-specific regulation of the c-myc gene by lymphocyte mitogens and platelet-derived growth factor. Cell *35*, 603-610.

Kelly, T.K., Miranda, T.B., Liang, G., Berman, B.P., Lin, J.C., Tanay, A., and Jones, P.A. (2010). H2A.Z maintenance during mitosis reveals nucleosome shifting on mitotically silenced genes. Mol Cell *39*, 901-911.

Kinoshita, Y., Jarell, A.D., Flaman, J.M., Foltz, G., Schuster, J., Sopher, B.L., Irvin, D.K., Kanning, K., Kornblum, H.I., Nelson, P.S.*, et al.* (2001). Pescadillo, a novel cell cycle regulatory protein abnormally expressed in malignant cells. Journal of Biological Chemistry *276*, 6656-6665.

Klebes, A., Sustar, A., Kechris, K., Li, H., Schubiger, G., and Kornberg, T.B. (2005). Regulation of cellular plasticity in *Drosophila* imaginal disc cells by the polycomb group, trithorax group and lama genes. Development *132*, 3753-3765.

Knoll, B., and Nordheim, A. (2009). Functional versatility of transcription factors in the nervous system: the SRF paradigm. Trends Neurosci *32*, 432-442.

Kocholaty, W., Ellis, W.W., and Jensen, H. (1952). Activation of plasminogen by trypsin and plasmin. Blood *7*, 882-890.

Koehler, K., Mielke, K., Schunck, M., Neumann, C., Herdegen, T., and Proksch, E. (2010). Distinct roles of JNK-1 and ERK-2 isoforms in permeability barrier repair and wound healing. Eur J Cell Biol.

Kragl, M., Knapp, D., Nacu, E., Khattak, S., Maden, M., Epperlein, H.H., and Tanaka, E.M. (2009). Cells keep a memory of their tissue origin during axolotl limb regeneration. Nature *460*, 60-U69.

Kudron, M.M., and Reinke, V. (2008). *C. elegans* Nucleostemin Is Required for Larval Growth and Germline Stem Cell Division. Plos Genet *4*, -.

Kumanogoh, H., Miyata, S., Sokawa, Y., and Maekawa, S. (2001). Biochemical and morphological analysis on the localization of Rac1 in neurons. Neurosci Res *39*, 189-196.

Kumar, A., Godwin, J.W., Gates, P.B., Garza-Garcia, A.A., and Brockes, J.P. (2007). Molecular basis for the nerve dependence of limb regeneration in an adult vertebrate. Science *318*, 772-777.

Kume, S. (2005). Stem-cell-based approaches for regenerative medicine. Development Growth & Differentiation *47*, 393-402.

Kwan, K.Y., Lam, M.M.S., Krsnik, Z., Kawasawa, Y.I., Lefebvre, V., and Sestan, N. (2008). SOX5 postmitotically regulates migration, postmigratory differentiation, and projections of subplate and deep-layer neocortical neurons. P Natl Acad Sci USA *105*, 16021-16026.

Lai, T., Jabaudon, D., Molyneaux, B.J., Azim, E., Arlotta, P., Menezes, J.R.L., and Macklis, J.D. (2008). SOX5 controls the sequential generation of distinct corticofugal neuron subtypes. Neuron *57*, 232-247.

Lamph, W.W., Wamsley, P., Sassone-Corsi, P., and Verma, I.M. (1988). Induction of proto-oncogene JUN/AP-1 by serum and TPA. Nature *334*, 629-631.

Latasa, M.U., Couton, D., Charvet, C., Lafanechere, A., Guidotti, J.E., Li, Z., Tuil, D., Daegelen, D., Mitchell, C., and Gilgenkrantz, H. (2007). Delayed liver regeneration in mice lacking liver serum response factor. Am J Physiol Gastrointest Liver Physiol *292*, G996-G1001.

Lau, L.F., and Nathans, D. (1987). Expression of a Set of Growth-Related Immediate Early Genes in Balb-C 3t3 Cells - Coordinate Regulation with C-Fos or C-Myc. P Natl Acad Sci USA *84*, 1182-1186.

Lee, M.G., Norbury, C.J., Spurr, N.K., and Nurse, P. (1988). Regulated expression and phosphorylation of a possible mammalian cell-cycle control protein. Nature *333*, 676-679.

Lee, Y., Hami, D., De Val, S., Kagermeier-Schenk, B., Wills, A.A., Black, B.L., Weidinger, G., and Poss, K.D. (2009). Maintenance of blastemal proliferation by functionally diverse epidermis in regenerating zebrafish fins. Developmental Biology *331*, 270-280.

Lemmon, M.A., and Schlessinger, J. (2010). Cell signaling by receptor tyrosine kinases. Cell *141*, 1117-1134.

Lens, S.M., Voest, E.E., and Medema, R.H. (2010). Shared and separate functions of polo-like kinases and aurora kinases in cancer. Nat Rev Cancer *10*, 825-841.

Lepilina, A., Coon, A.N., Kikuchi, K., Holdway, J.E., Roberts, R.W., Burns, C.G., and Poss, K.D. (2006). A dynamic epicardial injury response supports progenitor cell activity during zebrafish heart regeneration. Cell *127*, 607-619.

Lewis, J., Mathews, MB. (1980). Control of adenovirus early gene expression: a class of immediate early products. Cell *21*, 303-313.

Li, G.C., Gustafson-Brown, C., Hanks, S.K., Nason, K., Arbeit, J.M., Pogliano, K., Wisdom, R.M., and Johnson, R.S. (2003). c-Jun is essential for organization of the epidermal leading edge. Developmental Cell *4*, 865-877.

Li, L.H., and Gergen, J.P. (1999). Differential interactions between Brother proteins and Runt domain proteins in the *Drosophila* embryo and eye. Development *126*, 3313-3322.

Lien, C.L., Schebesta, M., Makino, S., Weber, G.J., and Keating, M.T. (2006). Gene expression analysis of zebrafish heart regeneration. PLoS Biol *4*, e260.

Lindahl, A.K., Sandset, P.M., Thune-Wiiger, M., Nordfang, O., and Sakariassen, K.S. (1994). Tissue factor pathway inhibitor prevents thrombus formation on procoagulant subendothelial matrix. Blood Coagul Fibrinolysis *5*, 755-760.

Lindh, N.O. (1957). The mitotic activity during the early regeneration in E*uplanaria polychroa*. Ark Zool *10*, 497-509.

Mace, K.A., Pearson, J.C., and McGinnis, W. (2005). An epidermal barrier wound repair pathway in *Drosophila* is mediated by grainy head. Science *308*, 381-385.

Mackay, D.R., Hu, M., Li, B.A., Rheaume, C., and Dai, X. (2006). The mouse Ovol2 gene is required for cranial neural tube development. Developmental Biology *291*, 38-52.

Mangone, M., Myers, M.P., and Herr, W. (2010). Role of the HCF-1 Basic Region in Sustaining Cell Proliferation. Plos One *5*, -.

Martin, P., and Parkhurst, S.M. (2004). Parallels between tissue repair and embryo morphogenesis. Development *131*, 3021-3034.

Mead, J.E., and Fausto, N. (1989). Transforming Growth Factor-Alpha May Be a Physiological Regulator of Liver-Regeneration by Means of an Autocrine Mechanism. P Natl Acad Sci USA *86*, 1558-1562.

Michalopoulos, G.K., and DeFrances, M.C. (1997). Liver regeneration. Science *276*, 60-66.

Miller, J., Horner, A., Stacy, T., Lowrey, C., Lian, J.B., Stein, G., Nuckolls, G.H., and Speck, N.A. (2002). The core-binding factor beta subunit is required for bone formation and hematopoietic maturation. Nat Genet *32*, 645-649.

Milunsky, J.M., Maher, T.A., Zhao, G., Roberts, A.E., Stalkers, H.J., Zori, R.T., Burch, M.N., Clemens, M., Mulliken, J.B., Smith, R.*, et al.* (2008). TFAP2A mutations result in branchio-oculo-facial syndrome. Am J Hum Genet *82*, 1171-1177.

Mohn, K.L., Laz, T.M., Hsu, J.C., Melby, A.E., Bravo, R., and Taub, R. (1991). The Immediate-Early Growth-Response in Regenerating Liver and Insulin-Stimulated H-35 Cells - Comparison with Serum-Stimulated 3t3 Cells and Identification of 41 Novel Immediate-Early Genes. Molecular and Cellular Biology *11*, 381-390.

Molina, M.D., Salo, E., and Cebria, F. (2007). The BMP pathway is essential for re-specification and maintenance of the dorsoventral axis in regenerating and intact planarians. Developmental Biology *311*, 79-94.

Molina, M.D., Salo, E., and Cebria, F. (2009). Expression pattern of the expanded *noggin* gene family in the planarian *Schmidtea mediterranea*. Gene Expression Patterns *9*, 246-253.

Monaghan, J.R., Epp, L.G., Putta, S., Page, R.B., Walker, J.A., Beachy, C.K., Zhu, W., Pao, G.M., Verma, I.M., Hunter, T.*, et al.* (2009). Microarray and cDNA sequence analysis of transcription during nerve-dependent limb regeneration. BMC Biol *7*, 1.

Moolten, F.L., and Bucher, N.L.R. (1967). Regeneration of Rat Liver - Transfer of Humoral Agent by Cross Circulation. Science *158*, 272-&.

Morales, A.V., Perez-Alcala, S., and Barbas, J.A. (2007). Dynamic Sox5 protein expression during cranial ganglia development. Dev Dynam *236*, 2702-2707.

Morgan, T.H. (1898). Regeneration in Planaria maculata. Science *7*, 196-197.

Morgan, T.H. (1901). Regeneration (New York, The Macmillan Company).

Morgan, T.H. (1904). Polarity and axial heteromorphosis. The American Naturalist *38*, 502-505.

Morgan, T.H. (1905). “Polarity” considered as a phenomenon of gradation of materials. J Exp Zool *2*, 495-506.

Morrison, J.I., Loof, S., He, P.P., and Simon, A. (2006). Salamander limb regeneration involves the activation of a multipotent skeletal muscle satellite cell population. Journal of Cell Biology *172*, 433-440.

Muller, L., and Lindberg, I. (1999). The cell biology of the prohormone convertases PC1 and PC2. Prog Nucleic Acid Res Mol Biol *63*, 69-108.

Muller, R., Bravo, R., Burckhardt, J., and Curran, T. (1984). Induction of c-fos gene and protein by growth factors precedes activation of c-myc. Nature *312*, 716-720.

Nechiporuk, A., and Keating, M.T. (2002). A proliferation gradient between proximal and msxb-expressing distal blastema directs zebrafish fin regeneration. Development *129*, 2607-2617.

Neff, T., Beard, B.C., and Kiem, H.P. (2006). Survival of the fittest: in vivo selection and stem cell gene therapy. Blood *107*, 1751-1760.

Newmark, P.A., Reddien, P.W., Cebria, F., and Sánchez Alvarado, A. (2003). Ingestion of bacterially expressed double-stranded RNA inhibits gene expression in planarians. Proc Natl Acad Sci U S A *100 Suppl 1*, 11861-11865.

Newmark, P.A., and Sánchez Alvarado, A. (2000). Bromodeoxyuridine specifically labels the regenerative stem cells of planarians. Dev Biol *220*, 142-153.

Newmark, P.A., and Sánchez Alvarado, A. (2002). Not your father's planarian: a classic model enters the era of functional genomics. Nat Rev Genet *3*, 210-219.

Nibu, Y., Zhang, H., Bajor, E., Barolo, S., Small, S., and Levine, M. (1998). dCtBP mediates transcriptional repression by Knirps, Kruppel and Snail in the *Drosophila* embryo. Embo J *17*, 7009-7020.

Nicolas, E., Morales, V., Magnaghi-Jaulin, L., Harel-Bellan, A., Richard-Foy, H., and Trouche, D. (2000). RbAp48 belongs to the histone deacetylase complex that associates with the retinoblastoma protein. Journal of Biological Chemistry *275*, 9797-9804.

Nimmo, R., and Woollard, A. (2008). Worming out the biology of Runx. Dev Biol *313*, 492-500.

Niwa, H. (2007). How is pluripotency determined and maintained? Development *134*, 635-646.

Norman, C., Runswick, M., Pollock, R., and Treisman, R. (1988). Isolation and properties of cDNA clones encoding SRF, a transcription factor that binds to the c-fos serum response element. Cell *55*, 989-1003.

O'Connor, M.B., Umulis, D., Othmer, H.G., and Blair, S.S. (2006). Shaping BMP morphogen gradients in the *Drosophila* embryo and pupal wing. Development *133*, 183-193.

Ogawa, K., Ishihara, S., Saito, Y., Mineta, K., Nakazawa, M., Ikeo, K., Gojobori, T., Watanabe, K., and Agata, K. (2002). Induction of a noggin-like gene by ectopic DV interaction during planarian regeneration. Dev Biol *250*, 59-70.

Oliver, G., Mailhos, A., Wehr, R., Copeland, N.G., Jenkins, N.A., and Gruss, P. (1995). Six3, a murine homologue of the sine oculis gene, demarcates the most anterior border of the developing neural plate and is expressed during eye development. Development *121*, 4045-4055.

Orii, H., Sakurai, T., and Watanabe, K. (2005). Distribution of the stem cells (neoblasts) in the planarian *Dugesia japonica*. Dev Genes Evol *215*, 143-157.

Oshima, H., Rochat, A., Kedzia, C., Kobayashi, K., and Barrandon, Y. (2001). Morphogenesis and renewal of hair follicles from adult multipotent stem cells. Cell *104*, 233-245.

Park, H.D., Ortmeyer, A.B., and Blankenbaker, D.P. (1970). Cell division during regeneration in Hydra. Nature *227*, 617-619.

Paro, R., and Hogness, D.S. (1991). The Polycomb protein shares a homologous domain with a hetero-chromatin-associated protein of *Drosophila*. Proc Natl Acad Sci U S A *88*, 263-267.

Pearson, B.J., Eisenhoffer, G.T., Gurley, K.A., Rink, J.C., Miller, D.E., and Alvarado, A.S. (2009). Formaldehyde-Based Whole-Mount *In Situ* Hybridization Method for Planarians. Dev Dynam *238*, 443-450.

Pearson, H. (2001). The regeneration gap. Nature *414*, 388-390.

Pedersen, K.J. (1959). Cytological studies on the planarian neoblast. Z Zellforsch Mikrosk Anat *50*, 799-817.

Pellettieri, J., and Alvarado, A.S. (2007). Cell turnover and adult tissue homeostasis: From humans to planarians. Annu Rev Genet *41*, 83-105.

Pellettieri, J., Fitzgerald, P., Watanabe, S., Mancuso, J., Green, D.R., and Alvarado, A.S. (2010). Cell death and tissue remodeling in planarian regeneration. Developmental Biology *338*, 76-85.

Pentek, J., Parker, L., Wu, A., and Arora, K. (2009). Follistatin preferentially antagonizes activin rather than BMP signaling in *Drosophila*. Genesis *47*, 261-273.

Petersen, C.P., and Reddien, P.W. (2008). Smed-beta-catenin-1 is required for anteroposterior blastema polarity in planarian regeneration. Science *319*, 327-330.

Petersen, C.P., and Reddien, P.W. (2009). A wound-induced Wnt expression program controls planarian regeneration polarity. P Natl Acad Sci USA *106*, 17061-17066.

Pires-daSilva, A., and Sommer, R.J. (2003). The evolution of signalling pathways in animal development. Nat Rev Genet *4*, 39-49.

Poser, S., Impey, S., Trinh, K., Xia, Z., and Storm, D.R. (2000). SRF-dependent gene expression is required for PI3-kinase-regulated cell proliferation. Embo J *19*, 4955-4966.

Potten, C.S., and Booth, C. (2002). Keratinocyte stem cells: a commentary. Journal of Investigative Dermatology *119*, 888-899.

Prockop, D.J. (1997). Marrow Stromal Cells as Stem Cells for Nonhematopoietic Tissues Science *276*, 71-74.

Ramanan, N., Shen, Y., Sarsfield, S., Lemberger, T., Schutz, G., Linden, D.J., and Ginty, D.D. (2005). SRF mediates activity-induced gene expression and synaptic plasticity but not neuronal viability. Nat Neurosci *8*, 759-767.

Randolph, H. (1892). The regeneration of the tail in lumbriculus. J Morphol *7*, 317-344.

Reddien, P.W., Bermange, A.L., Kicza, A.M., and Alvarado, A.S. (2007). BMP signaling regulates the dorsal planarian midline and is needed for asymmetric regeneration. Development *134*, 4043-4051.

Reddien, P.W., Bermange, A.L., Murfitt, K.J., Jennings, J.R., and Sánchez Alvarado, A. (2005a). Identification of genes needed for regeneration, stem cell function, and tissue homeostasis by systematic gene perturbation in planaria. Dev Cell *8*, 635-649.

Reddien, P.W., Oviedo, N.J., Jennings, J.R., Jenkin, J.C., and Sánchez Alvarado, A. (2005b). SMEDWI-2 is a PIWI-like protein that regulates planarian stem cells. Science *310*, 1327-1330.

Reddien, P.W., and Sánchez Alvarado, A. (2004). Fundamentals of planarian regeneration. Annu Rev Cell Dev Biol *20*, 725-757.

Reya, T., Morrison, S.J., Clarke, M.F., and Weissman, I.L. (2001). Stem cells, cancer, and cancer stem cells. Nature *414*, 105-111.

Richardson, H., Lew, D.J., Henze, M., Sugimoto, K., and Reed, S.I. (1992). Cyclin-B homologs in Saccharomyces cerevisiae function in S phase and in G2. Genes Dev *6*, 2021-2034.

Rink, J.C., Gurley, K.A., Elliott, S.A., and Alvarado, A.S. (2009). Planarian Hh Signaling Regulates Regeneration Polarity and Links Hh Pathway Evolution to Cilia. Science *326*, 1406-1410.

Robinson, M.D., McCarthy, D.J., and Smyth, G.K. (2010). edgeR: a Bioconductor package for differential expression analysis of digital gene expression data. Bioinformatics *26*, 139-140.

Ronquist, F., and Huelsenbeck, J.P. (2003). MrBayes 3: Bayesian phylogenetic inference under mixed models. Bioinformatics *19*, 1572-1574.

Royet, J., and Finkelstein, R. (1995). Pattern formation in *Drosophila* head development: the role of the orthodenticle homeobox gene. Development *121*, 3561-3572.

Rubinfeld, B., Albert, I., Porfiri, E., Fiol, C., Munemitsu, S., and Polakis, P. (1996). Binding of GSK3beta to the APC-beta-catenin complex and regulation of complex assembly. Science *272*, 1023-1026.

Sakai, F., Agata, K., Orii, H., and Watanabe, K. (2000). Organization and regeneration ability of spontaneous supernumerary eyes in planarians - Eye regeneration field and pathway selection by optic nerves. Zool Sci *17*, 375-381.

Salo, E., and Baguñà, J. (1985). Cell movement in intact and regenerating planarians. Quantitation using chromosomal, nuclear and cytoplasmic markers. J Embryol Exp Morphol *89*, 57-70.

Saló, E., and Baguñà, J. (1984). Regeneration and pattern formation in planarians. I. The pattern of mitosis in anterior and posterior regeneration in *Dugesia (G) tigrina*, and a new proposal for blastema formation. J Embryol Exp Morphol *83*, 63-80.

Saló, E., Baguñà, J., (1989). Regeneration and pattern formation in planarians II. Local origin and role of cell movements in blastema formation. . Development *107*, 69-76.

Sánchez Alvarado, A. (2000). Regeneration in the metazoans: why does it happen? Bioessays *22*, 578-590.

Sánchez Alvarado, A. (2003). The freshwater planarian *Schmidtea mediterranea*: embryogenesis, stem cells and regeneration. Curr Opin Genet Dev *13*, 438-444.

Sánchez Alvarado, A. (2004). Regeneration and the need for simpler model organisms. Philos Trans R Soc Lond B Biol Sci *359*, 759-763.

Sánchez Alvarado, A. (2006). Planarian regeneration: its end is its beginning. Cell *124*, 241-245.

Sánchez Alvarado, A., and Kang, H. (2005). Multicellularity, stem cells, and the neoblasts of the planarian *Schmidtea mediterranea*. Exp Cell Res *306*, 299-308.

Sánchez Alvarado, A., and Newmark, P.A. (1999). Double-stranded RNA specifically disrupts gene expression during planarian regeneration. Proc Natl Acad Sci U S A *96*, 5049-5054.

Sánchez Alvarado, A., Newmark, P.A., Robb, S.M., and Juste, R. (2002). The *Schmidtea mediterranea* database as a molecular resource for studying platyhelminthes, stem cells and regeneration. Development *129*, 5659-5665.

Sayles, L.P. (1927). Origin of the mesoderm and behavior of the nucleolus in regeneration in Lumbriculus. Biol Bull-Us *52*, 278-U278.

Schambra, U.B., Duncan, G.E., Breese, G.R., Fornaretto, M.G., Caron, M.G., and Fremeau, R.T., Jr. (1994). Ontogeny of D1A and D2 dopamine receptor subtypes in rat brain using in situ hybridization and receptor binding. Neuroscience *62*, 65-85.

Schneider-Poetsch, T., Ju, J.H., Eyler, D.E., Dang, Y.J., Bhat, S., Merrick, W.C., Green, R., Shen, B., and

Liu, J.O. (2010). Inhibition of eukaryotic translation elongation by cycloheximide and lactimidomycin. Nat Chem Biol *6*, 209-217.

Schreiber, S.S., Tocco, G., Shors, T.J., and Thompson, R.F. (1991). Activation of Immediate Early Genes after Acute Stress. Neuroreport *2*, 17-20.

Serikaku, M.A., and Otousa, J.E. (1994). *Sine Oculis* Is a Homeobox Gene Required for *Drosophila* Visual-System Development. Genetics *138*, 1137-1150.

Skar, R., Larsen, T.H., and Serck-Hanssen, G. (1994). Regulation of c-fos expression by IGF-I in bovine chromaffin cells: desensitization following cholinergic activation. Mol Cell Endocrinol *106*, 213-220.

Slack, J.M. (2003). Regeneration research today. Dev Dyn *226*, 162-166.

Smith-Bolton, R.K., Worley, M.I., Kanda, H., and Hariharan, I.K. (2009). Regenerative Growth in *Drosophila* Imaginal Discs Is Regulated by Wingless and Myc. Developmental Cell *16*, 797-809.

Solloway, M.J., and Harvey, R.P. (2003). Molecular pathways in myocardial development: a stem cell perspective. Cardiovasc Res *58*, 264-277.

Spangrude, G.J., Heimfeld, S., and Weissman, I.L. (1988). Purification and Characterization of Mouse Hematopoietic Stem-Cells. Science *241*, 58-62.

Speck, N.A., and Gilliland, D.G. (2002). Core-binding factors in haematopoiesis and leukaemia. Nat Rev Cancer *2*, 502-513.

Staley, B., Irvine, KD. (2010). Wars and Yorkie mediate intestinal regeneration by influencing stem cell proliferation. Curr Biol *20*, 1580-1587.

Stocum, D.L. (2001). Stem cells in regenerative biology and medicine. Wound Repair Regen *9*, 429-442.

Stramer, B., Winfield, M., Shaw, T., Millard, T.H., Woolner, S., and Martin, P. (2008). Gene induction following wounding of wild-type versus macrophage-deficient *Drosophila* embryos. Embo Rep *9*, 465-471.

Su, A.I., Guidotti, L.G., Pezacki, J.P., Chisari, F.V., and Schultz, P.G. (2002). Gene expression during the priming phase of liver regeneration after partial hepatectomy in mice. P Natl Acad Sci USA *99*, 11181-11186.

Sullivan, J.C., Sher, D., Eisenstein, M., Shigesada, K., Reitzel, A.M., Marlow, H., Levanon, D., Groner, Y., Finnerty, J.R., and Gat, U. (2008). The evolutionary origin of the Runx/CBFbeta transcription factors - Studies of the most basal metazoans. Bmc Evolutionary Biology *8*, -.

Takahashi, K., and Yamanaka, S. (2006). Induction of pluripotent stem cells from mouse embryonic and adult fibroblast cultures by defined factors. Cell *126*, 663-676.

Tam, S.W., Theodoras, A.M., Shay, J.W., Draetta, G.F., and Pagano, M. (1994). Differential Expression and Regulation of Cyclin D1 Protein in Normal and Tumor Human-Cells - Association with Cdk4 Is Required for Cyclin D1 Function in G1 Progression. Oncogene *9*, 2663-2674.

Taub, R. (1996). Liver regeneration .4. Transcriptional control of liver regeneration. Faseb Journal *10*, 413-427.

Taub, R. (2004). Liver regeneration: From myth to mechanism. Nat Rev Mol Cell Bio *5*, 836-847.

Taub, R., Greenbaum, L.E., and Peng, Y. (1999). Transcriptional regulatory signals define cytokine-dependent and -independent pathways in liver regeneration. Semin Liver Dis *19*, 117-127.

Thompson, J.D., Higgins, D.G., and Gibson, T.J. (1994). CLUSTAL W: improving the sensitivity of progressive multiple sequence alignment through sequence weighting, position-specific gap penalties and weight matrix choice. Nucleic Acids Res *22*, 4673-4680.

Thomson, S., Clayton, A.L., and Mahadevan, L.C. (2001). Independent dynamic regulation of histone phosphorylation and acetylation during immediate-early gene induction. Mol Cell *8*, 1231-1241.

Till, J.E., and Mc, C.E. (1961). A direct measurement of the radiation sensitivity of normal mouse bone marrow cells. Radiat Res *14*, 213-222.

Ting, S.B., Caddy, J., Hislop, N., Wilanowski, T., Auden, A., Zhao, L.L., Ellis, S., Kaur, P., Uchida, Y., Holleran, W.M.*, et al.* (2005). A homolog of *Drosophila* grainy head is essential for epidermal integrity in mice. Science *308*, 411-413.

Toyoda, H., Komurasaki, T., Uchida, D., Takayama, Y., Isobe, T., Okuyama, T., and Hanada, K. (1995). Epiregulin. A novel epidermal growth factor with mitogenic activity for rat primary hepatocytes. J Biol Chem *270*, 7495-7500.

Tsai, R.Y., and McKay, R.D. (2002). A nucleolar mechanism controlling cell proliferation in stem cells and cancer cells. Genes Dev *16*, 2991-3003.

Tsai, R.Y., and McKay, R.D. (2005). A multistep, GTP-driven mechanism controlling the dynamic cycling of nucleostemin. J Cell Biol *168*, 179-184.

Tullai, J.W., Schaffer, M.E., Mullenbrock, S., Sholder, G., Kasif, S., and Cooper, G.M. (2007). Immediate-early and delayed primary response genes are distinct in function and genomic architecture. J Biol Chem *282*, 23981-23995.

Uchida, N., Buck, D.W., He, D.P., Reitsma, M.J., Masek, M., Phan, T.V., Tsukamoto, A.S., Gage, F.H., and Weissman, I.L. (2000). Direct isolation of human central nervous system stem cells. P Natl Acad Sci USA *97*, 14720-14725.

Umesono, Y., Watanabe, K., and Agata, K. (1997). A planarian orthopedia homolog is specifically expressed in the branch region of both the mature and regenerating brain. Dev Growth Differ *39*, 723-727.

Wagers, A.J., and Weissman, I.L. (2004). Plasticity of adult stem cells. Cell *116*, 639-648.

Wan, H., and Ishihara, H. (2004). Expression of JunB induced by X-rays in mice. Biomed Environ Sci *17*, 327-332.

Wang, W.D., Grimmer, J.F., Van De Water, T.R., and Lufkin, T. (2004). *Hmx2* and *Hmx3* homeobox genes direct development of the murine inner ear and hypothalamus and can be functionally replaced by *Drosophila Hmx*. Developmental Cell *7*, 439-453.

Wang, Y., Shen, J., Arenzana, N., Tirasophon, W., Kaufman, R.J., and Prywes, R. (2000). Activation of ATF6 and an ATF6 DNA binding site by the endoplasmic reticulum stress response. J Biol Chem *275*, 27013-27020.

Wang, Y., Zayas, R.M., Guo, T., and Newmark, P.A. (2007). *nanos* function is essential for development and regeneration of planarian germ cells. Proc Natl Acad Sci U S A *104*, 5901-5906.

Weichselbaum, R.R., Hallahan, D., Fuks, Z., and Kufe, D. (1994). Radiation induction of immediate early genes: effectors of the radiation-stress response. Int J Radiat Oncol Biol Phys *30*, 229-234.

Weissman, I.L. (2000). Stem cells: Units of development, units of regeneration, and units in evolution. Cell *100*, 157-168.

Wenemoser, D., and Reddien, P.W. (2007). Cell biological changes in neoblasts following wounding in the planarian *Schmidtea mediterranea*. Diploma Thesis.

Westheide, W., Reinhard, R. (2007). Spezielle Zoologie (Muenchen, Spektrum Akademischer Verlag).

Whitehead, G.G., Makino, S., Lien, C.L., and Keating, M.T. (2005). fgf20 is essential for initiating zebrafish fin regeneration. Science *310*, 1957-1960.

Winkles, J.A. (1998). Serum- and polypeptide growth factor-inducible gene expression in mouse fibroblasts. In Progress in Nucleic Acid Research and Molecular Biology, Vol 58 (San Diego, Academic Press Inc), pp. 41-78.

Wolff, E. (1962). Recent researches on the regeneration of planaria. (New York, Ronald Press).

Wolff, E., and Dubois, F. (1948). Sur la migration des cellules de régénération chez les planaires. Revue Swisse Zool *55*, 218-227.

Wollnik, B., Kubisch, C., Maass, A.H., Vetter, H., and Neyses, L. (1993). Hyperosmotic Stress Induces Immediate-Early Gene-Expression in Ventricular Adult Cardiomyocytes. Biochem Bioph Res Co *194*, 642-646.

Woodbury, R.G., Brown, J.P., Yeh, M.Y., Hellstrom, I., and Hellstrom, K.E. (1980). Identification of a cell surface protein, p97, in human melanomas and certain other neoplasms. Proc Natl Acad Sci U S A *77*, 2183-2187.

Xu, Q., Mellitzer, G., Robinson, V., and Wilkinson, D.G. (1999). In vivo cell sorting in complementary segmental domains mediated by Eph receptors and ephrins. Nature *399*, 267-271.

Yan, D., and Lin, X. (2007). *Drosophila* glypican Dally-like acts in FGF-receiving cells to modulate FGF signaling during tracheal morphogenesis. Dev Biol *312*, 203-216.

Yin, V.P., Thomson, J.M., Thummel, R., Hyde, D.R., Hammond, S.M., and Poss, K.D. (2008). Fgf-dependent depletion of microRNA-133 promotes appendage regeneration in zebrafish. Gene Dev *22*, 728-733.

Yokota, Y., Eom, T.Y., Stanco, A., Kim, W.Y., Rao, S., Snider, W.D., and Anton, E.S. (2010). Cdc42 and Gsk3 modulate the dynamics of radial glial growth, inter-radial glial interactions and polarity in the developing cerebral cortex. Development *137*, 4101-4110.

Zagami, C.J., Zusso, M., and Stifani, S. (2009). Runx transcription factors: lineage-specific regulators of neuronal precursor cell proliferation and post-mitotic neuron subtype development. J Cell Biochem *107*, 1063-1072.

Zayas, R.M., Hernandez, A., Habermann, B., Wang, Y., Stary, J.M., and Newmark, P.A. (2005). The planarian Schmidtea mediterranea as a model for epigenetic germ cell specification: analysis of ESTs from the hermaphroditic strain. Proc Natl Acad Sci U S A *102*, 18491-18496.

7 Publications

Written publications

Wenemoser, D., and Reddien, P.W.: Cell biological changes in neoblasts following wounding in the planarian *Schmidtea mediterranea*. Diploma Thesis, Free University of Berlin, March 2007.

Wenemoser, D., and Reddien, P.W. (2010). Planarian regeneration involves distinct stem cell responses to wounds and tissue absence. Dev Biol *344*, 979-991.

Oral and poster presentations

Wenemoser, D., and Reddien, P.W.: Identification of cellular and molecular events that control regeneration initiation in planarians. Poster presentation, North-East Regional Meeting of the Society of Developmental Biology, Woods Hole, USA, April 2008.

Scimone, M.L., Wenemoser, D., and Reddien, P.W.: Characterization of neoblast-expressed genes in planarian regeneration. Poster presentation, 73rd Cold Spring Harbor Symposium: Control and Regulation of Stem Cells, Cold Spring Harbor, USA, July 2008.

Wenemoser, D., and Reddien, P.W.: Regeneration initiation in planarians. Oral presentation, 1st North-American Planaria Meeting, Chicago, November 2008.

Wenemoser, D., and Reddien, P.W.: Regulation of planarian stem cells during regeneration initiation. Poster presentation, North-East Regional Meeting of the Society of Developmental Biology, Woods Hole, USA, April 2009.

Wenemoser, D., and Reddien, P.W.: Planarian regeneration involves distinct stem cell responses to wounds and tissue absence. SDB 69th Annual Meeting, Albuquerque, NM, USA, August 2010.

Wenemoser, D., and Reddien, P.W.: Regulation of planarian stem cells during regeneration initiation. Poster presentation, International Society for Stem Cell Research, 7th Annual Meeting, Barcelona, Spain, July 2009.

Awards

First Jerome and Florence Brill Summer Graduate Fellow Award for outstanding work on stem cell-related research, July 2006.

8 Appendix

8.1 Abbreviations

˚C	Degree Celsius
amp	Ampicillin
AP	Alkaline Phophatase
AP-1	Activator protein 1
BCIP	5-Brom-4-chlor-3-indolyl-phosphate
BMP	Bone Morphogenetic Protein
bp	Base Pair
BrdU	5-Bromo-2'-deoxyuridine
BSA	Bovine Serum Albumin
c-Fos	cellular oncogene fos
cdc	cell division cycle
cdk	cyclin-dependent kinase
cDNA	Complementary DNA
CREB	Cyclic-AMP response element-binding protein
d	day
dH2O	Destilled Water
DNA	Deoxyribonucleic Acid
dNTP	Deoxynuceloside-5'-Triphosphat
dpp	Decapentaplegic
DTT	Dithiotreitol
EDTA	Ethylendiamintetraaceticacid
ES cell	Embryonic Stem Cell
EST	Expressed Sequence Tag
EtOH	Ethanol
FACS	Fluorescence Activated Cell Sorting
FL	Fluorescence Laser
FSC	Forward Scatter
g	Gram
G	Gap Phase
h	Hour
H2B	histone H2B
H3P	Serine 10 phosphorylated histone H3
hh	Hedgehog
Hox	Homeobox Protein
HRP	Horseradish Peroxidase
HU	Hydroxyurea
ICM	Inner Cell Mass
IPTG	Isopropyl beta-D-1-thiogalactopyranoside
JAK/STAT	Janus kinase signal transducer and activator of transcription
JNK	JUN amino-terminal kinase
kan	Kanamycin
M	Mitosis
MAPK	Mitogen-activated protein kinase
MASH	Achaete-Scute Homolog
MCM	Minichromosome Maintenance
mg	Milligram
min	Minute
MLL	myeloid/lymphoid or mixed-lineage leukemia
mm	Millimeter
MMTV	Mouse Mammary Tumor Virus

mRNA	Messenger RNA
NBT	Nitrobluetetrazoliumchloride
nlg1	noggin-like 1
OD	Optical Density
oligo-dT	Oligo-deoxy-Thymidin
Pax	Paired Box Protein
PBS	Phosphate Buffered Saline
PCNA	Proliferating Cell Nuclear Antigen
PCR	Polymerase Chain Reaction
PEG	Polyethyleneglycol
PI	Propidium Iodide
qtPCR	quantitative PCR
RACE	Rapid Amplification Of cDNA Ends
RNA	Ribonucleic Acid
RNAi	RNA interference
RNR	Ribonucleotide reductase
rpm	Rounds Per Minute
RT-PCR	Reverse Transcription PCR
S	S-phase
SOS	Son of sevenless
sox	SRY (sex determining region Y)-box
SSC	Side Scatter
TAE	Tris-Acetate-EDTA-Buffer
tet	Tetracyclin
TFAP2A	AP-2 alpha (activating enhancer binding protein 2 alpha)
TGFβ	Transforming Growth Factor-β
unc	Uncoordinated Behaviour
vW	von Willebrandt
Wnt	Wingless and int, MMTV integration site
µg	Microgram
µl	Microliter

8.2 List of genes that were significantly upregulated in the differentiated tissue following wounding as determined by microarray analysis

Table 8.1. Log2 ratios of (time point/control) for oligos that were significantly (FDR-adjusted p-value < 0.05) upregulated in wild-type (log2 > 0.3) and at the same time point in irradiated (log > 0.6) animals following wounding. For space reasons, only 387 of the 463 identified oligos were shown. Missing oligos represent homologs of cytoskeletal and structural components (actin, myosin, and tubulin).

SMED ID	Top human blastx hit	WT 30min	WT 1h	WT 3h	WT 6h	WT12h	IRR 30min	IRR 1h	IRR 3h	IRR 6h	IRR 12h
SMED_07471_V2_1	early growth response 1 (egr1b)	2.21	2.81	1.89	0.48	-0.90	1.75	2.76	2.24	0.41	-0.80
SMED_15412_V2_1	unknown	1.85	1.33	1.16	1.51	1.24	1.51	0.83	1.29	0.47	1.08
SMED_21076_V2_1	unknown	1.82	1.32	1.12	1.46	1.18	1.40	0.83	1.29	0.71	1.10
SMED_03762_V2_1	unknown	1.81	1.11	0.98	1.12	1.03	1.42	0.37	1.14	0.08	1.05
SMED_00001_V2_1	unknown	1.78	1.13	0.93	1.27	1.04	1.46	0.56	1.12	0.45	0.91
SMED_20032_V2_1	unknown	1.70	1.62	1.33	1.64	1.43	1.70	1.48	1.57	0.92	1.64
SMED_08137_V2_1	unknown	1.68	1.34	1.08	1.45	1.13	1.52	0.77	1.23	0.53	1.13
SMED_01464_V2_1	unknown	1.23	0.87	0.58	0.88	0.87	1.04	0.52	0.76	0.74	0.43
SMED_04167_V2_1	unknown	1.19	1.50	1.09	0.41	0.14	1.13	1.61	0.76	0.17	0.06
SMED_00025_V2_1	prostaglandin D2 synthase, hematopoietic	1.17	0.56	0.42	0.59	0.70	1.07	0.46	0.78	0.55	0.54
SMED_03061_V2_1	jun	1.14	1.61	1.51	0.77	0.99	1.10	1.59	1.28	0.42	0.93
SMED_20166_V2_1	unknown	1.09	0.88	0.91	1.02	0.99	0.94	0.77	0.96	0.88	1.08
SMED_35828_V2_1	early growth response (egr1)	1.08	1.60	1.29	0.48	0.01	1.31	2.69	1.89	0.57	0.38
SMED_06068_V2_1	pim-1 oncogene	0.94	0.65	0.03	-0.21	-0.06	0.87	0.88	0.06	-0.39	0.12
SMED_00148_V2_1	guanine nucleotide binding protein (G protein), beta polypeptide 1	0.93	0.73	0.71	0.68	0.61	0.74	0.62	0.75	0.84	0.63
SMED_14072_V2_1	baculoviral IAP repeat-containing 3	0.88	0.72	0.07	-0.02	-0.08	0.83	0.78	0.23	-0.12	-0.04
SMED_29852_V2_1	collagen, type VI, alpha 3	0.88	1.04	0.95	-0.27	-0.48	1.08	1.74	1.09	-0.28	-0.90
SmWIOct06_021580	unknown	0.86	0.73	0.59	-1.05	-1.04	0.86	1.03	0.47	-1.41	-0.92
SMED_15791_V2_1	unknown	0.85	0.70	0.52	-0.97	-0.89	0.87	0.95	0.45	-1.33	-0.84
SMED_06912_V2_1	protein phosphatase 1, regulatory (inhibitor) subunit 3B	0.82	0.84	-0.31	-0.18	-0.42	1.25	1.25	0.00	-0.27	-0.04
SMED_02282_V2_1	unknown	0.81	1.10	0.84	0.62	0.74	0.91	1.04	1.28	0.85	0.93
SMED_02735_V2_1	unknown	0.76	0.70	1.12	1.20	1.14	0.73	1.01	0.99	0.81	1.24
SMED_03084_V2_1	unknown	0.76	0.84	0.33	-0.09	-0.19	0.63	0.75	0.32	-0.15	-0.21
SMED_08052_V2_1	Ras suppressor protein 1	0.74	0.50	0.42	0.61	0.49	0.70	0.42	0.56	0.50	0.47
SMED_00418_V2_1	transmembrane 9 superfamily member 2	0.74	0.74	0.67	0.61	0.34	0.49	0.65	0.64	0.62	0.61
SMED_14876_V2_1	RAB5A, member RAS oncogene family	0.72	0.56	0.58	0.53	0.47	0.68	0.54	0.62	0.35	0.37
SMED_02435_V2_1	ubiquitin-conjugating enzyme E2Z	0.72	0.55	0.63	0.81	0.66	0.61	0.44	0.66	0.60	0.72
SMED_37361_V2_1	unknown	0.69	0.94	0.79	0.66	0.13	0.46	1.09	0.91	0.67	0.43
SMED_21473_V2_1	unknown	0.69	0.58	1.26	1.17	0.92	1.07	0.89	0.73	1.27	1.19
SMED_02238_V2_1	ankyrin 3, node of Ranvier (ankyrin G)	0.69	0.76	0.71	0.55	0.29	0.54	0.77	0.64	0.57	0.41
SMED_09699_V2_1	surfeit 4	0.68	0.43	0.50	0.83	0.72	0.56	0.22	0.43	0.61	0.72
SMED_03373_V2_1	ubiquitin-conjugating enzyme E2D 3 (UBC4/5 homolog, yeast)	0.67	0.53	0.65	0.74	0.58	0.63	0.56	0.64	0.40	0.61
SMED_01224_V2_1	ADP-ribosylation factor 1	0.67	0.28	0.43	0.59	0.44	0.63	0.40	0.44	0.51	0.59
SMED_03209_V2_1	RAB27B, member RAS oncogene family	0.67	0.57	0.49	0.72	0.70	0.64	0.48	0.58	0.70	0.57
SmWIOct06_013207	unknown	0.67	0.74	0.64	0.46	0.15	0.51	0.69	0.65	0.53	0.43
SMED_00211_V2_1	unknown	0.66	0.51	0.30	0.53	0.53	0.65	0.41	0.73	0.65	0.48
SMED_03620_V2_1	muscle RAS oncogene homolog	0.65	0.64	0.77	0.78	0.27	0.40	0.36	0.69	0.70	0.31
SMED_00151_V2_1	major facilitator superfamily domain containing 1	0.64	0.45	0.52	0.63	0.61	0.52	0.37	0.61	0.74	0.54
SMED_37908_V2_1	unknown	0.64	0.39	0.38	0.57	0.38	0.60	0.33	0.45	0.39	0.41
SMED_15081_V2_1	unknown	0.64	0.38	0.41	0.55	0.27	0.63	0.37	0.51	0.44	0.40
SMED_06632_V2_1	ADP-ribosylation factor-like 14	0.63	0.31	0.39	0.59	0.40	0.66	0.43	0.54	0.44	0.51
SMED_02036_V2_1	calpain 3, (p94)	0.63	0.55	0.59	0.49	0.59	0.77	0.60	0.66	1.08	0.58

SMED_00564_V2_1	KDEL (Lys-Asp-Glu-Leu) endoplasmic reticulum protein retention receptor 2	0.62	0.29	0.33	0.63	0.50	0.59	0.29	0.45	0.52	0.64
SMED_01480_V2_1	p21 protein (Cdc42/Rac)-activated kinase 3	0.62	0.68	0.57	0.42	0.18	0.42	0.63	0.53	0.46	0.33
SMED_02080_V2_1	unknown	0.61	0.32	0.53	0.73	0.73	0.76	0.71	0.69	0.64	0.90
SMED_28394_V2_1	RAB5B, member RAS oncogene family	0.61	0.55	0.54	0.50	0.34	0.69	0.52	0.62	0.30	0.41
SMED_14741_V2_1	ligand of numb-protein X 1	0.60	0.52	0.70	0.68	0.42	0.44	0.44	0.79	0.96	0.56
SMED_19979_V2_1	unknown	0.59	0.33	0.41	0.60	0.37	0.63	0.33	0.50	0.47	0.49
SMED_06604_V2_1	unknown	0.59	0.76	0.57	0.32	0.53	0.59	0.75	0.56	0.28	0.53
SMED_02727_V2_1	glia maturation factor, beta	0.59	0.39	0.51	0.70	0.63	0.59	0.43	0.52	0.37	0.61
SMED_00792_V2_1	docking protein 7	0.59	0.70	0.55	0.33	0.41	0.60	0.72	0.49	0.20	0.54
SMED_12340_V2_1	unknown	0.58	0.57	0.68	0.46	0.33	0.41	0.57	0.62	0.80	0.34
SMED_02965_V2_1	3'-phosphoadenosine 5'-phosphosulfate synthase 2	0.58	0.42	0.42	0.61	0.69	0.60	0.32	0.53	0.87	0.59
SMED_16449_V2_1	unknown	0.57	0.51	0.58	0.67	0.56	0.35	0.44	0.50	0.29	0.60
SMED_06418_V2_1	unknown	0.57	0.50	0.60	0.47	0.55	0.61	0.52	0.53	0.95	0.37
SMED_00055_V2_2	c-Fos	0.56	1.47	1.74	0.94	1.07	0.57	1.55	1.61	1.35	1.35
SMED_01777_V2_1	glutathione S-transferase mu 4	0.56	0.44	0.55	0.67	0.56	0.49	0.47	0.59	0.39	0.62
SMED_02142_V2_1	unknown	0.55	0.45	0.41	0.72	0.93	0.73	0.68	0.67	0.74	1.21
SMED_20504_V2_1	unknown	0.55	0.73	0.59	0.44	0.43	0.39	0.63	0.73	0.65	0.52
SMED_12389_V2_1	unknown	0.55	0.59	0.51	0.40	0.16	0.36	0.67	0.56	0.24	0.29
SMED_28060_V2_1	misshapen-like kinase 1 (zebrafish)	0.55	0.66	0.59	0.48	0.31	0.56	0.60	0.63	0.77	0.43
SMED_03835_V2_1	protein phosphatase 2 (formerly 2A), regulatory subunit A, alpha isoform	0.55	0.42	0.43	0.51	0.55	0.64	0.28	0.41	0.81	0.35
SMED_02433_V2_1	mitogen-activated protein kinase kinase kinase 1	0.55	0.59	0.63	0.58	0.47	0.37	0.61	0.64	0.84	0.51
SMED_02886_V2_1	translocase of outer mitochondrial membrane 40 homolog (yeast)	0.55	0.48	0.67	0.82	0.72	0.36	0.24	0.66	0.69	0.65
SMED_01154_V2_1	unknown	0.54	0.45	0.48	1.05	1.45	0.42	0.45	0.24	0.62	0.81
SMED_16035_V2_1	poly (ADP-ribose) polymerase family, member 3	0.53	0.64	0.57	0.39	0.26	0.59	0.60	0.63	0.77	0.42
SMED_08358_V2_1	mitochondrial ribosomal protein S25	0.53	0.47	0.69	0.78	0.66	0.46	0.57	0.55	0.36	0.68
SMED_14794_V2_1	unknown	0.53	0.29	0.33	0.50	0.48	0.61	0.29	0.40	0.48	0.42
SMED_03302_V2_1	unknown	0.52	0.62	0.72	0.61	0.44	0.43	0.63	0.54	0.50	0.62
SMED_04383_V2_1	unknown	0.52	0.31	0.43	0.47	0.46	0.60	0.24	0.36	0.64	0.41
SMED_12662_V2_1	unknown	0.51	0.45	0.67	0.71	0.49	0.53	0.42	0.76	0.44	0.17
SMED_14904_V2_1	unknown	0.51	0.58	1.86	2.17	1.96	0.49	0.67	1.74	2.01	1.93
SMED_06866_V2_1	bromodomain and WD repeat domain containing 1	0.50	0.75	1.17	0.48	0.62	0.42	0.92	1.43	0.37	0.92
SMED_11787_V2_1	unknown	0.50	0.47	0.48	0.60	0.63	0.91	0.70	0.80	1.33	0.77
SMED_03805_V2_1	solute carrier family 39 (zinc transporter), member 7	0.49	0.22	0.35	0.64	0.61	0.37	0.15	0.37	0.43	0.68
SMED_01392_V2_1	family with sequence similarity 98, member A	0.49	0.43	0.53	0.57	0.52	0.59	0.33	0.54	0.66	0.38
SMED_03106_V2_1	ADP-ribosylation factor-like 8B	0.49	0.29	0.37	0.60	0.52	0.54	0.37	0.45	0.37	0.62
SMED_02039_V2_2r	piccolo (presynaptic cytomatrix protein)	0.49	0.49	0.50	0.60	0.73	0.57	0.32	0.46	0.80	0.42
SMED_03989_V2_1	histone cluster 1, H1e	0.49	1.05	1.35	0.33	0.10	0.65	1.16	1.48	0.24	0.09
SMED_02439_V2_1	kinesin family member 5C	0.48	0.68	0.65	0.58	0.59	0.59	0.79	0.93	1.37	0.77
SMED_08087_V2_1	ferritin, heavy polypeptide 1	0.48	0.71	0.64	0.51	0.26	0.58	0.80	0.73	0.33	0.33
SMED_05872_V2_1r	calpain 9	0.48	0.54	1.14	1.09	0.84	0.45	0.65	1.23	1.11	1.16
SMED_01658_V2_1	S-adenosylhomocysteine hydrolase	0.48	0.32	0.43	0.83	1.21	0.37	0.19	0.43	0.70	1.13
SMED_00353_V2_1	myxovirus (influenza virus) resistance 1, interferon-inducible protein p78 (mouse)	0.48	0.45	0.33	0.49	0.46	0.58	0.52	0.52	0.82	0.58
SMED_11308_V2_1	zinc metallopeptidase (STE24 homolog, S. cerevisiae)	0.48	0.41	0.65	0.84	0.76	0.57	0.43	0.55	0.56	0.88
SMED_10023_V2_1	unknown	0.48	0.36	0.58	0.59	0.27	0.43	0.44	0.67	0.40	0.33
SMED_05057_V2_1r	hypothetical protein LOC100133521	0.48	0.46	0.57	0.62	0.67	0.29	0.25	0.45	0.87	0.50
SmWIOct06_003878	leukotriene A4 hydrolase	0.47	0.43	0.51	0.38	0.36	0.70	0.55	0.59	0.94	0.37
SMED_04865_V2_1	unknown	0.47	0.37	0.40	0.35	0.49	0.75	0.42	0.51	1.06	0.47
SMED_32427_V2_1	geranylgeranyl diphosphate synthase 1	0.47	0.32	0.49	0.61	0.50	0.42	0.34	0.44	0.32	0.61
SMED_17304_V2_1	unknown	0.47	1.13	0.98	0.69	-0.08	0.37	1.39	1.19	0.62	0.56

SMED_37290_V2_1	ankyrin repeat domain 28	0.47	0.57	0.51	0.50	0.39	0.60	0.66	0.52	0.06	0.41
SMED_20753_V2_1	unknown	0.47	0.45	0.59	0.46	0.42	0.67	0.54	0.66	0.98	0.41
SMED_14989_V2_1	unknown	0.47	0.16	0.12	0.52	0.68	0.43	-0.08	0.17	0.43	0.65
SMED_05938_V2_1	GNAS complex locus	0.47	0.46	0.48	0.60	0.62	0.71	0.44	0.58	1.01	0.66
SMED_01511_V2_1	myxovirus (influenza virus) resistance 1, interferon-inducible protein p78 (mouse)	0.47	0.44	0.36	0.48	0.43	0.62	0.56	0.52	0.82	0.55
SMED_19431_V2_1	unknown	0.45	0.67	0.51	0.42	0.05	0.36	0.72	0.63	0.63	0.25
SMED_27101_V2_1	solute carrier family 30 (zinc transporter), member 9	0.45	0.41	0.53	0.55	0.46	0.49	0.39	0.42	0.38	0.60
SMED_05579_V2_1	unknown	0.45	0.67	0.73	0.38	0.17	0.42	0.65	0.61	0.13	-0.03
SMED_04057_V2_1	phosphoinositide-3-kinase, catalytic, alpha polypeptide	0.45	0.41	0.57	0.55	0.57	0.58	0.37	0.44	0.84	0.43
SMED_02221_V2_1	mediator complex subunit 13	0.45	0.66	0.61	0.42	0.14	0.32	0.71	0.68	0.48	0.46
SMED_07779_V2_1	unknown	0.45	0.63	0.76	0.60	0.70	0.63	0.75	0.77	0.78	0.87
SMED_03008_V2_1	GRB2-associated binding protein 3	0.44	0.39	0.54	0.50	0.52	0.63	0.59	0.50	0.38	0.65
SMED_12796_V2_1	unknown	0.44	0.34	0.65	0.76	0.61	0.51	0.53	0.61	0.49	0.85
SMED_05266_V2_1	unknown	0.44	0.29	0.49	0.61	0.50	0.60	0.36	0.43	0.54	0.61
SMED_18265_V2_1	unknown	0.44	0.51	0.46	0.60	0.51	0.52	0.52	0.60	0.72	0.73
SMED_00839_V2_1	noggin	0.44	0.32	0.86	1.27	1.27	0.50	0.35	1.15	1.36	1.67
SMED_12193_V2_1	unknown	0.44	0.46	0.85	0.55	0.16	0.51	0.45	0.71	0.28	-0.01
SMED_15193_V2_1	phospholipid scramblase 1	0.44	0.76	0.65	0.47	0.05	0.31	0.74	0.57	0.37	0.40
SMED_36485_V2_1	unknown	0.44	0.46	0.63	0.49	0.51	0.28	0.57	0.49	0.61	0.67
SMED_09765_V2_1	unknown	0.43	0.23	0.22	0.53	1.36	0.35	0.25	0.11	0.37	1.93
SMED_04506_V2_1	unknown	0.43	0.57	0.86	0.94	0.71	0.11	0.53	0.78	0.39	0.52
SmWIOct06_029758	SWI/SNF related, matrix associated, actin dependent regulator of chromatin	0.43	0.71	0.65	0.49	0.05	0.27	0.75	0.61	0.34	0.32
SMED_20767_V2_1	unknown	0.43	0.62	0.56	0.37	0.14	0.50	0.73	0.64	0.60	0.39
SMED_00405_V2_1	unknown	0.43	0.25	0.33	0.45	0.58	0.42	0.29	0.30	0.61	0.41
SMED_36797_V2_1	unknown	0.43	0.57	0.57	0.29	0.26	0.32	0.67	0.50	0.49	0.47
SMED_01600_V2_1	kynureninase (L-kynurenine hydrolase)	0.41	0.72	0.71	0.44	-0.05	0.16	0.48	0.71	0.34	0.32
SMED_01615_V2_1	septin 11	0.41	0.55	0.61	0.55	0.57	0.28	0.56	0.67	0.72	0.71
SMED_10026_V2_1	small G protein signaling modulator 1	0.41	0.35	0.41	0.32	0.42	0.51	0.40	0.41	0.78	0.30
SMED_19330_V2_1	unknown	0.41	0.42	0.52	0.57	0.48	0.56	0.41	0.52	0.45	0.67
SMED_01688_V2_1	troponin T type 2 (cardiac)	0.41	0.66	0.50	0.37	0.33	0.73	0.87	0.90	0.86	0.68
SMED_00324_V2_1	calponin 1, basic, smooth muscle	0.41	0.23	0.29	0.48	0.45	0.54	0.29	0.41	0.25	0.69
SMED_15622_V2_1	R3H domain containing-like	0.41	0.34	0.43	0.56	0.59	0.37	0.38	0.64	0.47	0.88
SMED_00450_V2_1	pyruvate kinase, muscle	0.40	0.33	0.40	0.41	0.53	0.48	0.33	0.42	0.69	0.41
SMED_01868_V2_1	acyl-CoA synthetase long-chain family member 4	0.40	0.60	0.74	0.65	0.56	0.61	0.77	0.80	0.84	1.01
SMED_20251_V2_1	early growth response 2 (Krox-20 homolog, Drosophila) (egr2)	0.40	1.13	2.36	2.27	1.96	0.28	0.84	1.84	1.90	1.75
SMED_06511_V2_1	cytochrome P450, family 2, subfamily U, polypeptide 1	0.40	0.58	0.71	0.67	0.52	0.27	0.54	0.52	0.53	0.67
SMED_27198_V2_1	peptidoglycan recognition protein 4	0.40	0.57	0.42	0.17	-0.05	0.15	0.66	0.43	0.11	0.10
SMED_27511_V2_1	troponin T type 2 (cardiac)	0.40	0.68	0.53	0.40	0.39	0.75	0.93	0.93	0.92	0.74
SmWIOct06_012995	forkhead box A2	0.39	0.67	0.63	0.35	0.28	0.35	0.68	0.59	0.39	0.50
SMED_09339_V2_1	solute carrier family 22 (extraneuronal monoamine transporter), member 3	0.39	0.32	0.53	0.78	0.63	0.40	0.26	0.44	0.74	0.75
SMED_05117_V2_1	unknown	0.39	0.64	0.79	0.77	0.38	0.47	0.66	0.92	0.97	1.06
SMED_20693_V2_1	solute carrier family 16, member 9 (monocarboxylic acid transporter 9)	0.39	0.23	0.40	0.54	0.48	0.42	0.25	0.42	0.60	0.56
SMED_20222_V2_1	unknown	0.39	0.50	0.84	0.88	0.82	0.29	0.50	0.69	0.48	0.67
SMED_15789_V2_1	nucleotide binding protein 1 (MinD homolog, E. coli)	0.38	0.41	0.51	0.49	0.47	0.29	0.39	0.39	0.30	0.61
SMED_01509_V2_1	ankyrin repeat domain 52	0.38	0.71	0.68	0.46	0.49	0.56	0.80	0.82	1.15	0.50
SMED_03123_V2_1	unknown	0.38	0.48	0.54	0.51	0.35	0.70	0.64	0.74	0.96	0.57
SMED_35771_V2_1	transmembrane protein 135	0.38	0.24	0.47	0.77	0.60	0.36	0.08	0.45	0.68	0.67
SMED_04173_V2_1	unknown	0.38	0.48	0.66	0.43	0.18	0.24	0.41	0.64	0.09	-0.05

SMED_04707_V2_1	ras-related C3 botulinum toxin substrate 1 (rho family, small GTP binding protein Rac1)	0.38	0.54	0.85	0.61	0.33	0.18	0.60	0.93	0.44	0.30
SMED_00099_V2_1	glutamate-ammonia ligase (glutamine synthetase)	0.38	0.56	0.58	0.83	0.71	0.19	0.33	0.56	0.69	0.80
SMED_02892_V2_1	unknown	0.37	0.35	0.54	0.94	0.93	0.34	0.20	0.42	0.70	0.92
SMED_04963_V2_1	CWC15 spliceosome-associated protein homolog	0.37	0.19	0.39	0.50	0.42	0.46	0.28	0.44	0.29	0.62
SMED_09897_V2_1	ArfGAP with RhoGAP domain, ankyrin repeat and PH domain 2	0.37	0.26	0.36	0.47	0.45	0.69	0.26	0.43	1.01	0.32
SMED_08379_V2_1	HLA-B associated transcript 1	0.37	0.45	0.39	0.50	0.60	0.42	0.33	0.42	0.61	0.28
SMED_15128_V2_1	unknown	0.37	0.45	0.55	0.60	0.46	0.19	0.47	0.66	0.38	0.19
SMED_02194_V2_1	p21 protein (Cdc42/Rac)-activated kinase 2	0.37	0.47	0.24	0.04	0.01	0.44	0.61	0.40	0.12	0.14
SMED_14564_V2_1	unknown	0.36	0.32	0.56	0.57	0.23	0.36	0.47	0.65	0.37	0.40
SMED_01830_V2_1	procollagen-proline, beta polypeptide	0.36	0.32	0.44	0.55	0.70	0.47	0.35	0.47	0.84	0.65
SMED_04547_V2_1	unknown	0.36	0.32	0.37	0.31	0.55	0.41	0.38	0.36	0.76	0.45
SMED_08759_V2_1	chromosome 16 open reading frame 62	0.36	0.35	0.44	0.43	0.46	0.47	0.31	0.44	0.84	0.35
SMED_30124_V2_1	SNF1-like kinase 2	0.36	0.55	0.55	0.44	0.51	0.29	0.53	0.55	0.59	0.67
SMED_00682_V2_1	cathepsin C	0.36	0.33	0.43	0.54	0.66	0.44	0.29	0.63	0.58	0.75
SMED_17889_V2_1	unknown	0.36	0.48	0.52	0.44	0.41	0.47	0.64	0.66	0.42	0.70
SMED_05034_V2_1	unknown	0.35	0.43	1.01	1.63	1.99	0.32	0.30	0.69	0.96	1.08
SMED_33036_V2_1	GDP-mannose pyrophosphorylase B	0.35	0.51	0.58	0.49	0.49	0.28	0.60	0.64	0.47	0.87
SMED_04686_V2_1	dynamin 3	0.34	0.67	0.69	0.34	0.33	0.41	0.86	0.42	0.51	0.77
SMED_12958_V2_1	solute carrier family 35, member B4	0.34	0.16	0.16	0.52	0.59	0.31	0.08	0.15	0.31	0.66
SMED_06730_V2_1	unknown	0.34	0.60	1.02	0.63	0.27	0.27	0.56	1.16	0.93	0.54
SMED_07992_V2_1	unknown	0.34	0.54	0.66	0.55	0.49	0.43	0.63	0.64	0.67	0.64
SMED_08992_V2_1	unknown	0.34	0.67	0.33	-0.07	-0.10	0.11	0.60	0.33	0.19	0.01
SMED_20673_V2_1	unknown	0.34	0.29	0.39	0.41	0.40	0.44	0.35	0.43	0.65	0.41
SMED_08611_V2_1	unknown	0.34	0.61	0.40	0.24	0.01	0.30	0.63	0.33	0.18	0.25
SMED_05752_V2_1r	unknown	0.34	0.57	0.65	0.29	0.22	0.60	0.92	0.82	1.01	0.78
SMED_05282_V2_1	hexokinase 1	0.34	0.20	0.38	0.57	0.85	0.34	0.25	0.35	0.50	1.01
SMED_36825_V2_1	unknown	0.33	0.59	0.43	0.14	-0.06	0.32	0.72	0.59	0.66	0.34
SMED_09356_V2_1	low density lipoprotein receptor adaptor protein 1	0.33	0.09	0.24	0.34	0.47	0.62	0.33	0.38	0.52	0.68
SMED_00511_V2_1r	sphingomyelin phosphodiesterase, acid-like 3A	0.33	0.25	0.38	0.47	0.43	0.28	0.22	0.31	0.62	0.37
SMED_03435_V2_1	Putative UDP-GlcNAc:betaGal beta-1,3-N-acetylglucosaminyltransferase	0.33	0.25	0.52	0.66	0.38	0.41	0.20	0.51	0.65	0.39
SMED_01454_V2_1	multiple EGF-like-domains 6	0.33	0.32	0.35	0.42	0.54	0.34	0.38	0.39	0.62	0.68
SMED_18694_V2_1	unknown	0.33	0.28	0.49	0.63	0.37	0.33	0.37	0.58	0.61	0.58
SMED_32400_V2_1	dynamin 1	0.33	0.66	0.75	0.39	0.35	0.33	0.83	0.70	0.50	0.69
SMED_00850_V2_1	cell division cycle 27 homolog (S. cerevisiae)	0.33	0.60	0.73	0.43	0.16	0.20	0.51	0.83	0.78	0.23
SMED_07430_V2_1	castor zinc finger 1	0.32	0.50	0.39	0.37	0.15	0.30	0.57	0.57	0.70	0.41
SMED_12386_V2_1	chloride channel 5	0.32	0.31	0.40	0.37	0.38	0.50	0.41	0.48	0.88	0.32
SMED_27027_V2_1	TNF receptor-associated factor 3	0.32	0.49	0.51	0.40	0.37	0.42	0.64	0.60	0.52	0.63
SMED_00660_V2_1	protein disulfide isomerase family A, member 6	0.32	0.15	0.36	0.57	0.67	0.17	0.05	0.26	0.34	0.60
SMED_16665_V2_1	unknown	0.32	0.46	0.64	0.49	0.40	0.30	0.50	0.77	0.24	0.50
SMED_15924_V2_1	NAD kinase	0.32	0.24	0.67	0.81	0.75	0.26	0.22	0.60	0.54	0.78
SMED_03707_V2_1	CD151 molecule (Raph blood group)	0.32	0.33	0.49	0.58	0.56	0.22	0.43	0.47	0.34	0.71
SMED_08080_V2_1	four and a half LIM domains 2	0.31	0.20	0.23	0.60	0.82	0.46	0.20	0.31	0.48	0.81
SMED_19855_V2_1	unknown	0.31	-0.15	0.51	0.50	0.20	0.30	0.40	0.63	0.87	0.99
SMED_02317_V2_1	high-mobility group box 2	0.31	0.27	0.47	0.60	0.61	0.29	0.23	0.48	0.65	0.43
SMED_07833_V2_1	glucosamine-phosphate N-acetyltransferase 1	0.31	0.29	0.99	1.18	1.06	0.29	0.21	0.82	0.77	0.89
SMED_15941_V2_1	signal sequence receptor, delta (translocon-associated protein delta)	0.31	0.17	0.48	0.72	0.67	0.22	0.16	0.37	0.48	0.66
SMED_06551_V2_1	pim-3 oncogene	0.30	0.92	1.28	0.56	0.47	0.32	1.08	0.92	0.24	0.51
SMED_20532_V2_1	membrane-associated ring finger (C3HC4) 6	0.30	0.15	0.35	0.38	0.55	0.44	0.16	0.34	0.80	0.40
SMED_04384_V2_1	unknown	0.30	0.32	0.45	0.57	0.40	0.41	0.31	0.43	0.89	0.42
SMED_01404_V2_1	unknown	0.30	0.30	0.50	0.59	0.70	0.25	0.32	0.52	0.59	0.89

SMED_02407_V2_1	ubiquitin B	0.30	0.45	0.85	0.88	0.62	0.42	0.32	0.76	0.66	0.50
SMED_04273_V2_1	pim-3 oncogene	0.30	0.72	0.61	0.05	-0.23	0.42	0.91	0.74	0.17	-0.23
SMED_01261_V2_1	p21 protein (Cdc42/Rac)-activated kinase 2	0.30	0.47	0.26	-0.02	-0.03	0.46	0.64	0.44	0.11	0.14
SMED_21109_V2_1	unknown	0.30	0.41	0.50	0.23	0.01	0.22	0.47	0.60	0.48	0.22
SMED_03780_V2_1r	unknown	0.29	0.42	0.37	0.34	0.20	0.10	0.62	0.42	0.16	0.33
SmWIOct06_018226	SVOP-like	0.29	0.31	0.93	1.28	0.90	0.30	0.13	0.83	1.17	1.04
SMED_04997_V2_1	ornithine decarboxylase 1	0.29	0.23	0.53	0.83	1.09	0.34	0.25	0.54	0.97	1.33
SMED_27020_V2_1	unknown	0.29	0.48	0.59	0.36	0.37	0.46	0.65	0.64	0.62	0.76
SMED_10303_V2_1	B-cell CLL/lymphoma 3	0.28	0.32	0.47	0.54	0.61	0.24	0.34	0.41	0.54	0.67
SMED_34385_V2_1	potassium channel, subfamily K, member 18	0.28	0.26	0.40	0.52	0.32	0.38	0.28	0.52	0.75	0.33
SMED_06017_V2_1	tocopherol (alpha) transfer protein-like	0.28	0.22	0.29	0.58	0.52	0.33	0.37	0.39	0.64	0.50
SMED_00341_V2_1	methionine adenosyltransferase II, alpha	0.28	0.54	0.69	0.67	0.88	0.22	0.36	0.45	0.64	0.87
SMED_17458_V2_1	GLI pathogenesis-related 1 like 1	0.28	0.27	0.52	0.54	0.60	0.19	0.35	0.61	0.32	0.97
SMED_23057_V2_1	lactamase, beta	0.27	0.27	0.34	0.54	0.44	0.44	0.22	0.45	0.14	0.68
SMED_04365_V2_1	mucin 2, oligomeric mucus/gel-forming	0.27	0.34	0.40	0.38	0.36	0.37	0.37	0.37	0.31	0.63
SMED_19658_V2_1	ankyrin repeat domain 62	0.27	1.04	1.75	0.83	0.75	0.71	1.33	1.63	2.08	0.88
SMED_16228_V2_1	GRB10 interacting GYF protein 2	0.27	0.51	0.33	0.25	-0.05	0.27	0.63	0.47	0.36	0.21
SMED_08312_V2_1	neuro-oncological ventral antigen 2	0.27	0.37	0.41	0.39	0.42	0.51	0.39	0.53	0.69	0.47
SMED_03676_V2_1	unknown	0.27	0.19	0.46	0.85	0.92	0.29	0.21	0.53	0.72	0.96
SMED_29181_V2_1	unknown	0.27	0.54	0.68	0.38	0.33	0.22	0.74	0.69	0.65	0.57
SmWIOct06_040653	host cell factor C1 (VP16-accessory protein)	0.27	0.47	0.46	0.24	0.11	0.27	0.67	0.49	0.50	0.38
SMED_04444_V2_1	unknown	0.26	0.31	0.74	0.85	0.57	0.58	0.68	0.69	0.43	0.87
SMED_08420_V2_1	pim-1 oncogene	0.26	0.82	1.05	0.44	0.41	0.21	0.70	0.69	0.21	0.30
SMED_06494_V2_1	hexokinase 2	0.26	0.10	0.25	0.44	0.79	0.27	0.11	0.25	0.52	0.89
SMED_03492_V2_1	unknown	0.26	0.20	0.27	1.03	1.22	0.41	0.13	0.17	0.68	0.93
SMED_07580_V2_1	peroxidasin homolog (Drosophila)	0.25	0.50	0.70	0.68	0.74	0.11	0.54	0.80	1.09	1.10
SMED_06705_V2_1	epiregulin	0.25	0.29	0.68	0.21	-0.30	0.31	0.32	0.72	-0.03	-0.36
SMED_01282_V2_1	inhibin, beta A	0.25	0.38	0.50	0.85	0.82	0.29	0.33	0.67	0.91	1.13
SMED_02088_V2_1	fascin homolog 1, actin-bundling protein (Strongylocentrotus purpuratus)	0.25	0.36	0.93	1.32	1.59	0.54	0.48	1.14	1.72	1.70
SMED_10445_V2_1	neural cell adhesion molecule 1	0.25	0.43	0.54	0.53	0.64	0.00	0.19	0.34	0.56	0.87
SMED_02329_V2_1	FK506 binding protein 2, 13kDa	0.25	0.20	0.40	0.57	0.71	0.20	0.25	0.28	0.38	0.77
SMED_02705_V2_1	von Willebrand factor A domain containing 5A	0.24	0.62	0.51	0.03	0.07	0.45	0.76	0.66	0.81	0.35
SMED_01947_V2_1	MYC binding protein 2	0.24	0.47	0.35	0.24	-0.06	0.29	0.61	0.45	0.39	0.22
SMED_11940_V2_1	solute carrier family 10 (sodium/bile acid cotransporter family), member 2	0.24	0.34	0.60	0.50	-0.04	0.08	0.31	0.62	0.39	-0.06
SMED_02864_V2_1	reticulon 1	0.24	0.29	0.37	0.44	0.55	0.44	0.24	0.41	0.80	0.49
SMED_15976_V2_1	unknown	0.24	0.33	0.42	0.36	0.38	0.40	0.52	0.51	0.33	0.60
SMED_22858_V2_1	peptidylprolyl isomerase B (cyclophilin B)	0.23	0.25	0.50	0.73	0.76	0.36	0.20	0.51	0.68	0.81
SMED_03007_V2_1	SFRS protein kinase 1	0.23	0.52	0.43	0.27	0.16	0.38	0.84	0.79	0.67	0.54
SMED_03698_V2_1	unknown	0.23	0.43	0.36	0.46	0.45	0.61	0.62	0.66	0.81	0.72
SMED_10176_V2_1	metallophosphoesterase domain containing 1	0.23	0.49	0.88	0.23	0.03	0.25	0.44	0.88	0.08	-0.05
SMED_23132_V2_1	CDC-like kinase 2	0.23	0.22	0.37	0.38	0.58	0.15	0.12	0.33	0.60	0.66
SMED_02879_V2_1	unknown	0.23	0.24	0.50	0.48	0.75	0.29	0.17	0.45	1.00	0.56
SMED_16011_V2_1	cytochrome P450, family 2, subfamily C, polypeptide 19	0.23	0.23	0.38	1.01	1.20	0.43	0.21	0.59	1.21	1.44
SMED_02365_V2_1	moesin	0.23	0.49	0.67	0.86	1.06	0.56	0.63	0.87	1.29	1.38
SMED_08031_V2_1	enolase 3 (beta, muscle)	0.23	0.14	0.24	0.40	0.42	0.35	0.21	0.37	0.42	0.61
SMED_20366_V2_1	solute carrier family 35, member B1	0.23	0.03	0.35	0.75	0.65	0.21	0.01	0.23	0.45	0.76
SMED_37132_V2_1	unknown	0.22	0.37	0.25	0.20	0.15	0.31	0.69	0.40	0.13	0.35
SMED_19019_V2_1	unknown	0.22	0.05	0.03	0.35	0.64	0.09	-0.07	0.09	0.16	0.66
SMED_16101_V2_1	solute carrier family 4, sodium borate transporter, member 11	0.22	0.53	0.68	0.60	0.35	0.19	0.67	0.65	1.10	0.84
SMED_00017_V2_1	TNF receptor-associated factor 2	0.22	0.34	0.18	0.17	0.23	0.41	0.99	0.88	0.70	0.87
SMED_05687_V2_1	unknown	0.22	0.03	0.02	0.37	0.77	0.23	0.04	0.10	0.22	0.73

SMED_21674_V2_1	tripartite motif-containing 67	0.22	0.36	0.43	0.24	0.17	0.41	0.75	0.67	1.00	0.57
SMED_02029_V2_1	PRP8 pre-mRNA processing factor 8 homolog (S. cerevisiae)	0.22	0.38	0.41	0.23	0.11	0.22	0.87	0.73	0.43	0.58
SMED_09259_V2_1	lactamase, beta	0.21	0.17	0.27	0.43	0.49	0.47	0.23	0.35	0.19	0.74
SmWIOct06_012075	tissue factor pathway inhibitor (lipoprotein-associated coagulation inhibitor)	0.21	0.36	0.37	1.61	2.13	0.38	0.21	0.18	1.29	1.81
SMED_15201_V2_1	unknown	0.21	0.51	0.48	0.25	0.00	0.28	0.78	0.63	0.48	0.32
SMED_05818_V2_1	unknown	0.20	0.24	0.42	0.63	0.76	0.40	0.32	0.65	0.82	0.97
SMED_30572_V2_1	unknown	0.20	0.42	0.43	0.16	0.26	0.21	0.76	0.61	0.40	0.53
SMED_23904_V2_1	FYN oncogene related to SRC, FGR, YES	0.20	0.37	0.60	0.67	0.44	0.14	0.30	0.59	0.93	0.75
SMED_37709_V2_1	unknown	0.20	0.02	0.09	0.18	0.31	0.35	0.37	0.32	0.33	0.65
SMED_20731_V2_1	adducin 1 (alpha)	0.20	0.27	0.25	0.36	0.41	0.45	0.32	0.40	0.61	0.55
SMED_20770_V2_1	solute carrier family 33 (acetyl-CoA transporter), member 1	0.20	0.15	0.33	0.61	0.57	0.21	0.03	0.17	0.57	0.62
SMED_03434_V2_2	unknown	0.20	0.60	1.05	0.75	0.79	0.29	0.87	1.28	0.97	1.20
SMED_05540_V2_1	DnaJ (Hsp40) homolog, subfamily C, member 3	0.20	0.15	0.43	0.70	0.87	0.45	0.32	0.49	0.84	0.99
SMED_21560_V2_1	unknown	0.20	0.39	0.45	0.35	0.43	0.23	0.46	0.50	0.46	0.61
SMED_00498_V2_1	glycine amidinotransferase (L-arginine:glycine amidinotransferase)	0.19	0.54	0.97	0.85	0.85	-0.10	0.31	0.59	0.63	0.32
SMED_19195_V2_1	unknown	0.19	0.25	0.48	0.47	0.36	0.51	0.51	0.63	0.75	0.63
SMED_03304_V2_1	IMP (inosine monophosphate) dehydrogenase 2	0.19	0.21	0.34	0.41	0.64	0.28	0.33	0.37	0.70	0.96
SMED_10375_V2_1	unknown	0.19	0.62	-0.14	-0.36	-0.46	0.06	0.70	-0.03	-0.32	-0.26
SMED_12847_V2_1	unknown	0.19	0.34	0.28	0.22	0.23	0.10	0.78	0.42	0.20	0.33
SMED_00097_V2_1r	transmembrane protein 111	0.18	0.39	0.69	0.68	0.06	0.27	0.25	0.66	0.53	0.11
SMED_01527_V2_1	aminolevulinate, delta-, dehydratase	0.18	0.16	0.48	0.78	1.02	0.25	0.17	0.61	0.43	0.86
SMED_04943_V2_1	unknown	0.18	0.29	1.71	1.99	1.82	0.14	0.39	1.52	1.75	1.75
SMED_07661_V2_1	major facilitator superfamily domain containing 2	0.18	0.36	0.47	0.37	0.33	0.37	0.56	0.71	0.76	0.63
SMED_05374_V2_1	receptor tyrosine kinase-like orphan receptor 1	0.18	0.41	0.33	0.15	0.21	0.21	0.73	0.61	0.43	0.53
SMED_11930_V2_1	GA binding protein transcription factor, beta subunit 2	0.18	0.17	0.26	0.32	0.34	0.21	0.13	0.30	0.63	0.32
SMED_09938_V2_1	early growth response 1 (egr2a)	0.18	0.32	0.90	0.79	0.60	0.29	0.40	0.91	0.72	0.71
SMED_07580_V2_1r	peroxidasin homolog (Drosophila)	0.18	0.42	0.57	0.52	0.45	0.42	0.54	0.72	1.21	0.92
SMED_00143_V2_1	unknown	0.18	0.22	0.64	0.73	0.53	0.29	0.16	0.78	0.86	0.61
SMED_13944_V2_1	SET domain containing 1B	0.18	0.49	0.35	0.17	0.04	0.25	0.63	0.51	0.53	0.31
SMED_03388_V2_1	surfeit 4	0.17	0.10	0.37	0.56	0.45	0.22	0.12	0.28	0.51	0.70
SMED_14464_V2_1	unknown	0.17	0.45	0.41	0.22	0.05	0.17	0.68	0.54	0.38	0.27
SMED_21995_V2_1	unknown	0.17	0.28	0.61	0.24	0.35	0.38	0.69	0.70	0.93	0.69
SMED_34297_V2_1	suppression of tumorigenicity 13 (colon carcinoma) (Hsp70 interacting protein)	0.16	0.42	0.61	0.55	0.58	0.07	0.32	0.42	0.38	0.68
SMED_08635_V2_1	unknown	0.16	0.21	0.57	0.46	0.29	0.12	0.35	0.70	0.45	0.64
SMED_08717_V2_1	delta	0.16	-0.08	-0.15	0.14	1.94	0.05	-0.05	-0.40	0.16	2.45
SMED_02116_V2_1	low density lipoprotein-related protein 2	0.16	0.08	0.39	0.82	0.57	0.29	0.22	0.58	0.61	0.65
SMED_15891_V2_1	tissue factor pathway inhibitor (lipoprotein-associated coagulation inhibitor)	0.16	0.26	0.32	1.52	2.13	0.43	0.39	0.27	1.41	2.00
SMED_36533_V2_1	unknown	0.16	0.33	0.24	0.14	0.05	0.07	0.66	0.37	0.26	0.15
SMED_04485_V2_1	tissue factor pathway inhibitor (lipoprotein-associated coagulation inhibitor)	0.16	0.39	0.32	1.62	2.20	0.35	0.15	0.08	1.35	1.84
SMED_11730_V2_1	solute carrier family 35, member B1	0.16	0.05	0.40	0.75	0.66	0.12	0.01	0.21	0.45	0.74
SMED_23374_V2_1	FYN oncogene related to SRC, FGR, YES	0.16	0.18	0.61	0.71	0.52	0.06	0.13	0.59	0.90	0.59
SMED_13647_V2_1	thyroid hormone receptor, beta	0.15	0.51	0.74	0.51	0.51	-0.07	0.39	0.50	0.68	0.82
SMED_17626_V2_1	unknown	0.15	0.30	0.60	0.28	0.13	0.50	0.71	0.63	0.57	0.30
SMED_25200_V2_1	septin 7	0.15	0.24	0.52	0.51	0.62	0.03	0.17	0.49	0.77	0.56
SMED_13739_V2_1	unknown	0.15	0.12	-0.25	0.62	0.17	0.27	0.02	-0.04	1.16	0.14
SMED_10552_V2_1	protein tyrosine phosphatase, receptor type, N polypeptide 2	0.14	0.22	0.30	0.30	0.46	0.44	0.46	0.49	0.98	0.61
SMED_34413_V2_1	E74-like factor 1 (ets domain transcription factor)	0.14	0.34	0.77	0.47	0.39	0.19	0.44	0.74	0.78	0.41

SMED_02428_V2_1	cat eye syndrome chromosome region, candidate 5	0.14	0.33	0.33	0.23	0.29	0.40	0.62	0.63	0.53	0.71
SMED_09482_V2_1	UDP-Gal:betaGlcNAc beta 1,3-galactosyltransferase, polypeptide 1	0.14	0.35	0.64	0.79	0.55	0.16	0.23	0.63	0.77	0.58
SMED_13474_V2_1	leucine rich repeat and fibronectin type III domain containing 5	0.14	0.34	0.63	0.38	0.12	0.05	0.32	0.64	0.63	0.34
SmWIOct06_016868	ornithine decarboxylase 1	0.14	0.29	0.60	0.60	0.72	0.01	0.05	0.48	0.63	0.74
SMED_10870_V2_1	unknown	0.13	-0.05	0.01	0.54	0.78	-0.09	-0.01	0.26	-0.01	0.76
SMED_03513_V2_1	CTP synthase	0.13	0.22	0.52	0.53	0.39	0.16	0.12	0.51	0.67	0.10
SMED_04357_V2_1	IMP (inosine monophosphate) dehydrogenase 2	0.13	-0.03	-0.06	0.11	0.39	0.24	-0.07	0.08	0.64	0.61
SMED_37149_V2_1	unknown	0.13	0.21	0.22	0.22	0.32	0.44	0.65	0.58	0.56	0.88
SMED_01834_V2_1	unknown	0.13	0.19	1.02	0.98	0.99	0.14	0.18	0.96	1.18	1.08
SMED_37464_V2_1	zinc finger protein 607	0.13	0.49	0.34	0.16	0.01	-0.02	0.62	0.42	0.05	0.15
SMED_01183_V2_1	ADAM metallopeptidase domain 10	0.13	0.05	0.26	0.31	0.29	0.33	0.17	0.34	0.84	0.31
SMED_31874_V2_1	unknown	0.13	0.12	0.28	0.54	0.73	0.14	0.04	0.12	0.62	0.85
SMED_07121_V2_1	TNF receptor-associated factor 6	0.12	0.28	0.84	1.02	0.61	-0.09	0.19	0.85	0.89	0.81
SMED_14270_V2_1	unknown	0.12	0.11	0.38	0.48	0.38	0.27	0.17	0.52	0.68	0.52
SMED_00664_V2_1r	unknown	0.12	0.24	0.42	0.47	0.27	0.19	0.22	0.58	0.81	0.32
SMED_10286_V2_1	IQ motif and Sec7 domain 1	0.12	0.16	0.40	0.42	0.67	0.11	0.10	0.32	0.74	0.51
SMED_27203_V2_1	GLI pathogenesis-related 2	0.12	0.28	0.31	0.55	0.82	0.19	0.24	0.29	0.49	0.85
SMED_07127_V2_1	synaptotagmin II	0.12	-0.05	-0.06	0.33	0.66	0.07	-0.07	-0.04	0.02	0.71
SMED_16561_V2_1	tetratricopeptide repeat domain 25	0.11	0.39	0.41	0.36	0.34	0.38	0.77	0.79	0.79	0.75
SMED_33504_V2_1	unknown	0.11	0.10	0.31	0.59	1.09	0.08	0.03	0.25	0.53	1.21
SMED_02477_V2_1	peptidylprolyl isomerase B (cyclophilin B)	0.11	0.07	0.32	0.55	0.59	0.26	0.05	0.30	0.49	0.66
SMED_19200_V2_1	unknown	0.11	0.05	0.54	1.54	2.54	0.05	-0.09	0.28	0.71	0.79
SMED_01327_V2_1	bestrophin 3	0.11	0.29	0.37	0.60	0.75	0.10	0.19	0.34	0.53	0.66
SMED_05976_V2_1	unknown	0.11	0.25	0.36	0.43	0.43	0.20	0.35	0.55	1.03	0.84
SMED_09819_V2_1	purinergic receptor P2X, ligand-gated ion channel, 4	0.10	-0.05	0.06	0.37	0.44	0.10	-0.01	0.05	0.12	0.62
SMED_27420_V2_1	DEAD (Asp-Glu-Ala-Asp) box polypeptide 6	0.10	0.17	0.68	0.44	0.27	0.04	0.24	0.68	0.42	0.34
SMED_13757_V2_1	unknown	0.09	0.11	0.27	0.51	0.72	0.10	0.01	0.12	0.59	0.84
SMED_00466_V2_1	calreticulin	0.09	0.36	0.28	0.30	0.57	0.32	0.36	0.46	0.59	0.68
SMED_29161_V2_1	cubilin (intrinsic factor-cobalamin receptor)	0.09	0.41	0.38	0.23	-0.15	-0.11	0.64	0.49	0.22	0.13
SMED_07433_V2_1	FYN oncogene related to SRC, FGR, YES	0.09	0.13	0.73	0.49	0.47	0.21	0.21	0.60	0.62	0.45
SMED_09777_V2_1	Rab geranylgeranyltransferase, alpha subunit	0.09	0.24	0.49	0.46	0.32	0.41	0.20	0.55	0.81	0.24
SMED_11499_V2_1	thyrotropin-releasing hormone degrading enzyme	0.09	0.44	0.60	0.50	0.79	0.05	0.26	0.45	0.92	0.78
SMED_01731_V2_1	phospholipid scramblase 1	0.08	0.03	0.17	0.45	0.83	0.05	0.01	0.10	0.32	0.85
SMED_04503_V2_1	NAD kinase	0.08	0.09	0.58	0.67	0.68	0.03	0.01	0.43	0.44	0.66
SMED_01121_V2_1	polymerase (RNA) II (DNA directed) polypeptide A, 220kDa	0.08	0.35	0.16	0.11	0.09	0.15	0.65	0.54	0.21	0.27
SMED_23290_V2_1	fyn-related kinase	0.08	0.15	0.45	0.57	0.33	0.06	0.04	0.40	0.70	0.52
SMED_31833_V2_1	agrin	0.08	-0.03	0.17	0.26	0.45	0.14	-0.01	0.17	0.51	0.65
SMED_15461_V2_1	unknown	0.08	0.28	0.36	0.19	0.13	0.16	0.69	0.63	0.45	0.48
SMED_08509_V2_1	Williams Beuren syndrome chromosome region 27	0.08	-0.01	0.22	0.85	1.31	0.01	0.00	0.33	0.57	1.36
SMED_01360_V2_1	unknown	0.07	0.15	0.27	0.44	0.67	0.16	-0.05	0.25	0.26	0.77
SMED_27240_V2_1	plasminogen	0.07	0.19	0.22	0.85	1.06	0.11	0.10	0.20	0.99	1.37
SMED_11579_V2_1	GLI pathogenesis-related 2	0.06	0.26	0.29	0.51	0.77	0.14	0.21	0.26	0.45	0.85
SMED_10789_V2_1	unknown	0.06	0.45	0.76	0.02	0.08	0.00	0.37	0.72	0.36	0.29
SMED_02793_V2_1	(borderline1)	0.05	0.31	0.21	1.34	1.41	0.51	0.11	0.16	1.02	1.10
SMED_05022_V2_1	heparan sulfate proteoglycan 2	0.05	0.23	0.35	0.30	0.58	0.25	0.24	0.31	0.65	0.75
SMED_21648_V2_1	unknown	0.05	0.14	0.54	0.59	0.61	0.06	0.02	0.39	0.71	0.65
SMED_04030_V2_1	unknown	0.04	0.19	0.55	1.15	1.93	0.17	0.14	0.21	0.16	0.91
SMED_01940_V2_1	unknown	0.04	-0.20	-0.48	0.79	1.00	0.00	0.07	0.74	0.02	1.18
SMED_22086_V2_1	fascin homolog 2, actin-bundling protein, retinal (Strongylocentrotus purpuratus)	0.04	0.34	1.07	1.30	1.64	0.27	0.37	1.04	1.79	1.80

SMED_13192_V2_1	guanine nucleotide binding protein (G protein), alpha inhibiting activity polypeptide 1	0.04	0.17	0.52	0.35	0.10	0.06	0.28	0.69	0.40	0.28
SmWIOct06_013748	ornithine decarboxylase 1	0.03	0.01	0.25	0.52	0.82	-0.10	-0.25	0.00	0.34	0.66
SMED_06006_V2_1	antigen p97 (melanoma associated) identified by monoclonal antibodies 133.2 and 96.5	0.03	0.03	0.23	0.49	0.49	0.06	-0.02	0.23	0.54	0.66
SMED_02525_V2_1	UDP-glucose dehydrogenase	0.02	0.06	0.29	0.45	0.56	0.14	0.02	0.20	0.55	0.73
SMED_00748_V2_1	ATPase, Ca++ transporting, cardiac muscle, slow twitch 2	0.02	0.08	0.43	0.48	0.56	0.03	0.22	0.27	0.65	0.53
SMED_07998_V2_1	unknown	0.02	-0.11	0.25	0.55	0.73	0.20	0.19	0.25	0.83	0.93
SMED_15601_V2_1	solute carrier family 16, member 14 (monocarboxylic acid transporter 14)	0.02	0.02	0.32	0.42	0.90	-0.08	-0.11	0.21	0.48	0.99
SMED_05013_V2_1	eukaryotic translation termination factor 1	0.01	0.27	0.68	0.83	0.83	0.18	0.23	0.67	0.87	0.75
SMED_20788_V2_1	unknown	0.00	0.17	0.27	0.34	0.71	0.11	-0.05	0.17	0.23	0.81
SMED_09630_V2_1	pannexin 2	-0.01	0.14	0.91	1.11	1.13	-0.04	0.02	0.86	0.97	1.14
SMED_34863_V2_1	wingless-type MMTV integration site family, member 4	-0.01	0.11	0.25	0.20	0.35	-0.29	0.20	0.04	-0.07	0.71
SMED_06634_V2_1	solute carrier family 4, sodium borate transporter, member 11	-0.01	0.35	0.44	0.34	0.12	0.05	0.51	0.53	0.97	0.69
SMED_12880_V2_1	TNF receptor-associated factor 2	-0.01	0.19	0.80	0.91	0.57	0.16	0.25	0.92	1.16	0.75
SMED_28930_V2_1	wingless-type MMTV integration site family, member 1	-0.02	-0.01	0.07	0.17	0.31	-0.02	0.04	0.12	0.28	0.65
SMED_12438_V2_1	leishmanolysin-like (metallopeptidase M8 family)	-0.02	0.10	0.60	0.42	0.33	0.15	0.11	0.61	0.66	0.37
SMED_37906_V2_1	solute carrier family 2 (facilitated glucose transporter), member 1	-0.02	0.08	0.10	0.14	0.34	0.00	0.25	0.16	0.23	0.78
SMED_24961_V2_1	peptidylprolyl isomerase B (cyclophilin B)	-0.03	0.03	0.26	0.43	0.52	0.20	-0.03	0.25	0.41	0.66
SMED_28665_V2_1	transient receptor potential cation channel, subfamily M, member 2	-0.03	0.16	0.37	0.38	0.52	0.20	0.16	0.42	0.96	0.58
SMED_04485_V2_2	tissue factor pathway inhibitor (lipoprotein-associated coagulation inhibitor)	-0.03	0.29	0.22	1.49	2.08	0.16	0.12	0.03	1.22	1.93
SMED_17043_V2_1	ribosomal protein S6 kinase, 70kDa, polypeptide 1	-0.03	0.07	0.56	0.52	0.33	0.07	-0.01	0.61	0.86	0.43
SMED_09364_V2_1	unknown	-0.04	-0.02	0.29	0.80	1.14	0.10	0.08	0.39	0.87	1.27
SMED_00996_V2_1r	ankyrin 2, neuronal	-0.04	-0.18	0.14	0.35	0.25	0.29	0.08	0.29	0.82	0.48
SMED_05151_V2_1	unknown	-0.04	0.12	0.67	0.45	0.27	0.04	0.13	0.60	0.76	0.24
SmWIOct06_043148	solute carrier family 2 (facilitated glucose transporter), member 4	-0.05	0.22	0.13	0.12	0.47	-0.18	0.01	0.13	0.38	0.71
SMED_10377_V2_1	DDHD domain containing 1	-0.05	0.06	0.28	0.42	0.48	-0.01	-0.05	0.20	0.68	0.52
SMED_04768_V2_1r	argininosuccinate synthetase 1	-0.05	-0.20	0.34	0.45	0.88	0.42	0.24	0.36	0.88	0.67
SMED_19317_V2_1	septin 7	-0.05	-0.02	0.23	0.33	0.37	-0.03	-0.06	0.28	0.62	0.35
SMED_13523_V2_1	unknown	-0.05	-0.03	0.37	0.69	0.77	-0.04	-0.09	0.28	0.46	0.81
SMED_11394_V2_1	carboxypeptidase O	-0.07	-0.12	0.15	0.54	1.10	0.01	-0.14	0.13	0.56	1.16
SMED_09420_V2_1	G protein-coupled receptor 177	-0.07	-0.03	0.52	0.68	0.91	0.07	0.05	0.43	0.86	0.95
SMED_06008_V2_1	unknown	-0.08	0.09	0.26	0.32	0.39	0.30	0.36	0.63	0.86	0.66
SMED_10693_V2_1	angiotensin I converting enzyme (peptidyl-dipeptidase A) 1	-0.08	0.11	0.35	0.40	0.37	0.06	0.29	0.37	0.71	0.60
SMED_29274_V2_1	ADAM metallopeptidase with thrombospondin type 1 motif, 20	-0.08	-0.03	0.06	0.34	0.72	-0.09	-0.09	0.17	0.80	0.74
SMED_29811_V2_1	phytanoyl-CoA dioxygenase domain containing 1	-0.08	-0.22	-0.06	0.55	0.50	-0.12	-0.32	0.18	0.75	0.78
SMED_08508_V2_1	Williams Beuren syndrome chromosome region 27	-0.09	-0.19	-0.14	0.27	0.63	-0.05	-0.18	0.07	0.19	0.81
SMED_29539_V2_1	xin actin-binding repeat containing 2	-0.09	0.29	0.50	0.65	0.84	0.23	0.35	0.59	0.96	0.81
SMED_11855_V2_1	synaptotagmin-like 2	-0.10	-0.02	0.35	0.46	0.14	-0.17	-0.09	0.39	0.69	0.18
SMED_05034_V2_1r	unknown	-0.10	-0.13	0.69	0.83	1.40	0.60	0.47	0.57	1.49	1.09
SMED_37557_V2_1	unknown	-0.12	-0.08	-0.08	-0.07	0.36	-0.01	0.06	-0.07	0.18	1.15
SMED_07335_V2_1	slit homolog 2 (Drosophila)	-0.13	-0.14	0.30	0.47	0.48	0.07	0.01	0.19	0.65	0.65
SMED_24633_V2_1	cytochrome P450, family 2, subfamily B, polypeptide 6	-0.16	-0.19	-0.19	0.17	0.68	-0.05	-0.37	-0.13	0.04	0.73
SMED_18868_V2_1	unknown	-0.16	-0.01	0.57	0.44	0.63	-0.10	0.08	0.58	0.62	0.60
SMED_05460_V2_1	WAP, follistatin/kazal, immunoglobulin, kunitz and netrin domain containing 2	-0.16	0.05	0.28	0.81	1.56	0.21	0.26	0.33	0.23	0.90

SMED_05543_V2_1	unknown	-0.16	0.06	0.84	1.05	1.50	0.01	0.36	1.06	1.18	1.84
SMED_19280_V2_1	unknown	-0.17	0.24	0.42	0.26	0.62	-0.17	0.11	0.26	0.84	0.61
SMED_15999_V2_1	methionine adenosyltransferase II, alpha	-0.18	0.28	0.55	0.43	0.62	-0.23	0.03	0.13	0.33	0.67
SMED_05767_V2_1	xin actin-binding repeat containing 2	-0.18	0.20	0.45	0.58	0.73	0.33	0.45	0.62	0.96	0.74
SMED_36904_V2_1	unknown	-0.20	-0.01	0.51	0.39	0.30	0.05	0.11	0.53	0.88	0.31
SMED_15317_V2_1	unknown	-0.21	-0.32	-0.23	0.47	0.75	0.06	-0.15	0.46	-0.43	1.04
SMED_23858_V2_1	ezrin	-0.27	0.10	0.25	0.40	0.70	0.15	0.24	0.47	1.03	0.97
SMED_10656_V2_1	phytanoyl-CoA dioxygenase domain containing 1	-0.37	-0.39	-0.08	0.47	0.46	-0.35	-0.51	0.04	0.64	0.75

8.3 List of genes for which wound-induced expression patterns were determined by in situ hybridization

Table 8.2. Log2 ratios of (time point/control) for oligos that were significantly (FDR-adjusted p-value < 0.05) upregulated in wild-type (log2 > 0.3) and at the same time point in irradiated (log > 0.6) animals following wounding and for which expression following wounding was assessed by in situ hybridization. (WND = wound induction, Y = wound-induced, M = possibly wound-induced, N = not wound-induced or no signal).

SMED ID	Top human blastx hit	WT 30min	WT 1h	WT 3h	WT 6h	WT12h	IRR 30min	IRR 1h	IRR 3h	IRR 6h	IRR 12h	WND
SMED_07471_V2_1	early growth response 1 (egr1b)	2.21	2.81	1.89	0.48	-0.90	1.75	2.76	2.24	0.41	-0.80	Y
SMED_01464_V2_1	hypothetical protein	1.23	0.87	0.58	0.88	0.87	1.04	0.52	0.76	0.74	0.43	Y
SMED_03061_V2_1	jun	1.14	1.61	1.51	0.77	0.99	1.10	1.59	1.28	0.42	0.93	Y
SMED_35828_V2_1	early growth response 1 (Krox-20 homolog, Drosophila) (egr1)	1.08	1.60	1.29	0.48	0.01	1.31	2.69	1.89	0.57	0.38	Y
SMED_06912_V2_1	protein phosphatase 1, regulatory (inhibitor) subunit 3B	0.82	0.84	0.31	-0.18	-0.42	1.25	1.25	0.00	-0.27	-0.04	Y
SMED_03084_V2_1	blast to hepatic leukemia factor, bZIP TF, was NA	0.76	0.84	0.33	-0.09	-0.19	0.63	0.75	0.32	-0.15	-0.21	Y
SMED_09699_V2_1	surfeit 4	0.68	0.43	0.50	0.83	0.72	0.56	0.22	0.43	0.61	0.72	Y
SmWIOct06_013207	fibroblast growth factor receptor 2	0.67	0.74	0.64	0.46	0.15	0.51	0.69	0.65	0.53	0.43	Y
SMED_02142_V2_1	hypothetical protein	0.55	0.45	0.41	0.72	0.93	0.73	0.68	0.67	0.74	1.21	Y
SMED_02433_V2_1	mitogen-activated protein kinase kinase kinase 1	0.55	0.59	0.63	0.58	0.47	0.37	0.61	0.64	0.84	0.51	Y
SMED_00055_V2_1	c-Fos	0.54	1.23	1.68	0.84	1.08	1.02	1.88	1.78	1.96	1.44	Y
SMED_14904_V2_1	unknown	0.51	0.58	1.86	2.17	1.96	0.49	0.67	1.74	2.01	1.93	Y
SMED_06866_V2_1	bromodomain and WD repeat domain containing 1	0.50	0.75	1.17	0.48	0.62	0.42	0.92	1.43	0.37	0.92	Y
SMED_05579_V2_1	unknown	0.45	0.67	0.73	0.38	0.17	0.42	0.65	0.61	0.13	-0.03	Y
SMED_04057_V2_1	phosphoinositide-3-kinase, catalytic, alpha polypeptide	0.45	0.41	0.57	0.55	0.57	0.58	0.37	0.44	0.84	0.43	Y
SMED_00839_V2_1	noggin	0.44	0.32	0.86	1.27	1.27	0.50	0.35	1.15	1.36	1.67	Y
SMED_09765_V2_1	low van Willebrandt similarity, was NA	0.43	0.23	0.22	0.53	1.36	0.35	0.25	0.11	0.37	1.93	Y
SmWIOct06_029758	SWI/SNF related, matrix associated, actin dependent regulator of chromatin	0.43	0.71	0.65	0.49	0.05	0.27	0.75	0.61	0.34	0.32	Y
SMED_10026_V2_1	small G protein signaling modulator 1	0.41	0.35	0.41	0.32	0.42	0.51	0.40	0.41	0.78	0.30	Y
SMED_20251_V2_1	early growth response 2 (Krox-20 homolog, Drosophila) (egr2)	0.40	1.13	2.36	2.27	1.96	0.28	0.84	1.84	1.90	1.75	Y
SmWIOct06_012995	forkhead box A2	0.39	0.67	0.63	0.35	0.28	0.35	0.68	0.59	0.39	0.50	Y
SMED_05117_V2_1	dally-like	0.39	0.64	0.79	0.77	0.38	0.47	0.66	0.92	0.97	1.06	Y
SMED_06730_V2_1	docking protein 3 isoform 1	0.34	0.60	1.02	0.63	0.27	0.27	0.56	1.16	0.93	0.54	Y
SMED_08992_V2_1	unknown	0.34	0.67	0.33	-0.07	-0.10	0.11	0.60	0.33	0.19	0.01	Y
SMED_08611_V2_1	putative prolin-rich signal peptide protein	0.34	0.61	0.40	0.24	0.01	0.30	0.63	0.33	0.18	0.25	Y
SMED_08080_V2_1	four and a half LIM domains 2	0.31	0.20	0.23	0.60	0.82	0.46	0.20	0.31	0.48	0.81	Y
SMED_06551_V2_1	pim-3 oncogene	0.30	0.92	1.28	0.56	0.47	0.32	1.08	0.92	0.24	0.51	Y
SMED_10303_V2_1	B-cell CLL/lymphoma 3	0.28	0.32	0.47	0.54	0.61	0.24	0.34	0.41	0.54	0.67	Y
SMED_19658_V2_1	ankyrin repeat domain 62	0.27	1.04	1.75	0.83	0.75	0.71	1.33	1.63	2.08	0.88	Y
SMED_04444_V2_1	SmWIOct06_012995	0.26	0.31	0.74	0.85	0.57	0.58	0.68	0.69	0.43	0.87	Y
SMED_06705_V2_1	epiregulin	0.25	0.29	0.68	0.21	-0.30	0.31	0.32	0.72	-0.03	-0.36	Y
SMED_01282_V2_1	inhibin, beta A	0.25	0.38	0.50	0.85	0.82	0.29	0.33	0.67	0.91	1.13	Y
SMED_02705_V2_1	von Willebrand factor A domain containing 5A	0.24	0.62	0.51	0.03	0.07	0.45	0.76	0.66	0.81	0.35	Y
SMED_05818_V2_1	unknown	0.20	0.24	0.42	0.63	0.76	0.40	0.32	0.65	0.82	0.97	Y
SMED_10375_V2_1	hypothetical protein	0.19	0.62	-0.14	-0.36	-0.46	0.06	0.70	-0.03	-0.32	-0.26	Y
SMED_04943_V2_1	unknown	0.18	0.29	1.71	1.99	1.82	0.14	0.39	1.52	1.75	1.75	Y
SMED_13944_V2_1	SET domain containing 1B	0.18	0.49	0.35	0.17	0.04	0.25	0.63	0.51	0.53	0.31	Y
SMED_08717_V2_1	delta	0.16	-0.08	-0.15	0.14	1.94	0.05	-0.05	-0.40	0.16	2.45	Y
SMED_02116_V2_1	low density lipoprotein-related protein 2	0.16	0.08	0.39	0.82	0.57	0.29	0.22	0.58	0.61	0.65	Y
SMED_04485_V2_1	tissue factor pathway inhibitor (lipoprotein-associated coagulation inhibitor)	0.16	0.39	0.32	1.62	2.20	0.35	0.15	0.08	1.35	1.84	Y
SMED_23374_V2_1	FYN oncogene related to SRC, FGR, YES	0.16	0.18	0.61	0.71	0.52	0.06	0.13	0.59	0.90	0.59	Y
SMED_13647_V2_1	thyroid hormone receptor, beta	0.15	0.51	0.74	0.51	0.51	-0.07	0.39	0.50	0.68	0.82	Y
SMED_13474_V2_1	slit/leucine rich repeat and fibronectin type III domain containing 5	0.14	0.34	0.63	0.38	0.12	0.05	0.32	0.64	0.63	0.34	Y
SMED_37464_V2_1	zinc finger protein 607	0.13	0.49	0.34	0.16	0.01	-0.02	0.62	0.42	0.05	0.15	Y
SMED_10286_V2_1	IQ motif and Sec7 domain 1	0.12	0.16	0.40	0.42	0.67	0.11	0.10	0.32	0.74	0.51	Y
SMED_19200_V2_1	DUF2464	0.11	0.05	0.54	1.54	2.54	0.05	-0.09	0.28	0.71	0.79	Y
SMED_19200_V2_1	unknown	0.11	0.05	0.54	1.54	2.54	0.05	-0.09	0.28	0.71	0.79	Y
SMED_01154_V2_1r	cytochrome c oxidase sub3	0.10	0.16	0.36	0.35	0.63	0.29	0.48	0.30	0.63	0.63	Y
SMED_00466_V2_1	calreticulin	0.09	0.36	0.28	0.30	0.57	0.32	0.36	0.46	0.59	0.68	Y
SMED_07433_V2_1	FYN oncogene related to SRC, FGR, YES	0.09	0.13	0.73	0.49	0.47	0.21	0.21	0.60	0.62	0.45	Y

SMED_11499_V2_1	thyrotropin-releasing hormone degrading enzyme	0.09	0.44	0.60	0.50	0.79	0.05	0.26	0.45	0.92	0.78	Y
SMED_27240_V2_1	plasminogen	0.07	0.19	0.22	0.85	1.06	0.11	0.10	0.20	0.99	1.37	Y
SMED_02793_V2_1	borderline1	0.05	0.31	0.21	1.34	1.41	0.51	0.11	0.16	1.02	1.10	Y
SMED_04030_V2_1	unknown	0.04	0.19	0.55	1.15	1.93	0.17	0.14	0.21	0.16	0.91	Y
SMED_09420_V2_1	wntless	-0.07	-0.03	0.52	0.68	0.91	0.07	0.05	0.43	0.86	0.95	Y
SMED_18868_V2_1	unknown	-0.16	-0.01	0.57	0.44	0.63	-0.10	0.08	0.58	0.62	0.60	Y
SMED_15412_V2_1	unknown	1.85	1.33	1.16	1.51	1.24	1.51	0.83	1.29	0.47	1.08	M
SMED_00025_V2_1	prostaglandin D2 synthase, hematopoietic	1.17	0.56	0.42	0.59	0.70	1.07	0.46	0.78	0.55	0.54	M
SMED_06068_V2_1	pim-1 oncogene	0.94	0.65	0.03	-0.21	-0.06	0.87	0.88	0.06	-0.39	0.12	M
SMED_06604_V2_1	unknown	0.59	0.76	0.57	0.32	0.53	0.59	0.75	0.56	0.28	0.53	M
SMED_17304_V2_1	unknown	0.47	1.13	0.98	0.69	-0.08	0.37	1.39	1.19	0.62	0.56	M
SMED_03008_V2_1	GRB2-associated binding protein 3	0.44	0.39	0.54	0.50	0.52	0.63	0.59	0.50	0.38	0.65	M
SMED_20767_V2_1	unknown	0.43	0.62	0.56	0.37	0.14	0.50	0.73	0.64	0.60	0.39	M
SMED_27198_V2_1	peptidoglycan recognition protein 4	0.40	0.57	0.42	0.17	-0.05	0.15	0.66	0.43	0.11	0.10	M
SMED_01454_V2_1	multiple EGF-like-domains 6	0.33	0.32	0.35	0.42	0.54	0.34	0.38	0.39	0.62	0.68	M
SMED_02317_V2_1	high-mobility group box 2	0.31	0.27	0.47	0.60	0.61	0.29	0.23	0.48	0.65	0.43	M
SMED_04273_V2_1	pim-3 oncogene	0.30	0.72	0.61	0.05	-0.23	0.42	0.91	0.74	0.17	-0.23	M
SMED_17458_V2_1	GLI pathogenesis-related 1 like 1	0.28	0.27	0.52	0.54	0.60	0.19	0.35	0.61	0.32	0.97	M
SMED_19658_V2_1	traf/ankyrin repeat domain 62	0.27	1.04	1.75	0.83	0.75	0.71	1.33	1.63	2.08	0.88	M
SmWIOct06_040653	host cell factor C1 (VP16-accessory protein)	0.27	0.47	0.46	0.24	0.11	0.27	0.67	0.49	0.50	0.38	M
SMED_00097_V2_1r	transmembrane protein 111	0.18	0.39	0.69	0.68	0.06	0.27	0.25	0.66	0.53	0.11	M
SMED_05374_V2_1	receptor tyrosine kinase-like orphan receptor 1	0.18	0.41	0.33	0.15	0.21	0.21	0.73	0.61	0.43	0.53	M
SMED_34413_V2_1	E74-like factor 1 (ets domain transcription factor)	0.14	0.34	0.77	0.47	0.39	0.19	0.44	0.74	0.78	0.41	M
SMED_07121_V2_1	TNF receptor-associated factor 6	0.12	0.28	0.84	1.02	0.61	-0.09	0.19	0.85	0.89	0.81	M
SMED_23290_V2_1	fyn-related kinase	0.08	0.15	0.45	0.57	0.33	0.06	0.04	0.40	0.70	0.52	M
SMED_05022_V2_1	heparan sulfate proteoglycan 2	0.05	0.23	0.35	0.30	0.58	0.25	0.24	0.31	0.65	0.75	M
SMED_21904_V2_2	Jun-related antigen	-0.11	-0.14	0.26	0.11	0.23	0.53	0.40	0.49	1.02	0.72	M
SMED_07335_V2_1	slit homolog 2 (Drosophila)	-0.13	-0.14	0.30	0.47	0.48	0.07	0.01	0.19	0.65	0.65	M
SMED_05460_V2_1	WAP, follistatin/kazal, immunoglobulin, kunitz and netrin domain containing 2	-0.16	0.05	0.28	0.81	1.56	0.21	0.26	0.33	0.23	0.90	M
SMED_19280_V2_1	unknown	-0.17	0.24	0.42	0.26	0.62	-0.17	0.11	0.26	0.84	0.61	M
SMED_10870_V2_1	unknown	0.13	-0.05	0.01	0.54	0.78	-0.09	-0.01	0.26	-0.01	0.76	M
SMED_00148_V2_1	guanine nucleotide binding protein (G protein), beta polypeptide 1	0.93	0.73	0.71	0.68	0.61	0.74	0.62	0.75	0.84	0.63	N
SMED_15791_V2_1	hypothetical protein	0.85	0.70	0.52	-0.97	-0.89	0.87	0.95	0.45	-1.33	-0.84	N
SMED_08052_V2_1	Ras suppressor protein 1	0.74	0.50	0.42	0.61	0.49	0.70	0.42	0.56	0.50	0.47	N
SMED_15081_V2_1	unknown	0.64	0.38	0.41	0.55	0.27	0.63	0.37	0.51	0.44	0.40	N
SMED_02036_V2_1	calpain 3, (p94)	0.63	0.55	0.59	0.49	0.59	0.77	0.60	0.66	1.08	0.58	N
SMED_14741_V2_1	ligand of numb-protein X 1	0.60	0.52	0.70	0.68	0.42	0.44	0.44	0.79	0.96	0.56	N
SMED_00792_V2_1	docking protein 7	0.59	0.70	0.55	0.33	0.41	0.60	0.72	0.49	0.20	0.54	N
SMED_20504_V2_1	Y-box protein	0.55	0.73	0.59	0.44	0.43	0.39	0.63	0.73	0.65	0.52	N
SMED_28060_V2_1	misshapen-like kinase 1 (zebrafish)	0.55	0.66	0.59	0.48	0.31	0.56	0.60	0.63	0.77	0.43	N
SMED_16035_V2_1	poly (ADP-ribose) polymerase family, member 3	0.53	0.64	0.57	0.39	0.26	0.59	0.60	0.63	0.77	0.42	N
SMED_03805_V2_1	solute carrier family 39 (zinc transporter), member 7	0.49	0.22	0.35	0.64	0.61	0.37	0.15	0.37	0.43	0.68	N
SMED_05872_V2_1r	calpain 9	0.48	0.54	1.14	1.09	0.84	0.45	0.65	1.23	1.11	1.16	N
SMED_12796_V2_1	unknown	0.44	0.34	0.65	0.76	0.61	0.51	0.53	0.61	0.49	0.85	N
SMED_15193_V2_1	phospholipid scramblase 1	0.44	0.76	0.65	0.47	0.05	0.31	0.74	0.57	0.37	0.40	N
SMED_09356_V2_1	low density lipoprotein receptor adaptor protein 1	0.33	0.09	0.24	0.34	0.47	0.62	0.33	0.38	0.52	0.68	N
SMED_07430_V2_1	castor zinc finger 1	0.32	0.50	0.39	0.37	0.15	0.30	0.57	0.57	0.70	0.41	N
SMED_16228_V2_1	GRB10 interacting GYF protein 2	0.27	0.51	0.33	0.25	-0.05	0.27	0.63	0.47	0.36	0.21	N
SMED_19019_V2_1	unknown	0.22	0.05	0.03	0.35	0.64	0.09	-0.07	0.09	0.16	0.66	N
SMED_19019_V2_1	unknown	0.22	0.05	0.03	0.35	0.64	0.09	-0.07	0.09	0.16	0.66	N
SMED_06588_V2_1	mitogen-activated protein kinase 10	0.18	0.15	0.21	0.25	0.35	0.11	0.08	0.16	0.24	0.33	N
SMED_10552_V2_1	protein tyrosine phosphatase, receptor type, N polypeptide2	0.14	0.22	0.30	0.30	0.46	0.44	0.46	0.49	0.98	0.61	N
SMED_29161_V2_1	cubilin (intrinsic factor-cobalamin receptor)	0.09	0.41	0.38	0.23	-0.15	-0.11	0.64	0.49	0.22	0.13	N
SMED_11579_V2_1	GLI pathogenesis-related 2	0.06	0.26	0.29	0.51	0.77	0.14	0.21	0.26	0.45	0.85	N
SMED_10789_V2_1	unknown	0.06	0.45	0.76	0.02	0.08	0.00	0.37	0.72	0.36	0.29	N
SMED_08508_V2_1	Williams Beuren syndrome chromosome region 27	-0.09	-0.19	-0.14	0.27	0.63	-0.05	-0.18	0.07	0.19	0.81	N
SMED_15317_V2_1	tetratricopeptide domain-containing protein	-0.21	-0.32	-0.23	0.47	0.75	0.06	-0.15	0.46	-0.43	1.04	N

8.4 List of genes that were significantly upregulated in neoblasts and/or their descendents following wounding as determined by microarray analysis

Table 8.3. Log2 ratios of (time point/control) for oligos that were significantly (FDR-adjusted p-value < 0.05) upregulated in wild-type (log2 > 0.3) and at the same time point in irradiated (log > 0.<1t) animals following wounding.

SMED ID	top human blast hit	WT 30min	WT 1h	WT 3h	WT 6h	WT 12h	IRR 30min	IRR 1h	IRR 3h	IRR 6h	IRR 12h
SMED_12882_V2	lin-54 homolog (C. elegans)	0.37	0.62	0.47	0.34	-0.02	-0.10	0.50	0.43	0.02	-0.02
SMED_01461_V2	H2A histone family, member Y2	0.62	0.56	0.57	0.61	0.60	0.29	0.23	0.23	0.24	0.15
SMED_00808_V2	unknown	0.31	0.54	0.51	0.36	-0.08	-0.17	0.11	0.15	0.03	0.22
SMED_00046_V2	tumor suppressor candidate 3	0.49	0.46	0.50	0.63	0.48	-0.10	0.26	0.39	0.22	0.47
SMED_23464_V2	guanine nucleotide binding protein (G protein)	0.36	0.44	0.47	0.44	0.27	0.04	0.09	0.23	0.21	0.44
SMED_11734_V2	SRY (sex determining region Y)-box 13	0.09	0.42	0.35	0.05	-0.06	-0.15	0.28	0.17	-0.02	0.12
SMED_34812_V2	unknown	0.45	0.41	0.44	0.46	0.14	-0.12	0.29	0.15	0.15	0.04
SMED_26248_V2	BMP2 inducible kinase	0.12	0.41	0.34	0.12	0.09	-0.18	0.14	0.12	-0.05	0.06
SMED_25875_V2	YTH domain family, member 1	0.35	0.41	0.27	0.13	0.03	-0.03	0.15	0.14	0.02	-0.01
SMED_01000_V2	hydroxysteroid (17-beta) dehydrogenase 10	0.44	0.41	0.38	0.57	0.47	0.17	0.16	0.25	0.17	0.19
SMED_33561_V2	jumonji, AT rich interactive domain 1A	0.18	0.40	0.24	0.13	0.09	-0.03	0.20	0.23	0.01	0.11
SMED_04830_V2	unknown	0.43	0.39	0.45	0.47	0.57	0.11	0.06	0.10	0.25	-0.21
SMED_03518_V2	notchless homolog 1 (Drosophila)	0.20	0.39	0.40	0.36	0.26	0.04	0.17	0.27	0.25	0.24
SMED_20741_V2	Wolf-Hirschhorn syndrome candidate 1	0.32	0.38	0.54	0.51	0.59	0.20	0.12	0.22	0.23	0.12
SMED_18010_V2	unknown	0.30	0.38	0.54	0.59	0.46	0.11	0.18	0.18	0.05	0.14
SMED_02609_V2	unknown	0.31	0.37	0.04	-0.04	-0.16	0.01	0.10	-0.04	-0.46	-0.28
SMED_35033_V2	unknown	0.32	0.37	0.41	0.39	0.14	-0.09	0.31	0.15	0.06	0.15
SMED_12069_V2	SH3-domain GRB2-like 3	0.35	0.36	0.34	0.28	0.22	0.03	0.18	0.17	0.01	0.23
SMED_02961_V2	runt-related transcription factor 2 (runt2)	0.23	0.35	0.44	0.12	0.06	0.05	0.10	0.17	-0.14	0.14
SMED_01813_V2	unknown	0.37	0.33	0.43	0.43	0.21	0.03	0.00	0.06	0.12	0.07
SMED_05061_V2	SRY (sex determining region Y)-box 9	0.45	0.33	0.12	0.25	0.26	0.09	0.01	0.08	0.10	0.02
SMED_00240_V2	FK506 binding protein 6, 36kDa	0.33	0.33	0.29	0.28	0.40	0.21	0.17	0.19	0.18	0.23
SMED_17522_V2	SLIT and NTRK-like family, member 1	0.28	0.33	0.28	0.38	0.55	0.11	0.18	0.12	0.09	0.12
SMED_25372_V2	p21 protein (Cdc42/Rac)-activated kinase 1	0.30	0.32	0.24	0.11	0.03	-0.04	0.11	0.07	-0.02	0.04
SMED_34063_V2	unknown	0.31	0.31	0.40	0.29	0.05	-0.22	0.18	0.04	-0.02	-0.03
SMED_09445_V2	suppressor of variegation 4-20 homolog 1 (Drosophila)	0.17	0.31	0.25	0.10	-0.08	0.01	0.10	0.05	-0.06	0.11
SMED_31979_V2	BTB (POZ) domain containing 9	0.16	0.30	0.30	0.05	-0.10	-0.07	0.07	0.06	-0.07	0.06
SMED_07003_V2	runt-related transcription factor 2 (runt1)	0.10	0.29	1.51	2.07	1.72	-0.02	0.06	0.08	0.07	0.04
SMED_25898_V2	leukotriene A4 hydrolase	0.26	0.28	0.35	0.41	0.49	0.05	0.01	-0.01	0.09	**0.10**
SMED_00510_V2	unknown	0.42	0.28	0.45	0.77	0.87	0.31	0.08	0.11	0.15	0.10
SMED_03398_V2	glycine amidinotransferase (L-arginine:glycine amidinotransferase)	0.25	0.27	0.37	0.37	0.56	0.01	-0.04	0.00	0.08	-0.05
SMED_05753_V2	endothelial differentiation-related factor 1	0.44	0.26	0.35	0.49	0.44	0.32	0.05	0.11	0.09	0.14
SMED_02632_V2	unknown	0.37	0.26	0.42	0.63	0.68	0.13	0.13	0.21	0.17	0.44
SMED_08100_V2	retinoblastoma binding protein 4	0.22	0.26	0.30	0.28	0.21	0.10	0.09	0.17	0.11	0.05
SMED_05281_V2	unknown	0.15	0.25	0.41	0.38	0.38	0.01	0.10	0.08	0.14	0.06
SMED_20358_V2	unknown	0.38	0.24	0.32	0.23	0.39	0.03	-0.01	0.05	-0.04	-0.06
SMED_05663_V2	dyskeratosis congenita 1, dyskerin	0.35	0.24	0.35	0.43	0.32	0.15	0.04	0.05	0.06	-0.04
SMED_32895_V2	unknown	0.40	0.24	0.13	0.19	0.18	0.15	0.00	0.05	0.22	-0.07
SMED_02069_V2	unknown	0.54	0.23	0.38	0.76	0.87	0.11	0.13	0.22	0.11	0.09
SMED_00740_V2	unknown	0.42	0.23	0.23	0.33	0.09	0.00	0.18	0.20	-0.07	0.10
SMED_14572_V2	unknown	0.19	0.23	0.33	0.35	0.20	0.03	0.07	0.12	0.04	0.05
SMED_10009_V2	TNF receptor-associated factor 4	0.28	0.23	0.31	0.45	0.36	0.14	0.20	0.17	0.23	0.14
SMED_01433_V2	soc-2 suppressor of clear homolog (C. elegans)	0.16	0.23	0.36	0.02	-0.18	-0.04	0.13	0.12	0.17	-0.16

SMED_30137_V2	TRAF and TNF receptor associated protein	0.27	0.22	0.23	0.42	0.42	0.17	0.10	0.21	0.15	0.20
SMED_12638_V2	unknown	0.30	0.22	0.29	0.34	0.20	0.04	0.01	0.01	0.04	0.03
SMED_28088_V2	transmembrane protein 147	0.36	0.22	0.28	0.56	0.45	0.21	-0.02	0.18	0.08	0.29
SMED_16977_V2	unknown	0.30	0.22	0.20	0.18	0.14	0.03	-0.05	0.05	0.18	0.01
SMED_06914_V2	polycomb group ring finger 2	0.20	0.22	0.25	0.38	0.37	0.15	0.12	0.12	0.10	0.28
SMED_07099_V2	TIA1 cytotoxic granule-associated RNA binding protein	0.30	0.21	0.25	0.45	0.56	0.34	0.08	0.06	0.20	0.19
SMED_03729_V2	unknown	0.52	0.21	0.58	0.34	0.22	-0.51	0.08	-0.16	-0.03	-0.55
SMED_03896_V2	EPH receptor A1	0.32	0.21	0.32	0.44	0.49	0.24	0.04	0.15	0.09	0.27
SMED_27119_V2	ring finger protein 103	0.12	0.20	0.31	0.26	0.24	0.06	0.02	0.06	0.05	0.05
SMED_01226_V2	unknown	0.35	0.19	0.24	0.40	0.24	0.25	-0.73	-0.31	0.19	-1.93
SMED_04030_V2	unknown	0.04	0.19	0.55	1.15	1.93	0.17	0.14	0.21	0.16	0.91
SMED_05169_V2	unknown	0.42	0.18	0.35	0.74	0.79	0.15	0.17	0.24	0.14	0.18
SMED_12087_V2	jumonji domain containing 2A	0.26	0.18	0.25	0.40	0.40	0.17	0.07	0.16	0.18	0.35
SMED_05614_V2	F-box and leucine-rich repeat protein 11	0.16	0.18	0.17	0.16	0.37	0.09	-0.02	0.07	0.11	0.13
SMED_02305_V2	NME1-NME2 readthrough transcript	0.31	0.17	0.24	0.39	0.41	0.08	0.06	0.14	0.20	0.08
SMED_19894_V2	unknown	0.26	0.17	0.20	0.37	0.33	0.13	-0.04	0.06	0.05	0.13
SMED_09947_V2	unknown	0.36	0.16	0.24	0.46	0.39	0.25	0.01	0.14	0.09	0.17
SMED_14033_V2	ASF1 anti-silencing function 1 homolog A (S. cerevisiae)	0.23	0.16	0.20	0.33	0.31	0.17	0.06	0.04	0.01	0.09
SMED_03674_V2	H2A histone family, member Z	0.41	0.16	0.19	0.56	0.51	0.25	0.17	0.27	0.27	0.14
SMED_00523_V2	unknown	0.18	0.15	0.38	0.43	0.45	-0.10	-0.10	-0.07	0.09	-0.11
SMED_14658_V2	chromosome 9 open reading frame 85	0.33	0.15	0.24	0.37	0.18	0.19	0.05	0.16	0.01	0.05
SMED_04459_V2	Y box binding protein 2	0.28	0.14	0.19	0.44	0.48	0.22	-0.03	0.12	0.35	0.01
SMED_13795_V2	zinc finger, matrin type 5	0.38	0.14	0.18	0.40	0.36	0.29	0.06	0.09	0.02	0.09
SMED_19801_V2	unknown	0.30	0.14	0.29	0.54	0.46	0.29	0.02	0.16	0.10	0.14
SMED_11006_V2	transmembrane protein 177	0.28	0.13	0.15	0.38	0.24	0.18	-0.04	0.02	-0.02	0.18
SMED_02715_V2	KIAA1333	0.18	0.13	0.21	0.30	0.30	0.14	0.11	0.01	-0.01	0.17
SMED_21037_V2	receptor accessory protein 2	0.29	0.13	0.24	0.42	0.36	-0.04	0.02	0.06	-0.07	-0.07
SMED_11111_V2	zinc finger, MYM-type 1	0.15	0.13	0.16	0.08	0.35	0.05	0.17	0.17	0.09	0.05
SMED_08511_V2	WD repeat domain 82	0.12	0.13	0.23	0.32	0.21	-0.03	-0.05	0.05	-0.14	0.02
SMED_32027_V2	unknown	0.25	0.12	0.22	0.38	0.18	0.26	0.01	0.20	-0.01	0.10
SMED_12559_V2	four and a half LIM domains 3	0.15	0.12	0.20	0.28	0.45	0.18	0.04	0.09	0.27	0.19
SMED_02233_V2	chromobox homolog 1 (HP1 beta homolog Drosophila)	0.19	0.12	0.27	0.43	0.43	0.16	-0.02	0.11	0.12	0.10
SMED_07640_V2	zinc finger, HIT type 2	0.28	0.11	0.23	0.36	0.24	0.21	0.02	0.01	-0.12	0.05
SMED_16187_V2	reticulocalbin 1, EF-hand calcium binding domain	0.37	0.11	0.12	0.34	0.36	0.25	-0.09	-0.02	0.08	0.02
SMED_22268_V2	unknown	0.18	0.11	0.19	0.12	0.47	0.17	-0.01	0.06	0.19	0.12
SMED_07927_V2	SIX homeobox 6	0.29	0.10	0.25	0.29	0.32	0.22	0.12	0.15	-0.04	0.20
SMED_05722_V2	splA/ryanodine receptor domain and SOCS box containing 4	0.16	0.10	0.25	0.22	0.34	-0.15	-0.05	0.07	-0.12	0.10
SMED_06249_V2	hypothetical protein MGC12972	0.29	0.09	0.13	0.24	0.37	0.06	-0.02	-0.15	-0.33	-0.43
SMED_02617_V2	unknown	-0.02	0.09	0.26	0.69	0.94	-0.25	-0.13	-0.11	0.01	-0.31
SMED_30081_V2	unknown	0.11	0.08	0.08	0.59	0.83	0.26	0.06	0.22	0.18	0.31
SMED_01904_V2	tudor domain containing 1	0.04	0.07	0.22	0.24	0.37	0.10	-0.01	0.07	0.13	0.11
SMED_06212_V2	endothelin converting enzyme 2	0.21	0.07	0.18	0.37	0.27	0.13	0.06	0.06	-0.15	0.22
SMED_12730_V2	unknown	0.28	0.07	0.12	0.42	0.29	0.32	0.05	0.07	0.12	0.16
SMED_23095_V2	SET domain containing 1A	0.00	0.06	-0.02	-0.03	0.52	-0.03	0.09	-0.03	-0.06	0.02
SMED_07632_V2	Rho GTPase activating protein 18	0.04	0.05	0.26	0.22	0.41	-0.11	-0.05	-0.10	0.00	-0.34
SMED_01927_V2	WD repeat domain 61	0.11	0.05	0.10	0.30	0.22	0.10	-0.14	0.01	-0.04	-0.01
SMED_04692_V2	unknown	0.23	0.05	0.50	0.67	0.44	0.12	0.11	0.25	0.22	0.18
SMED_09747_V2	unknown	0.16	0.05	0.17	0.37	0.35	0.13	0.01	0.09	0.00	0.10

SMED_23187_V2	nuclear receptor binding SET domain protein 1	-0.05	0.04	0.16	0.16	0.36	-0.02	0.11	0.05	-0.03	-0.02
SMED_10541_V2	solute carrier family 7, (cationic amino acid transporter, y+ system) member 11	0.06	0.04	0.30	0.45	0.46	-0.02	-0.25	-0.06	0.11	0.01
SMED_06746_V2	unknown	0.28	0.04	0.29	0.49	0.05	0.09	-0.06	0.04	0.20	-0.05
SMED_32801_V2	unknown	0.24	0.03	0.08	0.26	0.41	0.14	0.02	0.08	0.15	0.09
SMED_05897_V2	chromosome 14 open reading frame 166	0.20	0.03	0.09	0.28	0.31	0.17	0.04	0.03	-0.04	0.14
SMED_07385_V2	defender against cell death 1	0.09	0.03	0.06	0.22	0.34	0.07	-0.05	0.05	0.07	-0.01
SMED_01564_V2	unknown	0.09	0.03	0.19	0.32	0.30	-0.01	-0.05	-0.05	-0.11	0.05
SMED_07668_V2	chromosome 2 open reading frame 63	-0.03	0.02	0.19	0.35	0.25	0.05	0.07	0.12	0.10	0.05
SMED_12883_V2	SUMO/sentrin specific peptidase family member 8	0.22	0.02	0.15	0.40	0.42	0.24	-0.04	0.05	0.01	0.21
SMED_04844_V2	unknown	-0.14	0.02	0.38	0.53	0.58	-0.10	0.10	0.25	0.17	0.21
SMED_18055_V2	unknown	0.20	0.01	0.00	-0.01	0.41	0.15	-0.01	-0.02	0.10	0.00
SMED_09062_V2	high-mobility group box 2	0.28	0.01	0.06	0.30	0.30	0.24	0.01	-0.03	-0.18	0.00
SMED_20554_V2	translocated promoter region (to activated MET oncogene)	0.07	0.01	0.01	0.01	0.38	0.13	-0.07	-0.04	0.08	0.05
SMED_34089_V2	thyrotropin-releasing hormone receptor	0.16	0.01	0.03	0.18	0.41	0.21	-0.01	0.02	0.15	0.17
SMED_06593_V2	zinc finger, CCHC domain containing 13	0.17	0.00	0.06	0.06	0.36	0.15	0.07	0.05	0.10	0.10
SMED_06245_V2	peptidase inhibitor 16	0.03	0.00	-0.02	0.40	0.43	0.01	-0.07	0.02	0.05	0.30
SMED_28067_V2	neural precursor cell expressed, developmentally down-regulated 1	0.17	-0.01	0.08	0.19	0.34	0.15	-0.04	0.03	-0.02	0.01
SMED_04628_V2	unknown	0.11	-0.01	0.13	0.25	0.59	-0.17	-0.12	-0.16	-0.08	-0.21
SMED_04681_V2	unknown	0.14	-0.01	0.19	0.38	0.46	0.13	-0.08	-0.01	0.05	0.29
SMED_16667_V2	chromosome 14 open reading frame 129	0.13	-0.02	0.06	0.32	0.31	0.19	-0.06	-0.01	-0.05	0.03
SMED_05824_V2	unknown	0.16	-0.02	0.05	0.34	0.53	0.13	-0.06	0.06	0.05	0.20
SMED_00701_V2	unknown	-0.01	-0.05	0.09	0.44	0.44	0.02	-0.15	-0.01	0.11	0.19
SMED_28346_V2	ring finger protein 8	0.09	-0.08	0.03	0.27	0.33	0.06	-0.03	0.02	0.05	-0.04
SMED_35689_V2	unknown	0.12	-0.08	0.30	0.44	0.32	0.16	-0.09	-0.02	-0.03	-0.07
SMED_20378_V2	unknown	-0.05	-0.10	0.29	0.58	0.56	-0.15	-0.21	-0.08	0.02	-0.17
SMED_26112_V2	phosphorylase, glycogen, liver	0.19	-0.10	-0.10	-0.09	1.99	0.13	-0.13	-0.09	-0.07	-0.01
SMED_04796_V2	unknown	0.15	-0.13	0.12	0.41	0.34	0.04	-0.02	0.03	0.09	0.06
SMED_21205_V2	retinoblastoma binding protein 4, was NA	-0.09	-0.15	0.20	0.53	0.89	-0.01	-0.12	-0.18	-0.11	0.19
SMED_05706_V2	crystallin, alpha B	0.39	-0.16	0.69	0.70	0.04	-0.02	-0.74	-0.11	-0.19	-1.49
SMED_02590_V2	FK506 binding protein 4, 59kDa	-0.05	-0.22	0.08	0.37	0.58	-0.01	-0.27	-0.14	0.11	0.15

8.5 Erklärung

Ich versichere hiermit, diese Arbeit selbstständig verfaβt, und nur die angegebenen Hilfsmittel und Hilfen in Anspruch genommen zu haben. Alle Experiemente und Analysen wurden von mir eigenständig durchgeführt, mit Ausnahme einiger Klonierungen und *in situ* Hybridisierungen (mit Alexander Wilkinson, Whitehead Institute, Cambridge, USA), der Microarrayhybridisierungen (Genome Technology Core, Whitehead Institute, Cambridge, USA) und der Normalisierung und Teils der statistischen Analysen der Microarraydaten und der Daten von den NanoString Experimenten (mit George Bell, BaRC, Whitehead Institute, Cambridge, USA).

Danielle Wenemoser Cambridge, January 2011

Acknowledgements

First of all, I would like to express my deep gratitude to Prof. Dr. Peter Reddien for providing outstanding guidance and advise throughout these years. Thanks, for letting me realize my own ideas and bringing me back on track, whenever things went wrong. It has been a great experience to work with him as an advisor and I am looking forward to the following months, where I will stay in his Laboratory to finalize the work presented here.

My thanks also go to Prof. Dr. Constanze Scharff from the Free University of Berlin for her interest in my work, providing me with her advise whenever I needed it and always making time for me in her busy schedule throughout all this time period.

It is very important for me to thank all the past and present members of the Reddien Lab, many of which I consider my family, especially the other graduate students - my baymate Sylvain Lapan, Daniel E. Wagner, Irving Wang, Jared Owen, as well as technicians - Jaclyn Ho, Alexander Wilkinson, and Jessica Witchley. Thanks (to everybody!!!) for the help, the lunch and coffee breaks (especially the ones with non-scientific discussion topics!), the unforgettable nights in South Boston, and so much more! I am incredibly happy that I got the chance to work with them every day and to profit from the stimulating and creative atmosphere in this laboratory.

Ganz besonders möchte ich mich bei meiner Familie bedanken, für ihren Glauben an mich und die Unterstützung, die sie mir jederzeiten gewährten. Dies gilt ganz besonders fuer meine Mutter, Barbara Wenemoser, die zu jeder Tages- und Nachtzeit bereit war, sich mein Gejammer anzuhören und die ueber die Verpflichtungen einer Mutter hinaus immer fuer mich da war. VIELEN VIELEN DANK!

Und natürlich möchte ich den lieben Freunden in der Heimat danken, vor allem Myriam Günther und Rebecca Finster. Es ist gut zu wissen, dass man nach so langer Zeit immer noch Freunde in der Heimat hat!

Moreover, I want to thank my non-work friends in Cambridge, especially Timea Pal and Chiara Lepore, for making me feel at home here and for all the great times we had; and Emma Doud, the best roommate in the world! Special thanks for feeding me in the last week of my thesis work!

But most importantly I want to thank Michael Alexander Gaviño, my Editor-in-chief, colleague, and best boyfriend that a girl could possibly wish for! There are no words or expressions that would do my feelings justice, and therefore I will spend no more words..... <3